PLUME DISPERSION MEASUREMENTS FROM AN OIL SANDS EXTRACTION PLANT, JUNE 1977

by

D. S. DAVISON
and
K. L. GRANDIA
Intera Environmental Consultants Ltd.

for

ALBERTA OIL SANDS ENVIRONMENTAL RESEARCH PROGRAM

PROJECT ME 2.3.2

March 1979

TABLE OF CONTENTS

		Page
DECLARATION		ii
LETTER OF TRANSMITTAL		iii
DESCRIPTIVE SUMMARY		iv
LIST OF TABLES		xii
LIST OF FIGURES		xiv
ABSTRACT		xxi
ACKNOWLEDGEMENTS		xxii
1.	INTRODUCTION	1
1.1	Terms of Reference	1
2.	EQUIPMENT	3
2.1	Air Chemistry Package	3
2.2	Airborne Turbulence Package	4
2.3	Airborne Data Acquisition System	7
2.4	Position Recovery	8
3.	FIELD PROCEDURES AND ANALYSIS METHODOLOGIES	10
3.1	Field Procedures	10
3.1.1	Selection of Flight Times	10
3.1.2	Flight Track Set-up	10
3.1.3	Plume Traverses	11
3.1.4	Turbulence Runs	12
3.2	Criteria for the Selection of Case Studies	12
3.3	Data Analysis Methodology	13
3.3.1	SO_2 Concentrations Along Flight Traverses	13
3.3.2	Plume Geometry Calculations	13
3.3.3	Plume Rise Predictions	16
3.3.4	Turbulence Analysis Methodology	17
3.3.4.1	Generation of the Turbulent Gust Velocities and System Limitations	17
3.3.4.2	Fluxes and Stability	19
3.3.4.3	Dissipation and Integral Statistics	21
3.3.4.4	Spectral Analysis	22
3.3.4.5	Modification of the Velocity Standard Deviations	23
4.	CASE STUDIES	24
4.1	Case Study for the Flight of 19 June 1977 (0745-1010 MDT)	24
4.1.1	Visual Plume Description	24
4.1.2	Flight Profiles	24

TABLE OF CONTENTS (CONTINUED)

		Page
4.1.3	Tethersonde Data	30
4.1.4	Isopleths and Selected Traverses	30
4.1.5	Plume Geometry	34
4.1.6	Turbulence Levels Related to Plume Structure.	40
4.2	Case Study for the Flight of June 19 1977 (1335-1793 MDT)	44
4.2.1	Visual Plume Description	44
4.2.2	Flight Profiles.	44
4.2.3	Tethersonde Data	44
4.2.4	Isopleths and Selected Traverses	48
4.2.5	Plume Geometry	48
4.2.6	Validation of Turbulence Analysis Procedures	53
4.2.7	Turbulence Levels Related to Plume Structure.	58
4.3	Case Study for the Flight of 20 June 1977 (1000-1500 MDT)	65
4.3.1	Visual Plume Description	65
4.3.2	Flight Profiles.	65
4.3.3	Tethersonde Data	65
4.3.4	Isopleths and Selected Traverses	65
4.3.5	Plume Geometry	71
4.3.6	Turbulence Levels Related to Plume Structure.	79
4.4	Case Study for the Flight of 22 June 1977 (1915-2305 MDT)	82
4.4.1	Visual Plume Description	82
4.4.2	Flight Profiles.	82
4.4.3	Tethersonde Data	82
4.4.4	Isopleths and Selected Traverses	89
4.4.5	Plume Geometry	89
4.4.6	Turbulence Levels Related to Plume Structure.	98
5.	DISCUSSION OF THE CASE STUDY RESULTS.	103
5.1	A Comparison of Plume Geometry with the Pasquill-Gifford Curves	103
5.1.1	A Discussion of the Pasquill-Gifford Curves	103
5.1.2	Comparison of the Observed Plume Geometry with the Pasquill-Gifford Curves	106
5.2	The Effects of Topography on Dispersion of the GCOS Plume.	112
5.2.1	Enhanced σ_y Values	112

TABLE OF CONTENTS (CONCLUDED)

		Page
5.2.2	Local Effects	112
5.2.3	Ground Cover Variations Versus Topography	113
5.3	Summary of Plume Rise Data	114
5.4	Relationships Between Plume Sigma Values and Turbulence Parameters	114
5.4.1	Statistical Theory of Dispersion	114
5.4.2	A Brief Outline of Lagrangian and Eulerian Measurements	118
5.4.3	Normalized Plume Spread	119
6.	CONCLUSIONS	130
7.	REFERENCES CITED	133
8.	APPENDICES	136
8.1	Emission Characteristics from GCOS Plant	136
8.2	The Appropriate Gaussian Equation for Normalized Axial Centre-Line Concentration	136
8.3	Additional Details of SO_2 Concentrations and Turbulence Statistics for the Flight of 19 June 1977 (0745-1010 MDT)	139
8.4	Additional Details of SO_2 Concentrations and Turbulence Statistics for the Flight of 19 June 1977 (1335-1735 MDT)	151
8.5	Additional Details of SO_2 Concentrations and Turbulence Statistics for the Flight of 20 June 1977 (1000-1500 MDT)	167
8.6	Additional Details of SO_2 Concentrations and Turbulence Statistics for the Flight of 22 June 1977 (1915-2305 MDT)	186
8.7	List of Symbols	203
8.8	Recommendations for Future Aerial Programs	204
8.8.1	Position Recovery	204
8.8.2	Stationarity Problems	204
8.8.3	Aircraft Operational Base	204
8.8.4	Types of Aircraft Measurements Desired	205
8.8.5	Subsequent Data Analyses and Field Trips	205
9.	LIST OF AOSERP RESEARCH REPORTS	206

LIST OF TABLES

Page

1. Run Information for the Flight of 19 June 1977 (0745-1010 MDT) 27
2. Plume Geometry, Mass Flux, and Plume Rise for the Flight of 19 June 1977 (0745-1010 MDT) 35
3. Summary of Turbulence Data for Groups of Runs from the Flight of 19 June 1977 (0745-1010 MDT) 41
4. Run Information for the Flight of 19 June 1977 (1335-1735 MDT) 47
5. Plume Geometry, Mass Flux, and Plume Rise for the Flight of 19 June 1977 (1335-1735 MDT) 54
6. Turbulence Statistics from Each Run for the Flight of 19 June 1977 (1335-1735 MDT) 60
7. Summary of Turbulence Data for the Flight of 19 June 1977 (1335-1735 MDT) 62
8. Run Information for the Flight of 20 June 1977 (1000-1500 MDT) 68
9. Plume Geometry, Mass Flux, and Plume Rise for the Flight of 20 June 1977 (1000-1500 MDT) 75
10. Summary of Turbulence Statistics for the Flight of 20 June 1977 (1000-1500 MDT) 81
11. Run Information for the Flight of 22 June 1977 (1915-2305 MDT) 87
12. Plume Geometry, Mass Flux, and Plume Rise for the Flight of 22 June 1977 (1915-2305 MDT) 94
13. Summary of Turbulence Statistics for the Flight of 22 June 1977 (1915-2305 MDT) 100
14. Stability Classifications According to Slade (1968) 104
15. Stability Classificaitons According to Pasquill (1961) . . 105
16. Summary of the Adopted Stability Classifications for all of the June 1977 Case Studies 107
17. Summary of Input Data Used for the Calculation of Normalized Plume Spread 120

LIST OF TABLES (CONCLUDED)

Page

18. Summary of Normalized Plume Spread 121

19. Comparison of Integral Time Scales to Estimates from Normalized Plume Spreads 128

20. Comparison of the Observed Effective Stack Heights With the Observed σ_z Values 138

21. Run Information from the Flight of 19 June 1977 (0745-1010 MDT) 140

22. Turbulence Statistics from Each Run for the Flight of 19 June 1977 (0745-1010 MDT) 141

23. Run Information for the Flight of 19 June 1977 (1335-1735 MDT) 152

24. Turbulence Statistics from Each Run for the Flight of 19 June 1977 (1335-1735 MDT) 153

25. Run Information for the Flight of 20 June 1977 (1000-1500 MDT) 168

26. Turbulence Statistics from Each Run for the Flight of (1000-1500 MDT) 169

27. Run Information for the Flight of 22 June 1977 (1915-2305 MDT) 187

28. Turbulence Statistics from Each Run for the Flight of 22 June 1977 (1915-2305 MDT) 188

LIST OF FIGURES

Page

1. Sign-X SO_2 Analyzer Flow Diagram 5
2. Flow Chart of Airborne Data Recovery System 8
3. Selected Photos for the Flight of 19 June 1977 (0745-1010 MDT) 25
4. Flight Profiles for the Flight of 19 June 1977 (0745-1010 MDT) 26
5. Tethersonde Profiles for 19 June 1977 (0723-0948 MDT) . . . 28
6. SO_2 Concentration Isopleths of 19 June 1977 (0745-1010 MDT) 31
7. Normalized SO_2 Concentrations for Run 1 on the Flight of 19 June 1977 (0745-1010 MDT) 32
8. Normalized SO_2 Concentrations for Run 2 on the Flight of 19 June 1977 (0745-1010 MDT) 33
9. Maximum SO_2 Concentrations Along Each Traverse as a Function of Altitude for the Flight of 19 June 1977 (0745-1010 MDT).. 36
10. Observed Horizontal Dispersion Coefficients Compared to Pasquill-Gifford Curves for the Flight of 19 June 1977 (0745-1010 MDT) 37
11. Observed Vertical Dispersion Coefficient Compared to Pasquill-Gifford Curves for the Flight of 19 June 1977 (0745-1010 MDT) 38
12. Comparison of Observed Normalized Centerline Concentrations with Pasquill-Gifford Predictions for the Flight of 19 June 1977 (0745-1010 MDT) 39
13. Turbulence Data for the Flight of 19 June 1977 (0745-1010 MDT) 42
14. Spectral Plots for the Flight of 19 June 1977 (0745-1010 MDT) 43
15. Selected Photos for the Flight of 19 June 1977 (0745-1010 MDT) 45

LIST OF FIGURES (CONTINUED)

Page

16. Flight Profiles for the Flight of 19 June 1977 (1335-1735 MDT) 46

17. Normalized SO_2 Concentrations for Run 15 on the Flight of 19 June 1977 (1335-1735 MDT) 49

18. Normalized SO_2 Concentrations for Run 16 on the Flight of 19 June 1977 (1335-1735 MDT) 50

19. Maximum SO_2 Concentrations Along Each Traverse as a Function of Altitude for the Flight of 19 June 1977 (1335-1735 MDT) 51

20. Integrated Concentrations Along Each Traverse for the Flight of 19 June 1977 (1335-1735 MDT) 52

21. Observed Horizontal Dispersion Coefficients Compared to Pasquill-Gifford Curves for the Flight of 19 June 1977 (1335-1735 MDT) 55

22. Observed Vertical Dispersion Coefficients Compared to Pasquill-Gifford Curves for the Flight of 19 June 1977 (1335-1735 MDT) 56

23. Comparison of Observed Normalized Centerline Concentrations with Pasquill-Gifford Predictions for the Flight of 19 June 1977 (1335-1735 MDT) 57

24. Turbulence Data for the Flight of 19 June 1977 (1335-1735 MDT) 59

25. Spectral Plots for the Flight of 19 June 1977 (1335-1735 MDT) 64

26. Plume Photographs for the Flight of 20 June 1977 (1000-1500 MDT) 66

27. Flight Profiles for the Flight of 20 June 1977 (1000-1500 MDT) 67

28. Tethersonde Profiles for 20 June 1977 (1248 MDT) 69

29. SO_2 Concentration Isopleths for the Flight of 20 June 1977 (1000-1500 MDT) 70

30. Normalized SO_2 Concentrations for Run 2 on the Flight of 20 June 1977 (1000-1500 MDT) 72

LIST OF FIGURES (CONTINUED)

Page

31. Normalized SO_2 Concentrations for Run 1 on the Flight of 20 June 1977 (1000-1500 MDT) 73

32. Maximum SO_2 Concentrations Along Each Traverse as a Function of Altitude for the Flight of 20 June 1977 (1000-1500 MDT) 74

33. Observed Horizontal Dispersion Coefficients Compared to Pasquill-Gifford Curves for the Flight of 20 June 1977 (1000-1500 MDT) 76

34. Observed Vertical Dispersion Coefficient Compared to Pasquill-Gifford Curves for the Flight of 20 June 1977 (1000-1500 MDT) 77

35. Comparison of Observed Normalized Centerline Concentrations with Pasquill-Gifford Predictions for the Flight of 20 June 1977 (1000-1500 MDT) 78

36. Turbulence Data for the Flight of 20 June 1977 (1000-1500 MDT) 80

37. Spectral Plots for the Flight of 20 June 1977 (1000-1500 MDT) 83

38. Selected Photos for the Flight of 22 June 1977 (1915-2305 MDT) 84

39. Flight Profiles for the Flight of 22 June 1977 (1915-2305 MDT) 86

40. Tethersonde Profiles for 22 June 1977 (1950 MDT) 88

41. SO_2 Concentration Isopleths for the Flight of 22 June 1977 (1915-2305 MDT) 90

42. Normalized SO_2 Concentrations for Run 16 on the Flight of 22 June 1977 (1915-2305 MDT) 91

43. Normalized SO_2 Concentrations for Run 14 on the Flight of 22 June 1977 (1915-2305 MDT) 92

44. Maximum SO_2 Concentrations Along Each Traverse as a Function of Altitude for the Flight of 22 June 1977 (1915-2305 MDT) 93

45. Observed Horizontal Dispersion Coefficients Compared to Pasquill-Gifford Curves for the Flight of 22 June 1977 (1915-2305 MDT) 95

LIST OF FIGURES (CONTINUED)

Page

46. Observed Vertical Dispersion Coefficients Compared to Pasquill-Gifford Curves for the Flight of 22 June 1977 (1915-2305 MDT) 96

47. Comparison of Observed Normalized Centerline Concentrations with Pasquill-Gifford Predictions for the Flight of 22 June 1977 (1915-2305 MDT) 97

48. Turbulence Data for the Flight of 22 June 1977 (1915-2305 MDT) 99

49. Spectral Plots for the Flight of 22 June 1977 (1915-2305 MDT) 102

50. Horizontal Dispersion Coefficient as a Function of Downwind Distance from the Source as Compared with Pasquill-Gifford Values for 1977 Flights 108

51. Vertical Dispersion Coefficient as a Function of Downwind Distance from the Source as Compared with Pasquill-Gifford Values for 1977 Flights 109

52. Observed Normalized Centerline Concentrations Compared with Pasquill-Gifford Values for 1977 Flights 110

53. Summary of Ratios of Calculated to Observed Effective Stack Heights for 1977 Flights 115

54. Normalized Vertical Plume Spread According to the Pasquill-Draxler Approach of Equation (5) 122

55. Normalized Vertical Plume Spread According to the Long Dispersion Time Predictions of Taylor's Statistical Theory. 123

56. Normalized Lateral Plume Spread According to the Pasquill-Draxler Approach of Equation (5) 124

57. Normalized Vertical Plume Spread According to the Long Dispersion Time Predictions of Taylor's Statistical Theory. 125

58. Run 1, 19 June 1977 142

59. Run 2, 19 June 1977 143

60. Run 5, 19 June 1977 144

LIST OF FIGURES (CONTINUED)

Page

61. Run 6, 19 June 1977 145
62. Run 7, 19 June 1977 146
63. Run 8, 19 June 1977 147
64. Run 9, 19 June 1977 148
65. Run 10, 19 June 1977 149
66. Run 11, 19 June 1977 150
67. Run 1, 19 June 1977 155
68. Run 2, 19 June 1977 156
69. Run 3, 19 June 1977 157
70. Run 4, 19 June 1977 158
71. Run 7, 19 June 1977 159
72. Run 8, 19 June 1977 160
73. Run 9, 19 June 1977 161
74. Run 11, 19 June 1977 162
75. Run 12, 19 June 1977 163
76. Run 13, 19 June 1977 164
77. Run 15, 19 June 1977 165
78. Run 16, 19 June 1977 166
79. Run 1, 20 June 1977 171
80. Run 2, 20 June 1977 172
81. Run 5, 20 June 1977 173
82. Run 6, 20 June 1977 174
83. Run 8, 20 June 1977 175
84. Run 9, 20 June 1977 176

LIST OF FIGURES (CONCLUDED)

Page

85. Run 10, 20 June 1977 177
86. Run 11, 20 June 1977 178
87. Run 12, 20 June 1977 179
88. Run 13, 20 June 1977 180
89. Run 14, 20 June 1977 181
90. Run 15, 20 June 1977 182
91. Run 16, 20 June 1977 183
92. Run 17, 20 June 1977 184
93. Run 18, 20 June 1977 185
94. Run 4, 22 June 1977 190
95. Run 5, 22 June 1977 191
96. Run 6, 22 June 1977 192
97. Run 8, 22 June 1977 193
98. Run 10, 22 June 1977 194
99. Run 12, 22 June 1977 195
100. Run 14, 22 June 1977 196
101. Run 15, 22 June 1977 197
102. Run 16, 22 June 1977 198
103. Run 17, 22 June 1977 199
104. Run 18, 22 June 1977 200
105. Run 20, 22 June 1977 201
106. Run 22, 22 June 1977 202

ABSTRACT

During June 1977, a plume survey field program was conducted about the Great Canadian Oil Sands (GCOS) site to determine the plume geometry and associated turbulent parameters. Airborne measurements were conducted by INTERA's research aircraft under various meteorological conditions co-ordinated with the June inter-agency field program.

Four flights were selected for detailed analysis of plume geometry and turbulence characteristics. Analysis of the SO_2 data included plume sigma and observed plume rise computation by several techniques, mass flux, and SO_2 concentration isopleth analyses. Turbulence analyses included derivation of the environmental gust velocities and their time-domain statistics, autocorrelation analysis for integral scales, second-order structure function analysis for dissipation estimates, and spectral analysis.

The turbulence data were applied to the statistical theory for lateral dispersion and gave remarkably good agreement except for the flight of 19 June. The vertical plume spread was not predicted well by the statistical theory. It was concluded that changes in integral scales, initial plume-induced turbulent mixing, and changes in stability with weight need to be simulated for reasonably accurate dispersion formulations.

ACKNOWLEDGEMENTS

This research project ME 2.3.2 was funded by the Alberta Oil Sands Environmental Research Program, a joint Alberta-Canada research program established to fund, direct, and co-ordinate environmental research in the Athabasca Oil Sands area of north-eastern Alberta.

1. INTRODUCTION

In June 1977, INTERA entered into a contract with the Alberta Oil Sands Environmental Research Program (AOSERP) to determine the behaviour and geometry of plumes from existing sources by means of aerial measurements.

This final report is submitted to AOSERP management as part of the terms of the contract. This report presents a review of the terms of references of the contract, a description of the equipment and methodologies used in the field and for data analysis, case study analyses, and discussion of the overall results of the study. Recommendations for improvements in future aerial programs are presented under separate cover.

1.1 TERMS OF REFERENCE

The terms of reference of this study, as defined in the contract, are presented below:

1. Design an aerial sampling scheme that will allow the determination of statistically reliable values of plume width and depth, plume height above ground, plume trajectory from source, plume cross-sectional areas, the three-dimensional concentration field, the SO_2 flux, atmospheric turbulence levels.
2. Using suitable instruments and aircraft, conduct plume surveys from the Great Canadian Oil Sands (GCOS) Power Plant source during the time of an intensive inter-agency field study in June-July 1977, under the direction of the Meteorology and Air Quality Research Manager. Instrumentation that should be considered includes a three-dimensional turbulence measurement package, a fast-response SO_2 continuous concentration monitor, data tape storage systems, position recovery system, and an air-to-ground communication system to be used with the Atmospheric Environment Service tethersonde operation.

3. Ascertain the degree to which the data deviate from the Gaussian distributions assumed in simple plume dispersion models and compare this deviation to that obtained in the reports of the March 1976 field study (Davison et al. 1977).
4. Derive the standard deviations of the horizontal and vertical distributions as a function of distance.
5. Compare the derived values with those given by Pasquill-Gifford.
6. Relate the derived standard deviation values to the measured levels of atmospheric turbulence, with suitable stability and height scaling parameters.
7. Determine the trajectory of the plume axis and the effects of topography upon that trajectory. Compare these results with those reported in the March 1976 study.
8. Compare the observed plume rise with the predicted by the more popular theoretical/empirical models, such as those of Briggs.
9. Calculate the SO_2 flux at various downwind distances and do a mass balance.
10. Present the average three-dimensional concentration fields in a pictorial and tabular form.
11. Determine a spectral analysis of turbulence data and perform those analyses that could relate turbulence to plume dispersion by considering the measurements of wind component standard deviations, plume sigma values, and the integral time scales as functions of height.
12. Under separate cover, make recommendations for improvements in aerial programs to be followed in future field studies.

2. EQUIPMENT

The specific objectives of this study required the accurate determination and recording of various meteorological state parameters, atmospheric turbulence data, and effluent SO_2 plume characteristics. The sensing and recording platforms for this field study were mounted on a light twin-engine aircraft, a Cessna 411. The five-seat passenger configuration was modified considerably to accommodate two standard 19 in. instrument racks and a technician's station. These racks housed the sensing and recording control units and the primary power distribution panel. The basic instrumentation system was similar to that used for the plume dispersion measurements of March 1976 made under contract ME 2.3.1 as outlined in AOSERP Report 13 (Davison et al. 1977).

An external sampling panel served the dual role of aircraft escape hatch and instrument mounting panel, which facilitated the installation of numerous instrument mounts without having to cut additional holes in the skin of the aircraft. The panel supported the isokinetic intake probes for the Sign-X SO_2 Analyzer and the E.G. & G. Dew Point Hygrometer.

The turbulence probe was mounted through the nose of the aircraft, parallel to the longitudinal axis. This probe consisted of isolated pitot and static pressure sources and two vanes. The vanes were orthogonally mounted pitch and yaw vanes. A sliding instrument tray was installed in the port nose compartment to house the pressure transducers and power distribution panel for the probe system.

2.1 AIR CHEMISTRY PACKAGE

The effective measurement of an effluent plume structure by an airborne platform requires sensitive, accurate, and rapidly responding samplers that are relatively easy to operate in the air. The accuracy and sensitivity requirements are common to any sampling device. However, the response characteristics become more critical in an aircraft that is normally operated at 60 m/sec (120 kn).

The air chemistry instrumentation used for the SO_2 measurements was the Sign-X SO_2 Analyzer. The Sign-X SO_2 Analyzer continuously measures the electro-conductivity of a sample of deionized water that dissolves all incoming SO_2 gases. Once the conductivity of this sample is measured, the SO_2 solution is converted back to deionized water, which is then recycled through the flow system. From manufacturer's specifications, the threshold sensitivity of the analyzer is 0.01 ppm, and the SO_2 readings have an accuracy of $\pm$ 5% of the calibrated range. The e-folding time constant for the readings is 2.5 sec, which is adequate for aerial sampling. The operation of this analyzer is shown schematically in Figure 1. In practice, the sensor had non-symmetric response characteristics, which are discussed in the analysis methodology section.

During the field study, the output signal from the Sign-X was monitored on an MFE chart record as well as digitized and recorded with all the other sensor outputs. The visual display of SO_2 concentration was used extensively by the on-board meteorologist to determine appropriate plume traverse heights. The Sign-X system was laboratory-calibrated before and after the field program.

2.2 AIRBORNE TURBULENCE PACKAGE

The measurement of turbulence is important in an assessment of plume diffusion by turbulent mixing. It is possible to measure the total amount of turbulent energy simply by measuring dissipation through the measurement of band-limited high-frequency pitot pressures. However, this technique of measuring turbulence levels is not advantageous if a careful study of plume dispersion is desired. To relate observed plume geometry to the turbulent mixing mechanisms, it is important to know how the turbulent energy is distributed at the larger size scales that dominate the mixing process. In addition, terrain-induced vertical mixing is difficult to document using dissipation measurements only. In most recent attempts to correlate plume sigma values to turbulence, for example, Draxler (1976) and Pasquill (1976), the turbulent parameters required are the standard

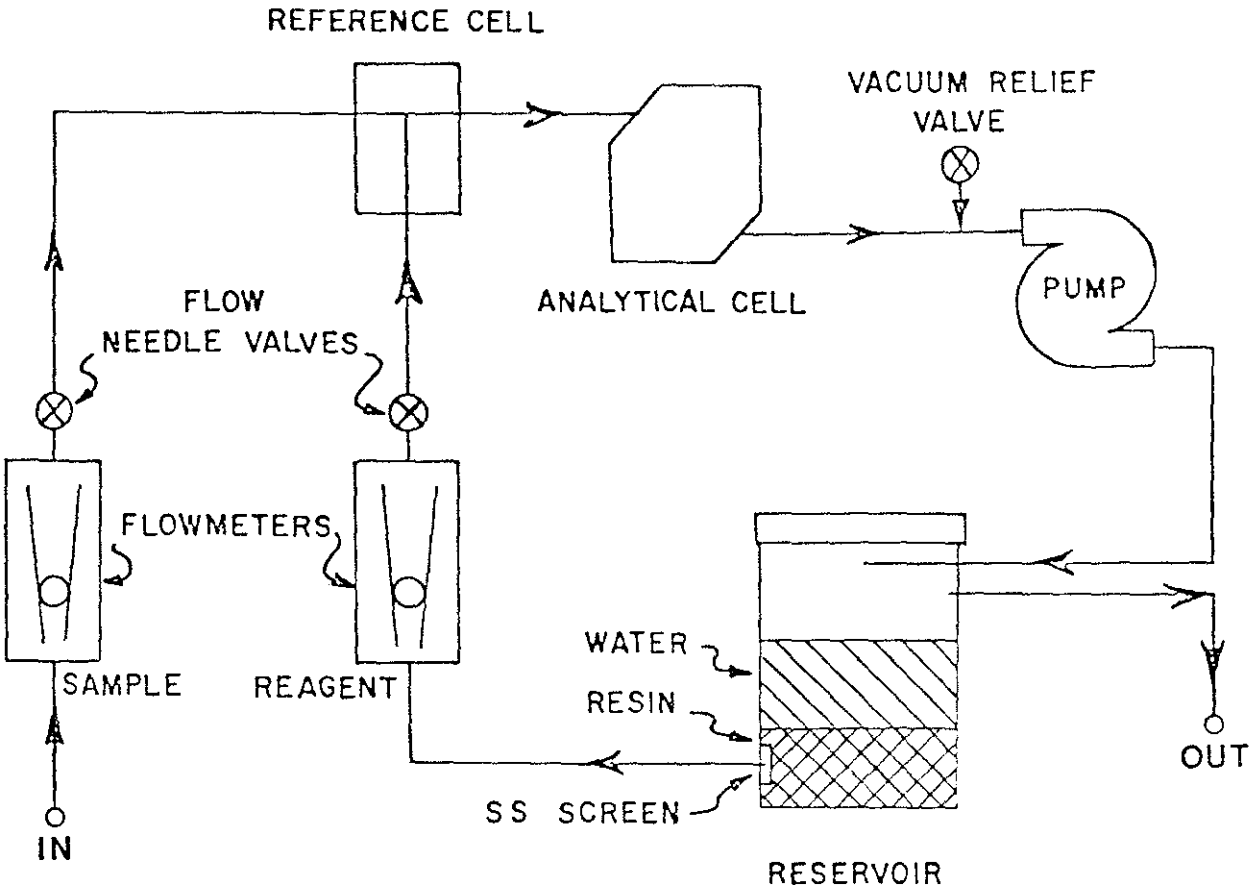

Figure 1. Sign-X SO_2 analyzer flow diagram.

deviations of the turbulent velocities and the integral scales. These parameters can be determined only by a system capable of resolving the gust velocities.

The turbulence system in INTERA's research aircraft can resolve these gust velocities so that that statistics for the horizontal and vertical components of turbulence can be examined separately. Direct measurement of stability as a function of height can be made using ratios of mechanical and thermal fluxes.

Measurement of the gust velocities is accomplished by measuring the wind with respect to the aircraft and the motion of the aircraft with respect to an inertial frame of reference. By removal of aircraft motion effects in digital analysis, the true environmental gust velocities can be estimated. This basic approach has been used successfully by many groups in the past decade to study atmospheric turbulence, for example, Mather (1967), Myrup (1967), Lenschow (1970), Donelan and Miyake (1973), Davison (1973), etc.

Aircraft motion was sensed by a system of accelerometers and gyroscopes. The rates of aircraft pitch, roll, and yaw were measured by three mutually orthogonal miniature gyroscopes aligned to the three axes of the aircraft. A three-axis accelerometer was used to measure motions in the x, y, and z directions. The gyros and accelerometers, which together measured all six possible modes of motion, were mounted on a platform close to the aircraft centre of gravity.

Pitch and yaw vanes were mounted on an instrument probe extended through the nose of the aircraft. The shaft from each vane drove a miniature autosyn motor, which related a vane deflection to a phase shift of the induced 400 Hz singal. The output signal was fed to a demodulator unit that produced a DC voltage according to the amount of phase shift between the vane-controlled 400 Hz signal and a reference 400 Hz signal.

Accurate static and dynamic pressures are required for the gust calculations. As mentioned above, the static and dynamic ports were mounted on the nose probe, outside the influence of the aircraft itself. Pressure lines from the ports were directed to transducers located at the base of the probe.

Temperature was measured using a Rosemount Model 102424 Total Temperature Probe (a fast-response platinum resistance element mounted under the port wing). The E.G. & G. Dew Point Hygrometer, also a fast-response system, was mounted on the instrument panel. After compensation for the effects of dynamic heating, absolute accuracies from these sensors are of the order of $\pm$ 0.5°C, with relative accuracies close to $\pm$ 0.1°C.

2.3 AIRBORNE DATA ACQUISITION SYSTEM

The analog signals from the various sensors were directed to the data acquisition system for subsequent recording. This system consisted of the Signal Conditioning Unit (SCU), the Monitor Labs 9400 Data Logger, and the Cipher Incremental Tape Drive. Figure 2 shows a schematic diagram of the Data Acquisition System.

The SCU included a bank of low pass filters designed to eliminate any significant aliasing effects on the incoming signal. In front of the filters was a bank of amplifiers to provide good dynamic range. After passing through the SCU, the signals were fed into the Monitor Labs 9400 Data Logger for digitization and formatting. The digital sampling period for an entire cross-channel sequence plus time and the positions of 10 sense switches was 0.5 sec.

The digitized, formatted channel sequence was then directed to the Cipher Incremental Tape Drive. This tape drive produced a 9-track, 800 bpi, computer-compatible tape in EBCDIC format for post-flight computer processing.

An analog trace of the signal from the Sign-X SO_2 Monitor was recorded on an MFE chart recorder. This signal was very helpful for deciding upon the appropriate plume traverse altitudes.

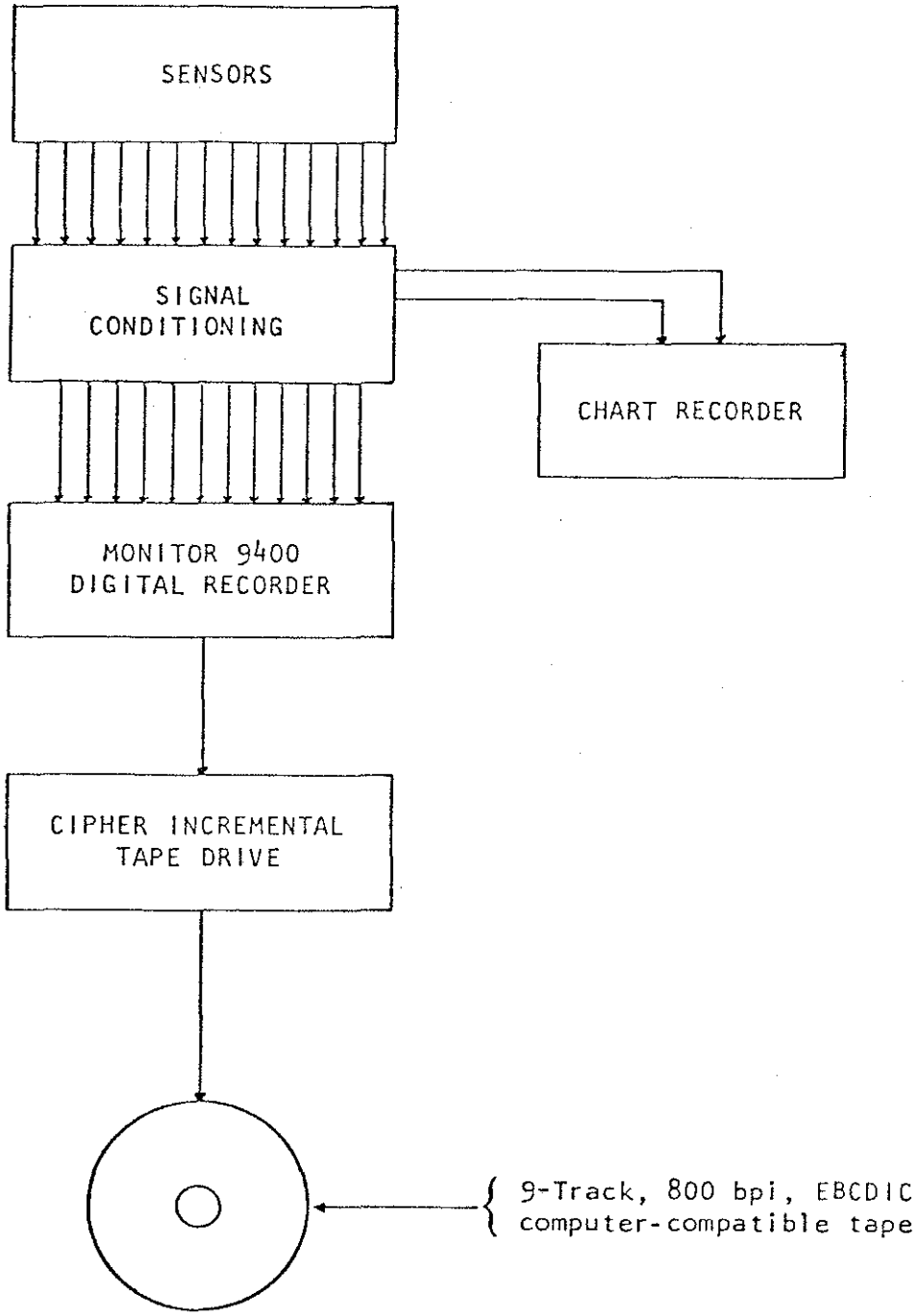

Figure 2. Flow chart of airborne data recovery system.

2.4 POSITION RECOVERY

The primary position recovery system was an ONTRAC III VLF Omega Navigation System. This system is a global navigation system that works on the principle of phase comparisons of signals from a series of transmitting stations around the world. When the system was functioning properly and was receiving more than four stations, position recovery for flight track selection was at least as good as the best visual checks could determine. Further details of the procedure used for setting up flight lines is presented in the section on field procedures in the next chapter.

3. FIELD PROCEDURES AND ANALYSIS METHODOLOGIES

The purpose of this chapter is to document the field and analysis techniques employed in this study in sufficient detail to enable meaningful comparisons with data from other sources. In addition, various procedures adopted in this study may be helpful in subsequent ones.

3.1 FIELD PROCEDURES

3.1.1 Selection of Flight Times

Due to the limitation on total flight hours (35 h for the study), a careful selection of flight times was made to optimize the data base. There were two criteria for flight time selection. First, there was a need to capture a variety of meteorological conditions that would be representative of early summer. Secondly, the flights needed to be co-ordinated with the activities of the other researchers in the field at the same time, and in particular with the tethered balloon operation. The aircraft was based at Fort McMurray Airport for aircraft servicing convenience. However, the AOSERP Mildred Lake Research Facility was visited several times using the local gravel airstrip. Detailed discussions in the field did not prove to be necessary; operating from Fort McMurray rather than Mildred Lake was more convenient.

3.1.2 Flight Track Set-Up

Upon approaching the GCOS site at the beginning of a flight, we carefully noted the bearing of the visual plume. The VLF navigation system was calibrated using the known position of the GCOS main stack as a reference position. A standard flight pattern was chosen with cross-wind traverses at 3.2 km and 8 km downwind from the stack. The waypoints defining the start and end of the traverses were entered as polar co-ordinates into the VLF navigation system computer. In this way, day-to-day changes in the bearing of the plume centerline resulted in one systematic change in all the angular inputs without any changes in the radial inputs. Thus,

the standard shape of the flight tracks was rotated about the stack depending upon plume bearing. Once the four way points defining the start and end points of the traverses at the two downwind distances were entered into the computer by the pilot, plume traverses could begin.

The downwind distances, 3.2 km and 8.0 km, were chosen to satisfy a number of constraints. An airborne traverse of a plume is a measure of relative dispersion about the centerline of the plume. The only way to obtain a direct measure of the time-averaged dispersion would be to make many traverses at the same height, combined with a very accurate positioning system. The procedure adopted here was to choose a downwind distance great enough so that relative dispersion was reasonably similar to time-averaged dispersion following criteria discussed by Pasquill (1974, Chapter 3). Another consideration was that the visual "lumpiness" of a plume usually disappeared by about 2 km downwind, indicating that sufficient downwind dispersion has taken place to enhance the repeatability of concentrations observed on plume traverses. The need to keep a good signal-to-noise ratio in the SO_2 sensor limited the further downwind distance. The adopted downwind distances appeared to be a reasonable compromise on the above constraints.

3.1.3 Plume Traverses

The concentration field associated with the GCOS plume was examined by a series of vertically stacked traverses at the two standard downwind distances. The flight altitudes were staggered so that any significant lack of stationarity would be detected as such and not as a height variation.

A racetrack pattern was adopted, partly for flight convenience but also as a stationarity check for the two downwind distances. The plume traverses were all 16 km long. This length was normally larger than necessary to capture the plume, but enabled more meaningful turbulence statistics to be measured during the plume traverses.

Occasionally, repeatability checks were made by repeated runs at the same altitude and the same downwind distance.

The height range that was flown was determined during the flights by the on-board meteorologist based upon ambient conditions.

3.1.4 Turbulence Runs

In addition to the crosswind plume traverses at the standard downwind distances, runs were often made parallel to the plume centerline to collect turbulence statistics. These statistics permitted a check on the degree of equivalence of the turbulence statistics of the lateral and longitudinal wind components, and an estimate on the magnitude of spatial variability of the turbulence statistics near plume centerline.

3.2 CRITERIA FOR THE SELECTION OF CASE STUDIES

There were two major criteria for the selection of the case studies. The first was relatively stationary meteorological conditions. The second was completeness of the profiles.

By the nature of the data collection procedures, stationary conditions were required. In order for us to determine concentration isopleths, mass flux, and plume geometry, all the traverses had to be assumed to be describing the same plume.

On some days, the data collected on a single flight had to be treated as two cases due to a significant change in stability during the flight.

In order to have a reasonably accurate estimate of the plume geometry, several traverses of the plume were necessary. Thus, cases in which there was obvious lack of stationarity before a fairly complete set of traverses was flown were not considered for detailed analysis.

3.3 DATA ANALYSIS METHODOLOGY

3.3.1 SO_2 Concentrations Along Flight Traverses

The data from the Sign-X sensor were converted into SO_2 concentrations in units of parts per million after digital processing to remove a floating baseline and reduce noise. The response characteristics of the Sign-X system were not symmetric: an increase in SO_2 concentration resulted in a different response curve than a decrease. After high concentrations were measured, the system sometimes exhibited a fall-off that did not return to the original baseline. In addition, there was a gradually increasing DC offset in the system throughout the 4 h of a typical flight.

A digital procedure was developed to automatically remove the floating baseline on the signal. On a given plume traverse, the average value along the entire traverse was removed from the signal producing negative and positive values. The average of the negative values was adopted as the baseline. Detailed comparisons with all types of plume sectionings indicated that this simple procedure produced a baseline that was virtually the same as the best eye-fitted estimate.

A noise limiter was introduced to set to zero any remaining concentration value less than about 0.01 ppm, which is the manufacturer's minimum sensitivity specification. The combined effects of the baseline removal and noise limiter proved to be generally satisfactory error recovery procedures.

The response delay of the Sign-X system after high concentrations proved to be a more difficult problem. The amount of apparent signal contamination did not reliably scale with concentration or with time. There were instances of high concentrations in narrow plumes that showed very little fall-off delay. The effect was probably not due to incomplete deionizing of the water in the Sign-X, because the flow rates and the reservoir size would indicate a much longer time constant for recirculation than the observed time constarts. It may possibly to due to adsorption of SO_2 onto the intake tubing walls, which would be a function of humidity, temperature,

particulate concentrations, etc. It was decided that adoption of any response correction function for this fall-off effect could lead to contamination of some apparently good data, and so no overall response correction function was used.

The nominal time constant of the Sign-X was 2.5 sec for the e-folding time. A typical plume traverse gave a standard deviation of 500 to 1000 m, corresponding to a time of about 40 to 80 sec for the traverse of 95% of the plume concentration. Thus, the normal time constant of the sensor did not represent a significant source of error.

A question may arise as to the sampling time of the measurements. As mentioned above, on a single traverse any airborne measuring system measures effectively instantaneous relative dispersion, not time-averaged dispersion. The speed of the traverse is not important; a slower traverse would mean a greater scatter in the population of repeated traverses, but would not improve an individual traverse, except for better sensor response. Sampling or averaging time is of concern in defining what time-average statistics are being used for comparison with the measurements of relative dispersion. The procedure adopted in this report was to present the measured plume geometry, with the recognition that these are measures of relative dispersion. The difference between relative and time-averaged dispersion will probably be small at the downwind distances flown. A detailed comparison will be possible from the ground-based COSPEC measurements being undertaken concurrently by the Atmospheric Environment Service (AES). From COSPEC measurements discussed by Millan (in Fanaki 1978) from the March 1976 field study, the differences between relative and time-averaged ($\simeq$30 min) plume spread (Millan's "Eulerian" and "pseudo-Lagrangian", respectively) at a downwind distance of 3.6 km were less than 5%. However, users of AOSERP data in subsequent projects will need to be aware that plume spread measurements obtained from traverses by airplanes, helicopters, or vehicles (COSPEC) are of relative dispersion. A more detailed discussion of this problem and a comparison of the various sensor systems' characteristics are part of another story.

3.3.2 Plume Geometry Calculations

The plume geometry was calculated from the concentration data along the plume traverses. In addition, visual notes by the on-board meteorologist and photography of the plume provided additional data, particularly as to whether there appeared to be fumigation to the ground.

There were three techniques used to estimate the plume centerline height. First, the height of the maximum concentration observed was noted. Secondly, from a plot of maximum concentrations versus height, the height of the center of mass was calculated. Visual notes and photography were used to estimate how to sketch in the near-ground profile. A sensitivity check showed that in most cases reasonable changes in the extrapolated concentration estimates did not affect the result significantly. The third technique was similar to the second except that the integrated concentrations along the traverse, rather than the maximum concentration values, were used.

Usually, the three plume height estimates agreed closely, but under certain conditions differences might be expected. If there was a strong capping inversion, then the maximum observed concentration might be higher than the center of mass of the maximum concentration profile. In the same situation, there might be enhanced dispersion at lower levels, which would reduce the concentrations observed there but which might still yield larger values of the integrated concentrations across the entire plume traverse. Although the incinerator stack had only about 10% of the output of the powerhouse stack, its lower plume rise would tend to lower the height of the center of mass.

All three estimates of plume centerline height were included in the summary statistics for each case study, so comparisons with the plume rise theories should be more meaningful.

On each traverse the lateral plume spread coefficient (σ_y) was estimated in two ways. A criterion based upon the area under the SO_2 concentration wave was adopted, as in the March 1976 study.

For a Gaussian distribution, minus and plus one standard deviation occur at distances such that the accumulated fractions of the total area under the curve are 0.159 and 0.841 respectively. The σ_y values were computed using the same area criteria. This procedure meant that the observed concentrations were being compared with a Gaussian distribution of the same area.

The second procedure for calculation of σ_y was the standard second moment technique. The σ_y values were computed for the first and second half of the concentration distribution to note any asymmetry in the profile. The average σ_y value from the area technique was used to normalize the concentration distribution for comparison with a Gaussian profile. All the traverses are presented in Appendices 8.3 to 8.6 of this report; selected traverses are presented in the case study discussions. The value of the centerline σ_y was estimated from traverses near the computed centerline height. For each case study, several traverses were used to improve the statistical reliability of the estimate if the data were available.

The vertical plume spread coefficient (σ_z) was estimated from the plot of the maximum concentration profile using the area technique. The upper, lower, and average σ_z values were presented for each case study.

The mass flux was computed by integrating the integrated concentration profile using a weighting function of the wind speed, estimated from the tethersonde wind profiles. The tethersonde data were measured and analyzed by R. Mickle of AES in Downsview.

3.3.3 Plume Rise Predictions

The observed plume centerline heights were compared to three plume rise prediction schemes: Briggs (1975), TVA (Montgomery et al. (1972) and Holland (U.S.W.B. 1953). Detailed discussions of these models have been presented previously, e.g., by Briggs (1969, 1975), and will not be repeated here.

For each case analyzed, emission data provided by GCOS were reduced to generate average stack exit temperature and flow rate. The stack characteristics are summarized in Appendix 8.1. Ambient temperature, wind speed, and temperature gradient were abstracted from the tethered balloon data collected by AES. Often there was more than one set of data over the plume survey period; they were averaged for the layer of the atmosphere between stack top and observed plume height. The tethersonde data upon which these plume rise calculations depended are presented in each study.

3.3.4 Turbulence Analysis Methodology

The turbulence data from all runs (both plume traverses and turbulence runs) were analyzed in blocks of 130 samples (65 sec). This time period was short enough to avoid drift problems in the gyroscopes. The statistics from many blocks were averaged after initial turbulence analysis, the groupings representing similar temporal and spatial characteristics of the turbulent field. Selection of groups of blocks for spectral analysis was made based upon temporal and spatial differences in the turbulence statistics and upon significance of the statistics at a given height for the plume dispersion on that particular day.

The blocks of 65 sec corresponded to a physical length scale of about 4.3 km for typical aircraft true air speeds. If a typical wind speed was, say 6 m/sec, then the physical length scale corresponded to an Eulerian averaging time of about 700 sec. Thus, the aircraft turbulence statistics were comparable to the tethersonde statistics (10 min averages) and were consistent with the length scales that could be expected to operate on the effluent plume at the downwind distances flown (3.2 and 8.0 km).

3.3.4.1 Generation of the turbulent gust velocities and system limitations. The turbulence system measures the wind with respect to a moving platform (the aircraft) whose motion is measured. Hence, it is possible to resolve the environmental gust velocities by computer reduction of the data. The same basic technique has

been used by several groups around the world to obtain turbulence data and is well accepted in the meteorological literature; see, for example, McBean and MacPherson (1976) or Donelan and Miyake (1973).

It is interesting to note that, since the air speed of the aircraft (about 66 m/sec) was typically 10 to 20 times faster than the wind speed, a 1 min aircraft data segment was equivalent to a 10 or 20 min ground-based observation. Even so, there were major averaging problems due to the inherent increase in intermittency of turbulence with increasing height, so many data blocks were usually required for a statistically reliable averaged turbulence value; in other words, the standard deviation of the population of similar means was small compared to the value itself.

There was a problem with inadequate pitot response characteristics. It was decided that the pitot pressure data could only be used to generate true air speed and not longitudinal turbulence statistics for the aircraft's direction of motion. There were usually sufficient runs parallel and perpendicular to the wind direction so that all three turbulence components could be estimated. Frequently there were more crosswind turbulence runs than along-wind runs, and so the longitudinal environmental gusts (those transverse to the aircraft) were better defined. The momentum stress is largely in the longitudinal-vertical plane, and so the estimates of the momentum stress were probably not degraded. The standard deviations of the lateral wind component would be more seriously affected. However, the assumption of equi-partition of energy in the two horizontal directions of typical plume heights is a reasonable approximation (McBean and MacPherson 1976), and so the average standard deviations of the horizontal wind components denoted by the subscript "UH" were used in place of σ_v. In individual case studies, comparisons of σ_v and σ_u from orthogonal runs were presented wherever possible to justify this approximation; see especially the flights of 19 June (1335-1735).

It is important to recognize some of the differences in the turbulence quantities presented. The standard deviations of the wind components are very frequently used to relate plume dispersion coefficients to turbulence, for example, by Pasquill (1971) and Draxler (1976). However, there are two important considerations to keep in mind when interpreting such data.

First, the standard deviations are sensitive to all velocity changes, whether turbulent or laminar. For example, wave motion would contribute to the standard deviations of the wind components but would have very little turbulent mixing effect, since the existence of the waves indicates the presence of stable layers. The same contribution to the standard deviations from truly turbulent eddies would cause significantly more mixing. In any region of irregular topography, the use of the standard deviations must be carefully examined, because potential flow over topographic features when intersected by the aircraft would contribute to the velocity standard deviations.

Another consideration is the inherent limitations of the instrumentation system. Any slight errors in the response or calibration of any of the motion sensors or vanes will lead to errors in the computed velocity components. Since all the sensors were passed through a signal conditioning unit, system errors could arise from several sources. Thus, there is a reliability limit on this or any other aircraft system that is diffiuclt to determine but that may be approached in very smooth, stable conditions. The lowest turbulent velocity standard deviation observed on this field trip was about 0.4 m/sec. This may represent a minimum turbulence level resolvable by the present system.

3.3.4.2 Fluxes and stability. The momentum fluxes are $\overline{W'U'}$ and $\overline{W'V'}$ (where the primes indicate fluctuating quantities, the overbar is a time average, and U, V, and W are the x, y, and z wind velocities, following standard meteorological sign conventions and nomenclature). In a mixed surface boundary layer, $\overline{W'U'}$ is negative, indicating

transfer of momentum toward the ground; that is, the wind feels the effects of the surface drag. If $\overline{W'U'}$ and $\overline{W'V'}$ are near zero, then there is very little mechanical turbulence. If $\overline{W'U'}$ is positive, then there may be a low-level jet. Obtaining a stable average value for the momentum flux requires a lot of data because of intermittency (Wyngaard 1973). Thus, only the values from heights with at least ten 1 min segments can be considered representative.

The heat flux, $\overline{W'T'}$, is a measure of the thermal stability. If the heat flux is positive, then heat is moving upward and the air mass is unstable. It is important to realize that, even in very unstable conditions, the temperature profile above the near surface layer is adiabatic and hence indistinguishable from a natural case.

The stability of an air mass is often defined in terms of the ratio of the mechanical to convective energy; the exact forms may be Richardson Numbers, Flux Richardson Numbers, Monin-Obukhov Lengths, or some other less frequently used parameters. The advantages of the above forms, compared to Pasquill-Gifford stability classes, is that the above forms are continuous variables that can be directly measured, as opposed to somewhat subjective and discrete classes. The Monin-Obukhov stability formulation has the widest use in the literature and was used in the discussions of the case studies. Stability is determined by the value of Z/L, where Z is height above ground and L is the Monin-Obukhov Length defined as:

$$L = \frac{-u_*^3 T}{Kg\ \overline{W'T'}}$$

where: u_* is the friction velocity: $u_* = [(\overline{U'W'})^2 + (\overline{V'W'})2^{1/2}]$ following McBean and MacPherson (1976)

T is the absolute temperature

g is acceleration due to gravity

K is von Karman's constant (0.4)

A negative Z/L value is unstable; a positive value is stable. Note that L depends upon the third power of the friction velocity, which is statistically a difficult parameter to measure reliably.

In practice, the value of dissipation discussed in the next section proved to be a good indicator of the height of the mixed layer. In very stable layers, the value of $\overline{W'U'}$ was dominated by large-scale features that clearly were not related to turbulent momentum flux, and so the value of L was not well defined.

3.3.4.3 Dissipation and integral statistics. Autocorrelation and second-order structure function analyses were routinely done as part of the turbulence analysis routines. From the integral of the autocorrelation of the velocity components, an estimate of the integral length scale could be made. Dissipation estimates were made from the second-order structure functions following the technique of Pond et al. (1963) and Paquin and Pond (1971).

The integral length scales are normally considered to be a measure of the memory of the turbulence. However, it must be recognized that any motion will contribute to the autocorrelation. Thus, laminar flow oscillations sectioned by the aircraft could result in quite large apparent integral length scales even when true three-dimensional turbulence is very weak. In stable conditions it was not unusual for the autocorrelation to exhibit a periodic shape about zero. The computed integral scales in such cases were taken to be the integrals up to the first zero crossing.

Dissipation is often considered to be a measure of the total amount of turbulent energy in the field. Dissipation appears in the energy equation as in the following approximate equation:

Time rate of change of turbulent energy	=	Mechanical energy production	+	Thermal energy production or sink	+	Vertical divergence of turbulent energy	+	dissipation

More detailed descriptions are available in any standard atmospheric turbulence text, such as Lumley and Panofsky (1964) or Tennekes and Lumley (1972). At GCOS, at typical plume heights, the time rate of change was generally small except near the edge of the mixed layer.

Within the mixed layer dissipation, ε has often been found to be nearly constant (Lenschow 1970, Kaimal et al. 1976) for fully convective boundary layers. This implies that the vertical divergence of turbulent kinetic energy changes with height to balance the decrease of heat flux with height associated with boundary layer heating. However, at GCOS, at typical plume heights, dissipation was usually found to decrease with height. This decrease of dissipation with height represented a decrease in the amount of smaller scale turbulent kinetic energy. For each case study, the dissipation and velocity standard deviations for every run were plotted to show the temporal and spatial changes in these turbulent parameters.

3.3.4.4 Spectral analysis. Groups of data blocks representing turbulence statistics of special interest were selected for spectral analysis. The objectives of the spectral analysis were basically three-fold. The spectral shapes could give clues as to the level of success of the removal of aircraft motion effects. Secondly, the spectral energy distribution estimated from the spectral shapes could be compared to that estimated from the values of dissipation and of the velocity standard deviation. Thirdly, the values of the turbulence parameters used in normalixing the plume spread could, perhaps, be optimized or better understood.

The spectral analysis was done using widely accepted analysis techniques following Blackman and Tukey (1959), Lee (1967), and Kanasewich (1975). The data segments were detrended in time domain, the IMSL routine for the fast Fourier transform was applied to blocks of 128 data points, the resulting coefficients were hanned and then band-averaged using logarithmic bandwidths, and the spectral estimates over the same frequency bands from all the analysis blocks in a group were logarithmically averaged. The spectral plots were

presented in a non-dimensional form normalized by the integral under the spectra, as function of wave number, k, where:

$$k = \frac{2\Pi f}{TAS}$$

k = wave number per metre

f = frequency per second

TAS = aircraft true air speed (m/sec)

3.3.4.5 Modification of the velocity standard deviations. The results of the spectral analysis indicated an apparently extraneous peak in energy at a wavelength of about 330 m (a period of about 5 sec) in both the vertical and lateral velocity components. The peak was considered to be extraneous due to its constant frequency regardless of height or turbulence intensity and due to the bump in the spectral plots that is inconsistent with spectral shapes measured in many other previous studies. Because the spectral estimates had been hanned, it was felt that removal of the effects of this extra energy could be accomplished with reasonable confidence. The removal of the effects of this extraneous energy resulted in a reduction of about 10-15% in the values of the velocity standard deviations. The values of the velocity standard deviation used for plume spread normalization were all modified in this fashion.

4. CASE STUDIES

In the following sections four flights have been analyzed in detail. Significant lack of stationarity required one of these flights to be divided into two case studies. In addition, another flight required a partial splitting of the case study. Thus, six distinct plume situations were identified. The case studies are presented chronologically.

4.1 CASE STUDY FOR THE FLIGHT OF 19 June 1977 (0745-1010 MDT)

4.1.1 Visual Plume Description

When the plume was approached at about 0800 Mountain Daylight Time (MDT), the sky was nearly cloudless, the air was smooth, and the plume was heading north down the Athabasca River valley. At the time of the first run, the plume appeared visually to be impinging on the west side of the river valley (Figure 3A). By about 0915 MDT, the flights were noticeably bumpier, and the top of the visual plume was not as smooth as previously (Figure 3B). The flight was then terminated due to anticipated changes in the plume structure as the mixed layer continued to rise.

4.1.2 Flight Profiles

The plume heading was visually estimated to be 320°M; a right-hand racetrack pattern at the standard downwind distances of 3.2 km and 8.0 km was set up (see Section 3.1 for further details of the procedure used to set up the way points needed to define the flight patterns for the VLF/Omega navigation system used as the positioning system). A series of five vertically stacked traverses was flown at the two downwind distances as shown in Figure 4 and Table 1. Run 11 was flown at the same height as Run 1 but was much bumpier, indicating changed meteorological conditions. Thus, the flight was terminated with a turbulence run on the west side of the Athabasca River valley on the return run to Fort McMurray.

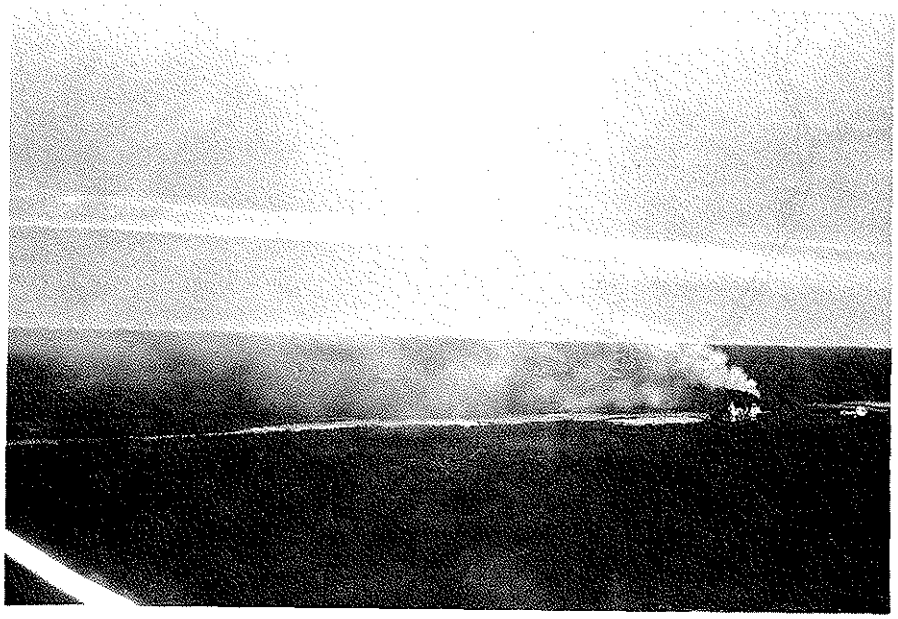

A

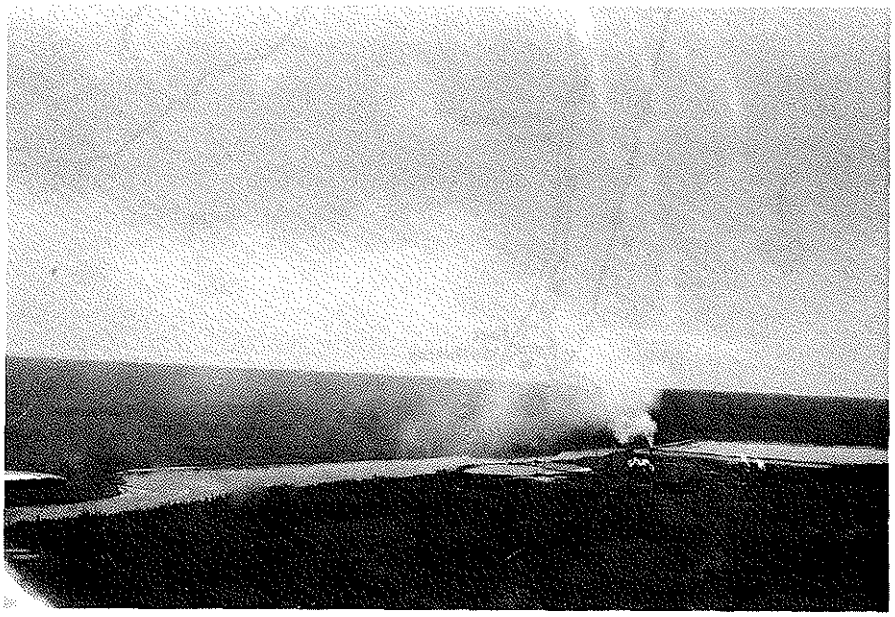

B

Figure 3. Plume photographs from the flight of 19 June 1977 (0745-1010 MDT). The upper photo (A) was taken at 0830 at an altitude of 610 m AMSL. The lower photo (B) was taken at 0940 (near the end of the flight) at an altitude of 610 m AMSL.

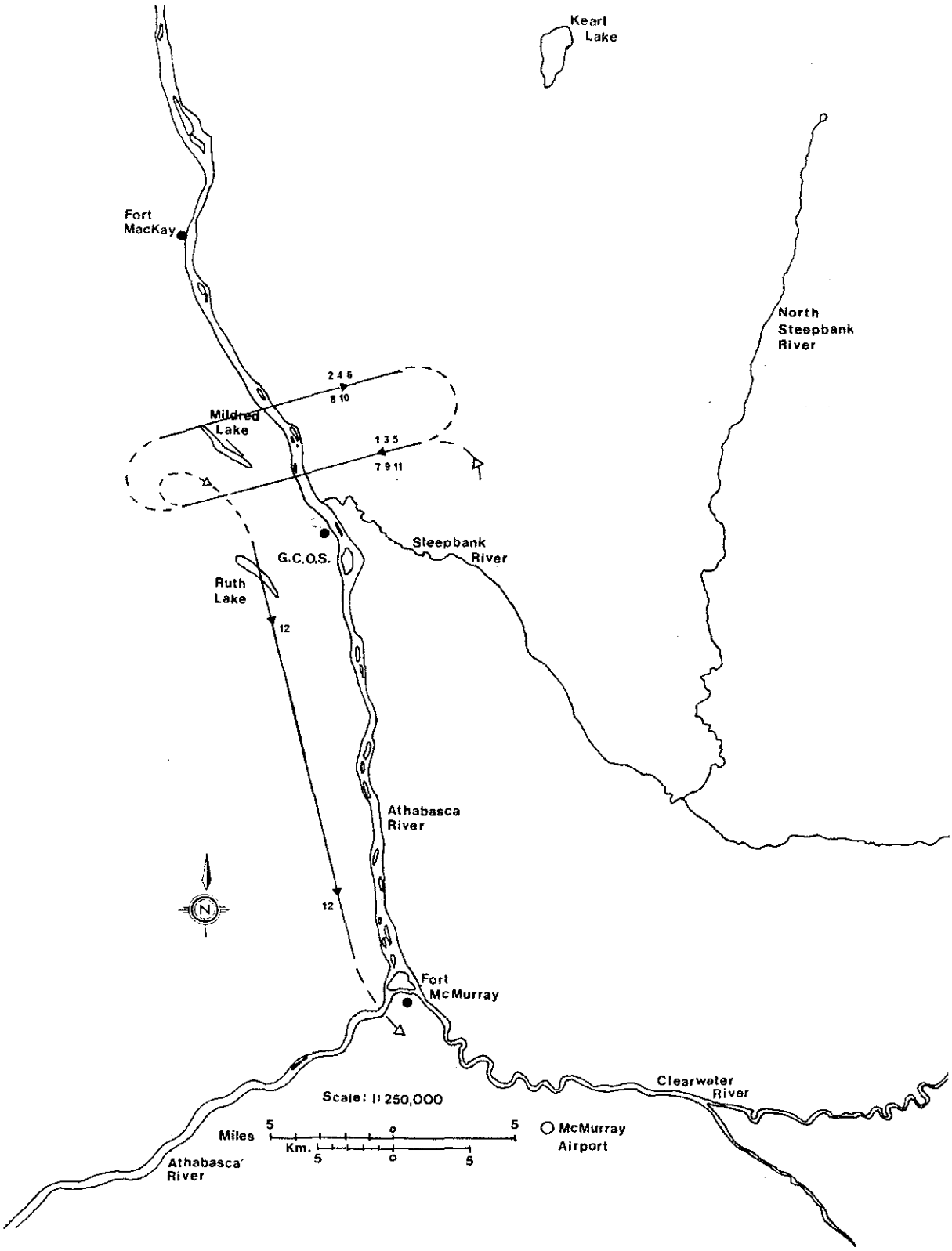

Figure 4. Flight profiles for 19 June 1977 (0745-1010 MDT).

Solid lines denote numbered runs and dashed lines denote interconnecting legs.

Table 1. Run information for flight of 19 June 1977 (0745-1010 MDT).

Run Number	Start Time (MDT)	Altitude (m MSL) ± 20	Downwind Distance (km) ± 0.3	σ_y (m) ± 100	Max. SO_2 Conc. (ppm) ± 0.02	Integrated Conc. (ppm-m) ± 50	Flight Dir. (From-To)
1	0828	610	3.2	1572	0.19	495	E-W
2	0834	610	8.0	2116	0.12	333	W-E
3[a]	0840	760	3.2	-	-	-	E-W
4[a]	0847	760	8.0	-	-	-	W-E
5	0856	519	3.2	4672	0.14	553	E-W
6	0902	519	8.0	4194	0.13	449	W-E
7	0909	671	3.2	1739	0.20	514	E-W
8	0916	671	8.0	5375	0.13	453	W-E
9	0923	564	3.2	5895	0.15	385	E-W
10	0930	564	8.0	5563	0.16	618	W-E
11	0938	610	3.2	3208	0.19	440	E-W
12T[b]	0949	610	-	-	-	-	N-S

[a] No detectable SO_2.

[b] T = turbulence run.

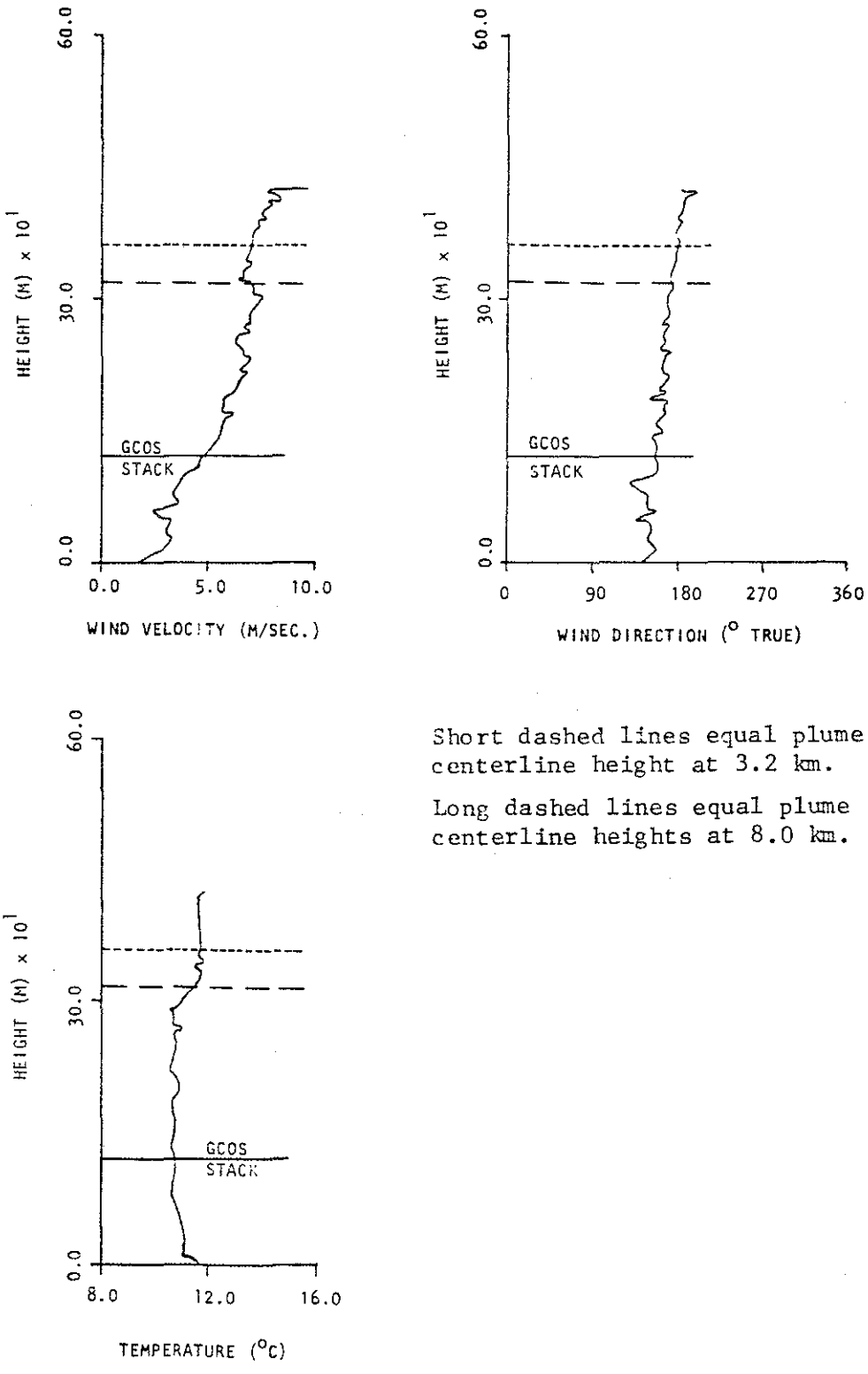

Short dashed lines equal plume centerline height at 3.2 km.

Long dashed lines equal plume centerline heights at 8.0 km.

Figure 5. Tethersonde profiles for 19 June 1977. 0723-0948 MDT. Data supplied by R. Mickle, AES.

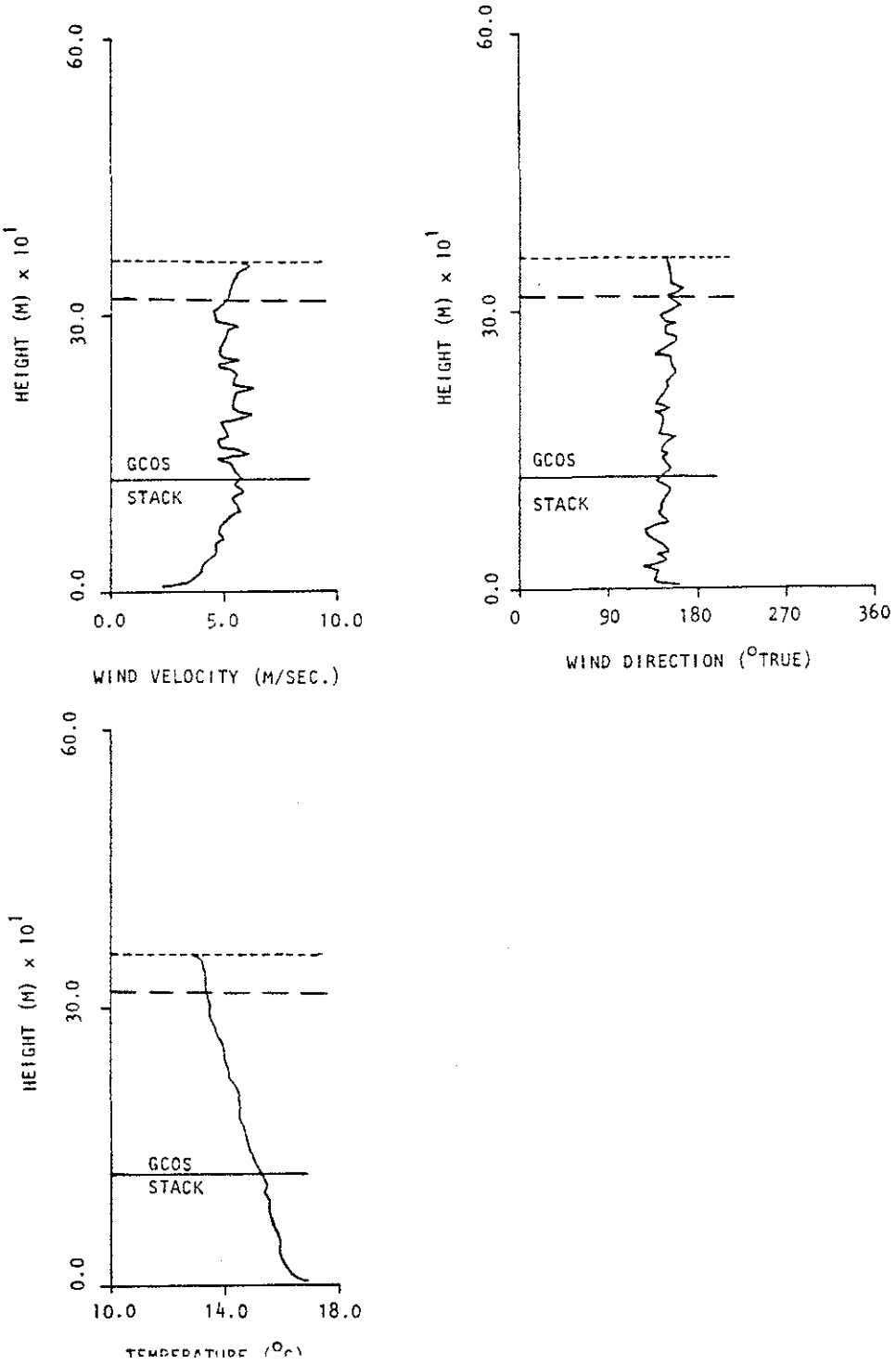

Figure 5. Concluded.

4.1.3 Tethersonde Data

The AES tethersonde data for the profiles beginning at 0723 and 0948 are shown in Figure 5. Note that, over the 2 h period between the profiles, the wind direction at about 300 m above ground level (AGL) had backed about 30°. The temperature and relative humidity profiles both indicate the presence of an inversion at about 300 m AGL or 545 m above mean sea level (AMSL), at about 0730 that had risen above the maximum tethersonde profiling height by 0950.

4.1.4 Isopleths and Selected Traverses

The isopleths in Figure 6 indicate that a very wide plume existed. Figures 7 and 8 show the actual plume traverses on Runs 1 and 2, which indicate that the plume cross-section showed some evidence of multiple source effects. If just the main peak is considered, the σ_y values for Runs 1 and 2 would be about one half of the raw computed value. Note that the traverses are plotted as normalized concentrations versus standard deviations. The zeroes in Figures 7 and 8 correspond to a Gaussian distribution with the same σ as computed using the area criterion; the crosses represent actual measured concentrations. The computed plume standard deviations for all the runs except Runs 1, 2, and 7 were very large due to small concentration values found near the ends of the runs. These extraneous values may have arisen due to fugitive emissions and a very low level wind direction shear or may have been unremoved system noise. In either case, these very large σ_y values have no significance as far as the main plume geometry is concerned. Run 8 was flown when convection was becoming important and may have been influenced by a combination of convective transport from below and the change of wind direction with time. The SO_2 concentration profiles for all runs are presented in Appendix 8.3.

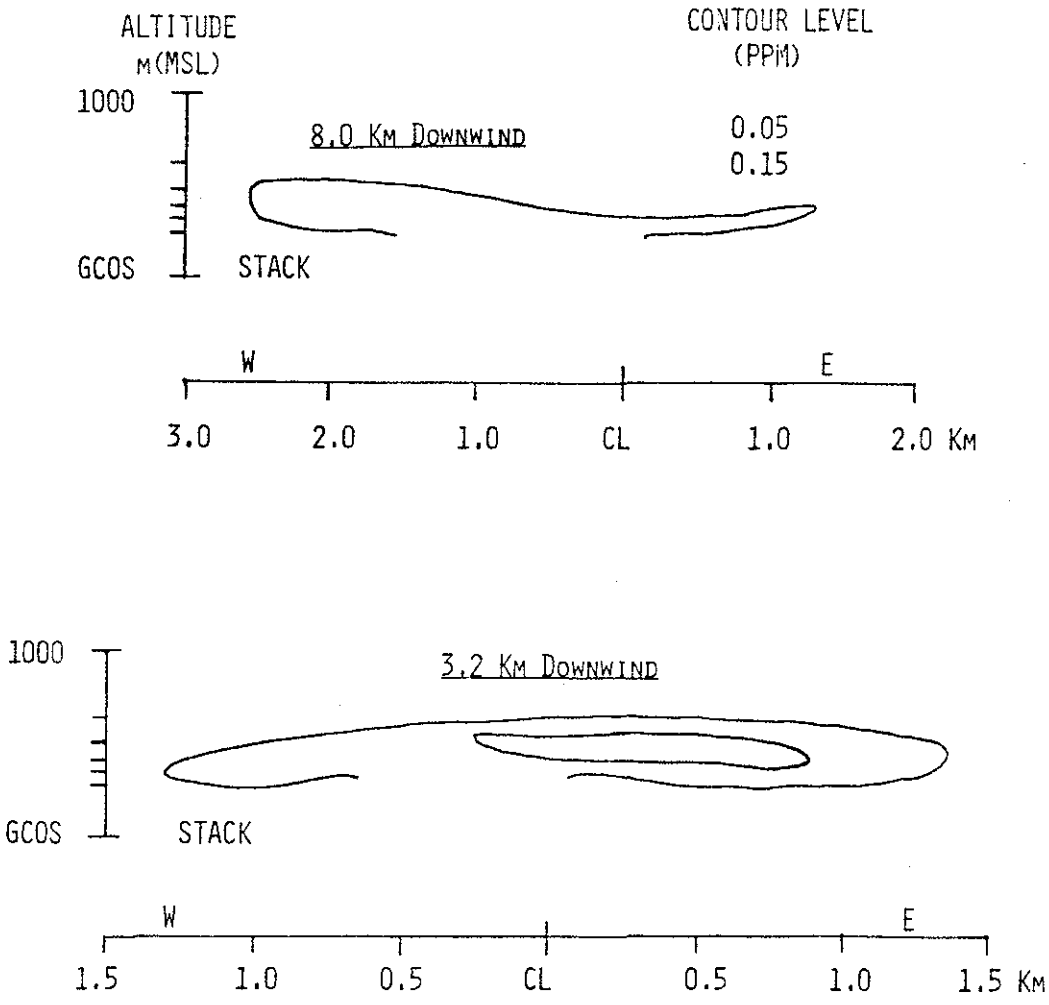

Figure 6. SO_2 concentration isopleths for the flight of 19 June 1977 (0745-1010 MDT).

Note: 8.0 km Isopleth has a 2X vertical exaggeration.
3.2 km Isopleth has no vertical exaggeration
Dashes on the left side of the vertical axes are flight levels.

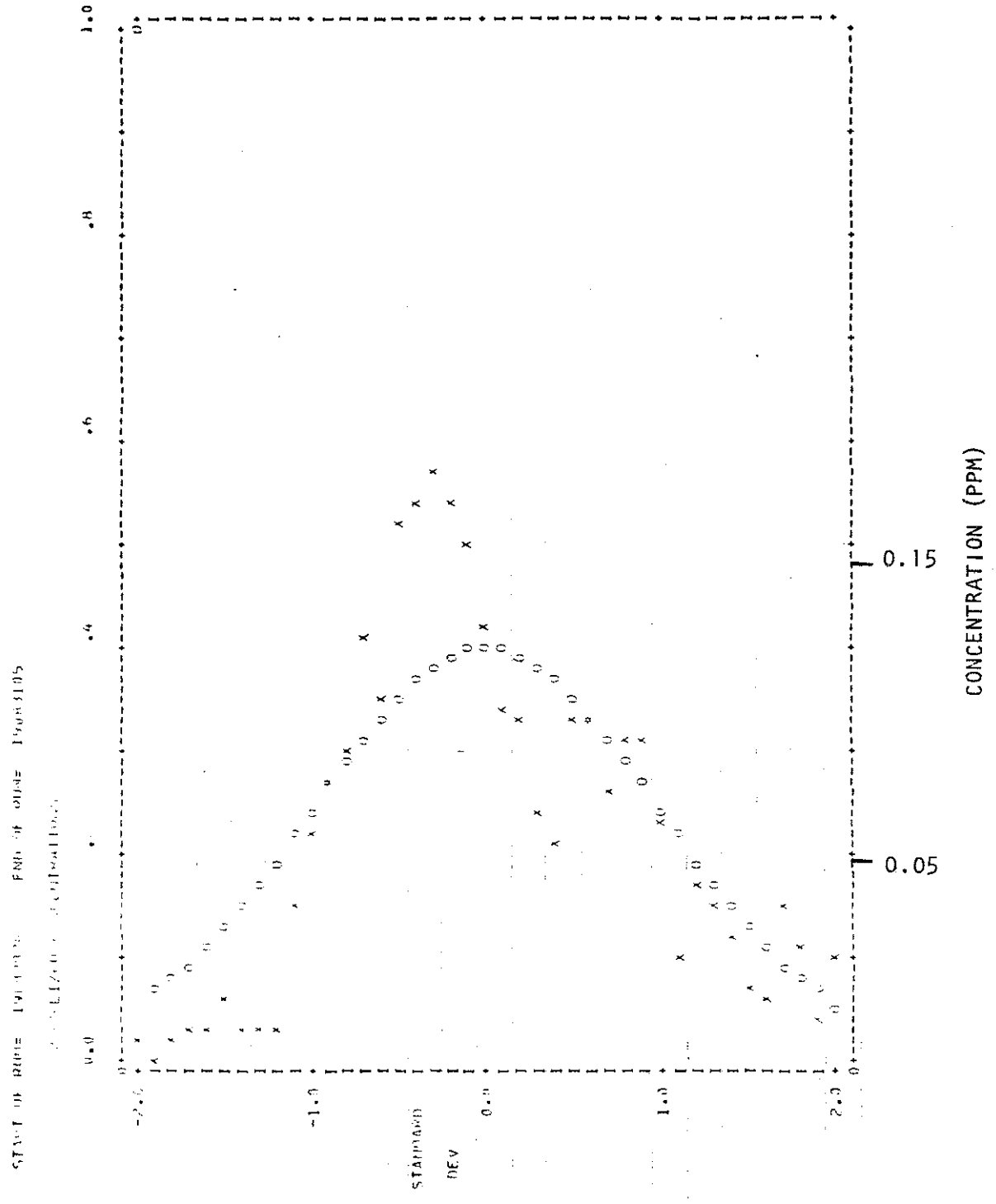

Figure 7. Normalized SO_2 concentrations for Run 1 on the flight of 19 June 1977 (0745-1010 MDT).

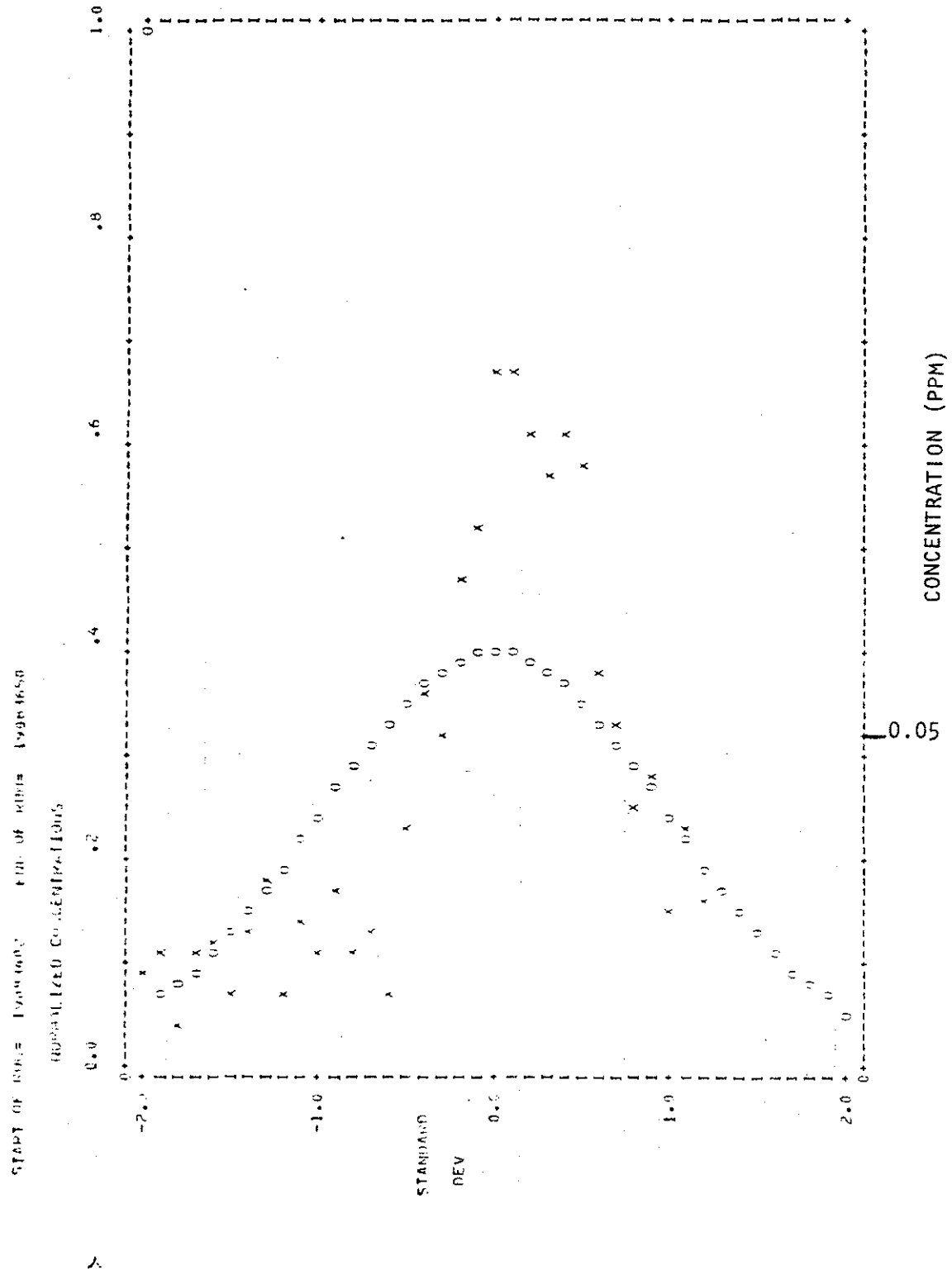

Figure 8. Normalized SO_2 concentrations for Run 2 on the flight of 19 June 1977 (0745-1010 MDT).

4.1.5 Plume Geometry

The major features of plume geometry are summarized in Table 2. The computation techniques for the various measurements of σ_y, σ_z, and plume height were discussed in the previous section. The difference between the upper and lower σ_z values was not considered significant, although the number of data points used to compute σ_z (see Figure 9) was not large. Note in Figure 9 that the maximum concentration values from Runs 9 and 10 (second lowest pair of values) were not inconsistent with the previous values. Thus, although penetrative convection may have affected the σ_y values, the maximum concentration values appear reasonable.

The observed values for σ_y, σ_z, and normalized axial concentrations were compared to the Pasquill-Gifford curves in Figures 10, 11, and 12. The appropriate Pasquill-Gifford stability class was chosen as D (see Section 5 for full description). The σ_y values are seen to be about eight times larger at 3.2 km and five times larger at 8.0 km than the Pasquill-Gifford curves. If a factor of two is allowed for possible multiple source effects, the discrepancy is similar to that found for most cases in the March 1976 study. The σ_z values did not increase with downwind distance, presumably due to the capping inversion. A more complete discussion of the observed plume sigma values compared to the Pasquill-Gifford curves is presented in the next section where data from all the case studies are consolidated.

The mass fluxes computed from the two tethersonde profiles differed by about 30%, but agreed with the emission data as well as could be expected, considering the changing meteorological conditions and the limited number of traverses.

The observed effective stack height was compared to the values predicted by the formulations of Briggs, TVA, and Holland. A comparison of the accuracies of the various prediction schemes is presented in the next section, where the data from all the case studies are synthesized.

Table 2. Plume geometry, mass flux, and plume rise for the flight of 19 June 1977 (0725-1010 MDT).

Parameter				Downwind Distance 3.2 [km]	8 [km]
σ_y cl	Area Criterion	[m]	± 50	1590	2120
	Second Moment	[m]	± 50	1700	2130
σ_z	Upper	[m]	± 20	68	76
	Lower	[m]	± 20	88	78
	Average	[m]	± 20	78	77
$\chi\bar{U}Q^{-1}$	Norm Axial Conc.	$10^{-6}m^{-2}$	± 0.3	1.37	1.07
SO_2	Mass Flux				
	[long tons·h^{-1}]		± 2	9.2 (6.7)	7.0 (5.6)
	[kg·sec^{-1}]		± 0.5	2.6 (1.9)	2.2 (1.6)
Observed centerline height		[m MSL]	± 20		
(i)	Height of center of mass from max conc. profile			600	560
(ii)	Height of center of mass from integrated conc. profile			585	555
(iii)	Height of max. conc. observed			670	565
Ratio of calculated to observed effective stack height					
(i)	Briggs			1.46	
(ii)	Holland			0.86	
(iii)	TVA			1.45	

Notes: 1. For the ratio of calculated to observed effective stack height, the following data were used: $\bar{U}$ = 5.5 (m/sec); $\partial T/\partial z$ = -0.38 (°C·100 m^{-1}). Observed effective stack height = 580 m MSL = 320 m AGL.

2. Values in parentheses for mass flux estimates are based upon the 0948 tethersonde profile; the other values, on the 0723 tethersonde profile. The source mass flux from data provided by GCOS was 2.7 kg·s^{-1} (9.4 long tons·h^{-1}).

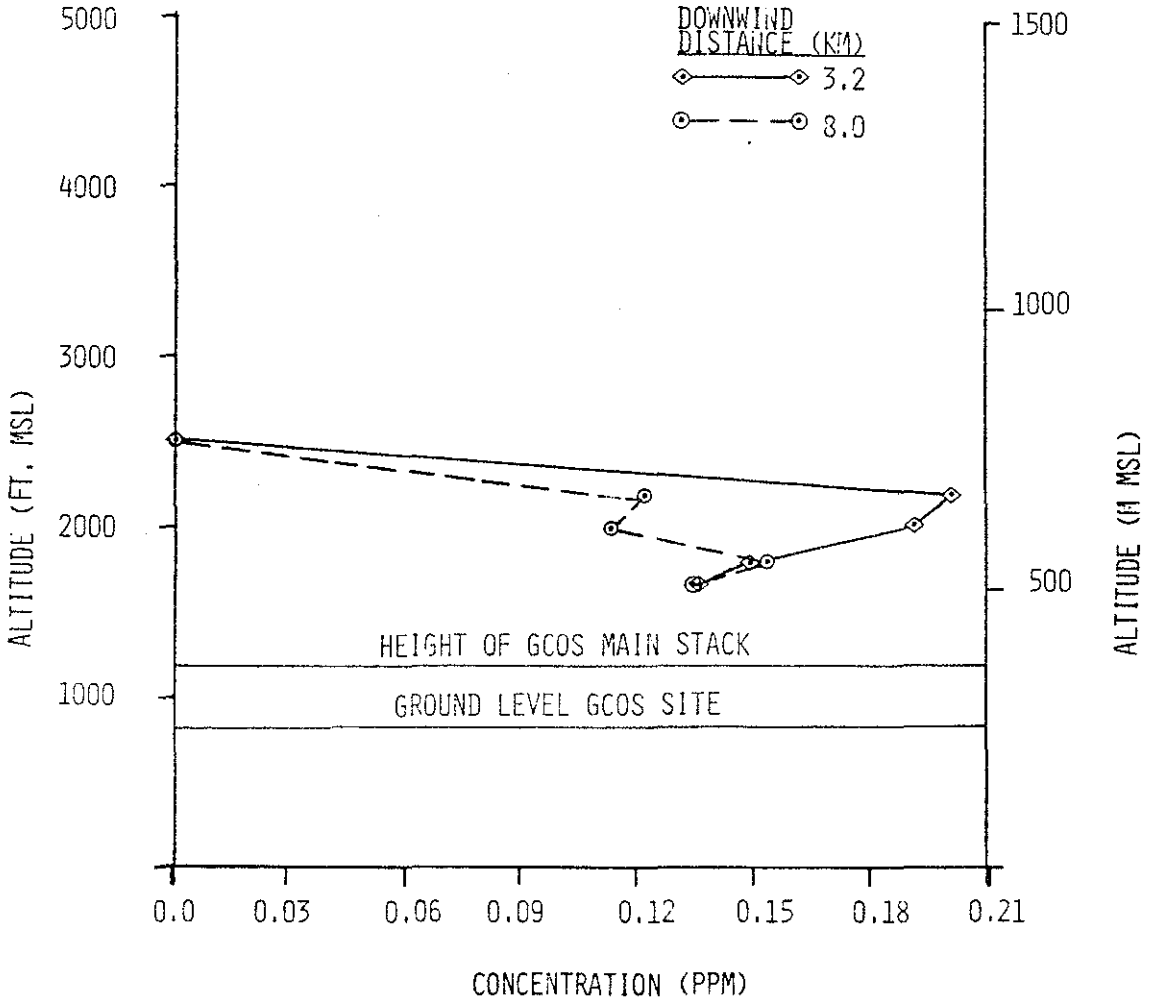

Figure 9. Maximum SO_2 concentrations along each traverse as a function of altitude for the flight of 19 June 1977 (0745-1010 MDT).

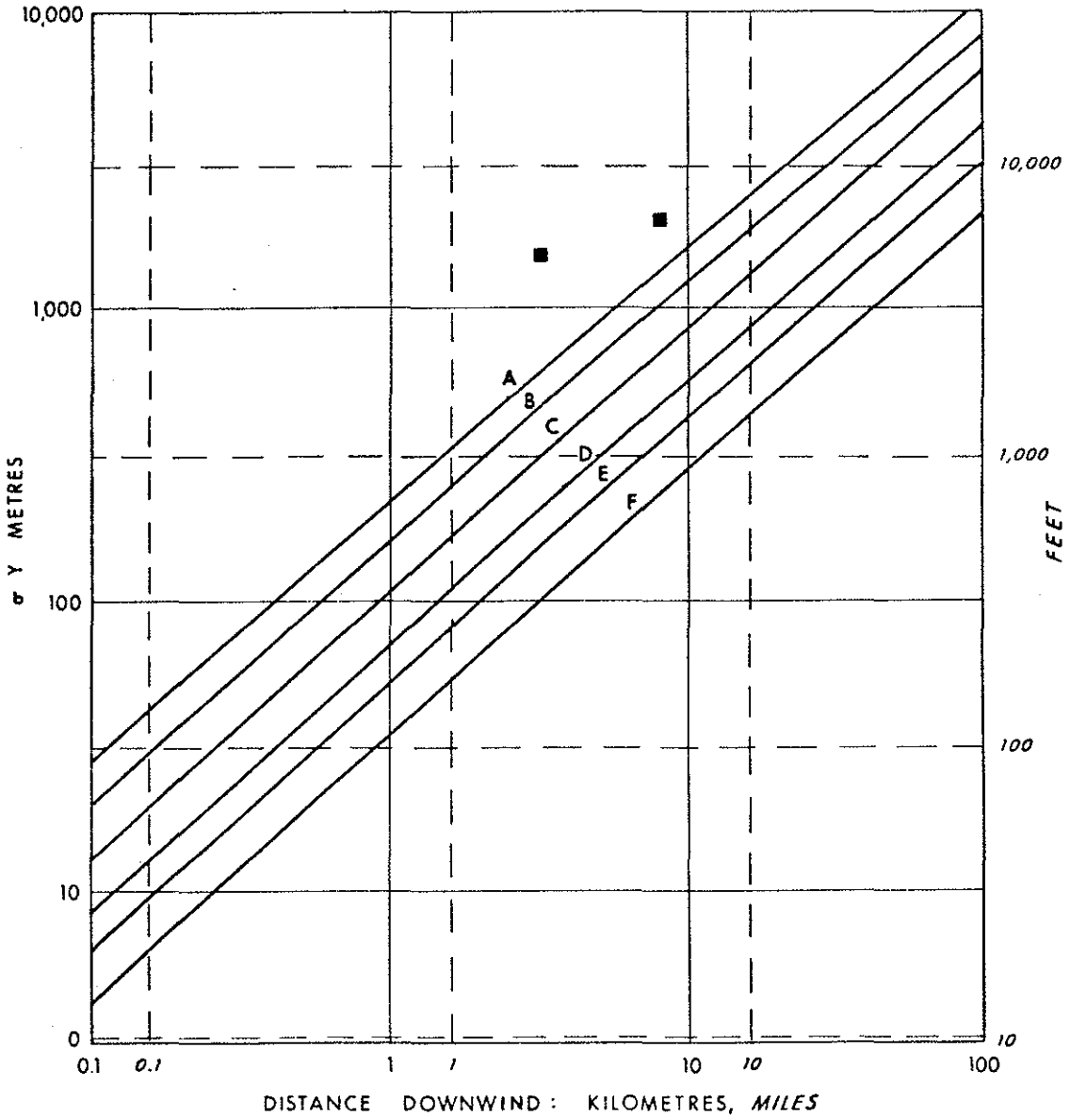

Figure 10. Observed horizontal dispersion coefficient compared to Pasquill-Gifford curves for the flight of 19 June 1977 (0745-1010 MDT).

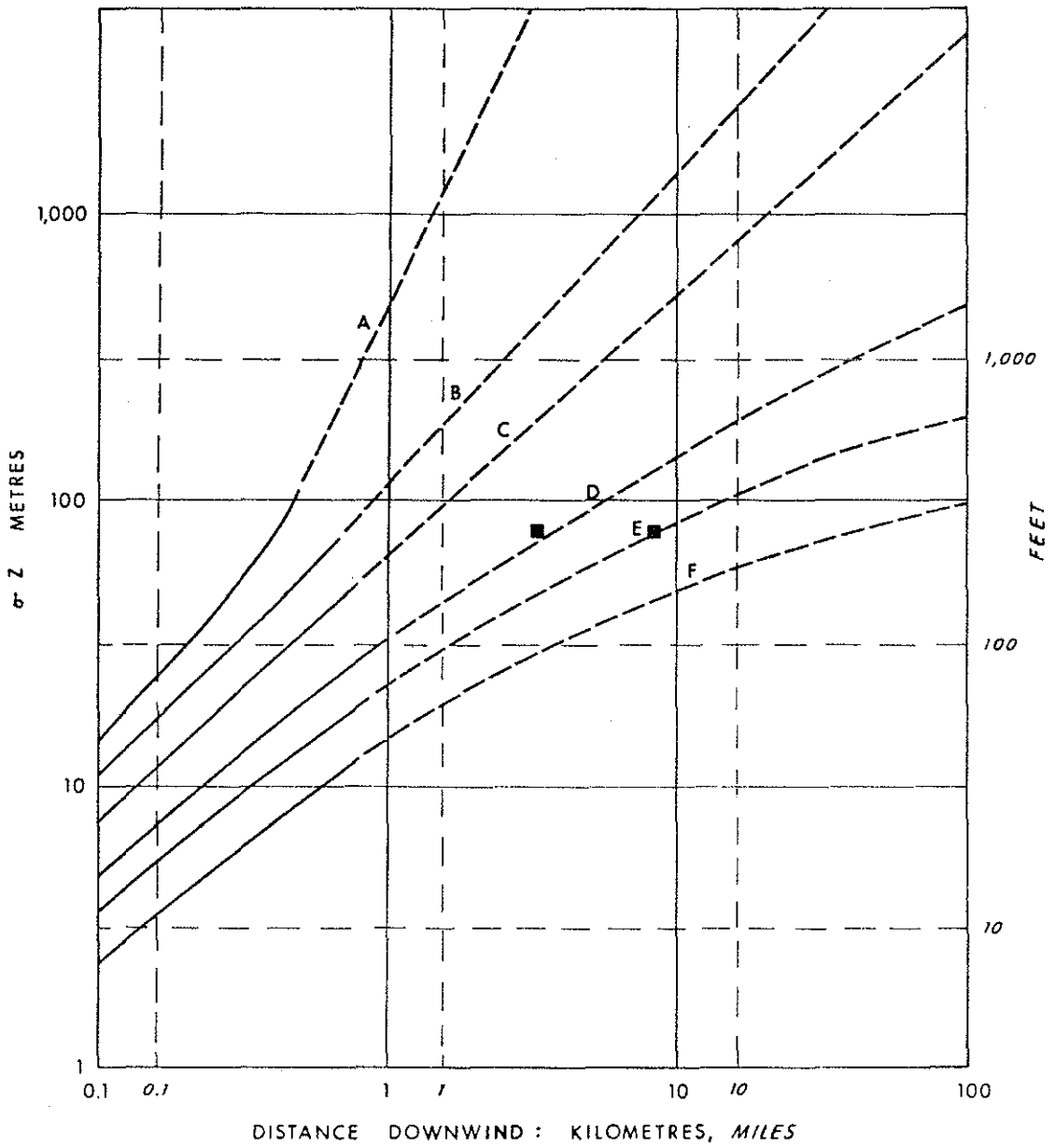

Figure 11. Observed vertical dispersion coefficient compared to Pasquill-Gifford curves for the flight of 19 June 1977 (0745-1010 MDT).

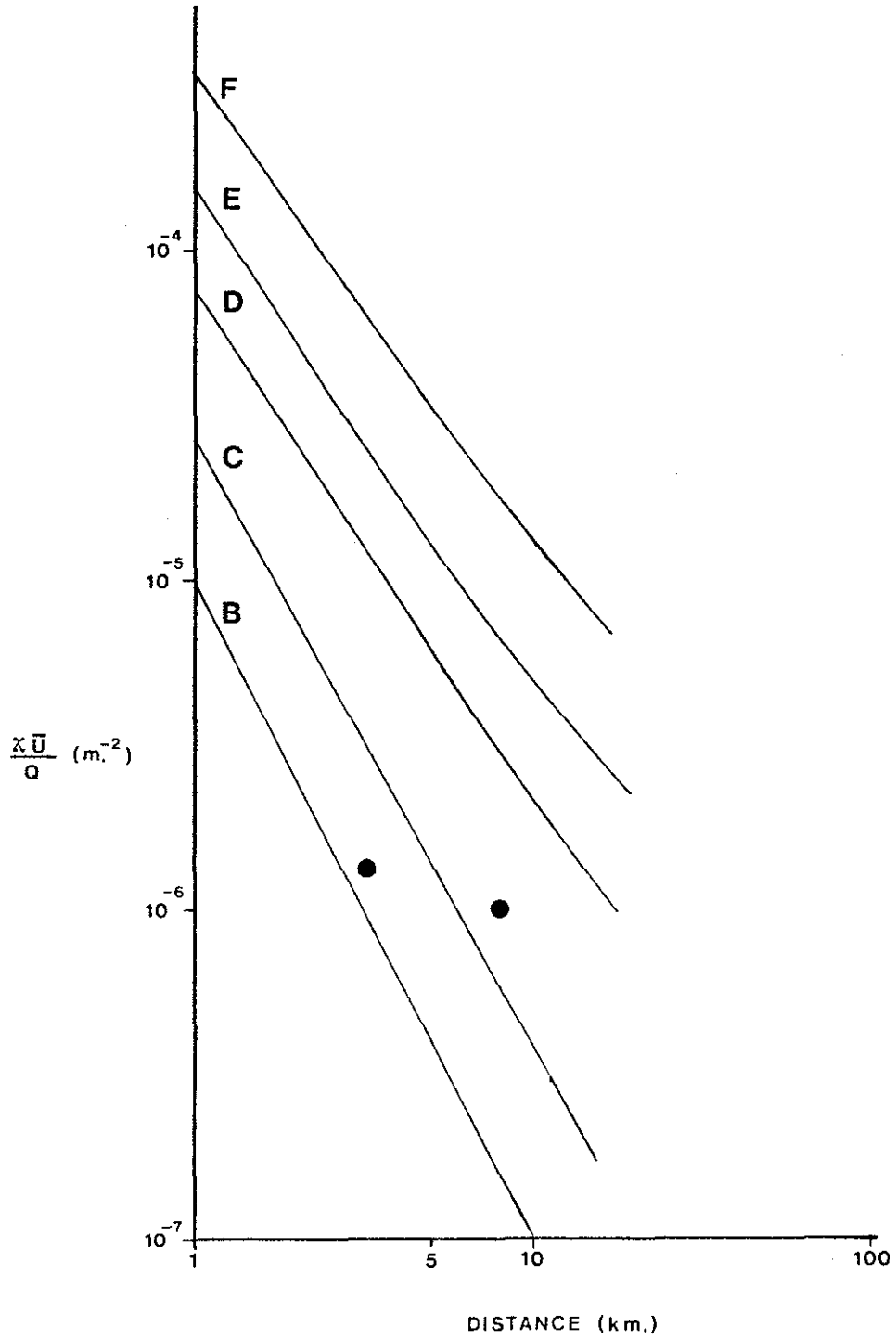

Figure 12. Comparison of observed normalized centerline concentrations with Pasquill-Gifford predictions for the flight of 19 June 1977 (0745-1010 MDT).

4.1.6 Turbulence Levels Related to Plume Structure

A summary of the turbulence data is presented in Figure 13; statistics from groups of runs are presented in Table 3. The changes of the turbulence parameters in Figure 13 with time are very noticeable, particularly for the dissipation values. The early runs generally show much reduced turbulence, compared to later runs. An exception is the final turbulence run heading south along the west side of the Athabasca River valley (Run 12); the statistics on the turbulence run indicated that the mixed layer along that path had not yet reached 600 m AMSL. The large value for σ_w on Run 8 is consistent with a previous suggestion of convective penetration at that level producing SO_2 concentration values removed from the central peak.

The statistics from the three groupings of runs shown in Table 3 show that the differences observed are statistically significant. Note that the standard deviation refers to the standard deviations of the population of similar mean values and is computed by dividing the data block standard deviation by the root of the number of blocks; see, for example, Baird (1962).

Spectral analysis was performed on the three groupings of runs for the vertical and lateral velocity channels (Figure 14). As mentioned in the previous section, the peak near the middle of the spectral plots, near log k = -2, was considered an extraneous peak. The values for σ_w and σ_v used in plume normalization in the next section were reduced by factors 0.9 and 0.84 respectively to remove the effects of this peak. The integrals under the spectra (the variances) agreed closely with the average values obtained from time domain computation, providing a check on the spectral analysis computation procedures. The shapes of the curves were not markedly dissimilar, all showing a falloff over part of their range not inconsistent with the $k^{-2/3}$ expected from similarity theory.

The vertical velocity spectral plot for Runs 9 and 10 did not show any low wave number fall-off. Since the first spectral estimate corresponds to a frequency of 64 sec and a wavelength of

Table 3. Summary of turbulence data for groups of runs from the flight of 19 June 1977 (0745-1010 MDT).

Runs	Description	No. of Blocks	σ_w [m/sec]	σ_{uH} [m/sec]	ε [cm^2/sec^3]	ℓ_w [m]	ℓ_v [m]
1, 2							
3, 4	Early	11	0.99	0.93	5	260	240
	Above inversion		(0.05)	(0.08)	(1)	(27)	(36)
5, 6	Early,	8	1.30	1.10	29	195	125
	Below inversion		(0.08)	(0.10)	(3)	(17)	(32)
9, 10	Later	8	1.55	1.81	55	200	230
	Below inversion		(0.10)	(0.18)	(7)	(14)	(34)

Note: Values in parentheses are the standard deviations of the population of mean values.

σ_w standard deviation of vertical velocity

σ_{uH} standard deviation of lateral velocity with respect to the aircraft

ε dissipation

ℓ_w integral length scale in the vertical

ℓ_v integral length scale in the lateral direction with respect to the aircraft.

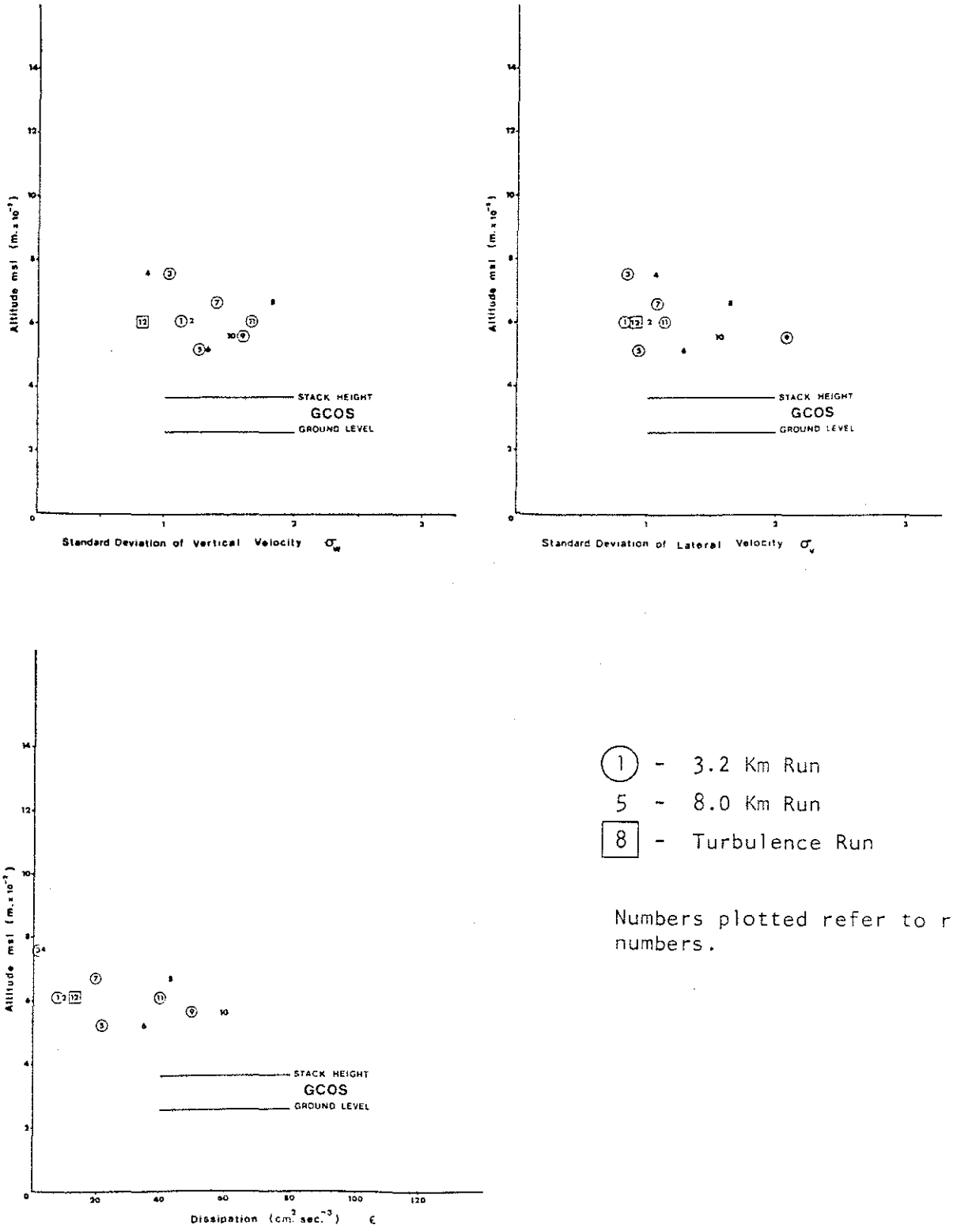

Figure 13. Turbulence data for flight of 19 June 1977 (0745-1010 MDT).

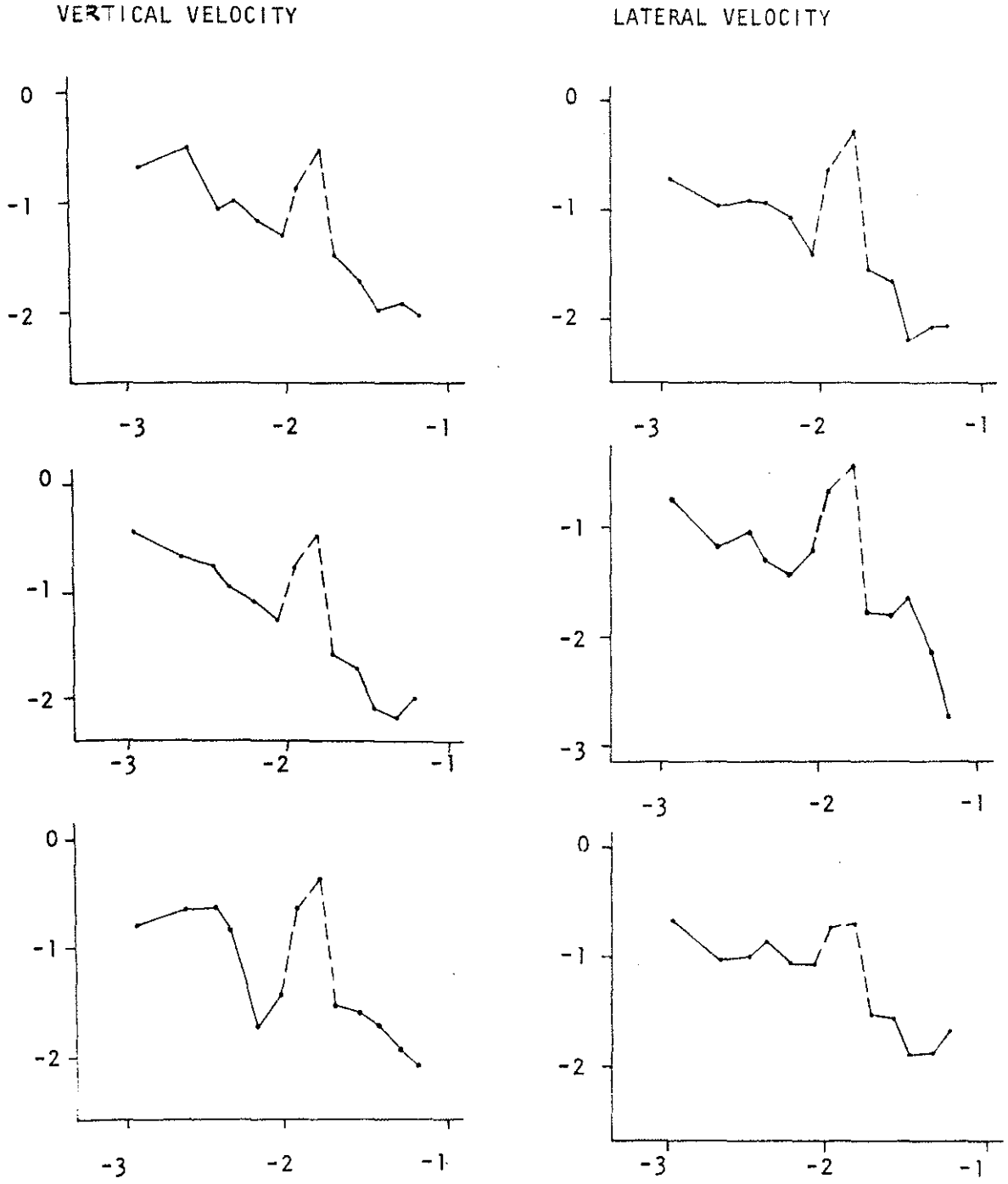

Figure 14. Spectral plots for the flight of 19 June 1977 (0745-1010 MDT). All plots are LOG$\left(\frac{K\ \phi\ (K)}{\sigma^2}\right)$ versus LOG K where K is wave-number (m^{-1}). From top to bottom the run groups are: 1, 2, 3, 4; 5, 6; 9, 10.

about 4 km, this lack of fall-off is somewhat surprising. The depth of the mixed layer was most certainly less than 1 km. However, it must be remembered that the aircraft samples at a constant pressure level, and so traverses across the river valley would be expected to show low frequency effects, especially in the vertical due to potential flow over the irregular terrain. The irregular terrain itself may generate motions with size scales typical of the terrain features. In this case, the motions may be part of the effective mixing process and so should be included in the σ_w and σ_{uH} values used for plume spread normalization in the next section.

4.2 CASE STUDY FOR THE FLIGHT OF 19 JUNE 1977 (1335-1735 MDT)

4.2.1 Visual Plume Description

In the afternoon of 19 June the plume was still heading northward with an estimated visual heading of 320°M, the same as in the morning flight. The runs were much bumpier at all levels than they had been in the morning flight. The plume exhibited looping characteristics, as shown in the two photographs in Figure 15. The looping of the plume means that the experimental error in the concentration distribution is largely due to lack of reproducibility in plume traverses. Nevertheless, documentation of the concentrations and associated meteorology are worthwhile because these meteorological conditions are not usual, and mixing to the ground was observed.

4.2.2 Flight Profiles

The flight profiles and some of the associated SO_2 concentration statistics are shown in Figure 16 and Table 4. The standard vertically stacked traverses at 3.2 and 8.0 km were followed by a series of turbulence runs parallel to the wind direction.

4.2.3 Tethersonde Data

The AES tethersonde was operated in a fixed level mode throughout the afternoon at a height of about 175 m AGL or about 420 m AMSL. The average wind speed from 1338 to 1458 was 6.9 m/sec,

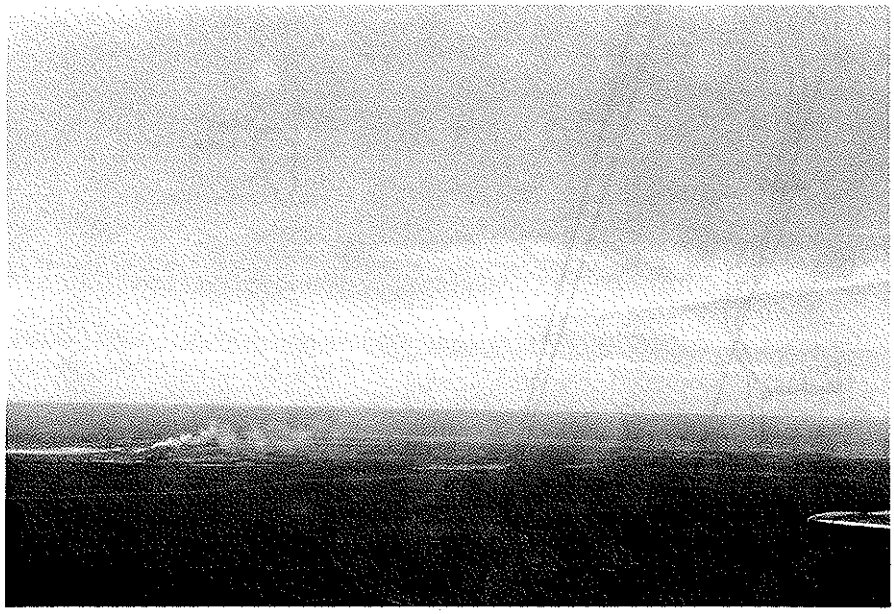

A

B

Figure 15. Plume photographs for the flight of 19 June 1977 (1335-1735 MDT). The upper photo (A) was taken at 1458 from approximately 5 km downwind (north) and 8 km east of GCOS at an altitude of 850 m AMSL. The lower photo (B) was taken at 1645 at an altitude of 1160 m AMSL.

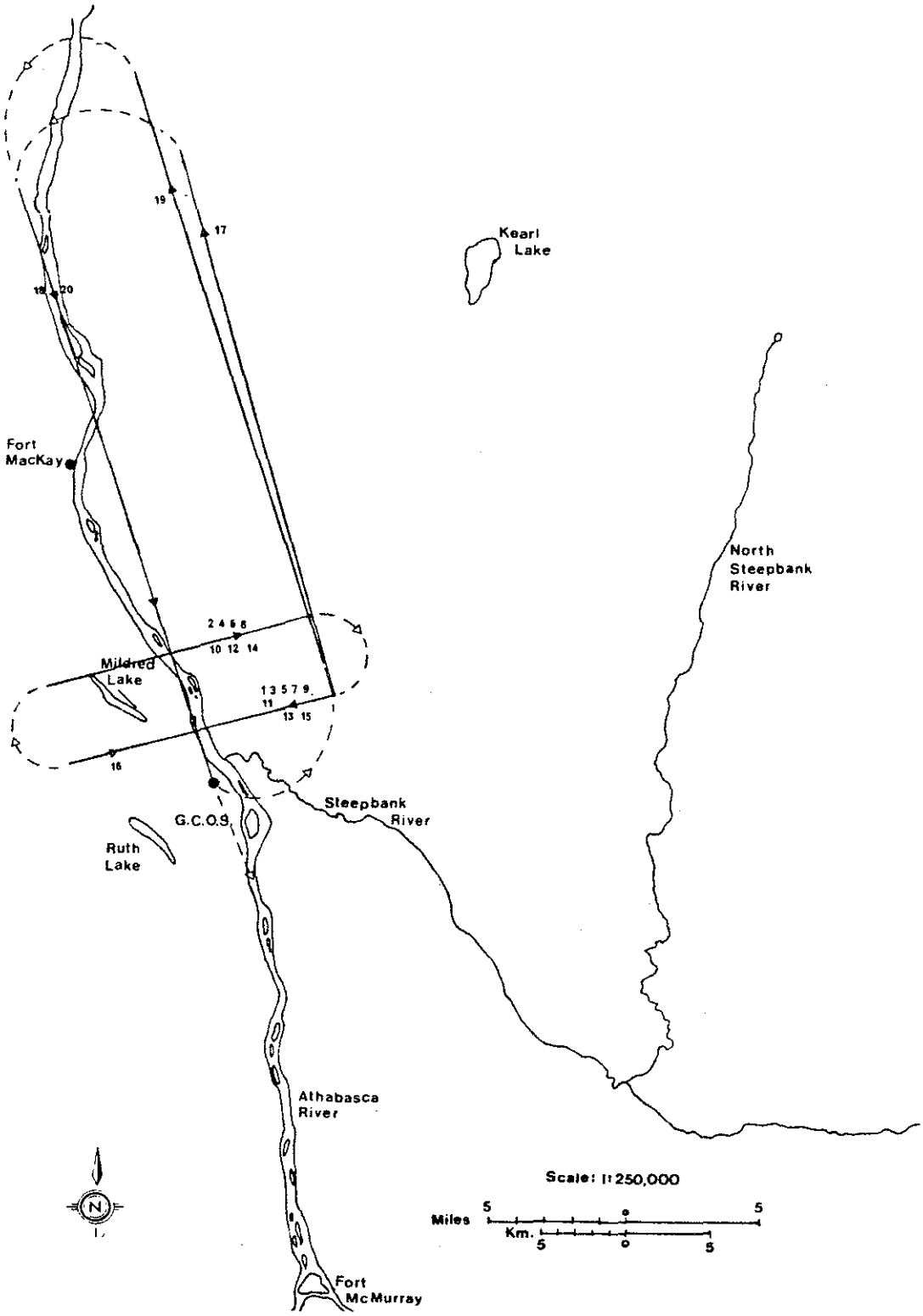

Figure 16. Flights profiles for 19 June 1977 (1335-1735 MDT).

Solid lines denote numbered runs and dashed lines denote interconnecting legs.

Table 4. Run information for flight of 19 June 1977 (1335-1735 MDT).

RUN NUMBER	START TIME (MDT)	ALTITUDE (m-MSL) ± 20	DOWNWIND DISTANCE (km) ± 0.3	σ_y (m) ± 100	MAX. SO_2 CONC. (ppm) ± 0.02	INTEGRATED CONC. (ppm-m) ± 50	FLIGHT DIR. (From-To)
1	1416	915	3.2	5137	0.088	221	E-W
2	1423	915	8.0	2628	0.092	303	W-E
3	1431	610	3.2	6251	0.098	423	E-W
4	1437	610	8.0	3747	0.070	225	W-E
5[a]	1445	1219	3.2	-	-	-	E-W
6[a]	1451	1219	8.0	-	-	-	W-E
7	1459	763	3.2	6641	0.19	479	E-W
8	1506	763	8.0	8003	0.079	368	W-E
9	1518	1373	3.2	517	0.067	68	E-W
10[a]	1524	1373	8.0	-	-	-	W-E
11	1532	1068	3.2	4798	0.073	160	E-W
12	1539	1068	8.0	1771	0.082	107	W-E
13	1549	519	3.2	6723	0.10	531	E-W
14[a]	1556	549	8.0	-	-	-	W-E
15	1602	793	3.2	5072	0.14	433	E-W
16	1609	793	3.2	5121	0.12	332	W-E
17T[b]	1618	610	-	-	-	-	S-N
18T	1630	610	-	-	-	-	N-S
19T	1648	1220	-	-	-	-	S-N
20T	1701	1220	-	-	-	-	N-S

[a] No detectable SO_2.

[b] T = turbulence run.

with a standard deviation within the 10 min averaging periods of 1 m/sec. The wind direction was measured as 132°M, indicating a plume heading of 310°M, with a standard deviation within the 10 min averaging periods of about 20°. The tethersonde fixed level height was only about one third of the actual plume height, and so some uncertainty exists as to the appropriate wind speed at plume height. The turbulence data from the aircraft indicated a mixed layer to above plume height. Since there are probably no significant wind shears within the mixed layer above 150 m, the adoption of the tethersonde winds for the higher levels is probably valid.

4.2.4 Isopleths and Selected Traverses

Due to the large variability between plume traverses and lack of reasonable plume cross-sections within individual traverses, reliable isopleths could not be drawn. The plume traverses on Runs 15 and 16 are shown in Figures 17 and 18. These two runs were made at the same height only a few minutes apart and yet showed considerable variation. Most of the runs encountered measurable SO_2 concentrations over a large portion of the run that led to very large σ_y values. The presence of other sources of SO_2 in the GCOS complex probably means that, for reasonable values of σ_y relating to the main plume under unstable conditions, a large value for the noise limiter is needed in the data reduction scheme to remove the effects of lower level sources.

4.2.5 Plume Geometry

The maximum concentration profiles and the integrated (along each traverse) concentration profiles are presented in Figures 19 and 20. In spite of the large fluctuations within the plume traverses, the values changed with height in a reasonable fashion. Note, however, that a puff of SO_2 was encountered at 3.2 km downwind at an altitude of over 1500 m AMSL (about 1250 m AGL), even though no SO_2 had been encountered at a lower level at 3.2 km or at the same heights at 8.0 km downwind.

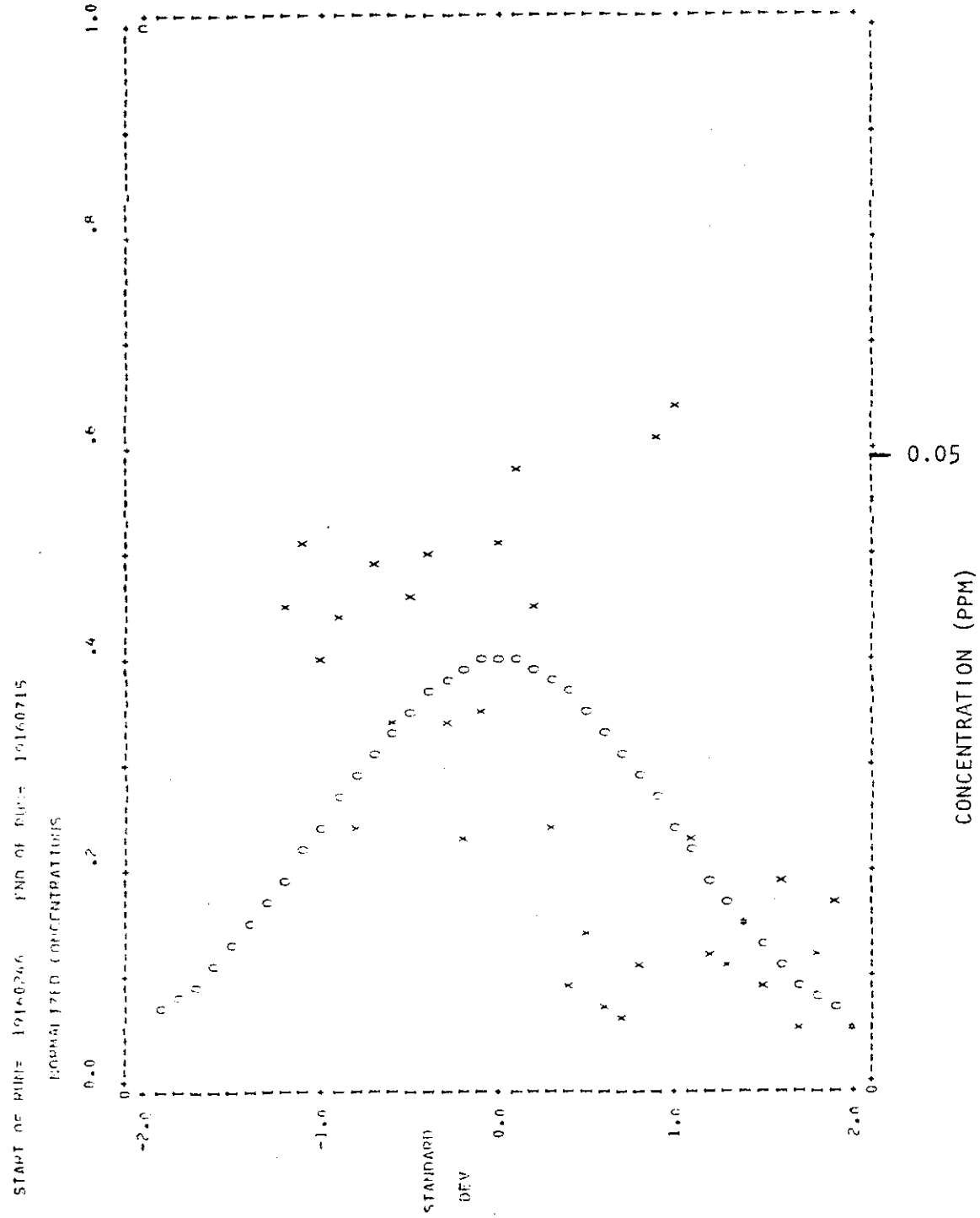

Figure 17. Normalized SO_2 concentrations for Run 15 on the flight of 19 June 1977 (1335-1735 MDT).

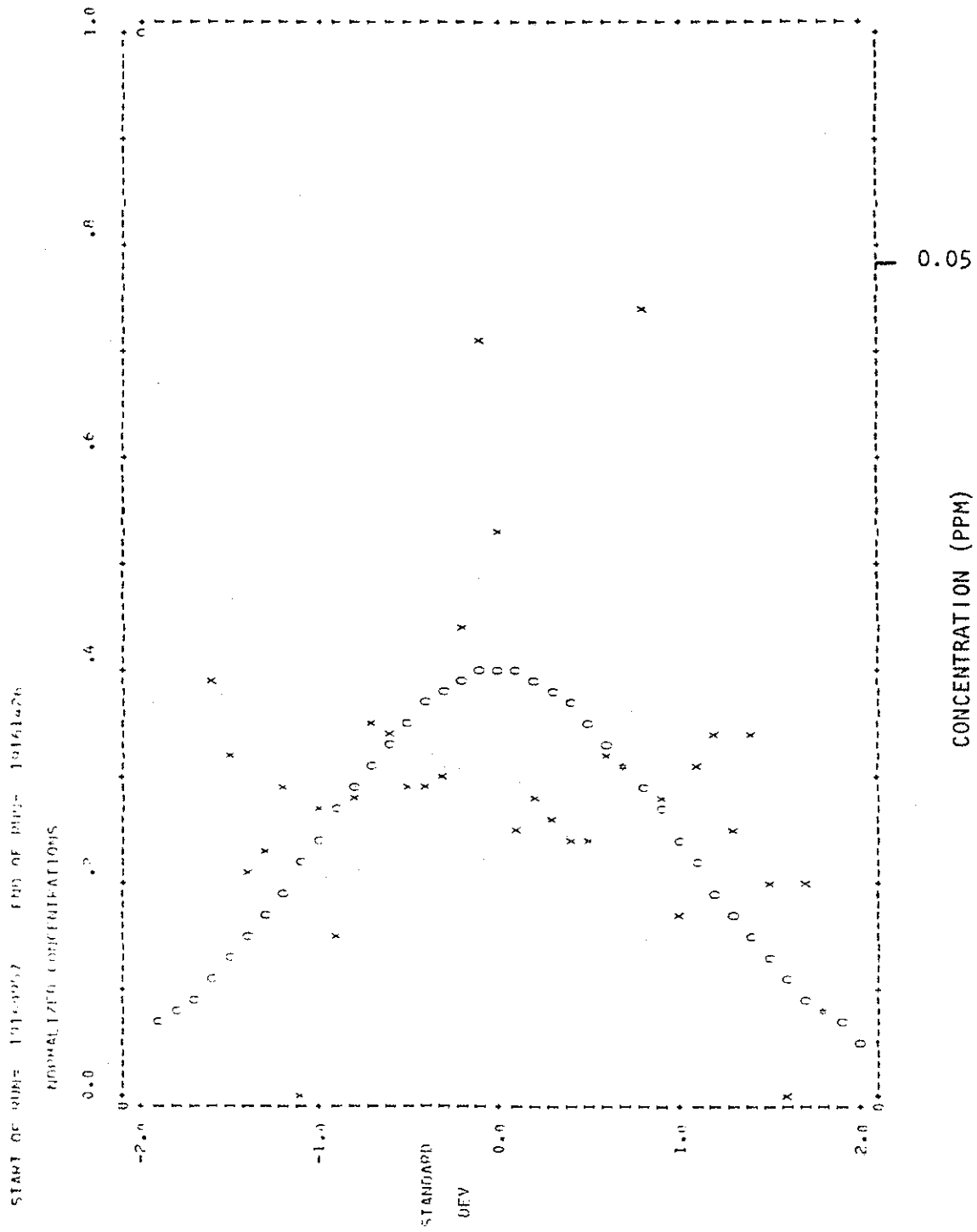

Figure 18. Normalized SO_2 concentrations for Run 16 on the flight of 19 June 1977 (1335-1735 MDT).

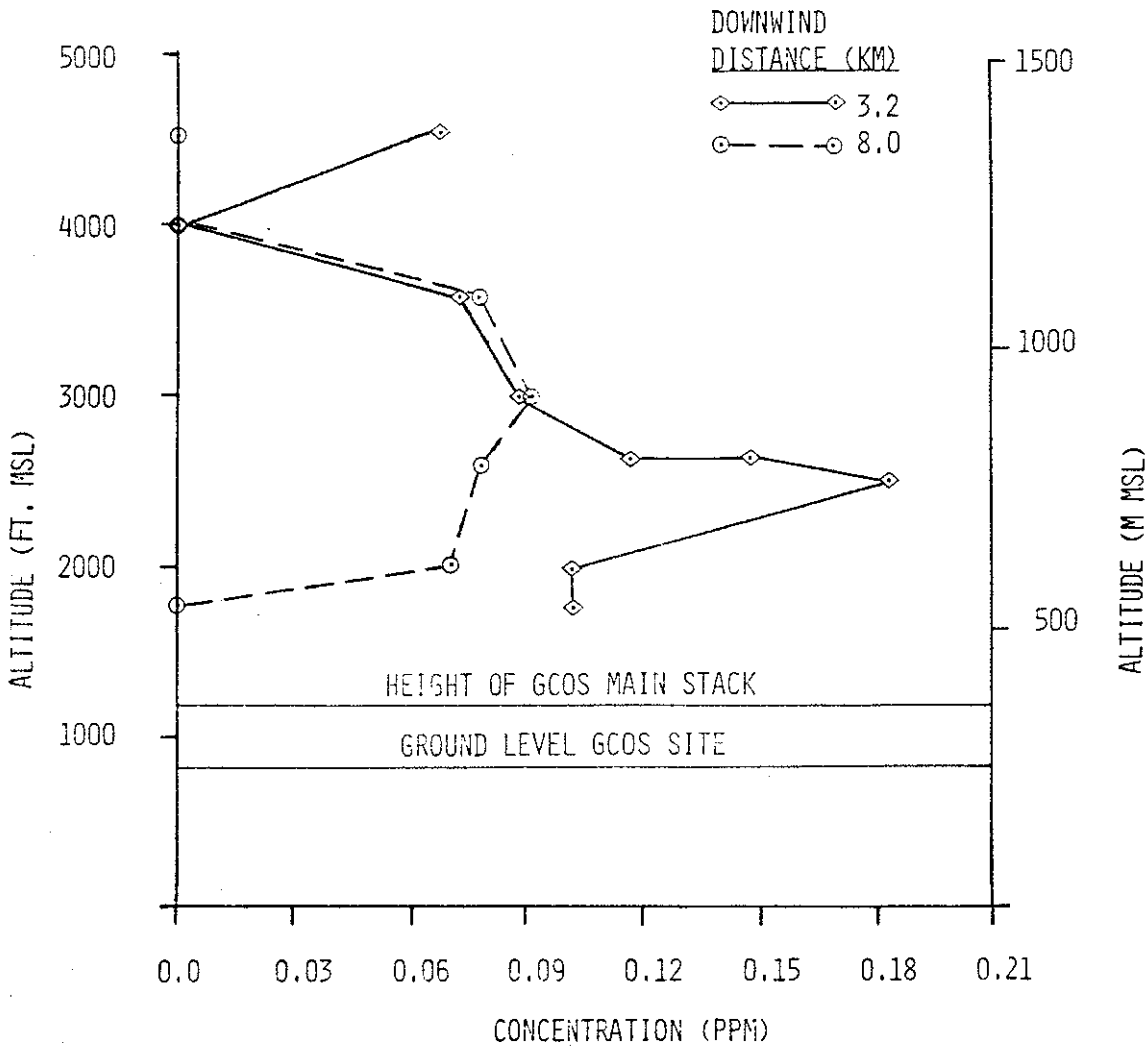

Figure 19. Maximum SO_2 concentrations along each traverse as a function of altitude for the flight of 19 June 1977 (1335-1735 MDT).

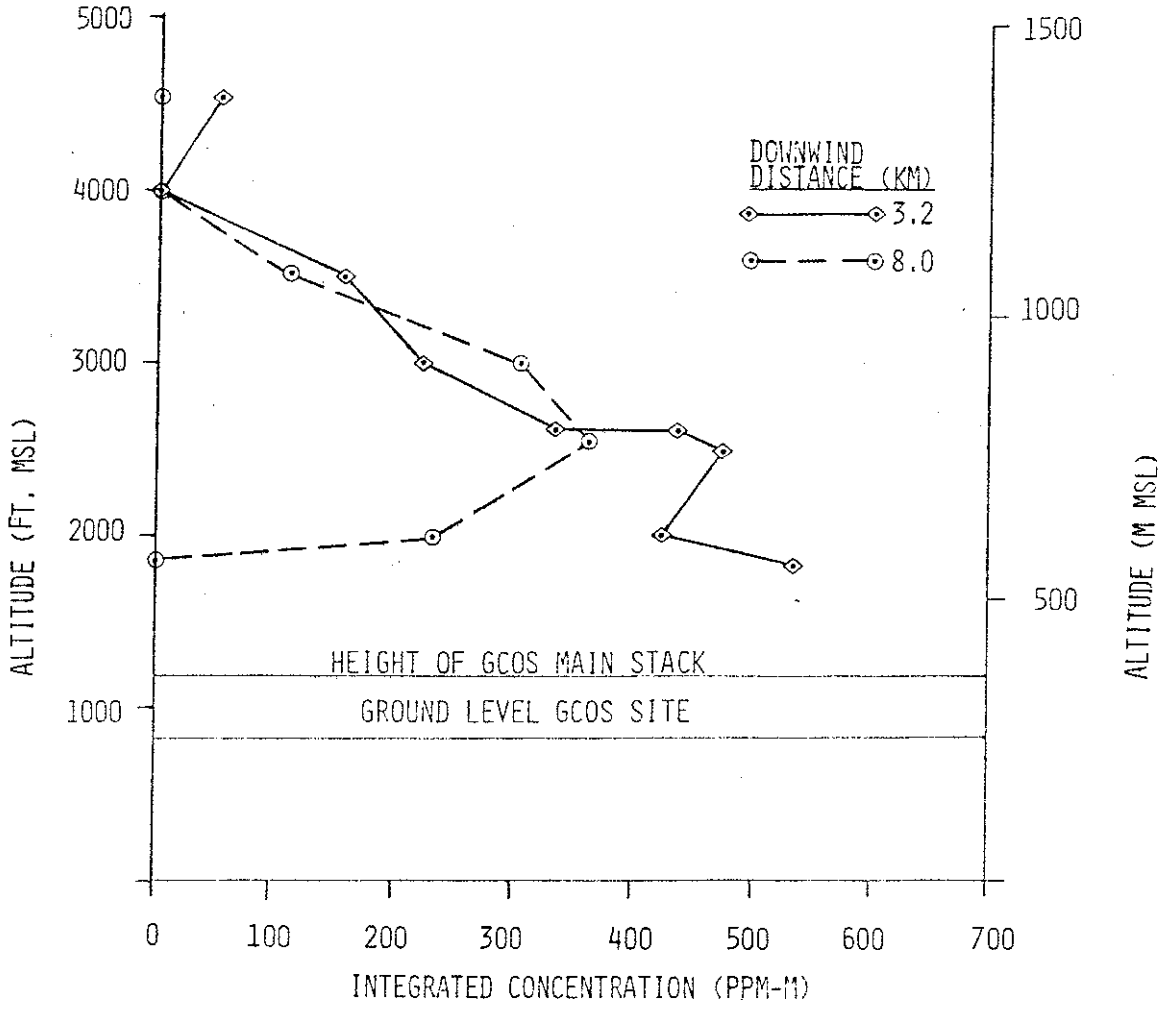

Figure 20. Integrated concentrations along each traverse for the flight of 19 June 1977 (1335-1735 MDT).

A summary of plume geometry statistics is presented in Table 5. Due to the variations in plume cross-sections, no reliable σ_y value could be estimated at 3.2 km downwind. A rough estimate was made for σ_y at 8.0 km; however, a very large uncertainty was assigned to it. Similarly, large values of uncertainty were assigned to the σ_z estimates.

The observed values for σ_y, σ_z, and normalized centerline concentrations were compared to the Pasquill-Gifford curves in Figures 21, 22, and 23. The σ_z and normalized centerline concentrations indicated slightly unstable conditions, which were present. The σ_y value, however, was much larger than the Pasquill-Gifford value. This discrepancy was at least partly due to the lack of a single source at the GCOS site.

The emission mass flux from GCOS was about 2.7 kg/sec or 9.7 long tons/h. The computed values have very good agreement considering the uncertainty in the wind speed and the integrated concentration profiles.

4.2.6 Validation of Turbulence Analysis Procedures

The data from the afternoon flight of 19 June provided an opportunity to test the validity of some of the assumptions made during the turbulence analysis. Statistics from all turbulence runs are presented in Table 6 and Figure 24.

As was mentioned in the previous section, spectral analysis indicated an extraneous peak in spectral energy in both the vertical and lateral velocities with a period of about 5 sec. The removal of this extraneous peak decreased the velocity standard deviations about 10 to 15%. However, the question remained whether any reasonable correlation between the velocity components could be made. In Table 6, the correlation $\overline{W'U'_e}$ has already been corrected for flight orientation; U'_e refers to fluctuations in the environmental longitudinal wind component. Since a racetrack pattern was flow at each level, any true wind stress should average out if the unmodified (in sign) values are averaged; this would mean that any significant residual could be due to a systematic correlation caused by a

Table 5. Plume geometry, mass flux, and plume rise for the flight of 19 June 1977 (1335-1735 MDT).

Parameter				Downwind Distance 3.2 [km]	8 [km]
$\sigma_{y_{cl}}$	Area Criterion	[m]	± 1000	[a]	3700
	Second Moment	[m]	± 1000	[a]	3900
σ_z	Upper	[m]	± 50	270	245
	Lower	[m]	± 50	270	285
	Average	[m]	± 50	270	260
$\bar{X}\bar{U}Q^{-1}$	Norm Axial Conc $10^{-6}m^{-2}$		± 0.3	1.35	0.66
SO_2	Mass Flux				
	[long tons·h^{-1}]		± 5	14	10.8
	[kg·sec^{-1}]		± 2	4	3.0
Observed centerline height		[m AMSL]	±		
(i)	Height of center of mass from max conc. profile			750	800
(ii)	Height of center of mass from integrated conc. profile			700	780
(iii)	Height of max. conc. observed			760	915
Ratio of calculated to observed effective stack height					
(i)	Briggs			0.79	
(ii)	Holland			0.49	
(iii)	TVA			1.06	

Notes: 1. For the ratio of calculated to observed effective stack height the following data were used: $\bar{U}$ = 6.7 [m/sec]; $\partial T/\partial z$ = -1.0 [°C·100 m^{-1}]. Observed effective stack height = 775 m AMSL = 515 m AGL.

[a] No reliable estimates of σ_y are availabe at 3.2 km due to wide fluctuations during plume traverse.

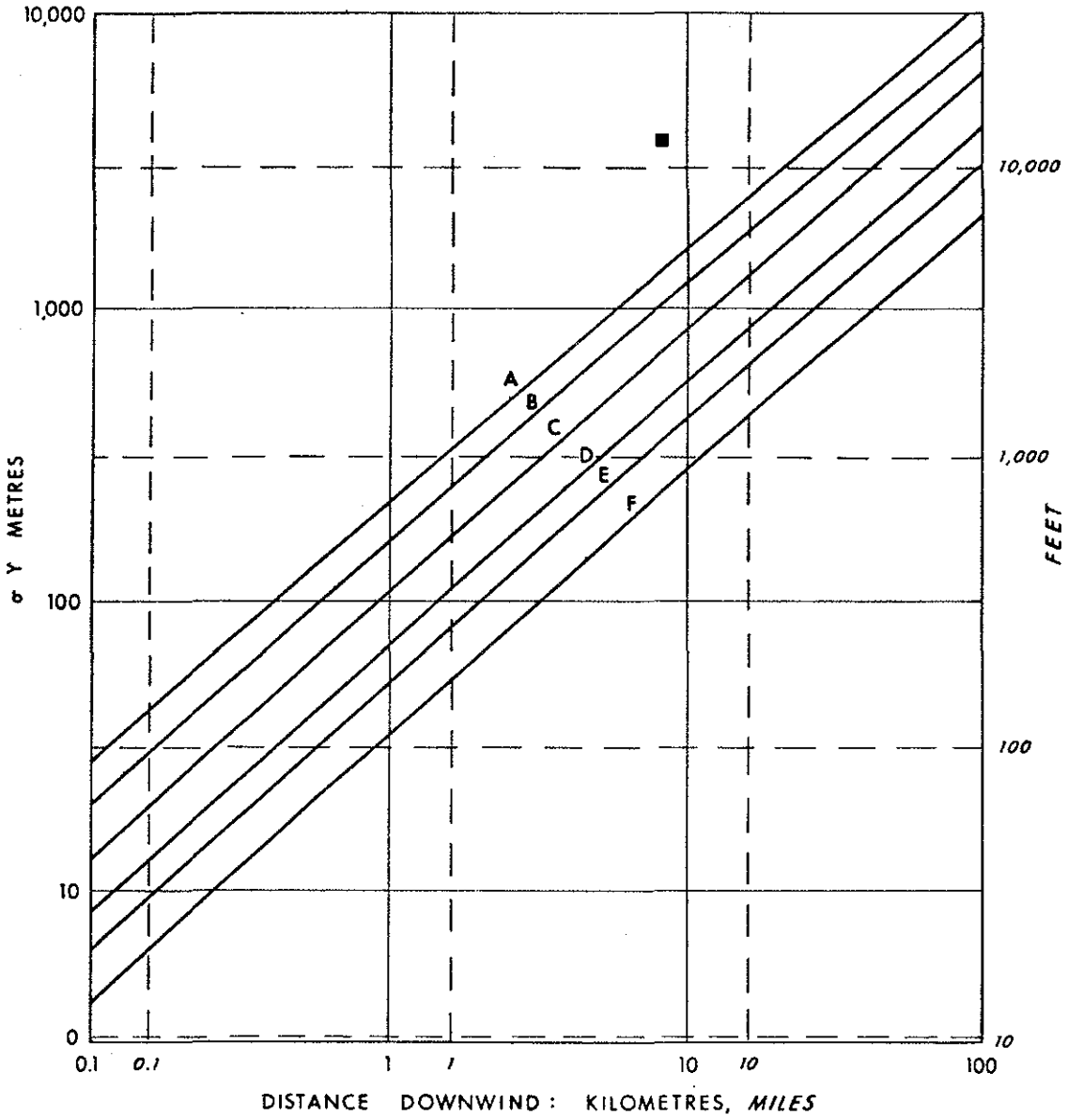

Figure 21. Observed horizontal dipsersion coefficient compared to Pasquill-Gifford curves for the flight of 19 June 1977 (1335-1735 MDT).

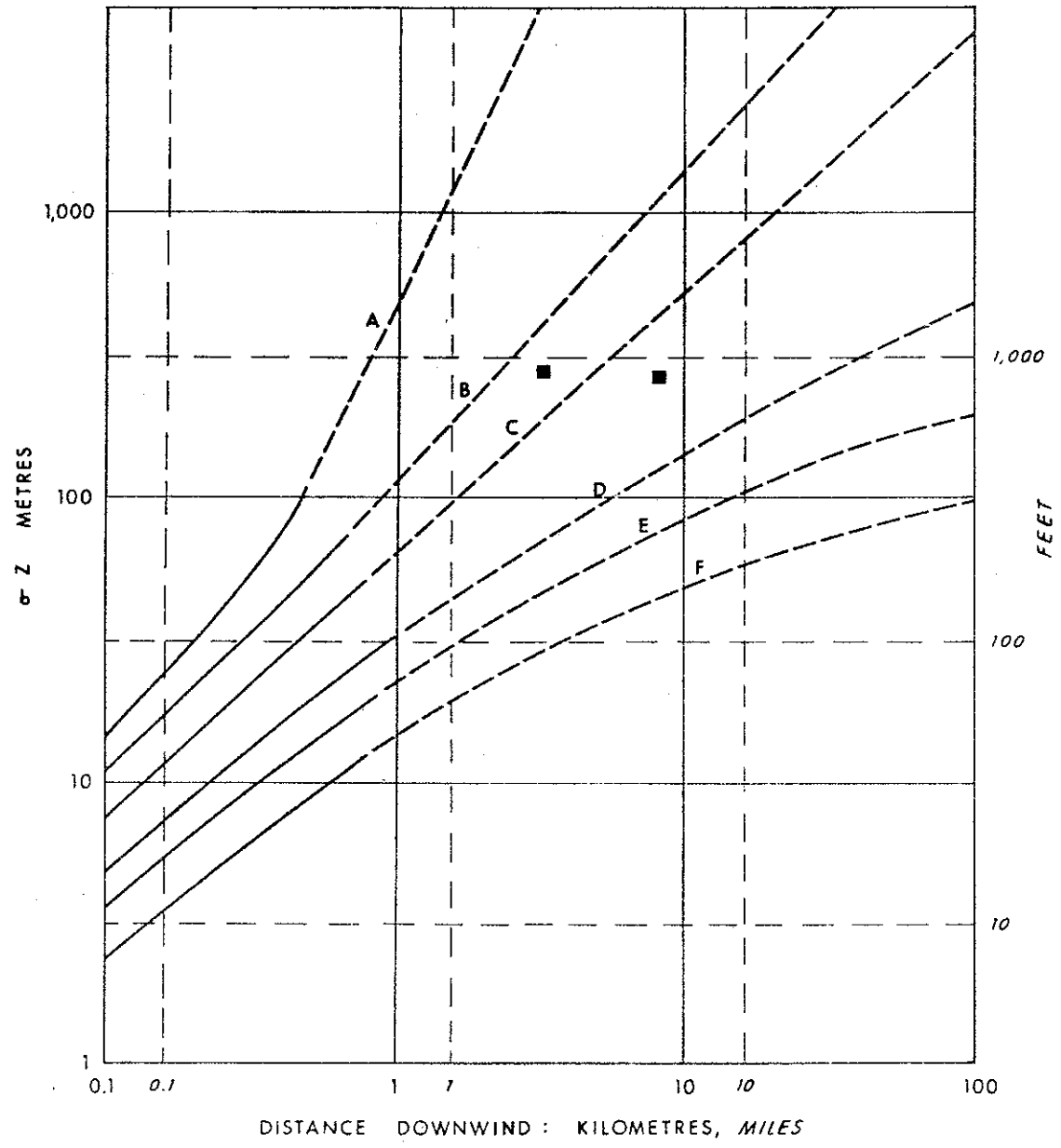

Figure 22. Observed vertical dispersion coefficient compared to Pasquill-Gifford curves for the flight of 19 June 1977 (1335-1735 MDT).

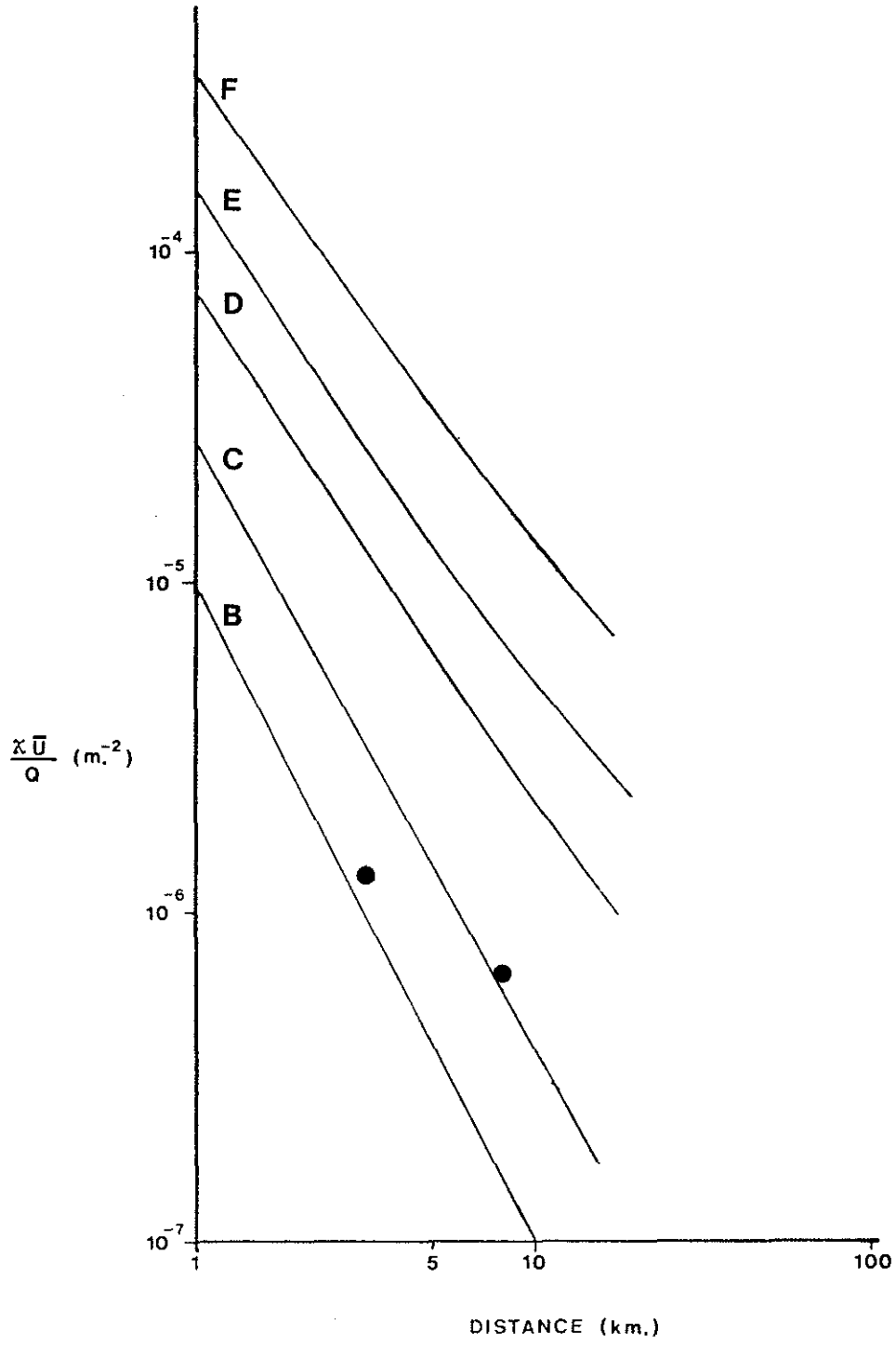

Figure 23. Comparison of observed normalized centerline concentrations with Pasquill-Gifford predictions for the flight of 19 June 1977 (1335-1735 MDT).

shortcoming in the motion removal routines or instrument calibration. Any velocity correlations arising from analysis problems should not depend upon the direction of flight with respect to the wind. Runs 1 to 16 represent eight flights towards the east and eight flights towards the west at various altitudes and with a total of 54 blocks of 64 sec duration each. The average value of $\overline{W'V'}$ without sign changes due to flight direction differences is -0.02 $(m/sec)^2$. Thus, it is reasonable to conclude that no large systematic correlation is due to any shortcomings of the motion removal procedures. This low level of correlation can be compared to the mean $\overline{W'U'}_e$ for all plume traverses between 600 and 800 m AMSL; this average value of $\overline{W'U'}_e$ = -0.40 $(m/sec)^2$ was computed with data from 20 blocks.

A second major assumption in the turbulence analysis was that the longitudinal velocity standard deviations were comparable to the lateral velocity standard deviations. The flight on the afternoon of 19 June provided data from two altitudes to test this assumption. Turbulence Runs 17 and 18 were flown at the same height (610 m AMSL) as crosswind Runs 3 and 4; similarly, Turbulence Runs 19 and 20 were flown at the same height (1220 m AMSL) as Runs 5 and 6. As can be seen in Figure 24 and Table 6, the values are comparable. At 610 m AMSL, σ_{ue} = 1.56 and σ_{ve} = 1.38 with standard deviations of the means of 0.18 and 0.08 respectively (all units are m/sec and subscript e refers to the environmental or wind-direction based coordinate system). At 1220 m AMSL, σ_{ue} = 1.37 and σ_{ve} = 1.30 with standard deviation of 0.2 and 0.06 m/sec respectively. The discrepancies are well within statistical error limits, with an average discrepancy of less than 10%. Thus, the adoption of some σ_{ue} values as approximations for σ_{ve} values when the latter are not available is a reasonable procedure.

4.2.7 Turbulence Levels Related to Plume Structure

The values for vertical and lateral velocity standard deviations with respect to the aircraft and dissipation for all runs are plotted against height in Figure 24. From a visual inspection of the graphs it appears that dissipation has a tendency to

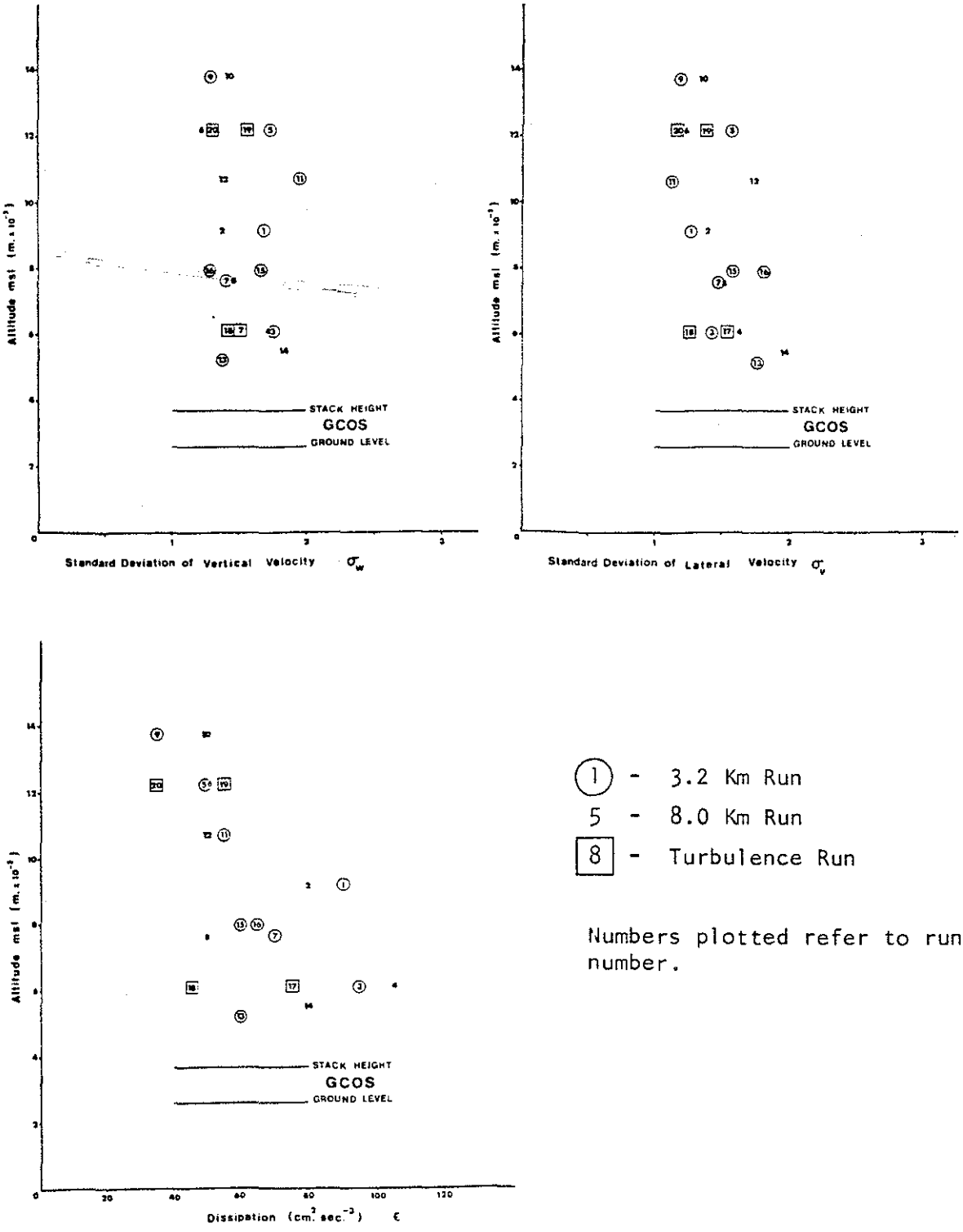

Figure 24. Turbulence data for the flight of 19 June 1977 (1335-1735 MDT).

Table 6. Turbulence statistics from each run for the flight of 19 June 1977 (1335-1735 MDT).

Run No.	HT. m MSL	X km	σ_w	σ_v	$\overline{W'V'}$	$\overline{W'T'}$	ℓ_w	ℓ_v	ϵ	N
1	915	3.2	1.69	1.28	-0.02	0.09	140	100	90	4
2	915	8.0	1.38	1.41	-0.40	-0.01	140	150	80	3
3	610	3.2	1.76	1.45	+0.03	-0.17	220	140	95	3
4	610	8.0	1.74	1.65	-0.44	0.03	170	150	105	4
5[a]	1219	3.2	1.74	1.65	-0.02	-0.03	180	230	50	2
6[a]	1219	8.0	1.22	1.25	-0.00	0.03	90	150	50	4
7	763	3.2	1.42	1.49	-0.69	0.14	140	160	70	4
8	763	8.0	1.46	1.53	-0.74	0.18	160	250	50	3
9	1373	3.2	1.30	1.20	-0.17	-0.01	160	140	35	4
10[a]	1373	8.0	1.43	1.34	0.10	0.02	250	240	50	2
11	1068	3.2	1.95	1.14	+0.39	0.00	260	90	55	4
12	1068	8.0	1.38	1.77	0.20	0.05	200	190	50	4
13	519	3.2	1.38	1.80	+0.42	0.04	190	210	60	3
14[a]	549	8.0	1.84	1.98	0.69	0.00	220	250	80	3
15	793	3.2	1.66	1.58	-0.11	-0.02	290	170	60	4
16	793	3.2	1.29	1.83	-0.42	0.05	130	230	65	3
17T	610	-	1.49	1.53	-0.34	0.13	170	140	75	5
18T	610	-	1.47	1.28	+0.13	0.06	190	130	45	8
19T	1220	-	1.57	1.39	0.08	0.05	150	160	55	7
20T	1220	-	1.30	1.21	-0.07	0.04	190	180	35	8

Notes: All units are MKS except dissipation, ϵ, which is expressed in $cm^2 \cdot sec^{-3}$.

X downwind distance from GCOS stack for crosswind flights

σ_w standard deviation of the vertical velocity

σ_v standard deviation of the lateral velocity with respect to the aircraft

$\overline{W'V'}$ product of fluctuating vertical and lateral velocities with sign changes so that crosswind flights express $\overline{W'U'}$ with respect to ground and along wind flights express $\overline{W'V'}$ with respect to ground using a right hand co-ordinate system with positive u in direction of wind.

$\overline{W'T'}$ product of fluctuating temperature and vertical velocity

ℓ_w integral length scale for vertical velocity

ℓ_v integral length scale for lateral velocity with respect to the aircraft

ϵ dissipation

N number of 65 sec analysis blocks in the run

T turbulence run flown parallel to wind

a No detectable SO_2

decrease with time and height, whereas σ_w and σ_v remain approximately constant.

The statistics from three groupings of runs are presented in Table 7. Note that the velocity standard deviation cannot be considered to be statistically different with a high degree of reliability (two standard deviations of each population of means). Nevertheless, the earlier values at 610 m AMSL (Runs 3 and 4) are somewhat larger than the values at 1220 m AMSL, and the values at about 780 m AMSL (Runs 7, 8, 15, and 16) measured about 1 h later. The dissipation values at 610 m (Runs 1 and 2) are significantly larger than the values for the other two groups of runs at higher altitudes.

The decrease in dissipation with height is not surprising. As outlined in Section 3, if the time rate of change of turbulent energy and the local energy divergence are small, then:

$$\varepsilon = u_*^2 \frac{\partial \bar{U}}{\partial Z} + \frac{g}{T} \overline{W'T'} - \frac{\partial}{\partial Z} \left(\overline{W' U'_i U'_i} \right)$$

where all symbols have usual meteorological significance and are defined in the appendix on nomenclature. If the field is convectively dominated, then the decrease of heat flux with height is approximately balanced by the divergence of the turbulent kinetic energy, leaving a constant (Kaimal et al. 1976). Note, however, that in the Minnesota study of Kaimal et al. the mixing height was constant in height and the boundary layer was vigorously convective during almost all their measurements. Thus, the more weakly convective boundary layer at GCOS may not be directly comparable. For the case of the afternoon of 19 June, convective energy is present, but mechanical energy is also being generated, probably enhanced by the topography. Thus, a slow decrease of ε with height is to be expected.

Table 7. Summary of turbulence statistics for the flight of 19 June 1977 (1335-1735 MDT).

Runs	Description	No. of Blocks	σ_w [m/sec]	σ_{uH} [m/sec]	ε [cm^2/sec^3]	ℓ_w [m]	ℓ_v [m]
3, 4	Early, lower	7	1.75	1.55	100	191	146
	Mixed layer		(0.22)	(0.18)	(23)	(24)	(30)
5, 6	Upper mixed	22	1.43	1.33	46	148	165
19, 20	layer		(0.88)	(0.07)	(5)	(23)	(15)
7, 8	Centerline	14	1.47	1.60	61	185	197
	height		(0.08	(0.09)	(10)	(37)	(22)

Note: Values in parentheses are standard deviations of the mean values.

σ_w standard deviation of vertical velocity

σ_{uH} standard deviation of lateral velocity with respect to the aircraft

ε dissipation

ℓ_w integral length scale in the vertical

ℓ_v integral length scale in the lateral direction with respect to the aircraft.

The momentum flux $\overline{W'U'}_e$ for runs between 600 and 800 m AMSL was found in the previous section to average -0.40 $(m/sec)^2$, indicating momentum transfer towards the surface, as expected. Runs 13 and 14 at altitudes between 520 and 550 m AMSL (within about 200 m of the ground) showed positive values. These values are attributed to large-scale flow effects associated with the river valley and are not considered to be turbulent momentum fluxes. The effects of topography upon the mean flow field would be expected to be most noticeable within the first 200 m of the ground. The heat flux over the same group of runs between 600 and 800 m AMSL (including the Turbulence Runs 17 and 18) averaged $\overline{W'T'} = 0.06$. A Monin-Obukhov stability can be calaculated using these elevated flux estimates as:

$$L \simeq -75 \text{ (m)}$$
$$Z/L \simeq -400/75 \simeq -5.3$$

This value of Z/L, if found in the surface layer, would indicate very unstable conditions. However, at a height of some 400 m above the ground, the height of the mixed layer may also be an important length scaling parameter.

The differences between the integral scale lengths in Table 7 are not statistically significant. As mentioned in the previous chapter, the integral scales were estimated from the integral of the velocity autocorrelation functions. The significance of the integral scales will be discussed in the next section.

The spectral plots for Runs 7, 8, 9, and 10 are presented in Figure 25. There is no low wavenumber fall-off, and the spectral shapes are similar to one another. The high wavenumber fall-offs follow the $k^{-2/3}$ prediction of similarity reasonably well although there is some scatter of data, presumably due to intermittency arising from the non-homogeneous surface.

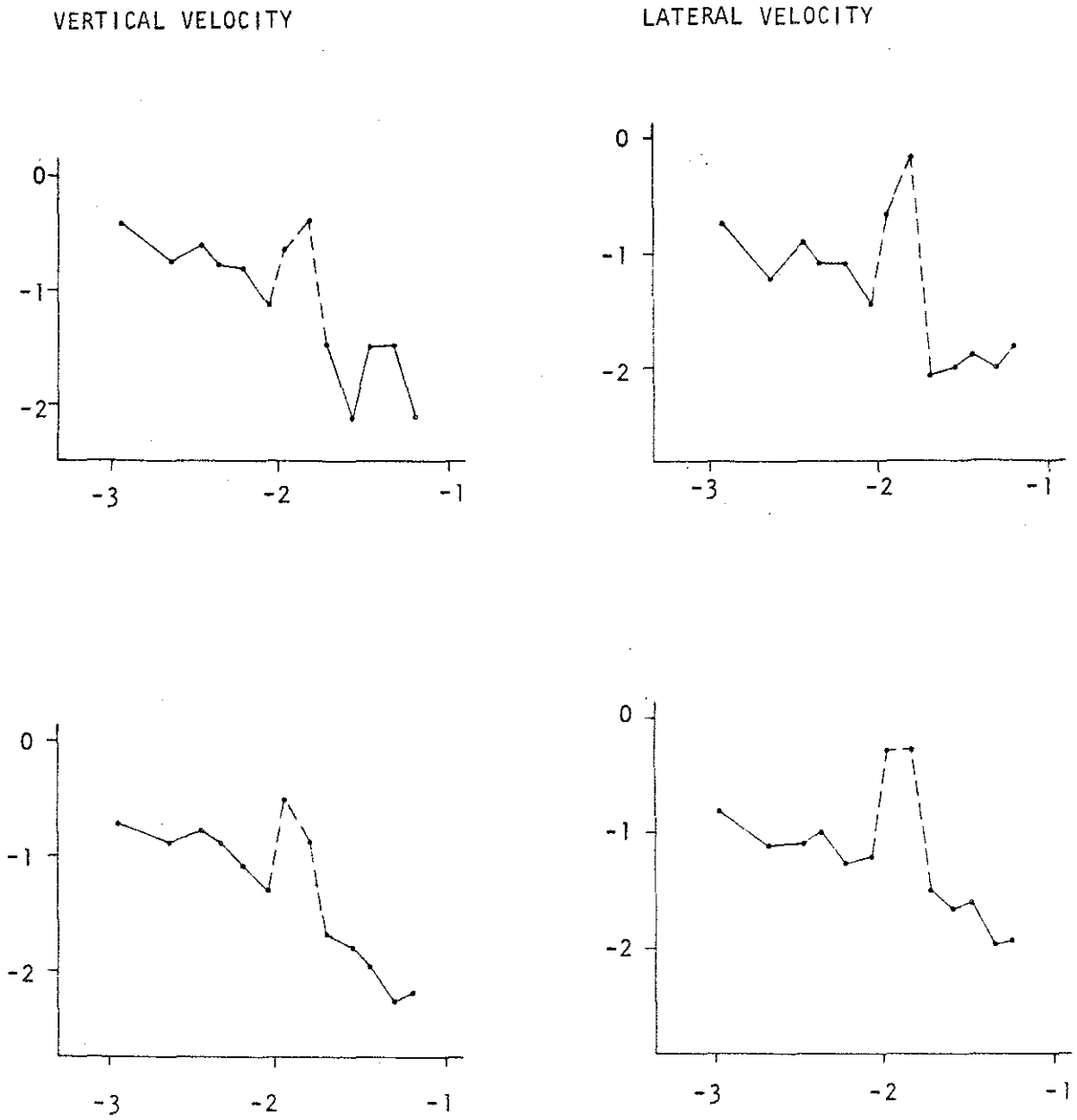

Figure 25. Spectral plots for the flight of 19 June 1977 (1335-1735 MDT). All plots are LOG $\left(\frac{K\ \phi\ (K)}{\sigma^2}\right)$ versus LOG K where K is wavenumber (m^{-1}). From top to bottom the run groups are: 7, 8; 15, 16.

4.3 CASE STUDY FOR THE FLIGHT OF 19 JUNE 1977 (1000-1500 MDT)

4.3.1 Visual Plume Description

The plume was approached shortly after 1000 MDT; it visually appeared to be fumigating to the surface. The plume centerline had a heading of 320°M, based upon airborne visual observations. There was about 0.8 altocumulus cloud cover, the wind was from the south, and a cold frontal passage was expected late in the day. At 1253 MDT during a traverse at 840 m AMSL, the flight was intermittently smooth, indicating that the top of the mixed layer was being encountered. By 1440 MDT, the turbulence flights at 1070 m AMSL were bumpy. Thus, the mixed layer clearly had risen throughout the flight. Figure 26 shows the plume at 1318 MDT near the end of the plume traverses.

4.3.2 Flight Profiles

The flight map and some of the SO_2 concentration statistics for the plume traverses are presented in Figure 27 and Table 8. The plume traverses were followed by turbulence runs parallel to the wind in the same fashion as for the afternoon flight of 19 June. However, for the 20 June flight, there were indications of lack of stationarity, which might limit the applicability of the data from the turbulence runs for plume spread normalization.

4.3.3 Tethersonde Data

The AES tethersonde profile commencing at 1243 MDT is shown in Figure 28. The mean wind speed near 300 m AGL (or 545 m AMSL) was about 5-6 m/sec; the lapse rate was adiabatic to the top of the profile about 600 m MSL.

4.3.4 Isopleths and Selected Traverses

The SO_2 concentration isopleths based upon plume traverses at eight heights are shown in Figure 29. The isopleths suggest a large SO_2 vertical gradient near the top of the plume at 3.2 km downwind. The visual observation of apparent fumigation to the surface was utilized in drawing the isopleths.

Figure 26. Plume photograph for the flight of 20 June 1977 (1000-1500 MDT). The photograph was taken at 1318 MDT from approximately 11 km west and 3 km north of GCOS at an altitude of 760 m AMSL.

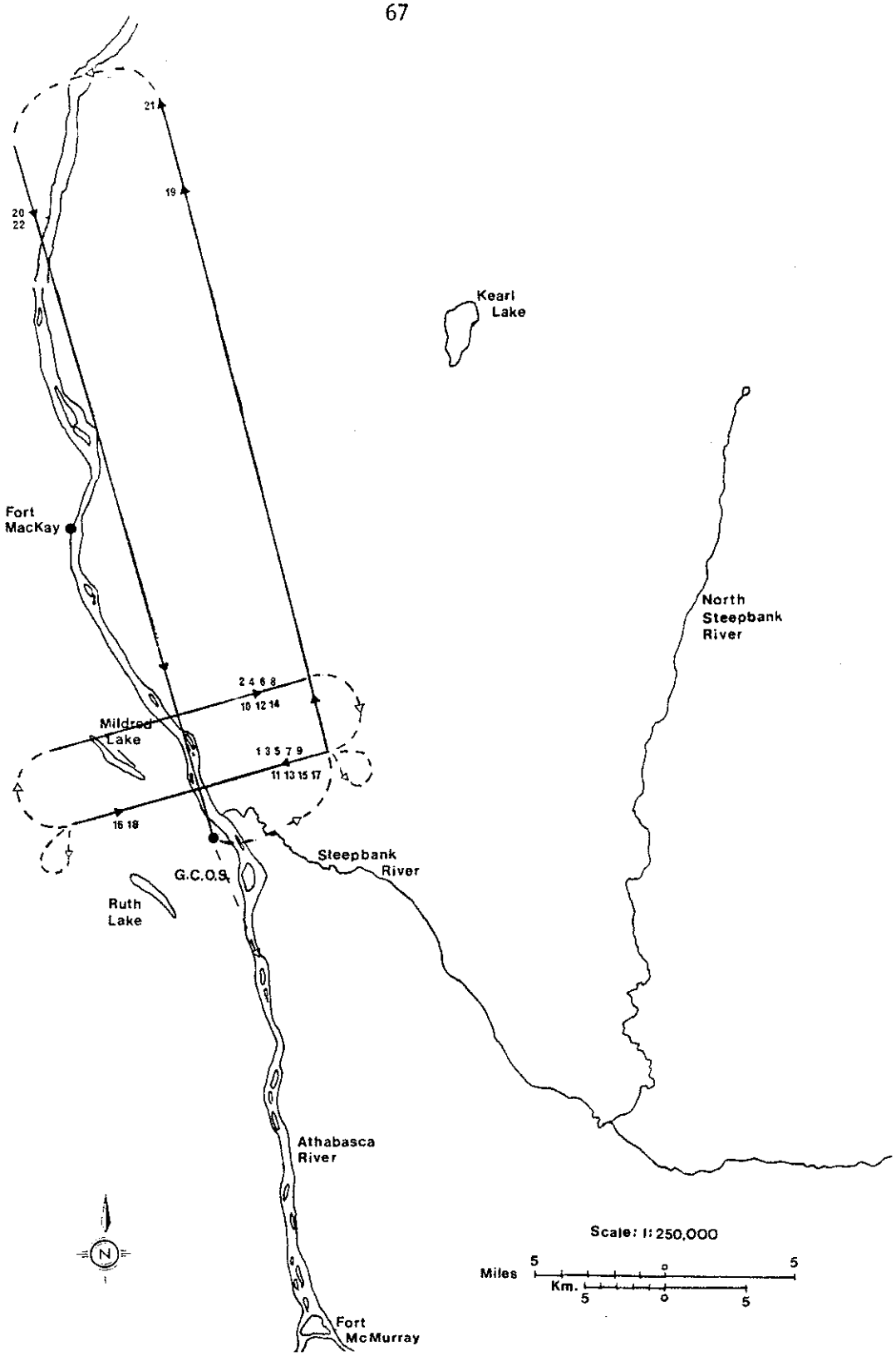

Figure 27. Flight profiles for 20 June 1977 (1000-1500 MDT).

Solid lines denote numbered runs and dashed lines denote interconnecting legs.

Table 8. Run information for the flight of 20 June 1977 (1000-1500 MDT).

Run Number	Start Time (MDT)	Altitude (m MSL) ± 20	Downwind Distance (km) ± 0.3	σ_y (m) ± 100	Max. SO_2 Conc. (ppm) ± 0.02	Integrated Conc. (ppm-m) ± 50	Flight Dir. (From-to)
1	1131	763	3.2	501	0.47	471	E-W
2	1137	763	8.0	726	0.24	384	W-E
3[a]	1146	1070	3.2	-	-	-	E-W
4[a]	1153	1070	8.0	-	-	-	W-E
5	1202	610	3.2	443	0.23	231	E-W
6	1208	610	8.0	1137	0.21	377	W-E
7[a]	1217	915	3.2	-	-	-	E-W
8	1224	915	8.0	6745	0.04	29	W-E
9	1231	519	3.2	585	0.35	406	E-W
10	1237	519	8.0	699	0.23	318	W-E
11	1246	839	3.2	516	0.64	552	E-W
12	1253	839	8.0	401	0.08	78	W-E
13	1259	686	3.2	508	0.38	387	E-W
14	1306	686	8.0	972	0.20	426	W-E
15	1313	763	3.2	502	0.20	195	E-W
16	1321	763	3.2	559	0.62	608	W-E
17	1335	839	3.2	534	0.25	276	E-W
18	1341	839	3.2	361	0.35	250	W-E
19T[b]	1350	763	-	-	-	-	S-N
20T	1402	763	-	-	-	-	N-S
21T	1421	1070	-	-	-	-	S-N
22T	1435	1070	-	-	-	-	N-S

[a] No detectable SO_2.

[b] T = turbulence run.

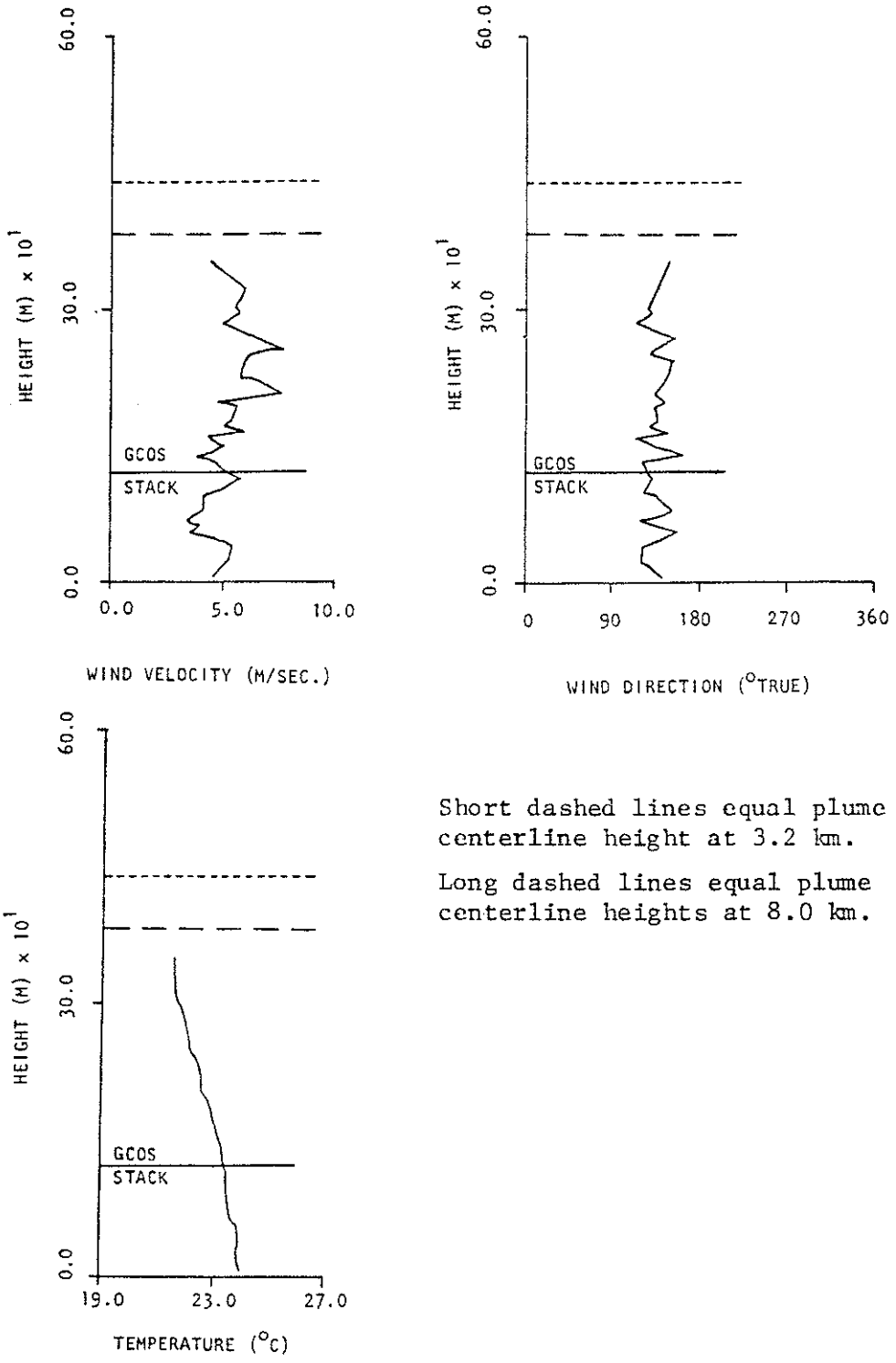

Short dashed lines equal plume centerline height at 3.2 km.

Long dashed lines equal plume centerline heights at 8.0 km.

Figure 28. Tethersonde profiles for 20 June 1977, 1243 MDT. Data supplied by R. Mickle, AES.

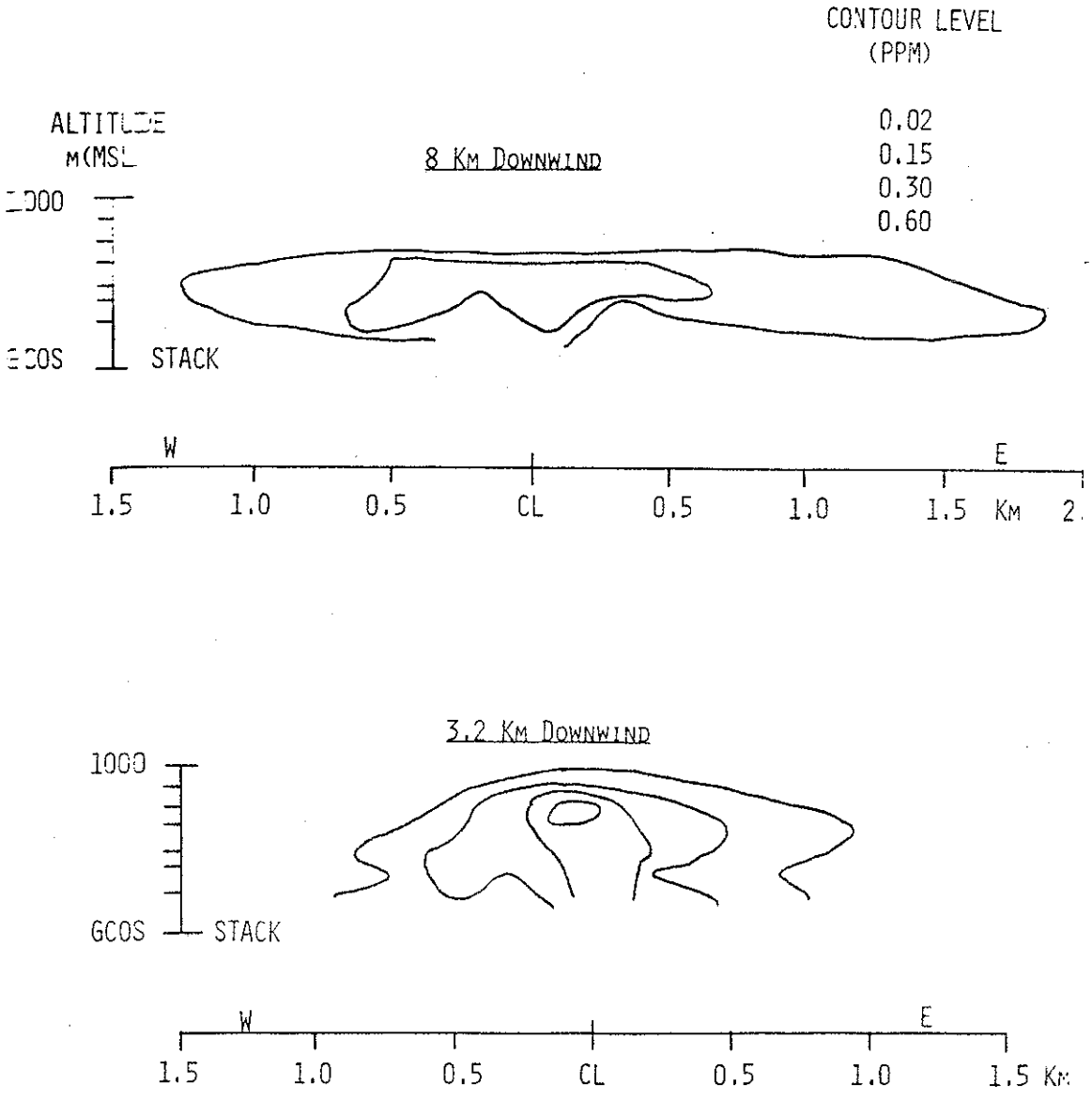

Figure 29. SO_2 concentration isopleths for the flight of 20 June 1977 (1000-1500 MDT).

NOTE: 8.0 km Isopleth has a 2X vertical exaggeration.
3.2 km Isopleth has no vertical exaggeration.
Dashes on the left side of the vertical axes are flight levels.

In marked contrast to the afternoon of 19 June, the plume traverses on 20 June showed consistently well formed SO_2 concentration profiles. Occasionally there were double peaks, but the σ_y values were, for the most part, representative of the main plume geometry. The plume traverses for Runs 1 and 2 at 763 m AMSL and at 3.2 and 8.0 km downwind respectively are shown in Figures 30 and 31. The plume cross-sections are both slightly more peaked than a Gaussian of the same area, but generally are reasonably approximated by the Gaussian. All of the plume traverses are presented in Appendix 8.5.

4.3.5 Plume Geometry

The maximum concentration profile is shown in Figure 32 and a summary of plume geometry statistics in Table 9. Note that the concentration scale in Figure 32 is a factor of 10 larger than for the corresponding Figure 19 for 19 June afternoon. The σ_y estimates are much better defined than for 19 June. There was an indication from the turbulence data to be presented below that the changes in meteorological conditions could have resulted in a plume that widened throughout the time of the flight. Thus, in Table 9, a second value of σ_y more appropriate for conditions later in the flight has been added. This second value is used in the discussion of normalized plume spread behaviour in the next section.

The observed values of σ_y, σ_z, and normalized axial concentrations were compared to the Pasquill-Gifford curves in Figures 33, 34, and 35. In Figure 34, the multiple σ_z values correspond to the upper, lower, and average σ_z values where they are significantly different.

The observed centerline height showed considerable difference among the methods of computation. The maximum concentration was found to be over 100 m higher than the centers of mass computed either from the maximum concentration or integrated concentration profiles. The physical situation giving rise to the difference is not uncommon: fumigation below a capping inversion. The average of the center of mass heights was used in comparisons with the predicted plume rises.

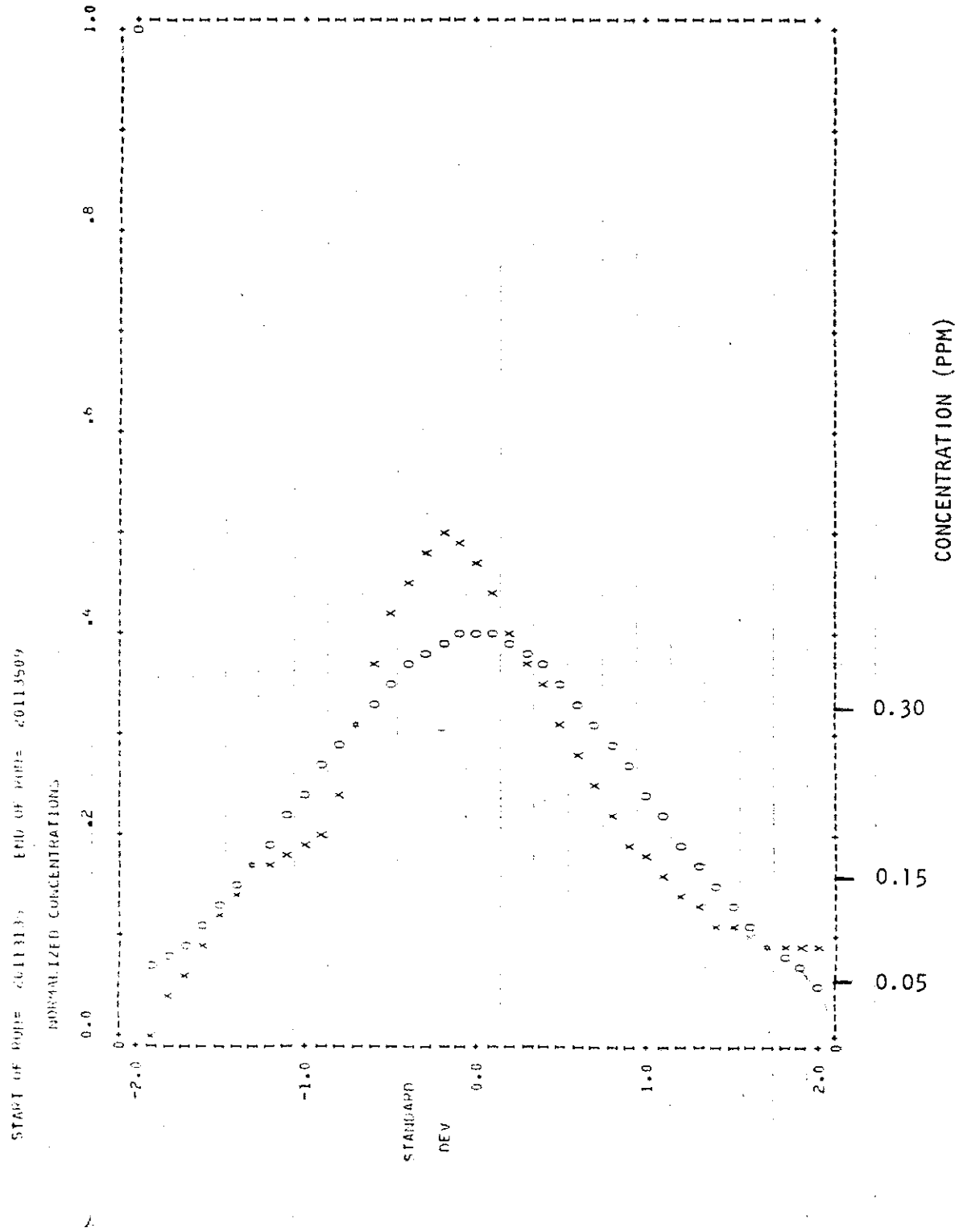

Figure 30. Normalized SO_2 concentrations for Run 1 on the flight of 20 June 1977 (1000-1500 MDT).

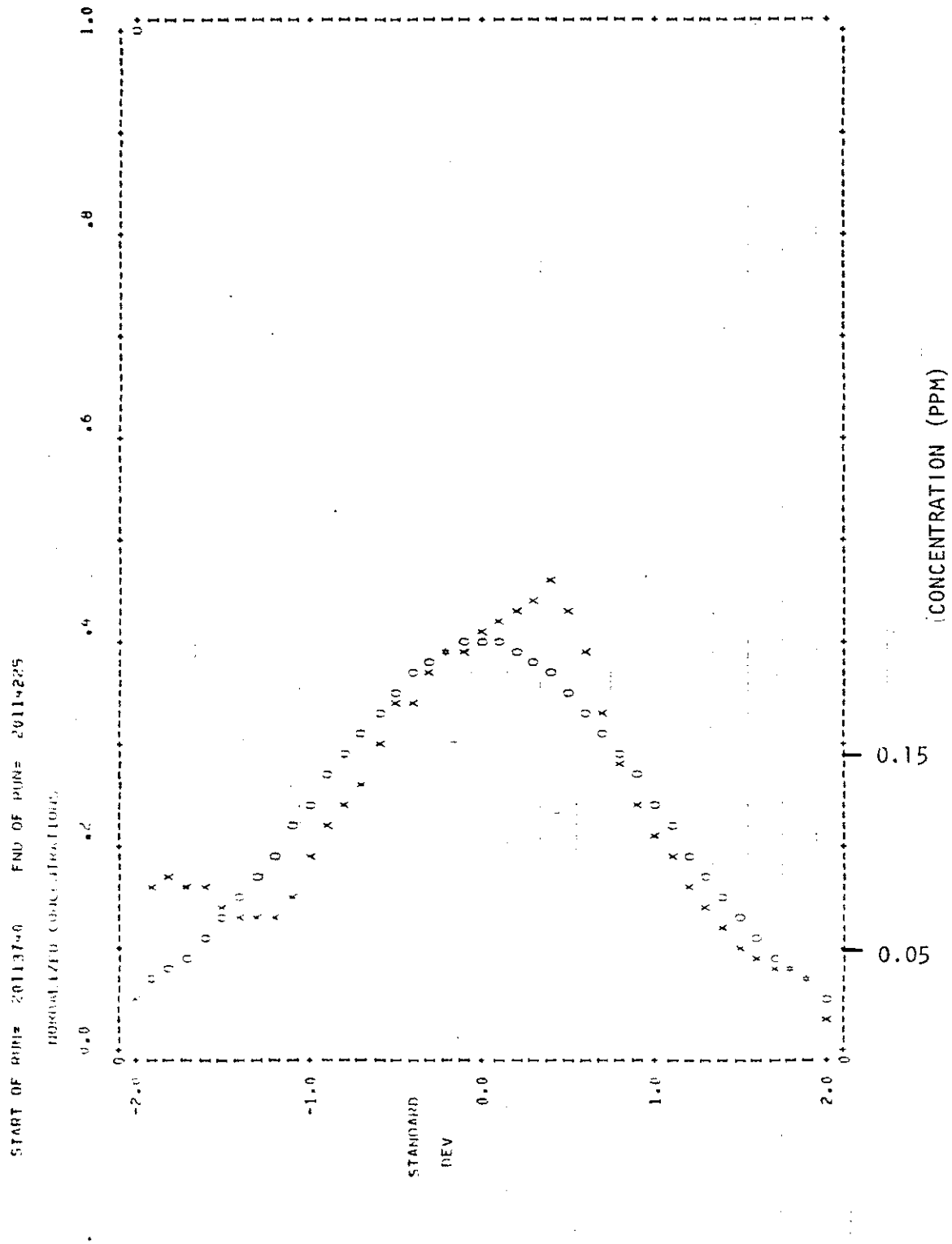

Figure 31. Normalized SO_2 concentrations for Run 2 on the flight of 20 June 1977 (1000-1500 MDT).

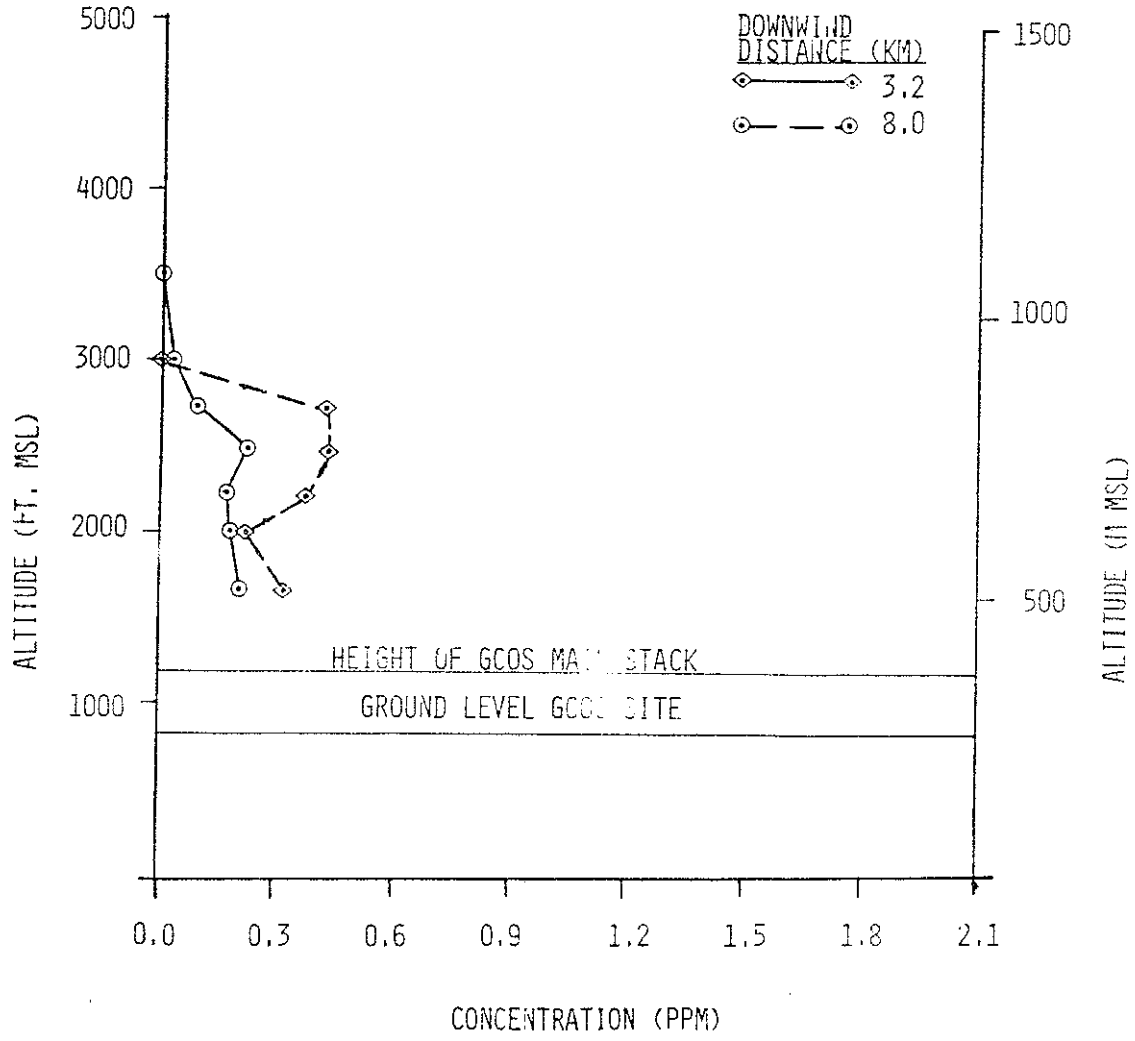

Figure 32. Maximum SO_2 concentrations along each traverse as a function of altitude for the flight of 20 June 1977 (1000-1500 MDT).

Table 9. Plume geometry, mass flux, and plume rise for the flight of 20 June 1977 (1000-1500 MDT).

Parameter			Downwind Distance 3.2 [km]	8 [km]
σ_{y}cl	Area Criterion [m]	± 20	520	725 970+
	Second Moment [m]	± 20	630	725 880+
σ_z	Upper [m]	± 20	120	155
	Lower [m]	± 30	220	195
	Average [m]	± 20	170	175
$X\bar{U}Q^{-1}$	Norm Axial Conc $10^{-6}m^{-2}$	± 0.3	3.3 (2.0)[a]	1.1
SO_2	Mass Flux			
	[long tons·h^{-1}]	± 3	11.0	8.2
	[kg·sec^{-1}]	± 1	3.1	2.3
Observed centerline height [m MSL]		± 20		
(i)	Height of center of mass from max conc. profile		700	610
(ii)	Height of center of mass from integrated conc. profile		710	630
(iii)	Height of max. conc. observed		840	760
Ratio of Calculated to Observed Effective Stack Height				
(i)	Briggs		1.16	
(ii)	Holland		0.69	
(iii)	TVA		1.41	

Notes: 1. For the ratio of calculated to observed effective stack height, the following data were used: $\bar{U}$ = 5.8 [m/sec]; $\partial T/\partial z$ = 0.8 [°C·100 m^{-1}]. Observed effective stack height = 655 m AMSL = 395 m AGL.

2. Value in parentheses is the normalized axial concentration taken at the height of the center of mass of the maximum concentration profile; the other value is at the height of the maximum concentration observed.

[a]Late afternoon σ_y; see text for discussion.

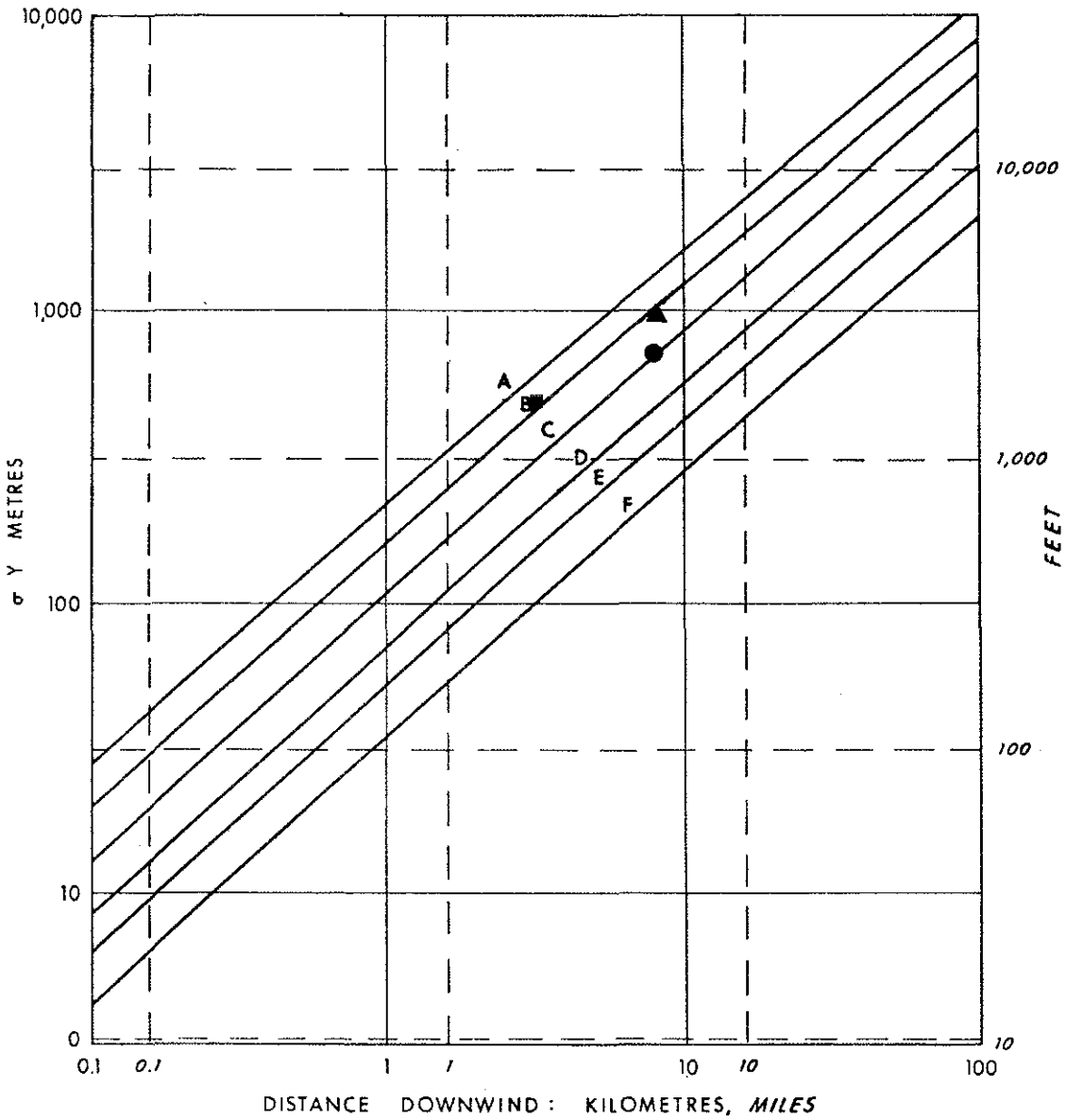

Figure 33. Observed horizontal dispersion coefficient compared to Pasquill-Gifford curves for the flight of 20 June 1977 (1000-1500 MDT).

● (1130-1230 MDT)
▲ (1230-1340 MDT)
■ (1000-1500 MDT)

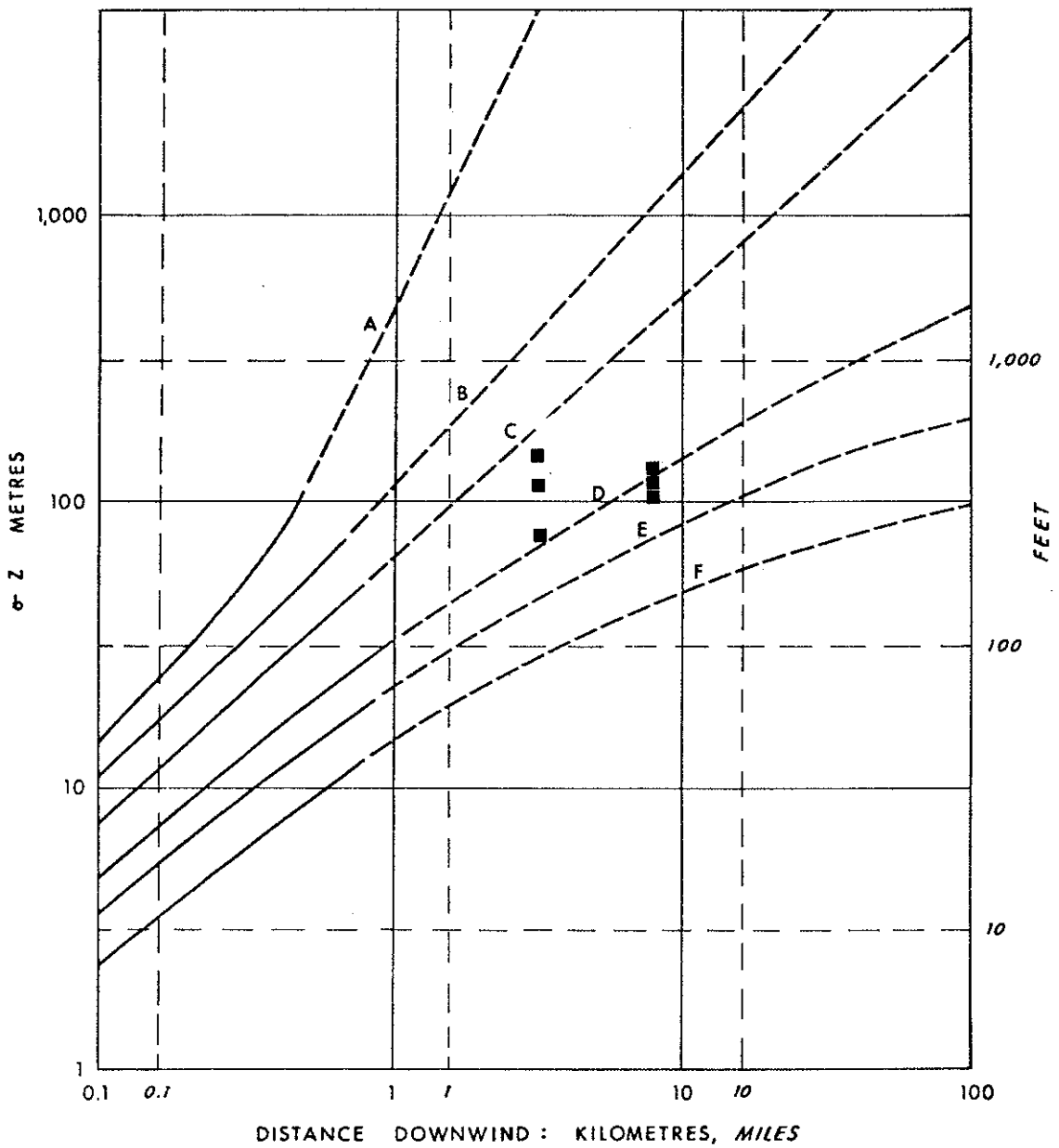

Figure 34. Observed vertical dispersion coefficient compared to Pasquill-Gifford curves for the flight of 20 June 1977 (1000-1500 MDT).

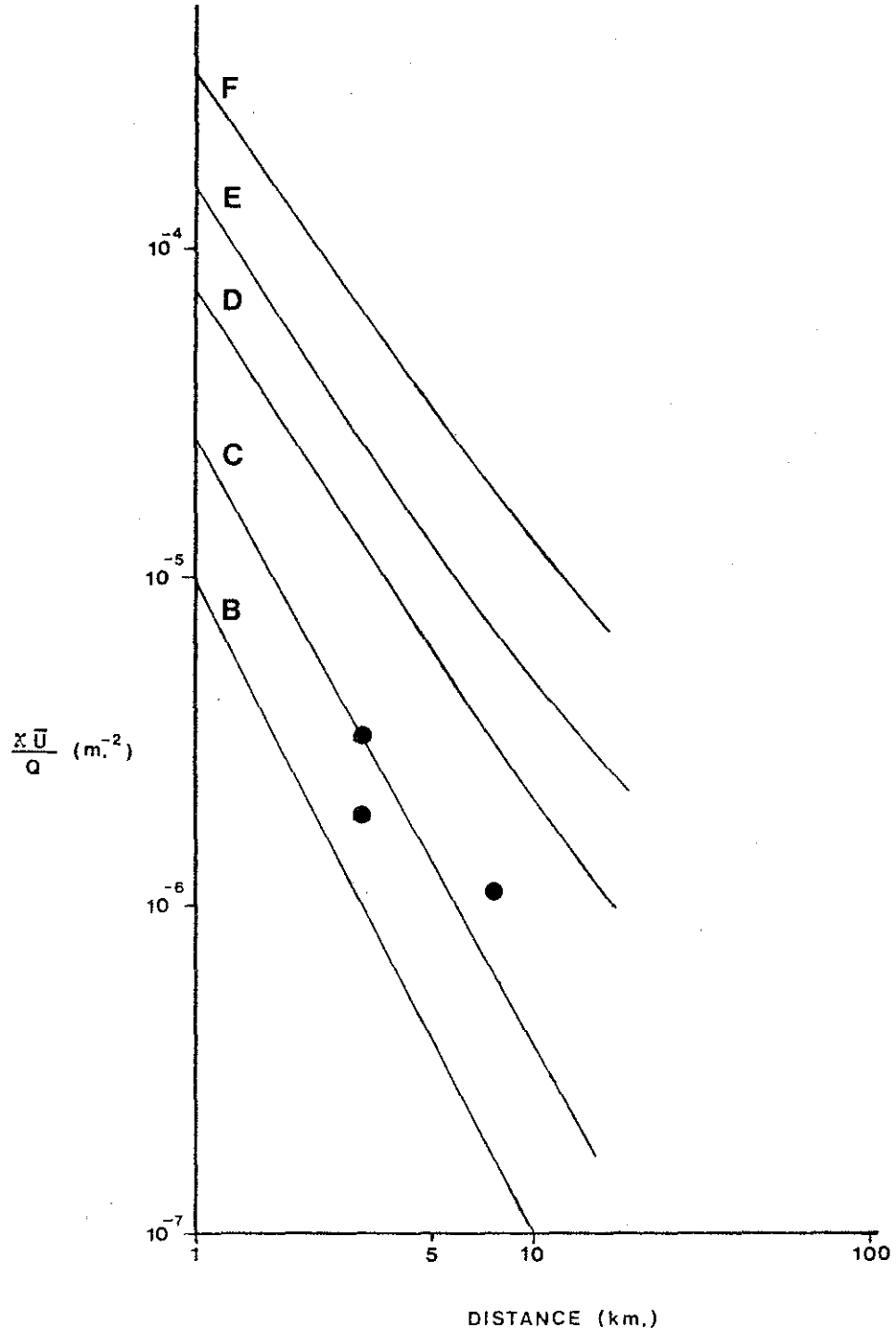

Figure 35. Comparison of observed normalized centerline concentrations with Pasquill-Gifford predictions for the flight of 20 June 1977 (1000-1500 MDT).

4.3.6 Turbulence Levels Related to Plume Structure

The values for dissipation and for vertical and lateral velocity standard deviations with respect to the aircraft for all runs are plotted as functions of height in Figure 36.

There are marked time changes in the statistics that are most noticeable for the dissipation values. The first 11 runs show a marked decrease of dissipation with height. Field notes described Run 12 as intermittently smooth, indicating that the edge of the mixed layer was at about 840 m AMSL at 1250 MDT. Note that the dissipation value for Run 12 is midway between the values for the smooth Run 11 and later values of Runs 17 and 18. The Turbulence Runs 19, 20, 21, and 22 all had quite large dissipation values compared to earlier runs.

The velocity standard deviations also show the rise of the mixed layer and the increase in turbulent energy throughout the afternoon in the lower and middle portions of the mixed layer. It is clear that the turbulence statistics from the turbulence runs cannot be directly applied for plume spread normalization. In the next section, this flight is broken into early and later sections for plume spread normalization, with Runs 1 and 2 and Runs 15 and 16 being used to typify the centerline turbulence for the two cases.

The turbulence statistics from four groups of runs are presented in Table 10. It can be seen that the differences between the early and later centerline conditions are statistically significant. The average heat flux for Runs 15 to 22 was $\overline{W'T'} = 0.06$ ($^{\circ}$C-m/sec), comparable to the values from the afternoon flight of 19 June. The friction velocity, u_*, however, averaged only 0.22 m/sec. for Runs 9, 10, 15, 16, 17, and 18. Thus, indications are that the afternoon of 20 June was more convectively dominated than the afternoon of 19 June.

The integral length scales shown in Table 10 had much lower standard deviations than the values from the afternoon of 19 June. The integral scales for the group of runs representing the stable conditions above the inversion had much longer integral scales than the groups of runs in the mixed layer.

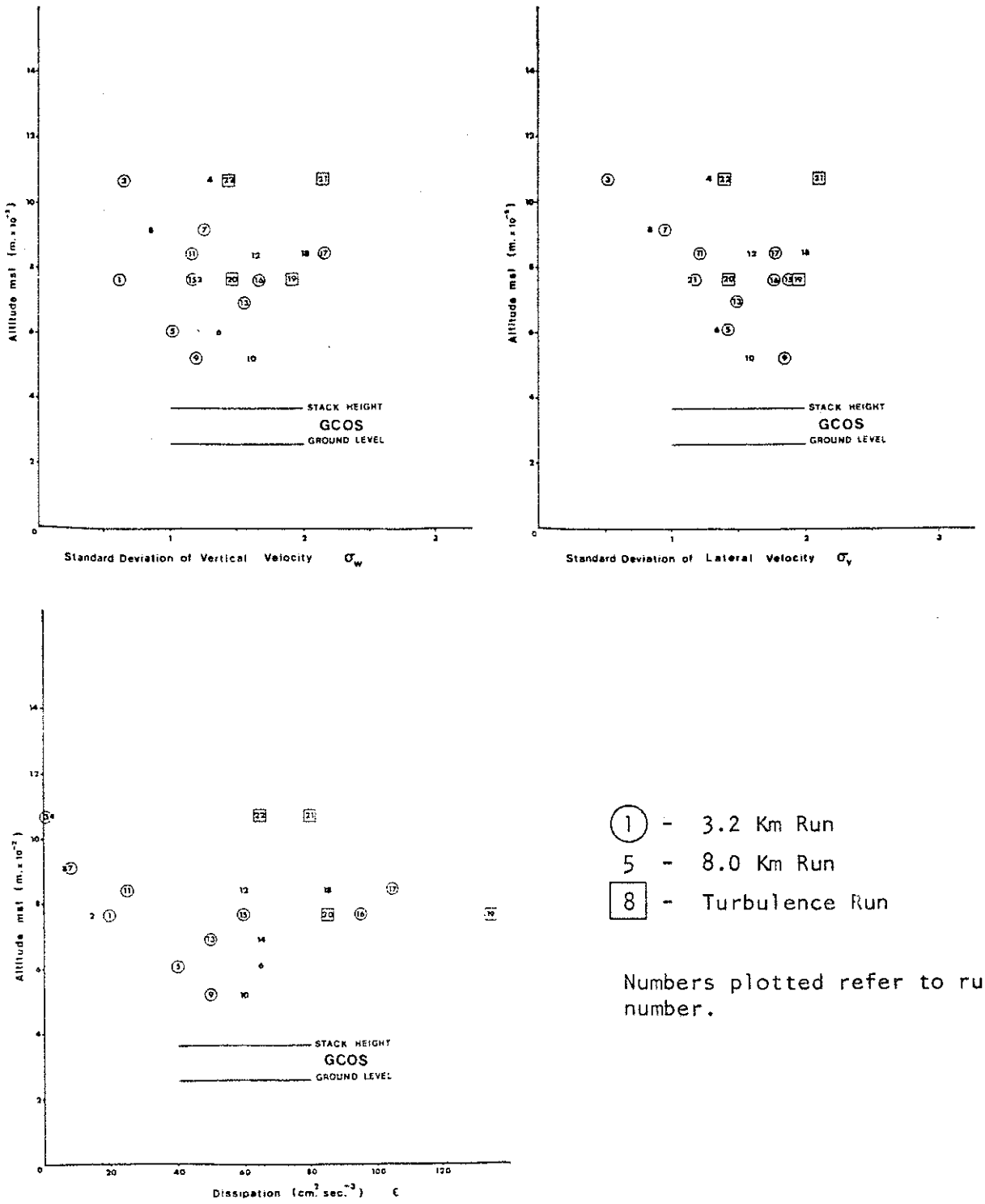

Figure 36. Turbulence data for the flight of 20 June 1977 (1000-1500 MDT).

Table 10. Summary of turbulence statistics for the flight of 20 June 1977 (1000-1500 MDT).

Runs	Description	Mean Height [m-AMSL)	No. of Blocks	σ_w [m/sec]	σ_{uH} [m/sec]	ε [cm^2/sec^3]	ℓ_w [m]	ℓ_v [m]
1, 2	Early	760	4	0.91	1.18	16	170	190
	centerline			(0.15)	(0.18)	(3)	(56)	(48)
3, 4	Early above	1000	13	0.96	0.86	5	280	355
7, 8	inversion			(0.12)	(0.08)	(1)	(12)	(12)
5, 6	Lower mixed	570	11	1.29	1.57	53	145	200
9, 10	layer			(0.13)	(0.14)	(6)	(12)	(10)
15, 16	Later,	760	8	1.42	1.83	78	140	210
	centerline			(0.13)	(0.09)	(7)	(16)	(29)

Notes: Values in parentheses are standard deviations of the mean values.

σ_w standard deviation of vertical velocity

σ_{uH} standard deviation of lateral velocity with respect to the aircraft

ε dissipation

ℓ_w integral length scale in the vertical

ℓ_v integral length scale in the alteral direction with respect to the aircraft.

The normalized spectral plots for the vertical and later velocities from Runs 1 and 2 and from Runs 15 and 16 are shown in Figure 37. For both groups of runs, the vertical velocity spectra appear to have levelled off and perhaps are beginning to fall off at the low wavenumber end of the spectrum.

4.4 CASE STUDY FOR THE FLIGHT OF 22 JUNE 1977 (1915-2305 MDT)

4.4.1 Visual Plume Description

This flight commenced in the early evening when the plume was oriented in an easterly direction with a heading of 070°M within a weakly mixed layer. As the evening progressed, a surface-based radiation inversion began to develop, creating a stable lower layer and a weakly mixed neutral upper layer. The three photographs in Figure 38 show the plume behaviour during the transition from daytime to late evening conditions.

4.4.2 Flight Profiles

The flight map and run information are presented in Figure 39 and Table 11. Runs 14 and later were treated as representing "evening" conditions, whereas the early runs were treated as "afternoon" runs. Since the flight was being made in conditions known to be changing, the maximum number of plume traverses was desired, and so no turbulence runs parallel to the wind were flown.

4.4.3 Tethersonde Data

The AES tethersonde profile commencing at 1950 MDT is presented in Figure 40. The temperature lapse rate was about $-0.7\ °C \cdot 100\ m^{-1}$, indicating slightly stable conditions. The wind speed averaged 7 to 8 m/sec for the upper parts of the profile. The plume centerlines in Figure 38 are seen to be much higher than the profile, so there is some uncertainty in extrapolating the wind speed. Also, the profile commencing at 1700 (not shown) indicated a mean wind speed over the same height range of about 4 m/sec. Thus, the mean wind field structure is not well known for this case study.

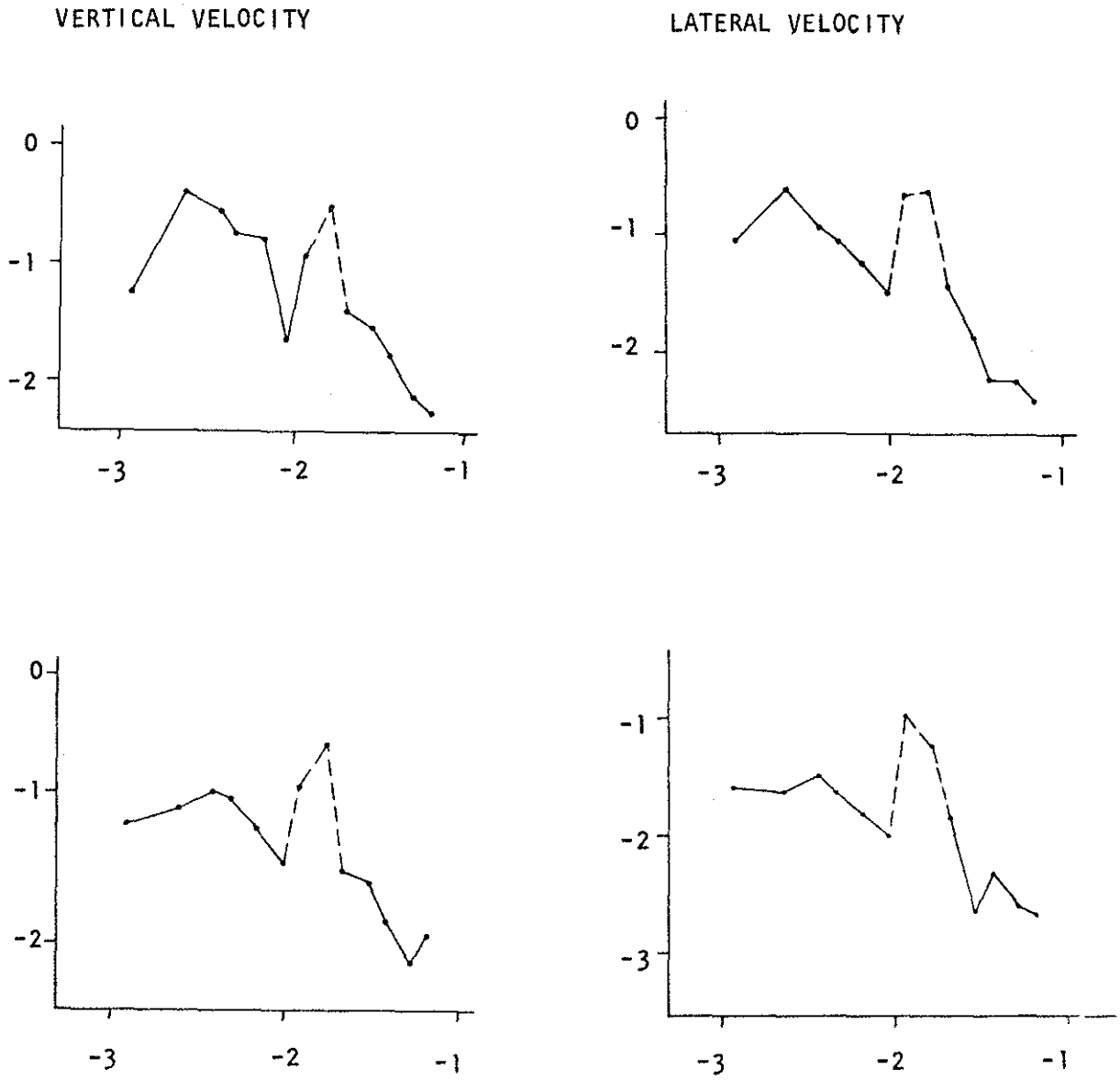

Figure 37. Spectral plots for the flight of 20 June 1977 (1000-1500 MDT). All plots are LOG $\left(\frac{K\ \phi\ (K)}{\sigma^2}\right)$ versus LOG K where K is wavenumber (m^{-1}).. From top to bottom the run groups are: 1, 2; 15, 16.

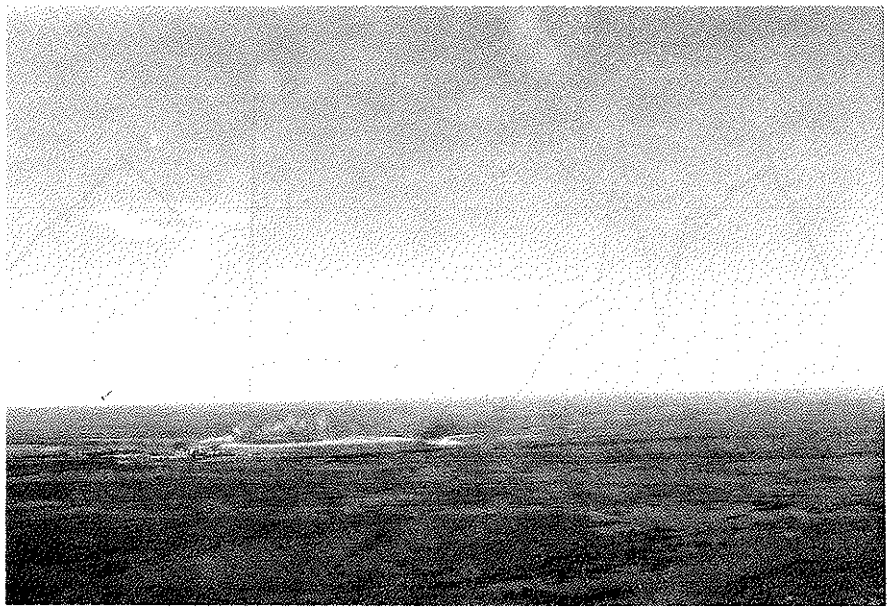

A

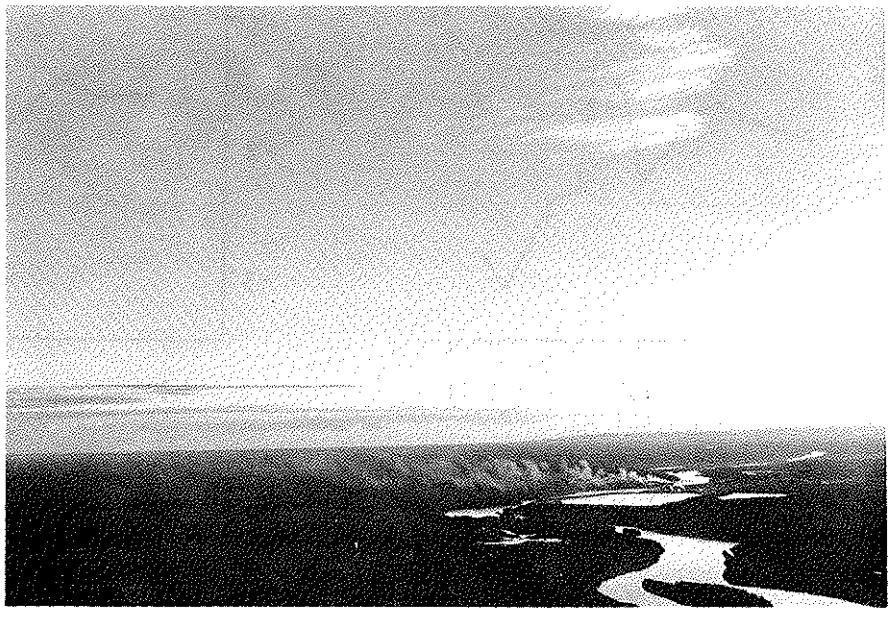

B

Figure 38. Plume photographs for the flight of 22 June 1977 (1915-2305 MDT): (A) taken at 2024 MDT from about 10 km northwest of GCOS at an altitude to 760 m AMSL; (B) taken at 1242 MDT from about 8 km south of GCOS at an altitude ot 915 m AMSL; and (C) at 2222 MDT at an altitude of 760 m AMSL.

C

Figure 38. Concluded.

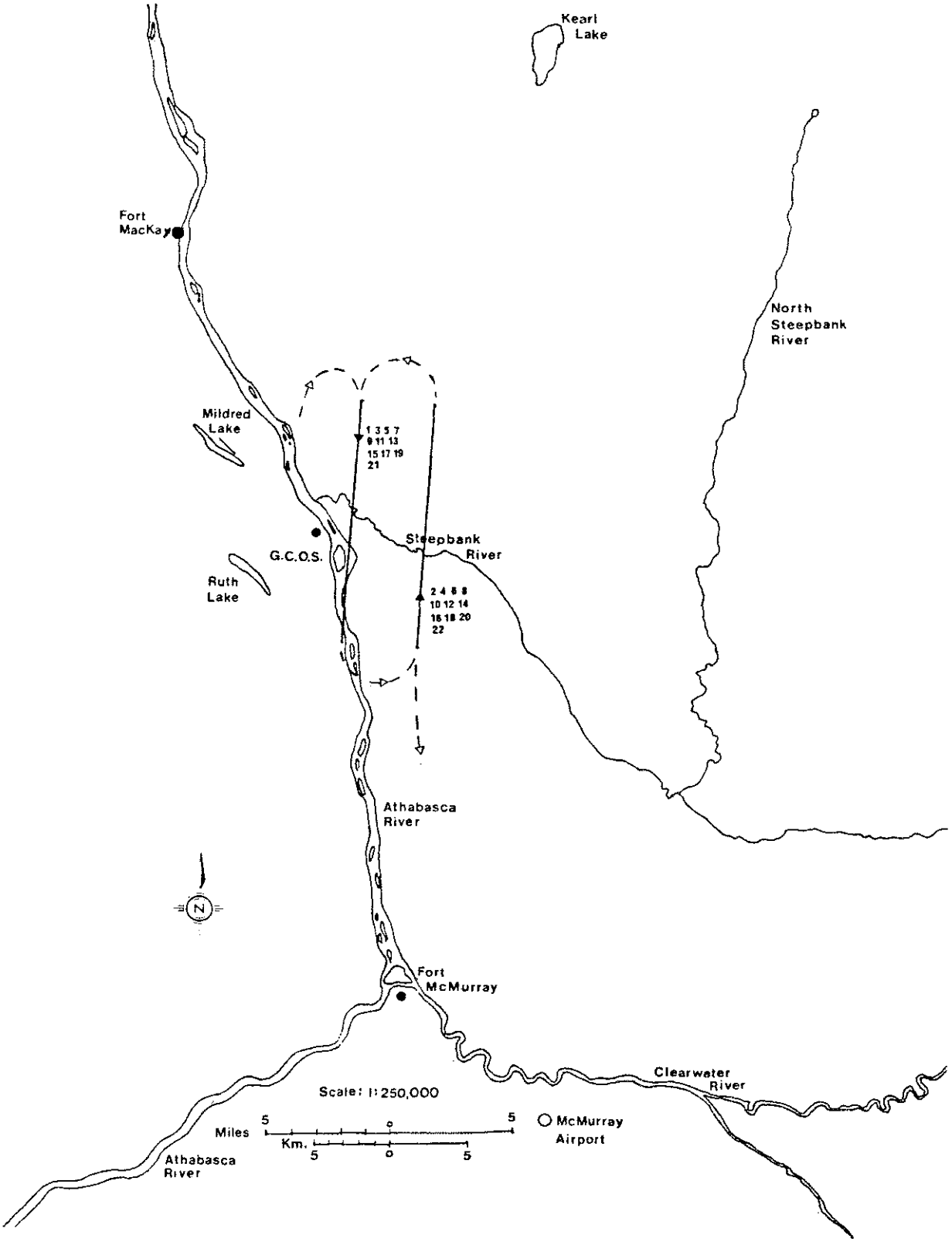

Figure 39. Flight profiles for 22 June 1977 (1915-2305 MDT).

Solid lines denote numbered runs and dashed lines denote interconnecting legs.

Table 11. Run information for the flight of 22 June 1977 (1915-2305 MDT).

Run Number	Start Time (MDT)	Altitude (m MSL) ± 20	Downwind Distance (km) ± 0.3	σ_y (m) ± 100	Max. SO_2 Conc. (ppm) ± 0.02	Integrated Conc. (ppm-m) ± 50	Flight Dir. (From-to)
1[a]	1953	1526	3.2	-	-	-	N-S
2[a]	1959	1526	8.0	-	-	-	S-N
3[a]	2012	915	3.2	-	-	-	N-S
4	2018	915	8.0	341	0.13	98	S-N
5	2025	610	3.2	435	0.43	313	N-S
6	2033	610	8.0	1448	0.08	75	S-N
7[a]	2045	1220	3.2	-	-	-	N-S
8	2053	1220	8.0	210	0.08	42	S-N
9[a]	2101	763	3.2	-	-	-	N-S
10	2108	763	8.0	438	0.17	182	S-N
11[a]	2121	1068	3.2	-	-	-	N-S
12	2130	1068	8.0	318	0.20	146	S-N
13[a]	2137	915	3.2	-	-	-	N-S
14	2144	915	8.0	728	0.09	78	S-N
15	2152	610	3.2	375	0.93	667	N-S
16	2159	610	8.0	452	0.31	303	S-N
17	2205	534	3.2	403	0.49	427	N-S
18	2212	549	8.0	796	0.19	362	S-N
19[a]	2221	763	3.2	-	-	-	N-S
20	2228	763	8.0	307	0.14	101	S-N
21[a]	2236	671	3.2	-	-	-	N-S
22	2243	671	8.0	482	0.77	642	S-N

[a]No detectable SO_2.

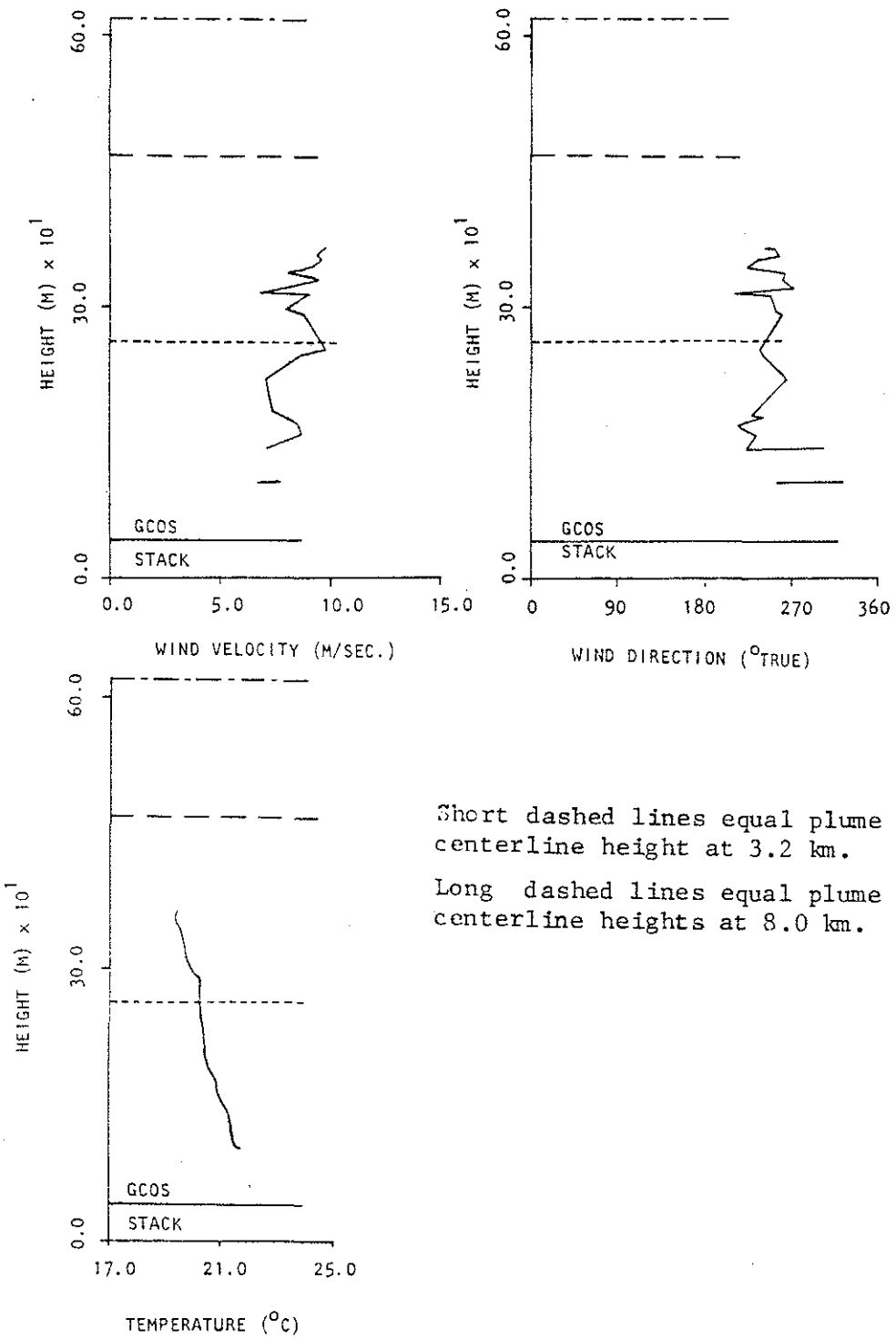

Figure 40. Tethersonde profiles for 22 June 1977. 1950 MDT. Data supplied by R. Mickle, AES.

4.4.4 Isopleths and Selected Traverses

The isopleths constructed for this flight are shown in Figure 41. The data at 3.2 km did not show large changes throughout the flight, and so only a single isopleth cross-section is shown. The differences between the afternoon and evening isopleths at 8.0 km are striking, with the evening plume becoming much flatter and wider.

The individual plume traverses showed consistent structure and hence reasonable values for standard deviation. Figure 42 shows the SO_2 concentration profile for Run 16 at 610 m AMSL at 8.0 km downwind from GCOS. This run is close to the evening centerline at 8.0 km downwind; the Gaussian fit is reasonable. Figure 43 shows the concentration profile for Run 14 at 915 m AMSL and at 8.0 km downwind. By the time of Run 14, there was clear evidence of a near-surface inversion suppressing all vertical motion near the surface; a smoke source at ground level was observed to be fanning out as it drifted eastward with no visible vertical motion. Run 14, however, shows two distinct peaks, suggesting oscillations in the top of the plume as sketched in the isopleths, even though surface convective support had ceased.

4.4.5 Plume Geometry

Figure 44 shows the vertical profile of the maximum concentrations; Table 12 presents a summary of the plume geometry measurements. Figures 45 and 46 compare the observed plume sigma values to the Pasquill-Gifford curves. The σ_y values at 8.0 km are small compared to those found on previous days. Note that the evening σ_y value at 8.0 km is greater than the afternoon value, even though conditions were more stable; this tendency is opposite to what the Pasquill-Gifford curves predict. The σ_z values appear to agree well with the Pasquill-Gifford curves, with the evening values in stable conditions and the afternoon value in slight unstable conditions.

The normalized centerline concentrations agree reasonably well with the Pasquill-Gifford curves (Figure 47). The value at 3.2 km downwind may be somewhat smaller than the curves would have predicted, but the observed centerline concentration is not well defined.

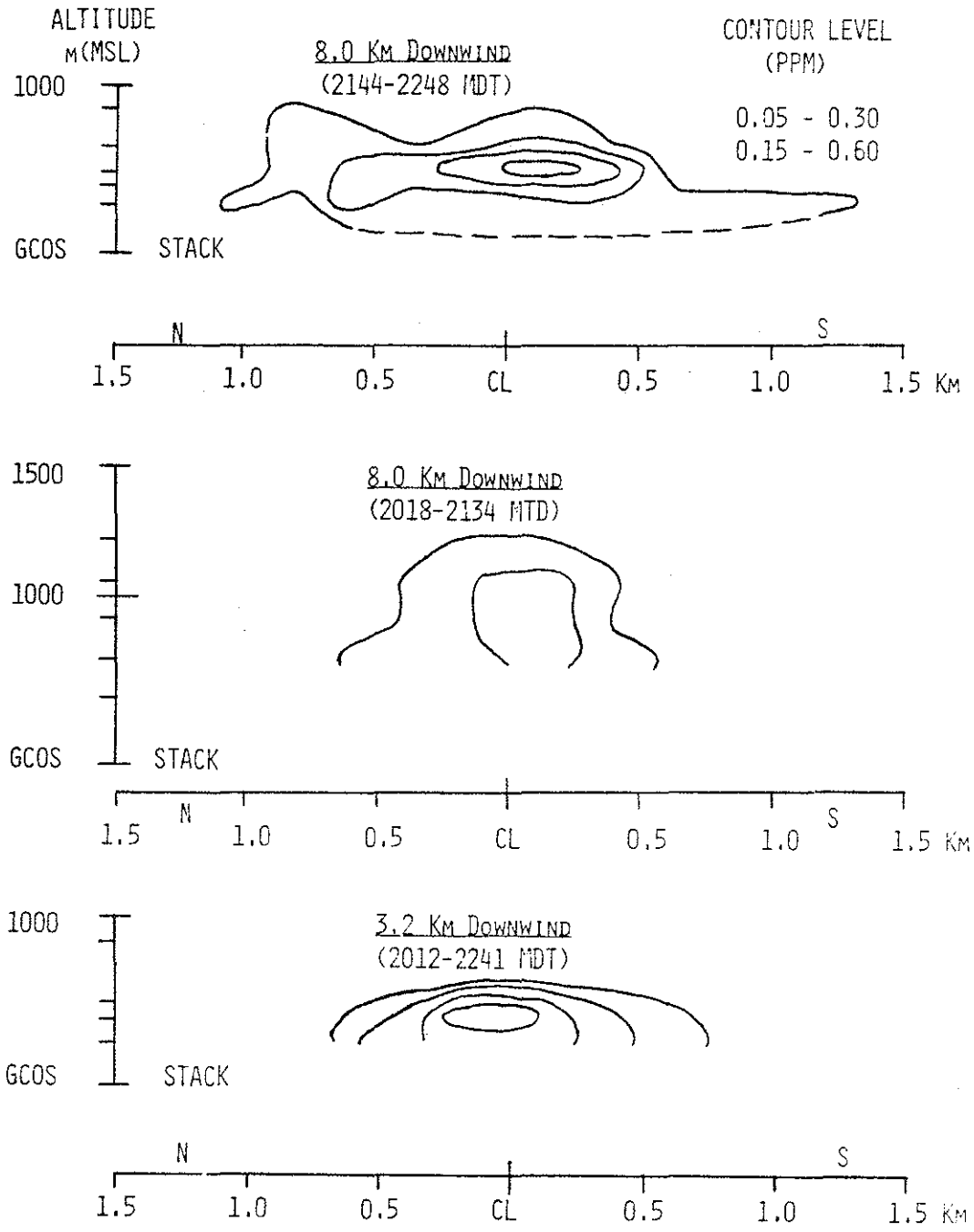

Figure 41. SO_2 concentration isopleths for the flight of 22 June 1977 (1915-2305 MDT).

NOTE: 8.0 km Isopleth has a 2X vertical exaggeration.
3.2 km Isopleth has no vertical exaggeration.
Dashes on the left side of the vertical axes are flight levels.

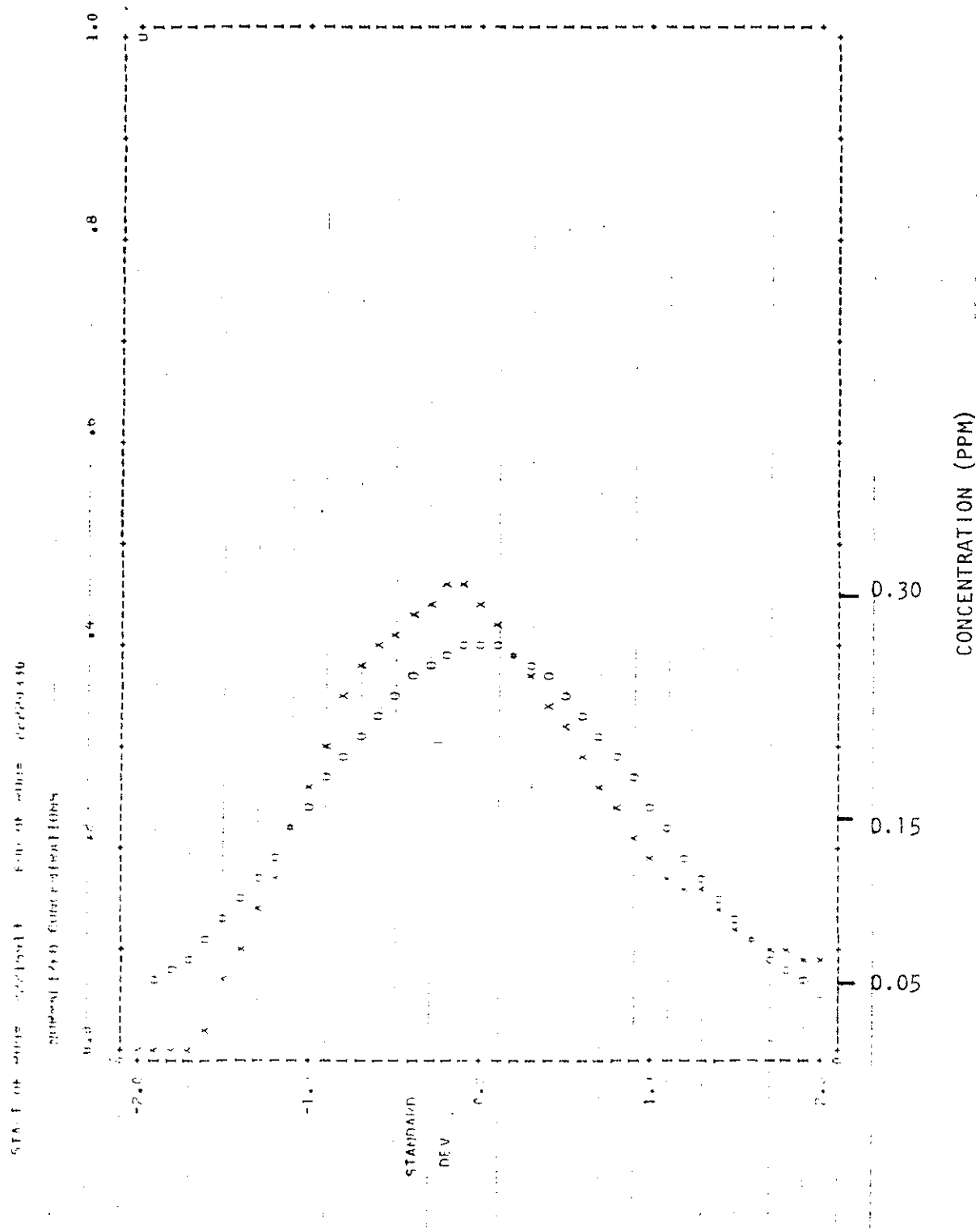

Figure 42. Normalized SO_2 concentrations for Run 16 on the flight of 22 June 1977 (1915-2305 MDT).

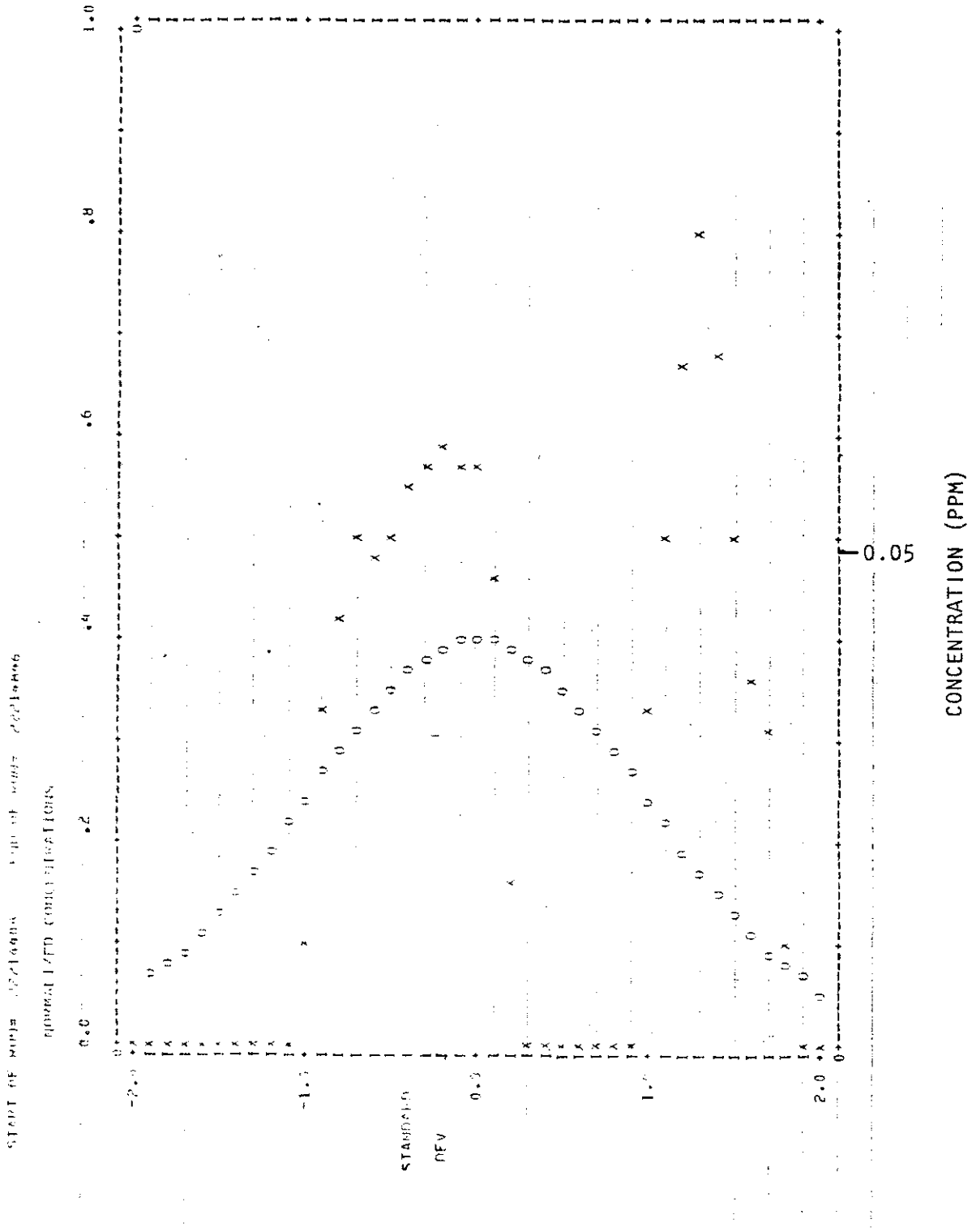

Figure 43. Normalized SO_2 concentrations for Run 14 on the flight of 22 June 1977 (1915-2305 MDT).

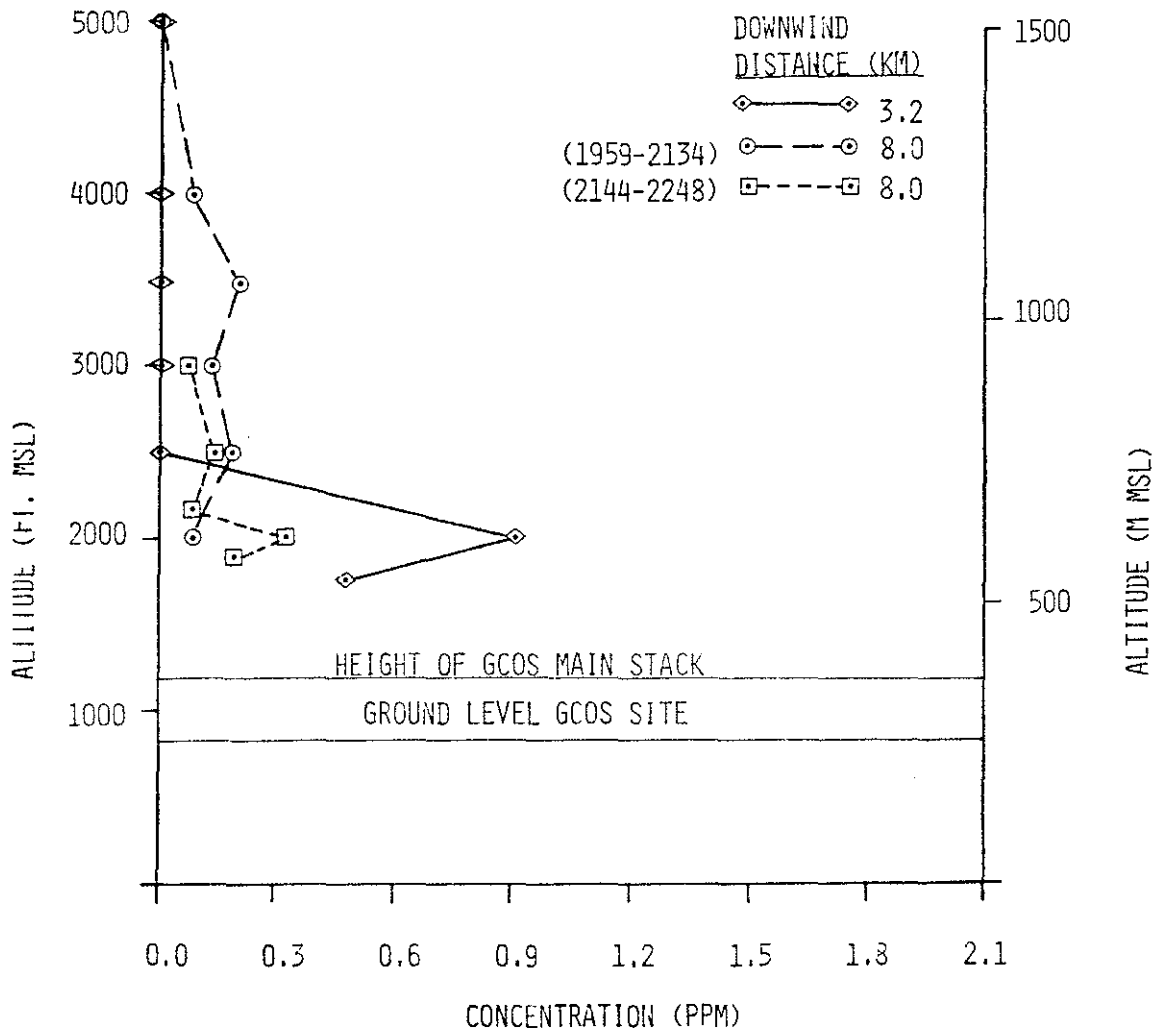

Figure 44. Maximum SO_2 concentrations along each traverse as a function of altitude for the flight of 22 June 1977 (1915-2305 MDT).

Table 12. Plume geometry, mass flux, and plume rise for the flight of 22 June 1977 (1915-2305 MDT).

Parameter			Downwind Distance (1950-2240)	(1950-2135)	(2140-2305)
σ_y cl	Area criterion [m]	± 30	375	340	480
	Second moment [m]	± 30	345	310	550
σ_z	Upper [m]	± 30	40	200	110
	Lower [m]	± 30	60	200	75
	Average [m]	± 30	50	200	90
$X\bar{U}Q^{-1}$	Norm Axial Conc. 10^{-6} m^{-2}	± 3	9.4	2.2(1.5)[a]	8.6
SO_2	Mass flux				
	[long tons·h^{-1}]	± 3	9.2	7.6	12.8
	[kg·sec^{-1}]	± 1	2.6	2.2	3.6
Observed centerline height [m MSL]		± 30	580	920	680
(i)	Height of center of mass from max. conc. profile		580	920	680
(ii)	Height of center of mass from integrated conc. profile		590	885	680
(iii)	Height of max. conc. observed		580	1070	670
Ratio of calculated to observed effective stack height					
(i)	Briggs		1.09	0.54	0.82
(ii)	Holland		0.67	0.33	0.51
(iii)	TVA		1.13	0.64	0.72

Notes: 1. For the ratio of calculated to observed effective stack height, the following data were used: $\bar{U}$ = 7.5 (m/sec), $\partial T/\partial Z$ = -0.7 (°C·100 m^{-1}) - 1950-2135; $\bar{U}$ = 7.5 (m/sec), $\partial T/\partial Z$ = 0.0 (°C·100 m^{-1}) (E-stability) - 2140-2305. The height of the center of mass from the concentration profile less the height of the base of the stack (259 m MSL) was used as the observed height.

[a] Value in parentheses is the normalized axial concentration for the observed concentration at the height of the center of mass from the maximum concentration profile.

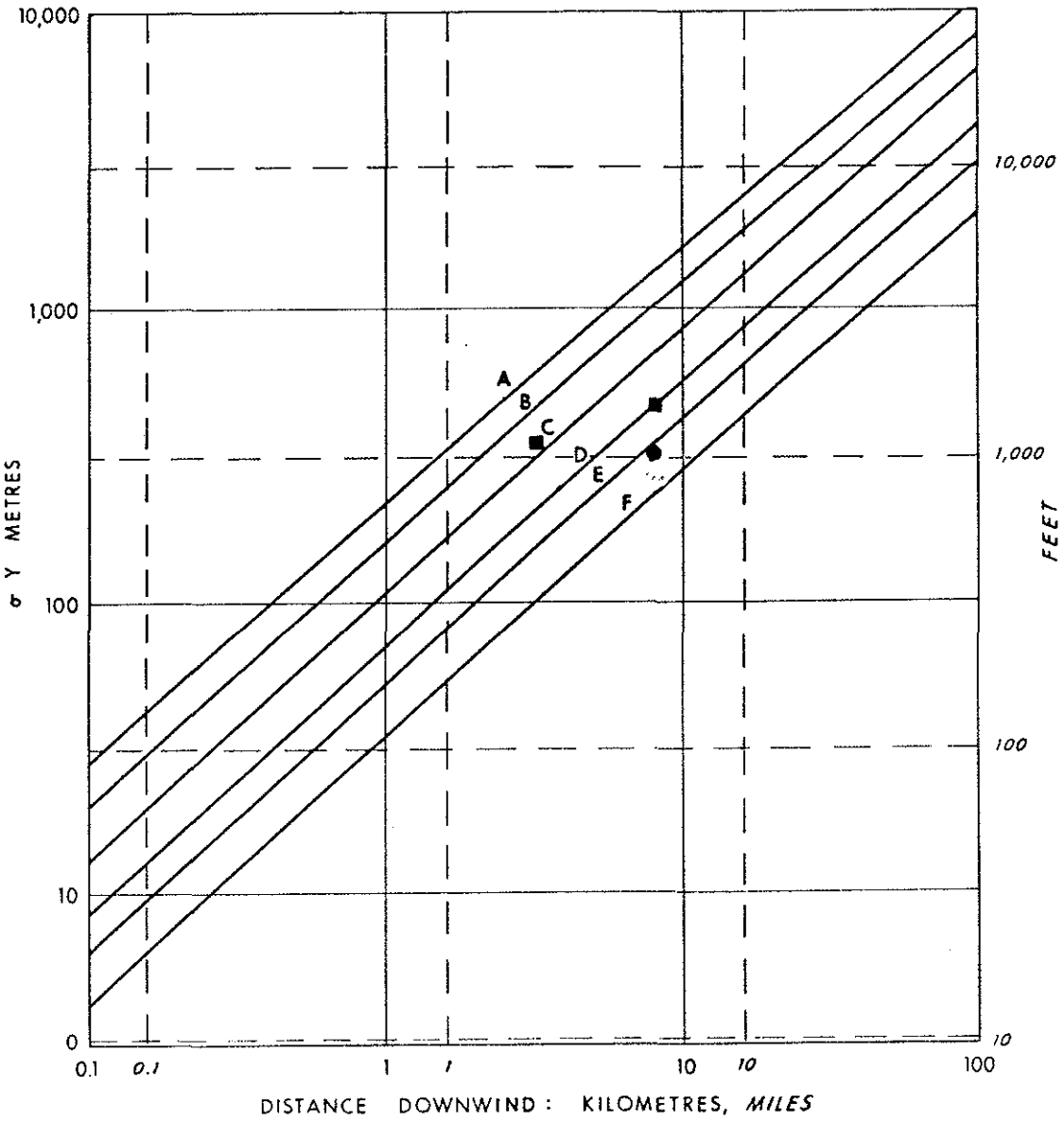

Figure 45. Observed horizontal dispersion coefficients compared to Pasquill-Gifford curves for the flight of 22 June 1977 (1915-2305 MDT).

● (1953-2134 MDT)

■ (2144-2248 MDT)

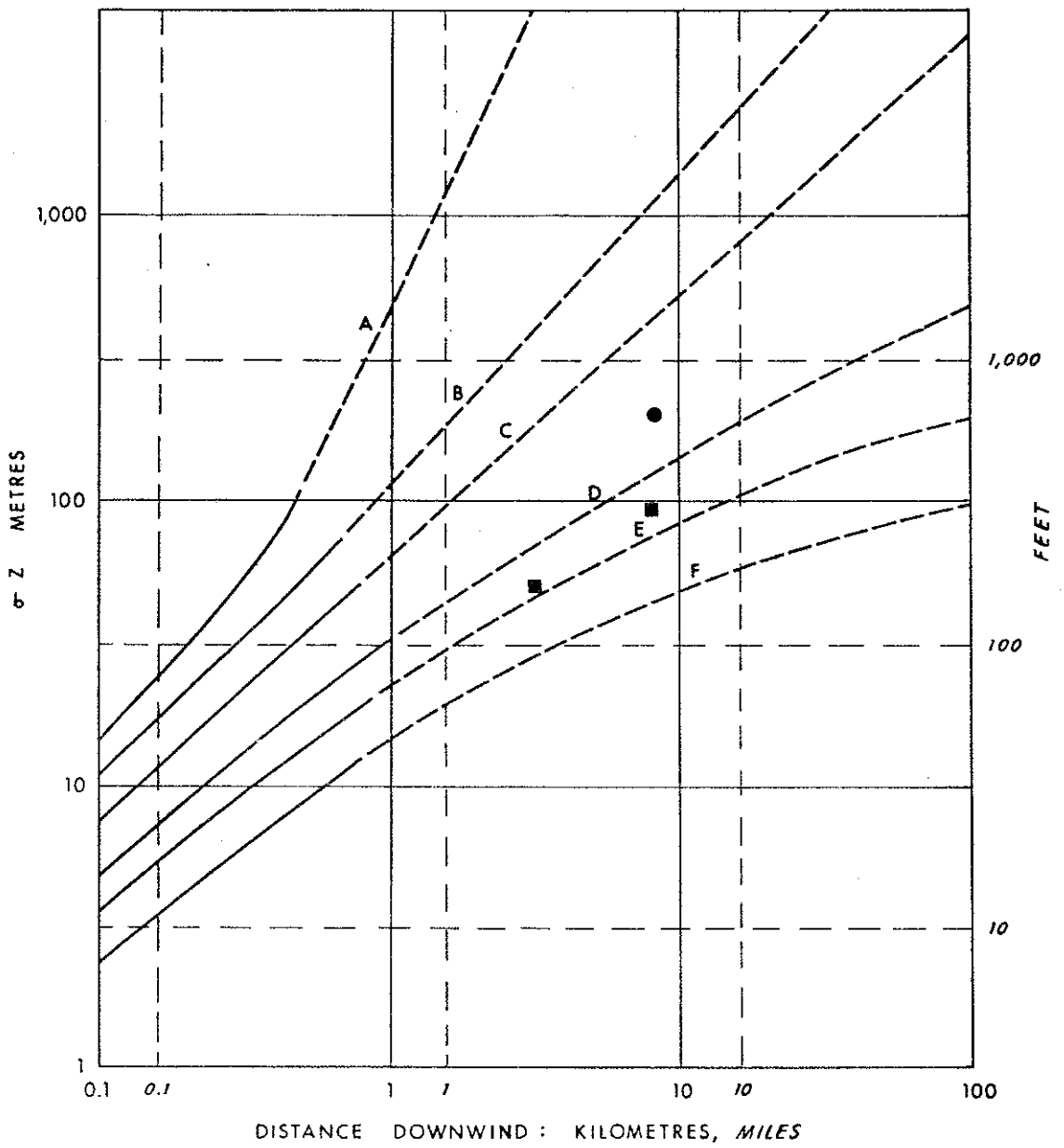

Figure 46. Observed vertical dispersion coefficients compared to Pasquill-Gifford curves for the flight of 22 June 1977 (1915-2305 MDT).

● (2018-2137 HR)
■ (2144-2241 HR)

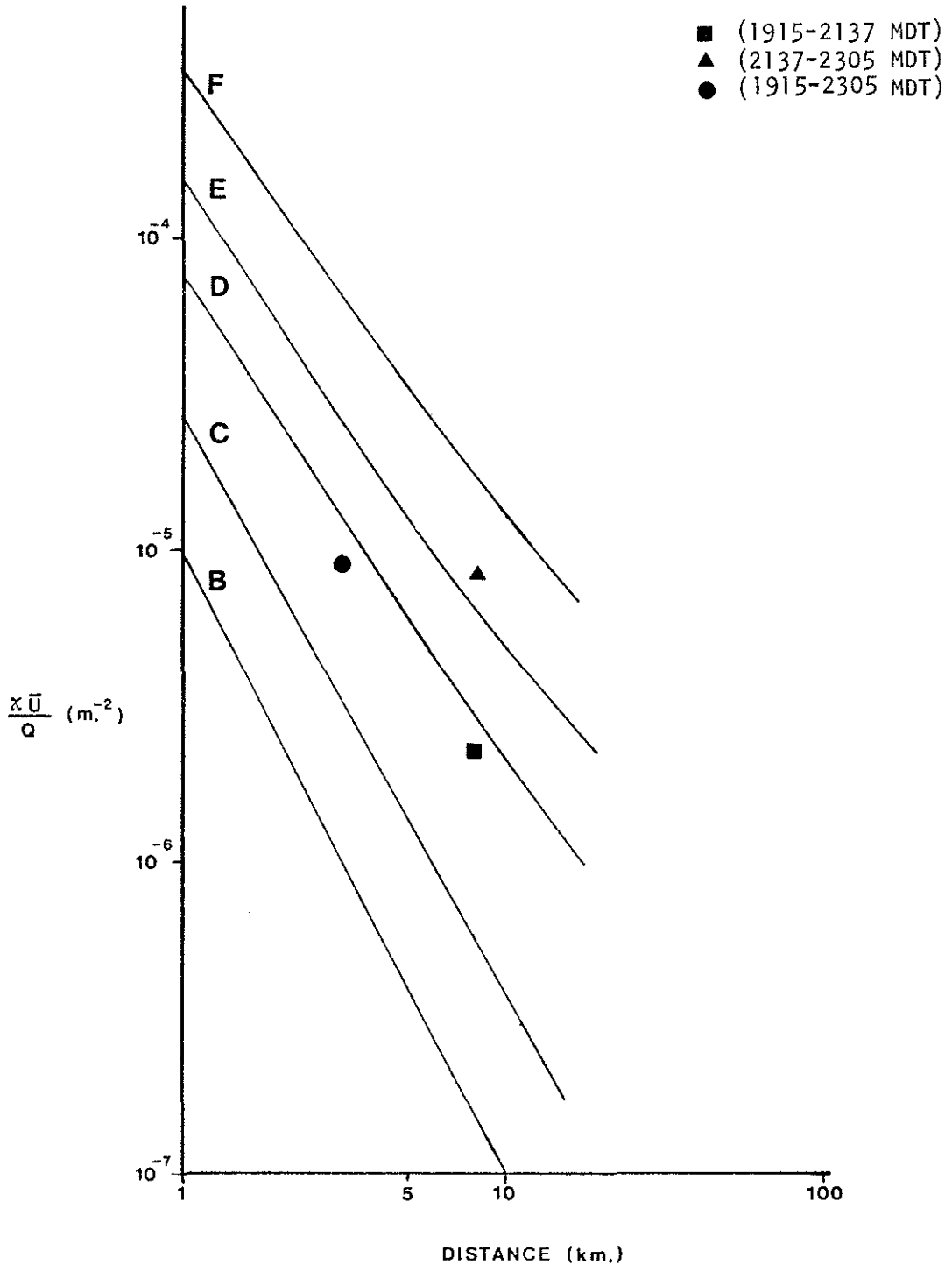

Figure 47. Comparison of observed normalized centerline concentrations with Pasquill-Gifford predictions for the flight of 22 June 1977 (1915-2305 MDT).

The mass fluxes show reaonable agreement with the source emission of about 2.5 kg/sec or 8.7 long tons/h. The larger discrepancy for the later estimate at 8.0 km may suggest that the wind speed had continued to increase at the plume centerline height throughout the evening.

The observed centerline heights did not vary markedly according to the technique used for their computation. The greater variation for the afternoon estimate at 8.0 km is understandable, considering the greater vertical range over which the plume existed. Note that all the plume rise formulations underestimated the observed plume height at 8.0 km. The values at 3.2 km, derived by averaging the plume predictions for the two sets of conditions, gave good agreement. The continued increase of plume height with increased downwind distance is not adequately handled by the three plume rise formulations examined.

4.4.6 Turbulence Levels Related to Plume Structure

The dissipation and velocity standard deviations are plotted as functions of height in Figure 48. The differences between the early and later runs are obvious. Runs 15 and 17, at 3.2 km downwind at altitudes of 610 and 530 m AMSL respectively, have each been split into two parts. Runs 15A and 17A represent single analysis blocks during plume passage. These sections of the runs had markedly more turbulent energy than the remaining sections of the runs. The increased turbulent energy, which corresponded to the plume passage, occurred above the Steepbank River near where it joins the Athabasca. During both of these runs, the increased turbulence was quite noticeable by the aircraft crew.

A summary of the statistics from four groups of runs is presented in Table 13. As expected, the velocity standard deviations and dissipation show statistically significant differences between most of the groupings. Thus, it is appropriate to break up the flight into two segments.

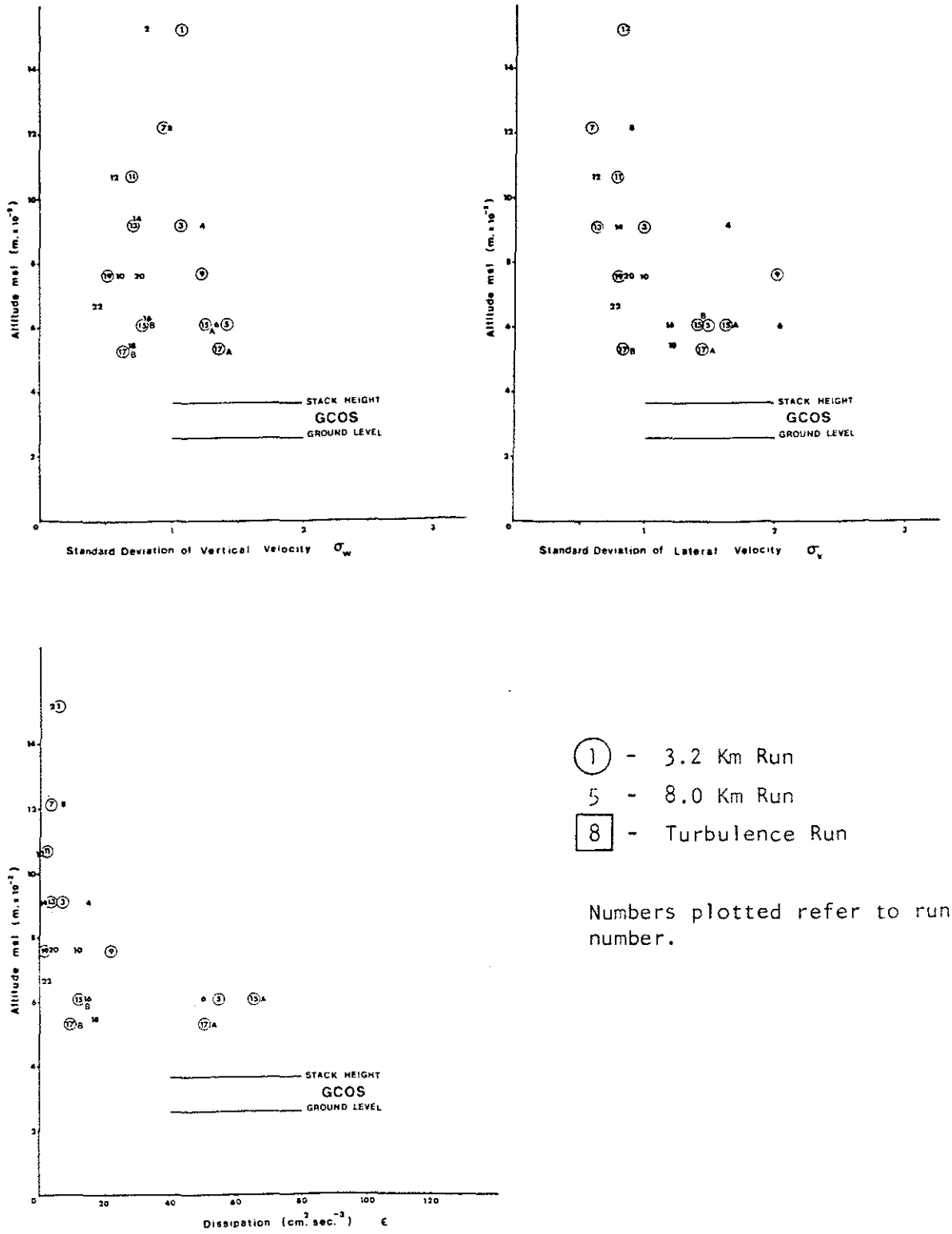

Figure 48. Turbulence data for the flight of 22 June 1977 (1915-2305 MDT).

Table 13. Summary of turbulence statistics for the flight of 22 June 1977 (1915-2305 MDT).

Runs	Description	Average Run Altitude [m-AMSL]	No. of Blocks	σ_w [m/sec]	σ_{uH} [m/sec]	ε [cm^2/sec^3]	ℓ_w [m]	ℓ_v [m]
5, 6	Afternoon[a] 3.2 km CL[a]	610	7	1.38 (0.12)	1.72 (0.17)	53 (6)	200 (24)	200 (30)
3, 4	Afternoon 8 km CL	915	5	1.17 (0.15)	1.38 (0.19)	12 (2)	250 (45)	250 (40)
15B,16 17B,18	Evening 3.2 km CL	575	12	0.74 (0.04)	1.20 (0.12)	13 (2)	175 (15)	240 (38)
19, 20 22	Evening 8 km CL	750	6	0.58 (0.07)	0.81 (0.04)	2 (1)	240 (35)	305 (25)

Notes: Values in parentheses are standard deviations of the mean values.

σ_w standard deviation of vertical velocity

σ_{uH} standard deviation of lateral velocity with respect to the aircraft.

ε dissipation

ℓ_w integral length scale in the vertical

ℓ_v integral length scale in the lateral direction with respect to the aircraft.

[a] CL = centerline

The spectral plots for two groups of runs (5, 6 and 19, 20) are presented in Figure 49. The vertical velocity spectrum for the low level afternoon flight appears to have more low wavenumber energy than the corresponding spectrum for the evening flight. The removal of the extraneous peaks meant a reduction in the velocity standard deviations of about 15%.

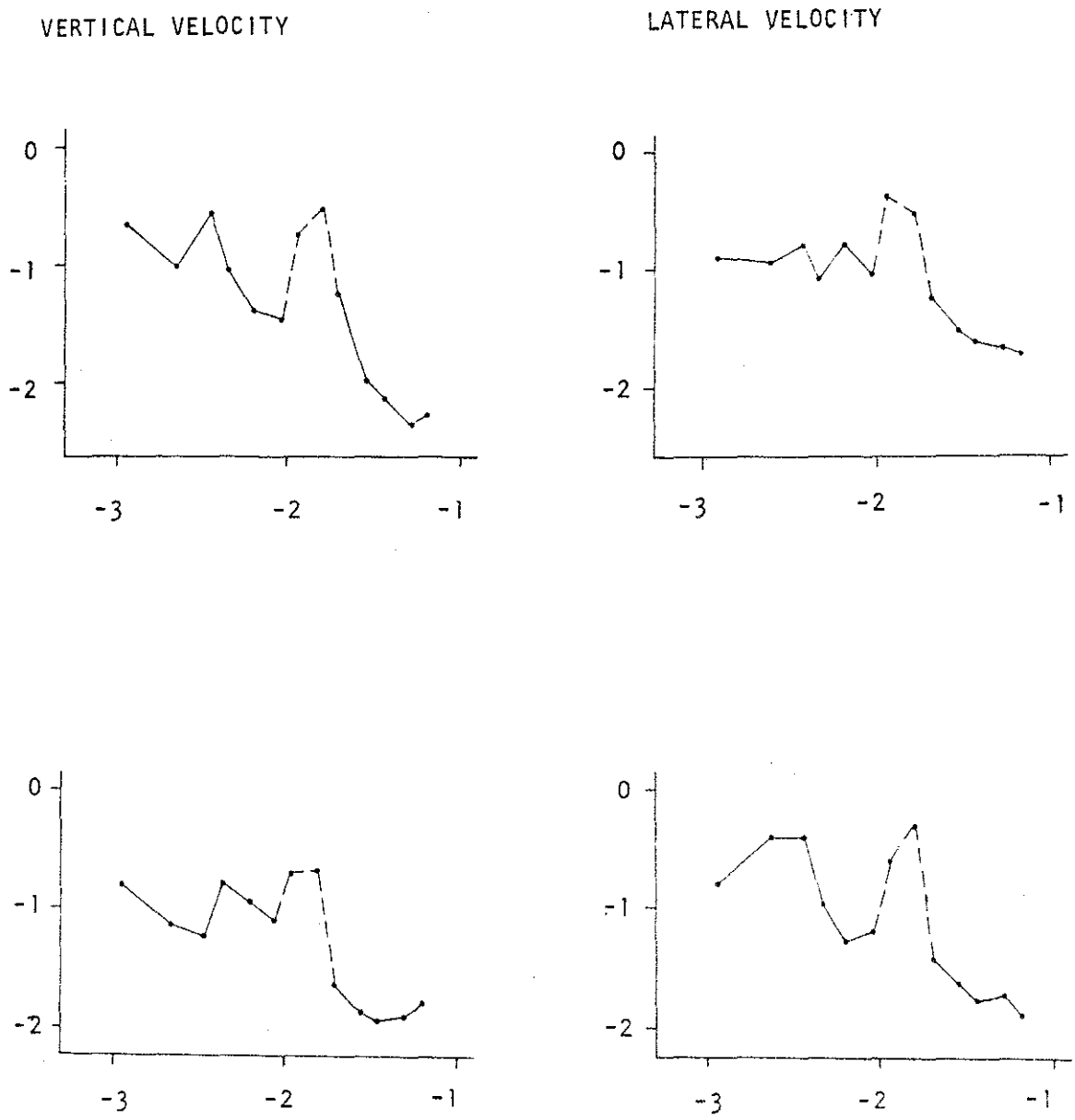

Figure 49. Spectral plots for the flight of 22 June 1977 (1915-2305 MDT). All plots are LOG $\left(\frac{K\,\phi\,(K)}{\sigma^2}\right)$ versus LOG K where K is wavenumber (m^{-1}). From top to bottom the run groups are: 5, 6; 19, 20.

5. DISCUSSION OF THE CASE STUDY RESULTS

5.1 A COMPARISON OF PLUME GEOMETRY WITH THE PASQUILL-GIFFORD CURVES

5.1.1 A Discussion of the Pasquill-Gifford Curves

For each of the case studies presented in the previous section, the observed values of σ_y, σ_z, and normalized centerline concentration were compared to the so-called Pasquill-Gifford curves, which are actually the "Turner Workbook" curves (Turner 1970). These curves, originally developed by Gifford (1961), are based mostly upon ground level concentration measurements made up to 800 m downwind of a ground level source over smooth, flat terrain. Values of σ_z were available at only a few downwind distances, and so generally σ_z as a function of distance had to be inferred from a Gaussian distribution. In practice, the Pasquill-Gifford curves have been extrapolated far beyond the distances of supporting measurements. Because of the widespread use of these curves, it is worthwhile comparing the observed plume geometry with them.

The Pasquill-Gifford curves are families of curves that depend upon a stability classification. The two commonly used procedures for defining stability were presented by Slade (1968) and Turner (1970), the latter one based upon work by Pasquill (1961). These two procedures are summarized in Tables 14 and 15. Note that the temperature lapse rate must be measured close to the surface, preferably at heights not greater than 10 m, since a super-adiabatic lapse rate is not observed even under the most unstable conditions above the near-surface layer. It is clear that these stability classification schemes can only be treated as very rough approximations, because the surface characteristics have not been taken into account.

Physically, it is to be expected that mixing of any plume will depend upon the ratio of the mechanical and convective energy terms and upon the turbulence intensity. The Pasquill-Gifford curves attempt to express the mixing in terms of a single parameter. There is, however, a linear scaling effect with wind speed inherent in the

Table 14. Stability classifications according to Slade (1968).

Stability Classification	Pasquill Categories	Temperature Change with height (°C/100 m)
Extremely unstable	A	< 1.9
Moderately unstable	B	-1.0 to -1.7
Slightly unstable	C	-1.7 to -1.5
Neutral	D	-1.5 to -0.5
Slightly stable	E	-0.5 to 1.5
Moderately stable	F	1.5 to 4.0
Extremely stable	G	> 4.0

Table 15. Stability classifications according to Pasquill (1961).

Surface Wind Speed m/sec	Daytime Insolation			Night-time Conditions	
	Strong	Moderate	Slight	Thin overcast or ≥ 4/8 Cloudiness[a]	≤ 3/8 Cloudiness
<2	A	A-B	B		
2	A-B	B	C	E	F
4	B	B-C	C	D	E
6	C	C-D[b]	D	D	D
>6	C	D	D	D	D

[a]The degree of cloudiness is defined as that fraction of the sky above the local apparent horizon which is covered by clouds.
[b]D-stability is used for heavy overcast, day or night.

formulations, since the plume geometry characteristics are expressed in terms of downwind distance. Thus if the wind speed is doubled, there will be increased mechanical turbulent mixing but less time for that mixing to take place by a given downwind distance. The Pasquill-Gifford curves assume that these effects exactly cancel or will be seen in a stability change.

5.1.2 Comparison of the Observed Plume Geometry with the Pasquill-Gifford Curves

The Pasquill-Gifford stability class appropriate to each case study is shown in Table 16. The adopted stability classes were based upon both the Pasquill and Slade formulations together with the meteorological description based upon the aircraft turbulence measurements.

The wind speed and temperature profiles are based upon the AES tethersonde data. Thus, these data refer to elevated conditions well displaced from the near-surface layer. Under stable conditions, this does not present any problems, but an adiabatic profile will be observed for both neutral and unstable conditions, limiting the usefulness here of the Slade formulation.

In Figures 50, 51, and 52, the observed plume sigma values and normalized concentrations for all case studies are compared to the Pasquill-Gifford curves. There are several significant features apparent.

The σ_y values in Figure 50 do not tend to increase with downwind distance as quickly as predicted. The σ_y values agree with the curves reasonably well for 20 June. However, for both flights on 19 June, the observed σ_y values were about a factor of 4 larger at 8.0 km than the curves and close to a factor of 10 larger at 3.2 km. Note that in the case study of 22 June the σ_y value for the later time period was larger than for the earlier period when conditions were less stable. This is opposite to what the Pasquill-Gifford curves predict. The σ_y value for the later part of the flight of 22 June at 8.0 km downwind is about a factor of 4 larger than the Pasquill-Gifford curves predict.

Table 16. Summary of the adopted stability classifications for all of the June 1977 case studies.

Time of Plume Traversing [MDT]	Meteorological Description	Elevated Wind Speed [m/sec]	Elevated Temp. Lapse Rate [°C/100 m]	Adopted Stability Class
19 June (0825-0945)	Fumigating plume with capping inversion	5.5	-0.4	D
19 June (1415-1615)	Mixed layer extended above plume	6.9	-1.0	C
20 June (1130-1345)	Convectively dominated mixed layer which increased in height and intensity during the flight	5.8	-0.8	B-C
22 June (1950-2135)	Weakly mixed, early evening	7.5	-0.7	D
(2140-2305)	Late evening, surface-based radiation inversion	7.5	0.0[a]	E

[a]The temperature profile for the later part of the flight on 22 June was estimated from E-stability criterion because no tethersonde data were available.

The wind speed and temperature lapse rates were measured by the AES tethersonde system above the near-surface layer.

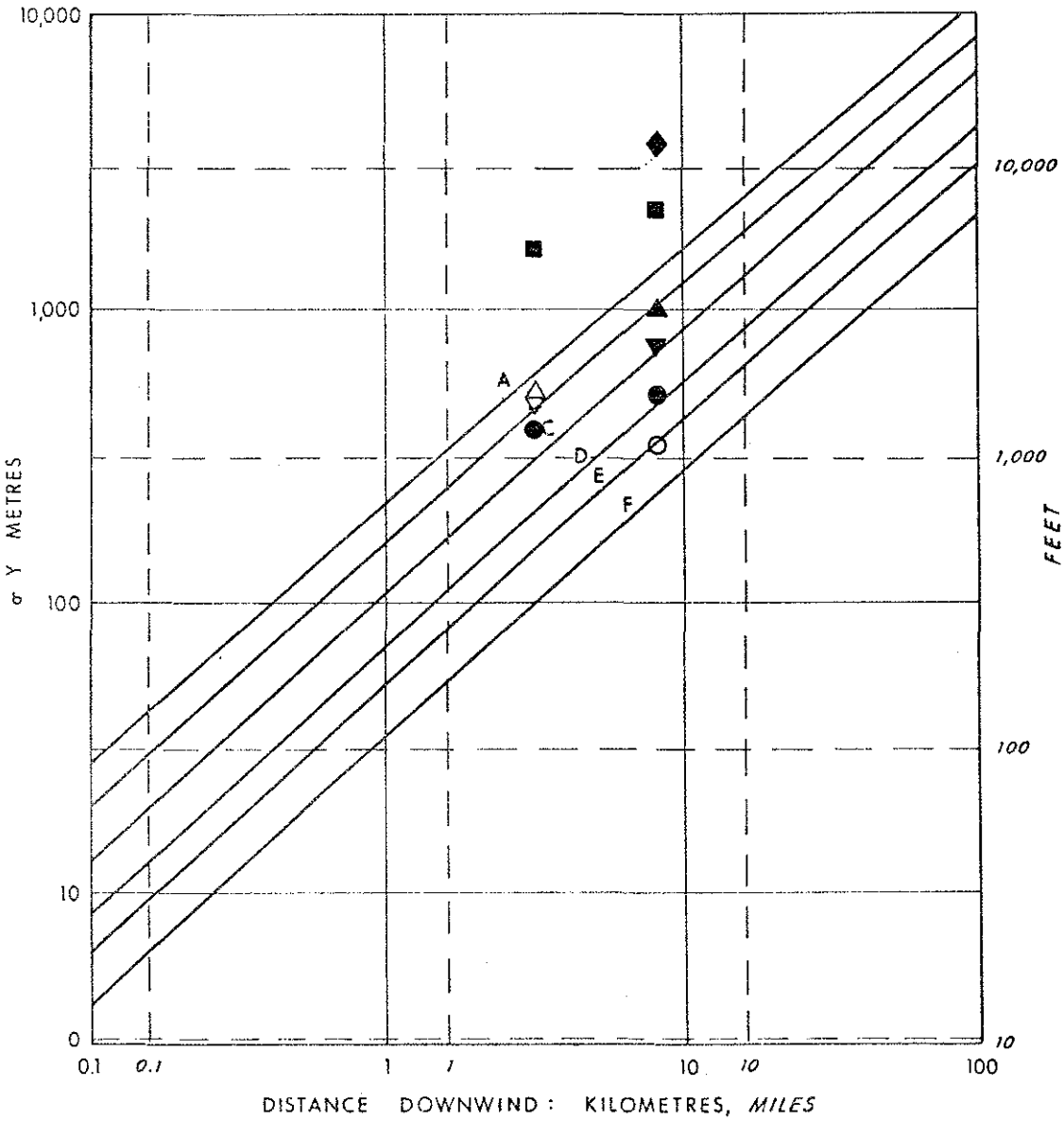

Figure 50. Horizontal dispersion coefficient as a function of downwind distance from the source compared with Pasquill-Gifford values for 1977 flights.

- ■ 19 June a.m.
- ◆ 19 June a.m.
- ◇ 20 June (1000-1500 MDT)
- ▼ 20 June (1130-1230 MDT)
- ▲ 20 June (1230-1340 MDT)
- ○ 22 June (1953-2134 MDT)
- ● 22 June (2144-2248 MDT)

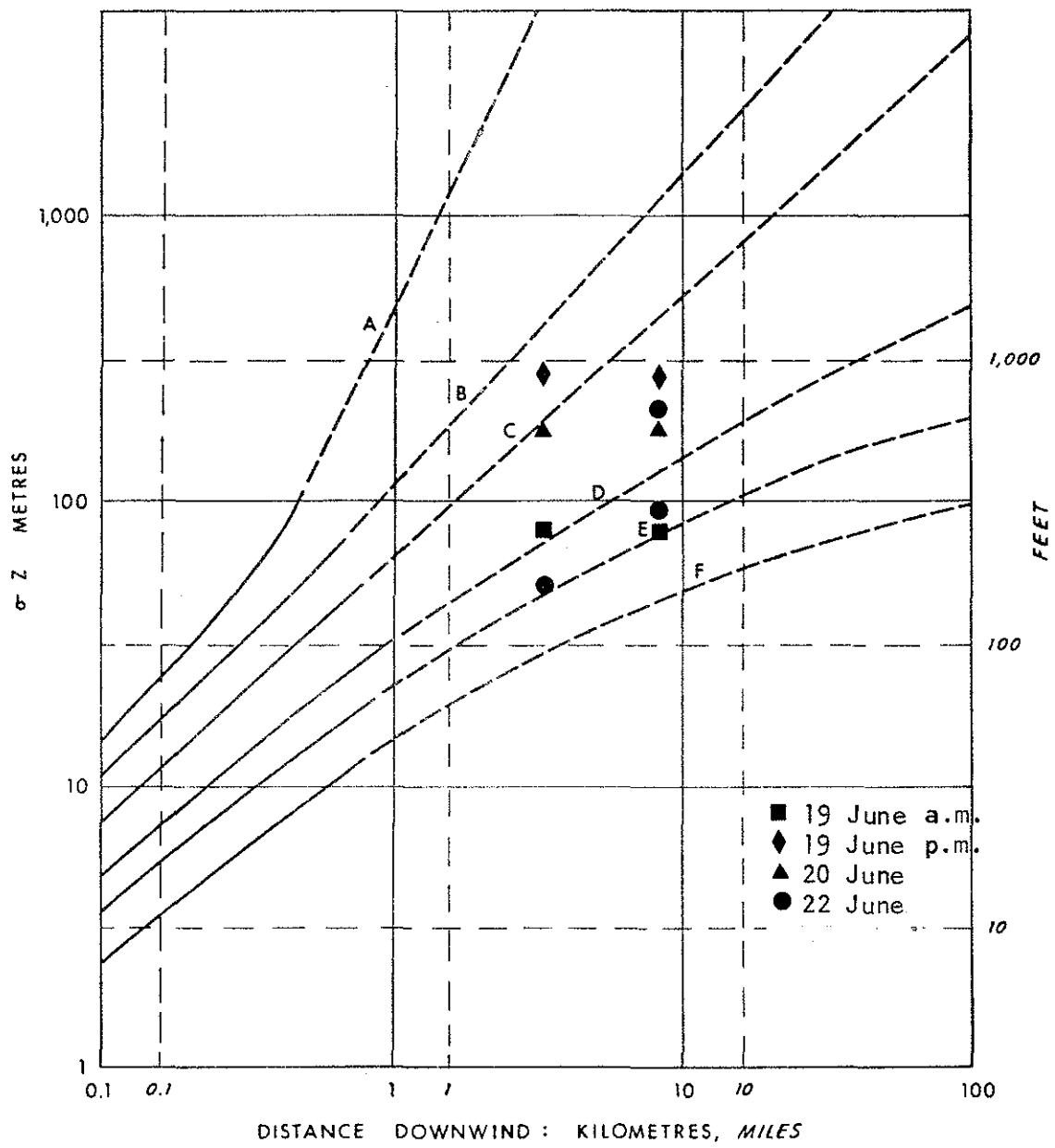

Figure 51. Vertical dispersion coefficient as a function of downwind distance from the source compared with Pasquill-Gifford values for 1977 flights.

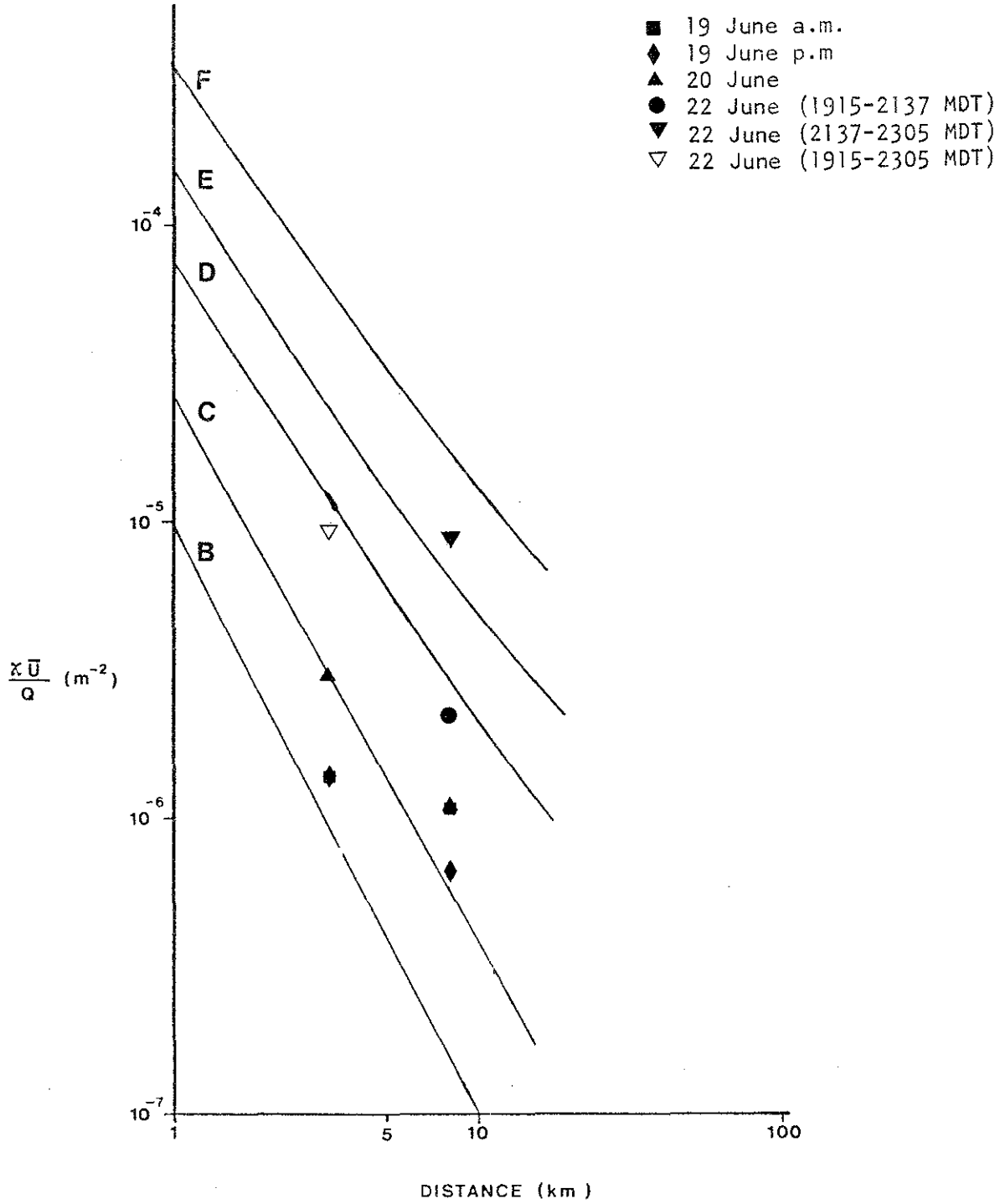

Figure 52. Observed normalized centerline concentrations compared with Pasquill-Gifford values, for 1977 flights.

In the March 1976 field study most of the observed σ_y values were also much larger than predicted, by about the same factors as the discrepancies for the case studies of 19 June and the evening of 22 June.

The σ_z values in Figure 51 showed very little increase with downwind distance except for the case study of 22 June. For the 19 June morning flight, a capping inversion limited vertical development. On the afternoon flight of 19 June, there were experimental errors due to sampling that were larger than the apparent decrease in σ_z. On 20 June, there was more vertical mixing at 3.2 km, presumably due to river valley effects. The σ_z values agreed reasonably well in magnitude with the Pasquill-Gifford curves at 3.2 km downwind. At 8.0 km, the major discrepancies occurred for 20 June (possibly a spatial inhomogeneity affect) and for the morning flight of 19 June. In both of these cases the observed σ_z values were less than predicted.

The results of the comparison of the observed σ_z values to the Pasquill-Gifford curves in this study are in marked contrast to the results found in the March 1976 study. In the March 1976 study, the σ_z values did not increase with distance as much as predicted either, but the magnitudes of the observed σ_z values were typically a factor of two or three larger than the predicted values.

The normalized centerline concentrations in Figure 50 agree reasonably well with the Pasquill-Gifford curves except that the observed concentrations tended to be slightly lower and to decrease less quickly with distance than predicted. These results appear to be consistent with the σ_y and σ_z values, which they must, if the Gaussian description is at all valid. The data from the March 1976 study showed more scatter than those in this study. In the March 1976 study, there were similar findings of lower concentrations than predicted and a slower fall-off with distance than predicted.

5.2 THE EFFECTS OF TOPOGRAPHY ON DISPERSION OF THE GCOS PLUME

5.2.1 Enhanced σ_y Values

In the March 1976 study, the increased values of both σ_y and σ_z were partially attributed to enhanced turbulent mixing due to topographic effects. In this study, some of the σ_y values were larger than predicted, but the σ_z values generally agreed with the Pasquill-Gifford curves. The Pasquill-Gifford curves are not based upon extensive measurements of elevated plumes, and so part of the discrepancies for the σ_y values may be due not to topography, but rather to inaccuracies in the Pasquill-Gifford curves for elevated plume geometry estimates. Since the σ_z values agree reasonably, then enhanced three-dimensional turbulence is probably not present. Topography could, however, generate more horizontal meanderings, which would enhance the lateral dispersion over flat terrain dispersion. A comparison of these low-frequency effects is probably best done using tower data where there are not the uncertainties in the measurement of low-frequency motions that exist for aircraft and to a lesser degree for tethersonde data.

5.2.2 Local Effects

On the 22 June flight, Runs 15 and 17, there was a marked increase in turbulence during plume passage at lower levels at 3.2 km downwind. The enhanced turbulence was noticed at a position above the Steepbank River valley near where it enters the Athabasca River valley. This phenomenon could represent a local effect of the rugged topography associated with the junction of the river valleys. If this interpretation is correct, then localized concentrations at ground level might be increased due to the enhanced local mixing. An alternative explanation is that the plume buoyancy generated its own turbulence, which was significantly larger than the background tubulence levels.

On other flights, turbulence parameters were noted to decrease in intensity on low-level flights over the disturbed area around the Syncrude developments. Presumably the stripping of the ground cover resulted in less surface wind drag and less turbulence generation.

5.2.3 Ground Cover Variations Versus Topography

In the March 1976 field study, crosswind turbulence runs were made parallel to the river valley on both sides of the river valley (wind from the west). It was shown that there were no statistically significant differences in the turbulence levels at typical plume height. Thus, it was concluded that the Athabasca River valley itself probably did not generate significant turbulence from the point of view of dispersion of the main plume.

In this study, there were turbulence flights parallel to the plume centerline as it headed north down the river valley. Flights on the afternoon of 19 June and on 20 June were made along the plume centerline approximately over the river valley and parallel to the centerline but displaced 8 km towards the east. In all four cases (two heights on each of the two days), the turbulence was slightly greater along the runs east of the river than along the river valley itself (see the turbulence statistics tables in the Appendix for details). If the turbulence was significantly affected by topography, then it would be expected that the turbulence over the river valley would be larger, due to the effects of the winding river valley walls.

A possible explanation for the differences is land cover variation effects. The flight lines were compared to a vegetative cover map being prepared for AOSERP by INTERA under the direction of M.D. Thompson. It was apparent that there were significant variations from black spruce to open muskeg to low scrub along and upwind of the flight line east of the Athabasca River. The size scale of fluctuations in ground cover varied considerably, but there were many blocks of landcover types with sizes of 0.5 to 1 km. These

variations in surface roughness and surface heat flux may have contributed to variations in turbulence intensity. Thus, it may be important to consider the surface characteristics and their variations in determining dispersion characteristics in the AOSERP study area.

5.3 SUMMARY OF PLUME RISE DATA

In each case study, the observed plume centerline height was compared to predicted heights according to the formulations of Briggs (1975), Holland (U.S.W.B. 1953), and TVA (Montgomery et al. 1972). The input data to the plume rise formulations were available from the AES tethersonde data. Figure 53 shows the overall accuracy of the plume rise predictions. Note that the data in Figure 53 are plotted on a logarithmic scale so that, say, a factor of two error in either direction gives the same deviation on the plot. Note also that the ratios of predicted and observed effective stack heights (not plume rise) are shown.

The data in Figure 53 indicate that the TVA formulation is slightly better than the Briggs formulation. The Holland formulation consistently underestimates the plume rise. The conclusion that the Briggs and TVA formulations are reasonable predictors for the GCOS plume is consistent with the results of the March 1976 field study.

5.4 RELATIONSHIPS BETWEEN PLUME SIGMA VALUES AND TURBULENCE PARAMETERS

5.4.1 Statistical Theory of Dispersion

In recent years, there has been considerable effort in attempting to apply the statistical theory of dispersion to industrial effluent plumes. The Pasquill-Gifford curves have been recognized as being very rough approximations that should be used only if on-site measurements are not available (Pasquill 1976). In a recent review of the state-of-the-art of dispersion theory, Pasquill (1974) concluded

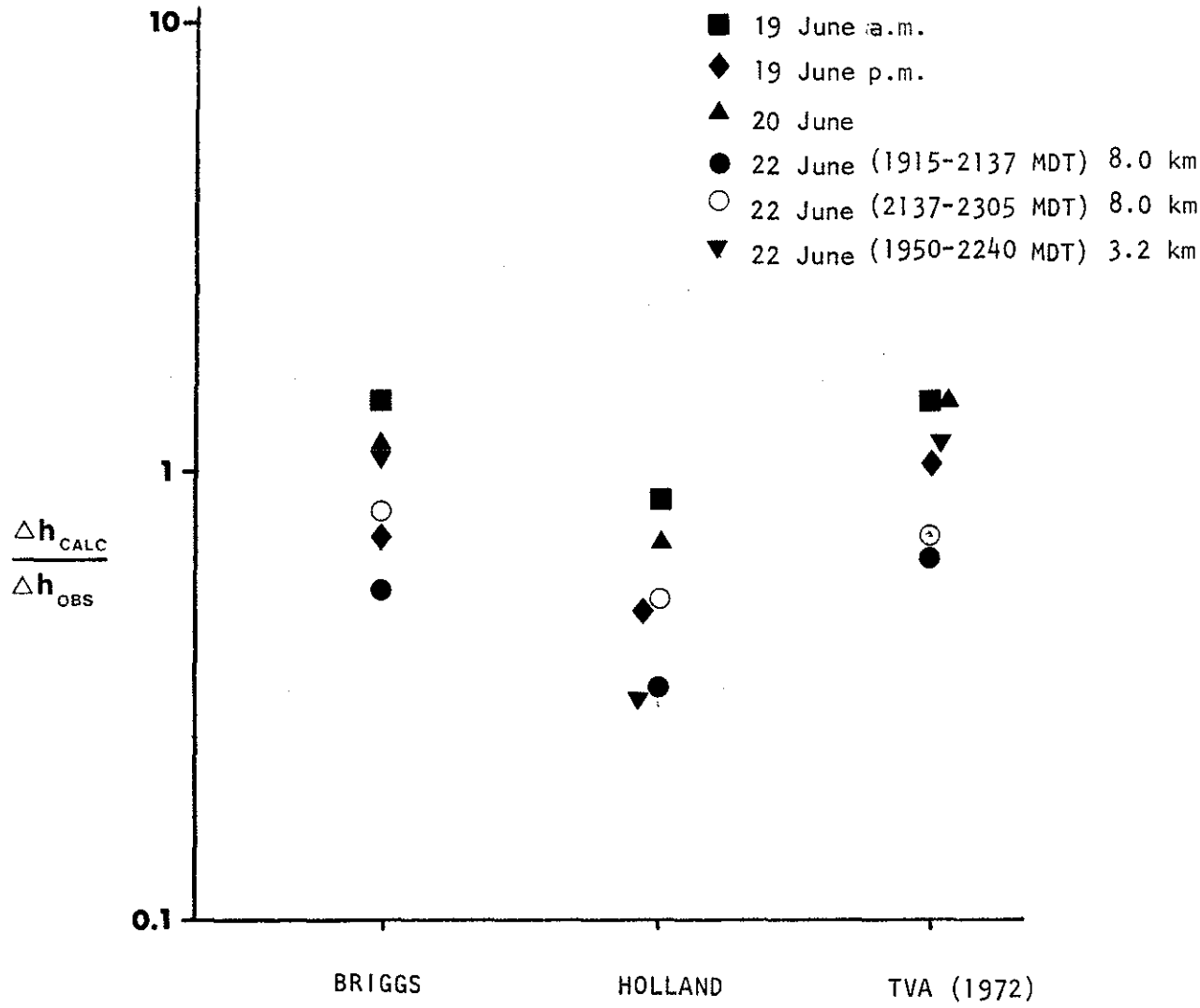

Figure 53. Summary of ratios of calculated to observed effective stack heights, for 1977 flights.

that the statistical theory is the most appropriate theoretical framework for lateral dispersion at all levels and for vertical dispersion for elevated sources when σ_z is less than the effective stack height.

The statistical theory of turbulent diffusion was largely developed by Taylor, who developed an expression relating particle displacements to the autocorrelation function for homogeneous, stationary turbulence

$$\sigma_y^2 = 2\sigma_v^2 \int_o^T \int_o^\tau R(\xi)\, d\xi\, d\tau \qquad (1)$$

where T is the dispersion time and where R is the Lagrangian autocorrelation function of the appropriate velocity component. A similar equation relates σ_z to σ_w. At very short dispersion times, the Lagrangian autocorrelation coefficient is approximately unity, and so

$$\sigma_y^2 = \sigma_v^2\, T^2. \qquad (2)$$

For large dispersion times, T, equation (1) reduces to

$$\sigma_y^2 = 2\,\sigma_v^2\, t_L\, T \qquad (3)$$

where t_L is the Lagrangian integral time scale given by

$$t_L = \int_o^\infty R(\xi)\, d\xi. \qquad (4)$$

(See next section for a brief explanation of the differences between Lagrangian and Eulerian measurements.)

Pasquill (1976) and Draxler (1976) utilized the statistical theory using the following formula as a starting point:

$$\frac{\sigma_y}{\sigma_v T} = f\left(\frac{T}{t_L}\right) \tag{5}$$

where the function f is an expression involving T/t_L to be defined. Pasquill recast Equation (5) in the form:

$$\frac{\sigma_y}{\sigma_\theta x} = f(x) \tag{6}$$

where σ_θ is the standard deviation of the horizontal wind angle. Pasquill suggested that empirical measurements suggested the f(x) was approximately invariant to changes in surface conditions and stability, and he presented suggested values of f(x). The suggested values of f(x) decrease from unity near the source, giving agreement with equation (2), to $0.33\ (10/X)^{1/2}$ where X is downwind distance in kilometres for X > 10 km. This long dispersion time limit gives agreement with equation (3), with t_L taken as a constant. If the empirical data upon which the suggested values of f(x) are examined, it is seen that the data have a range of about a factor of 4, presumably due partly to the neglect of variations in the integral scales.

In this study, plume measurements were taken at 3.2 and 8.0 km downwind of the source. Thus, it is worthwhile to consider the long dispersion time form of the statistical theory, i.e., equation (3). It can be recast as

$$\frac{\sigma_y}{\sigma_v T^{1/2}} = \sqrt{2t_L} \tag{7}$$

Thus, if equation (3) is valid, the value of the plume spread, when normalized as in (7), should be invariant with distance, and its value should lead to an estimate of the Lagrangian integral time scale. From the Lagrangian integral time scale and the intensity

of the turbulence, it is possible to estimate the integral length scales using the expressions

$$\ell_L \simeq \ell_E = \bar{U} t_E = \frac{\bar{U} t_L}{\beta} \tag{8}$$

where $\beta i = 0.44$, from empirical results

and where i is the intensity of turbulence ($i \simeq \sigma_v/\bar{U}$ in the horizontal)

$\bar{U}$ is the mean wind speed

t_E is the Eulerian integral time scale

ℓ_E is the Eulerian integral length scale

ℓ_L is the Lagrangian integral length scale

These expressions follow the review by Pasquill (1974, pp. 87 ff). The separation of experimental data when plooted according to (7) and the resultant integral scale estimates according to equation (8) can be compared to the observed integral scales.

5.4.2 A Brief Outline of Lagrangian and Eulerian Measurements

Throughout turbulence theory, reference is made to Lagrangian and Eulerian statistics and measurements. A Lagrangian measurement is a measurement taken by following an individual particle. For example, the Lagrangian velocity of a particle, as a function of time, is the velocity of a particular marked particle. The Eulerian velocity, however, is the velocity measured at a fixed point in space or along a given path that is not the path of a particular particle. The theory of turbulent diffusion usually involves Lagrangian velocity autocorrelations, which refer to how long (or how far) a particle is correlated with its past motion. The time integral of the Lagrangian autocorrelation is the Lagrangian integral time scale and is often considered the "memory" of turbulence. The Eulerian integral time scale of velocity, however, is a measure of how long the motion at a particular point in space is correlated. It turns out that the Lagrangian time scales are typically two to four times longer than the Eulerian time scales (Pasquill 1974).

This means that the motion of a particular particle changes more slowly than the motion at a fixed point in space. However, measurements are almost always Eulerian measurements, and so one of the major problems in dispersion theory is how to relate the Eulerian measurements of the structure of the turbulence to the Lagrangian-based theoretical formulations. Although in recent years the Eulerian-Lagrangian relationships have been somewhat better understood, there is still no completely adequate theoretical framework, and the experimental data still have significant uncertainties associated with them.

5.4.3 Normalized Plume Spread

The observed plume sigma values and the associated standard deviations of the turbulent velocities are presented in Table 17. The turbulent velocity standard deviations have been corrected for the effects of the extraneous energy peak noted in spectral analysis plots. In Table 18 are presented the normalized plume spread values for both the Pasquill-Draxler formulation of equation (5) and the statistical theory formulation of equation (7). Figures 54, 55, 56, and 57 show plots of the normalized plume spread versus downwind distance.

Figures 54 and 55 show that there is considerable scatter in the data for the normalized vertical plume spread. The result is not surprising, since some of the case studies indicated very little change in σ_z from 3.2 to 8.0 km. Since the effluent plume is buoyant, it is to be expected that the plume itself will generate turbulent mixing, which may dominate the ambient mixing in the vertical, particularly for stable situations. This effect has been noted in a summary of recommendations recently developed by an AMS workshop (Hanna et al. 1977). Thus a simple normalization of vertical plume spread by ambient conditions will lead to considerable scatter.

Figure 56 shows the lateral spread normalized according to equation (5) with Pasquill's recommended values of f(x) drawn in. Although the observed values have a fall-off with distance, there is a large offset, especially for the 19 June case studies.

Table 17. Summary of input data used for the calculation of normalized plume spread.

Date (1977)	Times [m]	Downwind Distance [km]	σ_z [m]	σ_y [m/sec]	σ_y [m]	σ_{uH} [m/sec]	$\bar{U}$ [m/sec]
19 June	0828-0935	3.2	78	0.93	1570	0.76	7
		8.0	77	0.93	2120	0.76	7
19 June	1415-1610	3.2	270	1.32	-[a]	1.28	7
		8.0	260	1.32	3700	1.28	7
20 June	1130-1230	3.2	170	0.82	501	1.06	5.2
		8.0	175	0.82	725	1.06	5.2
20 June	1230-1340	3.2	170	1.14	528	1.46	5.2
		8.0	175	1.14	970	1.46	5.2
22 June	1915-2130	3.2	50	1.17	375	1.46	9
		8.0	200	0.99	340	1.17	9
22 June	2145-2245	3.2	50	0.63	375	1.02	9
		8.0	90	0.49	480	0.69	9

[a]No reliable data available.

20 June: Runs 1 and 2 (1130-1145) typified the early portion; Runs 15 and 16 (1310-1325), typified the later portion; the plume geometry values were not changing rapidly except for σ_y at 8.0 km downwind.

22 June: The velocity standard deviations were derived from the following runs:
Afternoon, 3.2 km: Runs 5, 6
Afternoon, 8.0 km: Runs 3, 4
Evening, 3.2 km: Runs 15B, 16, 17B, 18
Evening, 8.0 km: Runs 19, 20, 22

Table 18. Summary of normalized plume spread.

Date (1977)	Data Times [MDT]	Downwind Distance [km]	$\frac{\sigma_z}{\sigma_w T}$	$\frac{\sigma_z}{\sigma_w T}^{1/2}$ [$sec^{1/2}$]	$\frac{\sigma_y}{\sigma_{uH} T}$	$\frac{\sigma_y}{\sigma_{uH} T}^{1/2}$ [$sec^{1/2}$]
19 June	0828-0935	3.2	0.18	3.9	4.5	97
		8.0	0.07	2.5	2.5	83
19 June	1415-1610	3.2	0.45	9.6	-[a]	-[a]
		8.0	0.19	6.5	2.5	86
20 June	1130-1230	3.2	0.34	8.4	0.80	20
		8.0	0.14	5.5	0.44	17
20 June	1230-1340	3.2	0.24	6.0	0.58	14
		8.0	0.10	3.9	0.43	17
22 June	1915-2130	3.2	0.12	2.3	0.72	14
		8.0	0.22	6.7	0.33	10
22 June	2145-2245	3.2	0.22	4.2	1.04	20
		8.0	0.21	6.1	0.79	23

[a]No reliable data available.

20 June: Runs 1 and 2 (1130-1145) typified the early portion; Runs 15 and 16 (1310-1325), typified the later portion; the plume geometry values were not changing rapidly except for σ_y at 8.0 km downwind.

22 June: The velocity standard deviations were derived from the following runs:
Afternoon, 3.2 km: Runs 5, 6
Afternoon, 8.0 km: Runs 3, 4
Evening, 3.2 km: Runs 15B, 16, 17B, 18
Evening, 8.0 km: Runs 19, 20, 22.

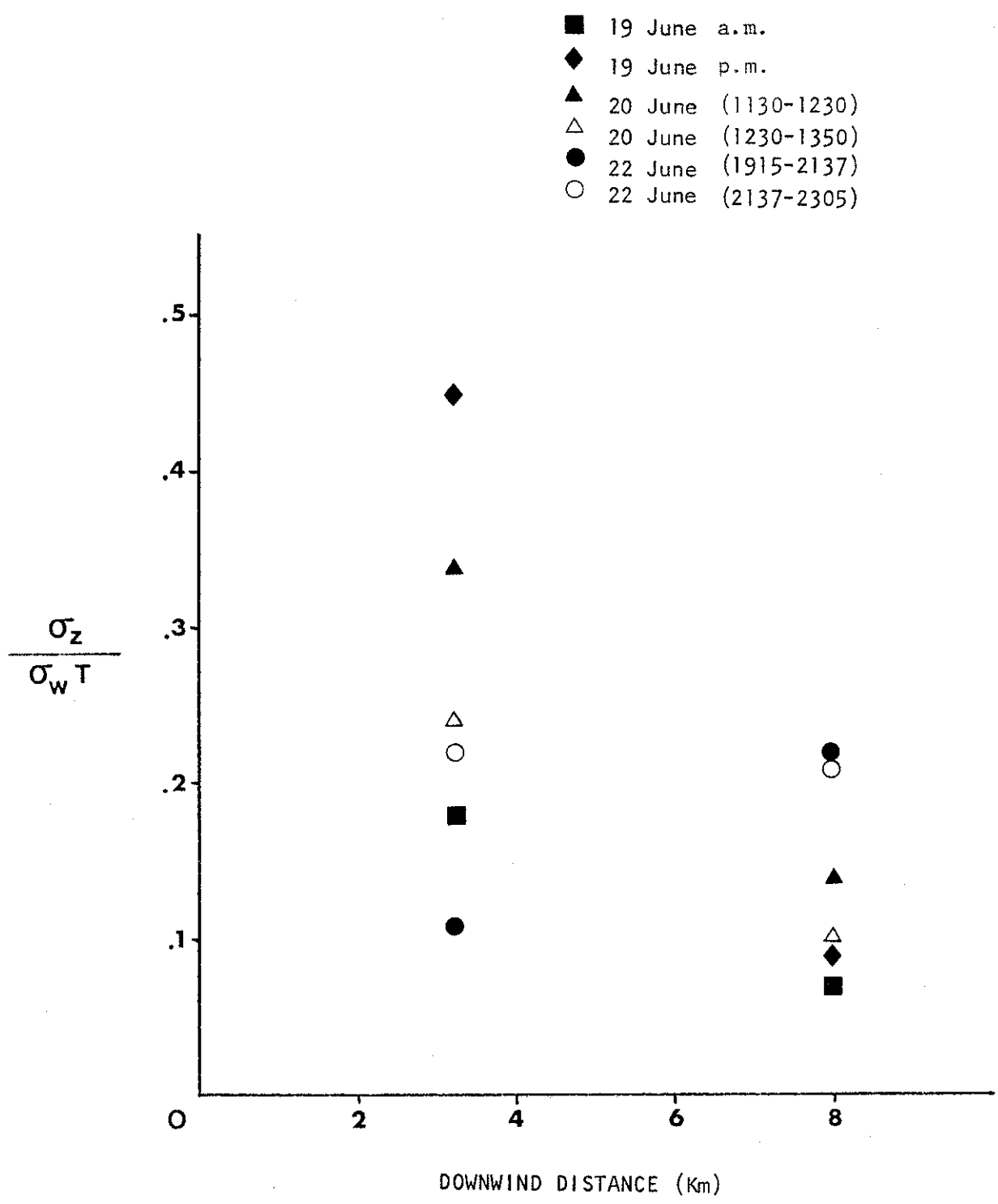

Figure 54. Normalized vertical plume spread according to the Pasquill-Draxler approach of equation (5).

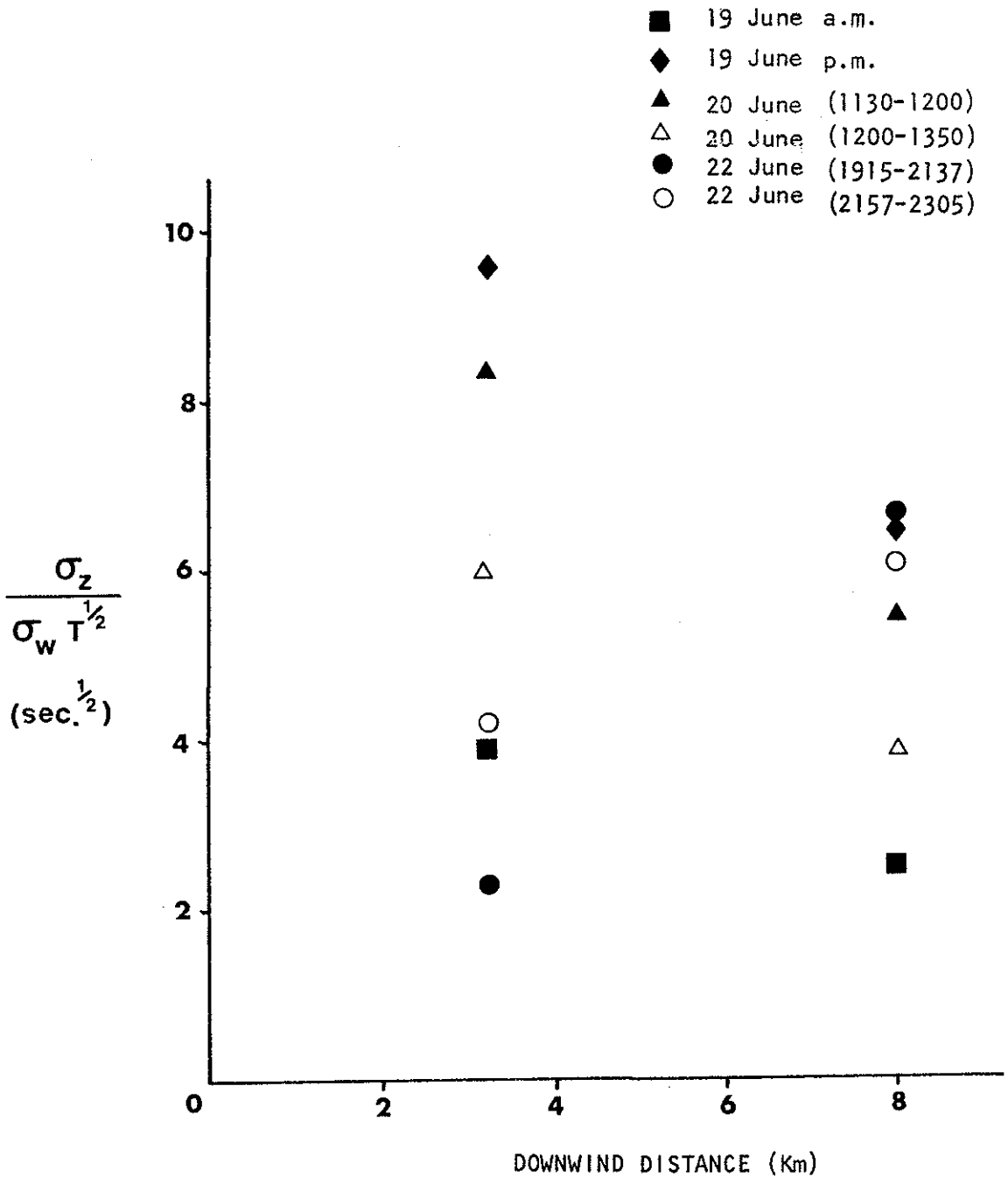

Figure 55. Normalized vertical plume spread according to the long dispersion time predictions of Taylor's statistical theory.

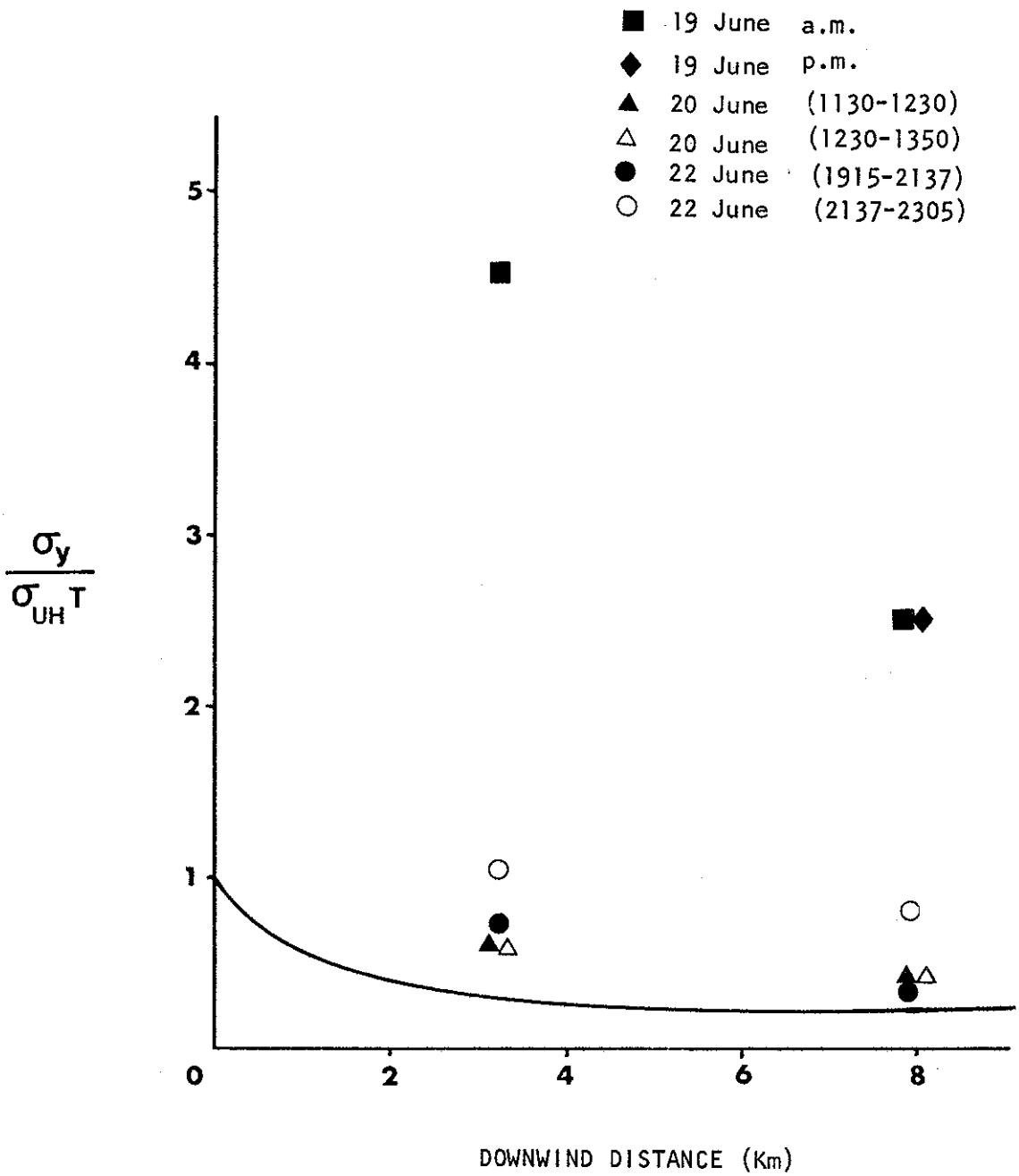

Figure 56. Normalized lateral plume spread according to the Pasquill-Draxler approach of equation (5). The curve on the figure represents Pasquill's recommended curve for the downwind decay of the normalized plume spread.

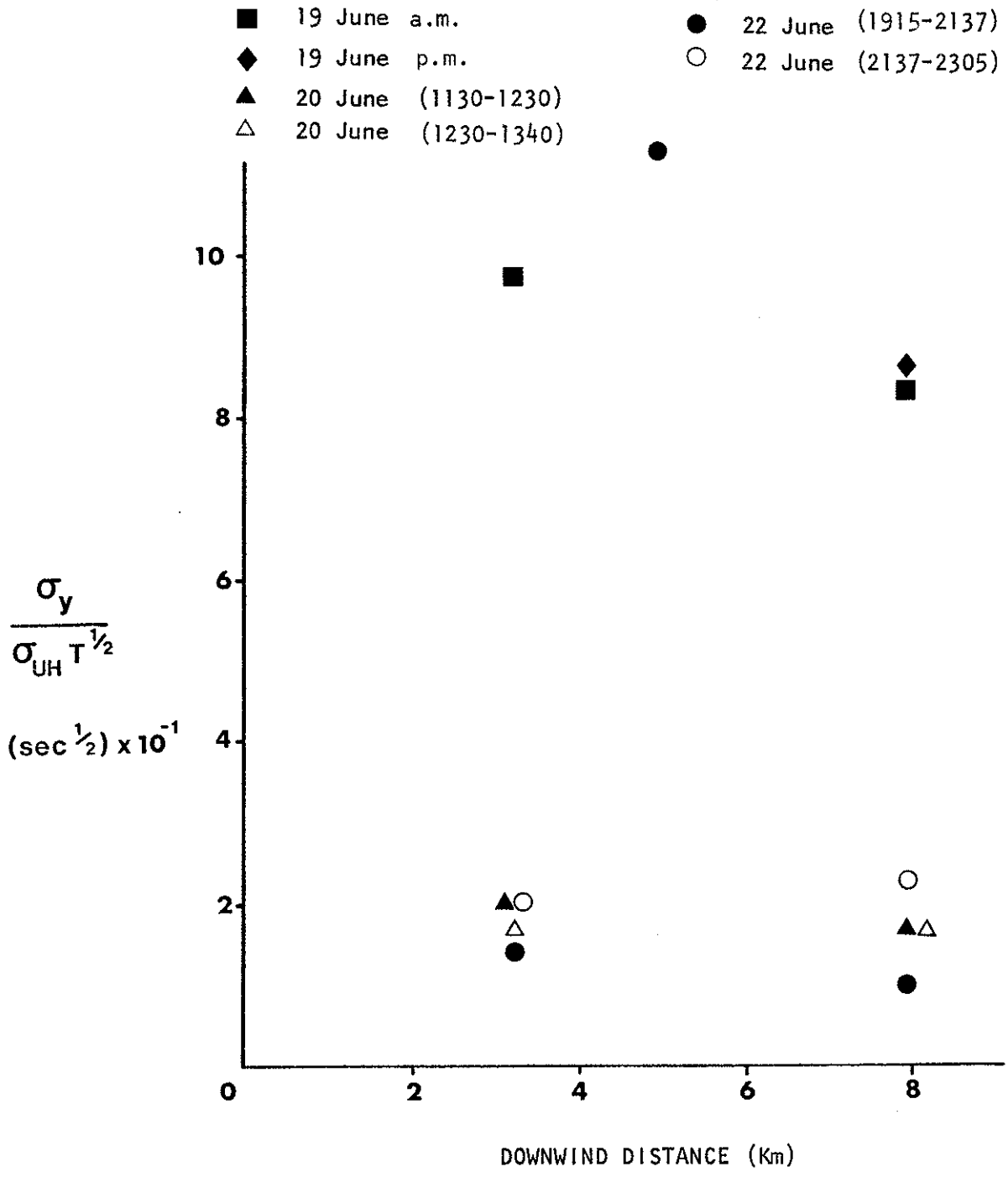

Figure 57. Normalized lateral plume spread according to the long dispersion time predictions of Taylor's statistical theory.

Figure 57 shows the lateral plume spread normalized according to equation (7). If equation (7) is satisfied, then the data should form horizontal lines for each day, since there should be no remaining time (or distance) dependence. If the normalized plume spread is compared to

$$\frac{\sigma_y}{\sigma_{uH}} = \alpha T^n \tag{9}$$

where α and n are constants, then the data produce a value of $n = 0.42$ with a standard deviation of the mean of 0.1, in good agreement with the long-dispersion time form of Taylor's theory (0.5).

It is instructive to consider the effect on plume spread normalization of an intial value of σ_y. If the plume undergoes initial, enhanced dispersion due to turbulence generated by its own buoyancy and momentum and due to the initial diameter of the plume (or multiple sources), then after a long dispersion time the dispersion according to the statistical theory becomes

$$\sigma_y = \sigma_{yo} + \sigma_y (2t_L)^{1/2} T^{1/2} \tag{10}$$

where σ_{yo} is the equivalent initial value of σ_y, accounting for the effects of plume-generated turbulent dispersion and the finite size of the initial source. When reformulated as in equation (7), (10) becomes

$$\frac{\sigma_y}{\sigma_v T^{1/2}} = \frac{\sigma_{yo}}{\sigma_v T^{1/2}} + (2t_L)^{1/2} \tag{11}$$

The effects of the first term on the right hand side of equation (11) are seen to be an increased value of the normalized plume spread that gradually decreases as the dispersion time increases. These are exactly the effects observed.

The Lagrangian integral time scales were estimated from the measured Eulerian length scales using equation (8). It must be cautioned that the measured integral scales showed considerable

variability and so do not have a high degree of statistical reliability. Furthermore, the extraneous spectral energy peak discussed previously may have contaminated some of the integral scale estimates. Table 19 shows the estimate of the Lagrangian integral time scales, t_L, together with, β, the parameter relating Eulerian and Lagrangian time scales and values of $(2t_L)^{1/2}$, which can be compared with the normalized plume spread estimates. The general agreement, except for the flights of 19 June is very good. The fact that the normalized plume spread values are higher than $(2t_L)^{1/2}$ is in agreement with the discussion leading to equation (11).

The reason for the very large σ_y values for both flights of 19 June is unclear. The mass fluxes for these flights gave reasonable agreement with emission data, and the shapes of the plume cross sections were reasonable. The wind speed of 7 m/sec from the AES tethersonde was midway between the values of 20 June and 22 June. The presence of a capping inversion in the morning and multiple source problems in the afternoon of 19 June may be at least partial explanations.

The values for β in Table 19 are in general agreement with previous values. Pasquill (1974) suggested that β has a range of about 2-4, depending upon stability with the larger values occurring in stable conditions. In this study, the ranges of β were slightly larger, but the stability dependence was the same as suggested by Pasquill. Note that these values of β are not from independent measurements of the Langrangian and Eulerian time scales but rather from the approximations in equation (8).

Except for the case of 19 June, this analysis shows that it is worthwhile to pursue the full Taylor theory approach according to equation (7) for the normalization of the lateral plume spread. A useful procedure may be to document integral scales as functions of stability and turbulent intensity with the aid of recent boundary layer theory. In this way the factor of 4 scatter in Pasquill's formulation may be reduced substantially by applying rough estimates of integral scales to the full statistical theory approach of equation (7) even when accurate estimates are not available.

Table 19. A comparison of integral time scales to estimates from normalized plume spreads.

Date (1977)	Data Times [MDT]	Downwind Distance [km]	β	t_L [sec]	$(2t_L)^{1/2}$ $[sec]^{1/2}$	$\frac{\sigma_y}{\sigma_u T^{1/2}}$ [a] $[sec]^{1/2}$
19 June	0828-0935	3.2 & 8.0	4	114	15	90
19 June	1415-1610	8.0	2.4	68	12	86
20 June	1130-1230	3.2 & 8.0	2.2	79	13	19
	1230-1340	3.2 & 8.0	1.6	63	11	16
22 June	1915-2130	3.2	2.7	60	11	14
		8.0	3.4	94	14	10
	2145-2245	3.2	3.9	104	14	20
		8.0	5.7	194	20	23

Note: Averages of values of 3.2 and 8.0 km were used wherever values for combined distances are indicated.

β is the rate of Lagrangian to Eulerian integral time scales

$\beta = t_L/t_E$

[a] This last column is reproduced from the normalized plume spread table for convenience of comparison with $(2t_L)^{1/2}$.

Further progress in normalization of the vertical plume spread (even when capping inversions are not present and σ_z is significantly less than the effective stack height) will probably depend upon simulating the initial plume expansion and finite source size.

The values of the Lagrangian integral time scale presented in Table 19 are much smaller than the values suggested by Draxler (1976). For elevated sources and for horizontal diffusion, Draxler suggested values of the Lagrangian integral time scale of about 600 sec. If that values was appropriate, then the $T^{1/2}$ behaviour according to Taylor's theory would not be exhibited until perhaps 3 integral time scales, or about 12 km downstream from the stack. The observed $T^{1/2}$ behaviour occurred typically within 3 km of the stack, consistent with the values of Lagrangian integral time scale presented in Table 19.

6. CONCLUSIONS

The experimental design and the equipment mobilized for this study could adequately define the effluent plume geometry and associated turbulence levels so as to accomplish the goals of the project. From the analysis and interpretation of the data several specific conclusions can be made.

The observed values of the lateral plume spread coefficient, σ_y, increased more slowly with distance than the Pasquill-Gifford curves predicted. Although the magnitude of some of the σ_y values agreed reasonably well with the Pasquill-Gifford curves, the σ_y values were a factor of about four larger for two case studies. In the March 1976 study (AOSERP Report 13), the σ_y values were consistently greater than the Pasquill-Gifford curves by a factor of two to four.

The observed values of the vertical plume spread coefficient, σ_z, had reasonable agreement with the Pasquill-Gifford curves at 3.2 km downwind from the source, but often did not increase substantially at farther downwind distances. The effects of reduced vertical mixing due to increased thermal stability with height were considered to be the reason for the discrepancy. These results are similar to those from the March 1976 study.

The normalized axial centerline concentrations generally were in reasonable agreement with the Pasquill-Gifford curves, except that the observed concentrations were usually lower and decreased less rapidly with distance than predicted.

The SO_2 mass flux could be calculated by vertical integration of the crosswind integrated concentration values from the various plume traverses, using a vertical weighting depending upon wind speed. Typical accuracy, compared to emission data supplied by GCOS, was about 10% to 20%. There were three major sources of error: uncertainty of the appropriate wind speed profile whenever the AES tethersonde did not reach effective stack height, limited vertical resolution due to a limited number of plume traverses,

and lack of stationarity in the meteorological conditions. Nevertheless, the mass flux computation provided a very useful check on the calibration of the SO_2 sensor.

The Gaussian shape of the plume was a reasonable approximation for the shape of the lateral concentration profile except when a secondary plume was present and in unstable convective conditions. It is recognized that the Gaussian profile is normally treated as a time-averaged profile, so that lack of a Gaussian shape in aircraft plume traverses in unstable conditions does not mean that the time-averaged or ensemble-averaged profile would not be Gaussian. The Gaussian shape was not as common in the vertical, due to changing stability conditions with height.

Significant vertical and temporal changes in the turbulence parameters were observed in every case study. A single stability case was seldom adequate to describe the boundary layer structure in which the plume existed. Interpretation of the SO_2 concentrations within the case studies was made much more reliable by detailed information on the turbulence structure.

From comparisons of turbulence statistics from runs parallel to the wind at the same altitude but along different paths, it was concluded that there was no enhanced turbulence generated by winds flowing down the Athabasca River at typical plume heights. On the contrary, turbulence levels over the region about 8 km east of the river and parallel to the river were somewhat greater than above the river. Variations in ground cover rather than topography were suggested to be the causes of the enhanced dispersion. On two runs within one case study, markedly enhanced turbulence was detected during the actual plume traverses at 3.2 km downwind from the stack while above the junction of the Steepbank River and the Athabasca River. It is probable that this effect is due to the complex topography, but turbulence generated by the buoyancy and initial momentum of the plume itself may also be a cause.

The observed values of plume rise were compared to the formulations by Briggs, TVA, and Holland. The TVA formulation was marginally better than the Briggs formulation; the Holland formulation consistently underpredicted the actual plume rise. These results are consistent with the results of the March 1976 study.

The increase in σ_y with downwind distance from 3.2 and 8.0 km followed the predictions of Taylor's statistical theory for the long dispersion times. The average exponent of time dependence was 0.42, with a standard deviation of the mean of 0.1. This value can be compared to the Taylor theory prediction of 0.5 and the March 1976 value of 0.46.

The magnitude of the normalized plume spread according to Taylor's theory should be $(2t_L)^{1/2}$ where t_L is the Lagrangian integral time scale. Except for the flights of 19 June, the estimates of t_L from the velocity autocorrelation analysis agreed well with the observed magnitudes of the normalized lateral plume spread. The σ_y values for 19 June were markedly larger than those predicted by both the statistical theory and the Pasquill-Gifford curves.

It was shown that the effects of the initial enhanced plume spread due to plume-generated turbulence and finite source size could at least partially explain the wide scatter observed for the normalized vertical plume spread. Taylor's theory was found to be inadequate to describe vertical dispersion, even close to the stack.

The small discrepancy in the exponent of time dependence for the normalized lateral plume spread (0.42 rather than 0.5) is precisely the effect expected in the presence of initial plume-induced turbulent mixing or finite source size. The effect should decrease with distance, leaving the $T^{1/2}$ behaviour valid at longer dispersion times.

The formulation recently presented by Pasquill (1976) and recommended as a modification to the Turner Workbook (Hanna et al. 1977) would have significantly underestimated the σ_y values in every case examined.

7. REFERENCES CITED

Baird, D.C. 1962. Experimentation: an introduction of measurement theory and experiment design. Prentice Hall, Englewood Cliffs, N.J. 198 pp.

Blackman, R.B., and J.W. Tukey. 1959. The measurement of power spectra. Dover, New York. 190 pp.

Briggs, G.A. 1969. Plume rise. AEC. Crit. Rev. Ser. TID-27075.

Briggs, G.A. 1975. Plume rise predictions. D.A. Haugen, ed. Lectures on air pollution and environmental impact analyses. Am. Meteorol. Soc., Boston. 296 pp.

Davison, D.S. 1973. The structures of convention in the planetary boundary layer. Ph.D. Thesis. Univ. of British Columbia. 152 pp.

Davison, D.S., C.C. Fortems, and K.L. Grandia. 1977. Plume dispersion measurements from an oil sands extraction plant, March 1976. Project ME 2.3.1, Alberta Oil Sands Environmental Research Program, Oxbridge Place, Edmonton. AOSERP Report 13. 195 pp.

Donelan, M., and M. Miyake. 1973. Spectra and fluxes in the boundary layer of the trade wind zone. J. Atmos. Sci. 30:444-464.

Draxler, R.R. 1976. Determination of atmospheric diffusion parameters. Atmos. Environ. 10:99-105.

Fanaki, F. 1978. Meteorology and air quality winter field study, March 1976. AOSERP Project ME 1.5.3 (in prep.).

Gifford, F.A. 1961. Use of routine meteorological observations for estimating atmospheric dispersion. Nucl. Saf. 2:47-51.

Hanna, S.R., G.A. Briggs, J. Deardorff, B.A. Egan, F.A. Gifford, and F. Pasquill. 1977. AMS workshop on stability classification schemes and sigma curves - summary of recommendations. Bull. Am. Meteorol. Soc. 58:1305-1309.

Kaimal, J.C., J.C. Wyngaard, D.A. Haugen, O.R. Cote, Y. Izumi, S.J. Caughey, and C.J. Readings. 1976. Turbulence structure in the convective boundary layer. J. Atmos. Sci. 33:2152-2169.

Kanasewich, E.R. 1975. Time sequence analysis in geophysics. Univ. of Alberta Press, Edmonton. 363 pp.

Lee, Y.W. 1967. Statistical theory of communication. Wiley, New York. 509 pp.

Lenschow, D.H. 1970. Airplane measurements of planetary boundary layer structure. J. Appl. Meteorol. 9:874-884.

Lumley, J.L., and H.A. Panofsky. 1964. The structure of atmospheric turbulence. Interscience, New York. 239 pp.

Mather, G.K. 1967. The NAE turbulence research aircraft. Report LR-474, National Aeronautical Establishment. National Research Council. 12 pp.

McBean, G.A., and J.I. MacPherson. 1976. Turbulence above Lake Ontario: velocity and scalar statistics. Submitted for publication.

Montgomery, T.L., S.B. Carpenter, W.C. Colbaugh, and F.W. Thomas. 1972. Results of recent TVA investigations of plume rise. J. Air Pollut. Control Assoc. 22:779-784.

Myrup, L.O. 1967. Temperature and vertical velocity fluctuations in strong convection. Q.J.R. Soc. 93:350-360.

Paquin, J.E., and S. Pond. 1971. The determination of the Kolmogoroff constants for velocity, temperature and humidity fluctuations from second- and third-order structure functions. JFM, 50:part 2:257-269.

Pasquill, F. 1961. The estimation of windborne material. Meteorol. Mag. 90:33-49.

Pasquill, F. 1971. Atmospheric dispersion of pollution. J. Meteorol Soc. 97:369-395.

Pasquill, F. 1974. Atmospheric diffusion. Ellis Horwood, Chichester, U.K. 429 pp.

Pasquill, F. 1976. Atmospheric dispersion parameters in Gaussian plume modelling. Part II. Possible requirements for change in the Turner Workbook values. U.S. EPA Report EPA-600/4-76-030b. Research Triangle Park, North Carolina.

Pond, S., R.W. Stewart, and R.W. Burling. 1963. Turbulence spectra in the wind over waves. J. Atmos. Sci. 20:319-324.

Slade, D.H. (ed.). 1968. Meteorology and atomic energy 1968. U.S. Atomic Energy Commission. TID-24190.

Tennekes, H., and J.L. Lumley. 1972. A first course in turbulence. MIT Press, Cambridge, Mass. 300 pp.

Turner, B.D. 1970. Workbook of atmospheric dispersion estimates. U.S. Department of Health, Education, and Welfare, Public Health Service Publ. 999-AP-26.

Wyngaard, J.C. 1973. On surface-layer turbulence. In D.A. Haugen (ed.), Workshop on micrometeorology. Am. Meteorol. Soc., Science Press, Ephrata, Pa. 392 pp.

8. APPENDICES

8.1 EMISSION CHARACTERISTICS FROM GCOS PLANT

Emission characteristics used to calculate the plume rise were provided by GCOS for the period of the field program. These are summarized for the two main stacks.

1. Incinerator stack

height	107 m
diameter	1.8 m
altitude of stack top	366 m AMSL
exit temperature	603 $\pm$ 18°C
exit velocity	16.6 $\pm$ 1.2 m/sec

2. Powerhouse stack

height	107 m
diameter	5.8 m
altitude of stack top	366 m AMSL
exit temperature	280 $\pm$ 18°C
exit velocity	20.1 $\pm$ 1.2 m/sec

8.2 THE APPROPRIATE GAUSSIAN EQUATION FOR NORMALIZED AXIAL CENTERLINE CONCENTRATION

The observed normalized centerline concentrations of SO_2 were compared with the predictions of a Gaussian model using dispersion coefficients commonly referred to as the Pasquill-Gifford coefficients. The time-averaged concentration field in the Gaussian model is given by (Pasquill 1971):

$$\frac{X\,(x,y,x)\;\bar{U}}{Q} = \frac{1}{2\Pi\;\sigma_y\;\sigma_z}\left[\exp - \frac{y^2}{2\;\sigma_y^{\,2}}\right]\left[\exp - \frac{(H-z)^2}{2\;\sigma_y^{\,2}} + \exp - \frac{(H+z)^2}{2\;\sigma_z^{\,2}}\right] \quad \text{(A-1)}$$

where Q is the source strength and H the height of the source. The above formulation assumes complete "reflection" of the plume from the ground; the second term in the square brackets is a virtual source required to simulate the complete reflection at the surface.

Using the above model, the axial centerline concentrations are given by

$$\frac{X\ (x,0,H)\ \bar{U}}{Q} = \frac{1}{2\Pi\ \sigma_y\ \sigma_z}\left[1 + \exp = \frac{4H^2}{2\ \sigma_z^2}\right] \qquad \text{(A-2)}$$

Again, the second term in the square bracket simulates the complete reflection at the surface. Physically, it is clear that for downwind distance for which σ_z is less than or of a similar size to H, the effects of reflection of the plume at the surface cannot have a significant effect at plume centerline. For large downwind distances, the second term due to the virtual source approaches unity.

If no virtual source is assumed, then the predicted concentration field at axial centerline is given by:

$$\frac{X\ (x,o,H)\ \bar{U}}{Q} = \frac{1}{2\Pi\ \sigma_y\ \sigma_z} \qquad \text{(A-3)}$$

On physical grounds, it is clear that equation (A-3) is more appropriate than (A-2) for axial centerline concentrations at downwind distances where σ_z is similar in size to or smaller than the effective plume height, or equivalently until the plume is well mixed in the vertical.

The observed 8.0 km σ_z values were always a factor of two less than the observed effective stack height (see Table 20).

Thus, equation (A-3) without a virtual source was adopted as the equation for comparison of the observed axial concentrations to Gaussian predictions in all of the case studies.

Table 20. Comparison of the observed effective stack heights with the observed σ_z values.

Case Study	Adopted Pasquill-Gifford Stability Class	Observed Effective Stack Height [m AGL][a]	Observed 8.0 km σ_z [m]
19 June a.m.	D	300	77
19 June a.m.	C	540	260
20 June	B-C	350	175
22 June early	D	660	200
22 June late	E	420	90

[a]The effective stack height is referenced to the height of the base of the stack; depending upon the direction of plume motion, the effective stack height based upon local ground elevation could be up to 100 m less.

8.3 ADDITIONAL DETAILS OF SO_2 CONCENTRATIONS AND TURBULENCE STATISTICS FOR THE FLIGHT OF 19 JUNE 1977 (0745-1010 MDT).

Table 21. Run information for flight of 19 June 1977 (0745-1010 MDT).

Run Number	Start Time (MDT)	Altitude (m AMSL) ± 20	Downwind Distance (km) ± 0.3	σ_y (m) ± 100	Max. SO_2 Conc. (ppm) ± 0.02	Integrated Conc. (ppm-m) ± 50	Flight Dir. (from-to)
1	0828	610	3.2	1572	0.19	495	E-W
2	0834	610	8.0	2116	0.12	333	W-E
3[a]	0840	760	3.2	-	-	-	E-W
4[a]	0847	760	8.0	-	-	-	W-E
5	0856	519	3.2	4672	0.14	553	E-W
6	0902	519	8.0	4194	0.13	449	W-E
7	0909	671	3.2	1739	0.20	514	E-W
8	0916	671	8.0	5375	0.13	453	W-E
9	0923	564	3.2	5895	0.15	385	E-W
10	0930	564	8.0	5563	0.16	618	W-E
11	0938	610	3.2	3208	0.19	440	E-W
12T	0949	610	-	-	-	-	N-S

[a]No detectable SO_2.

T = turbulence run.

Table 22. Turbulence statistics from each run for the flight of 19 June 1977 (0745-1010 MDT).

Run No.	HT. m AMSL	X km	σ_w	σ_v	$\overline{W'V'}$	$\overline{W'T'}$	ℓ_w	ℓ_v	ε	N
1	610	3.2	1.12	0.81	+0.36	-0.03	270	190	8	2
2	610	8.0	0.95	1.00	0.25	0.13	180	130	10	2
3[a]	760	3.2	1.03	0.84	-0.34	0.01	300	270	2	3
4[a]	760	8.0	0.86	1.05	-0.17	-0.00	290	360	2	4
5	519	3.2	1.26	0.91	+0.29	-0.01	230	80	22	3
6	519	8.0	1.33	1.28	0.41	0.02	160	170	35	4
7	671	3.2	1.39	1.07	+0.28	-0.12	190	160	20	4
8	671	8.0	1.82	1.63	-1.01	0.31	270	200	43	4
9	564	3.2	1.59	2.07	-0.15	-0.04	210	280	0	4
10	564	8.0	1.51	1.54	-0.84	-0.03	190	180	60	4
11	610	3.2	1.67	1.12	+0.35	-0.01	180	120	40	3
12T	610	-	0.83	0.89	-0.06	0.00	180	210	13	3

Notes: All units are MKS except dissipation, ε, which is expressed in $cm^2 \cdot sec^{-3}$.

X downwind distance from GCOS stack for crosswind flights

σ_w standard deviation of the vertical velocity

σ_v standard deviation of the lateral velocity with respect to the aircraft

$\overline{W'V'}$ product of fluctuating vertical and lateral velocities with sign changes so that crosswind flights express $\overline{W'U'}$ with respect to ground and along wind flights express $\overline{W'V'}$ with respect to ground using a right hand co-ordinate system with positive u in direction of wind.

$\overline{W'T'}$ product of fluctuating temperature and vertical velocity

ℓ_w integral length scale for vertical velocity

ℓ_v integral length scale for lateral velocity with respect to the aircraft

ε dissipation

N number of 65 sec analysis blocks in the run

T turbulence run flown parallel to wind.

[a]No detectable SO_2.

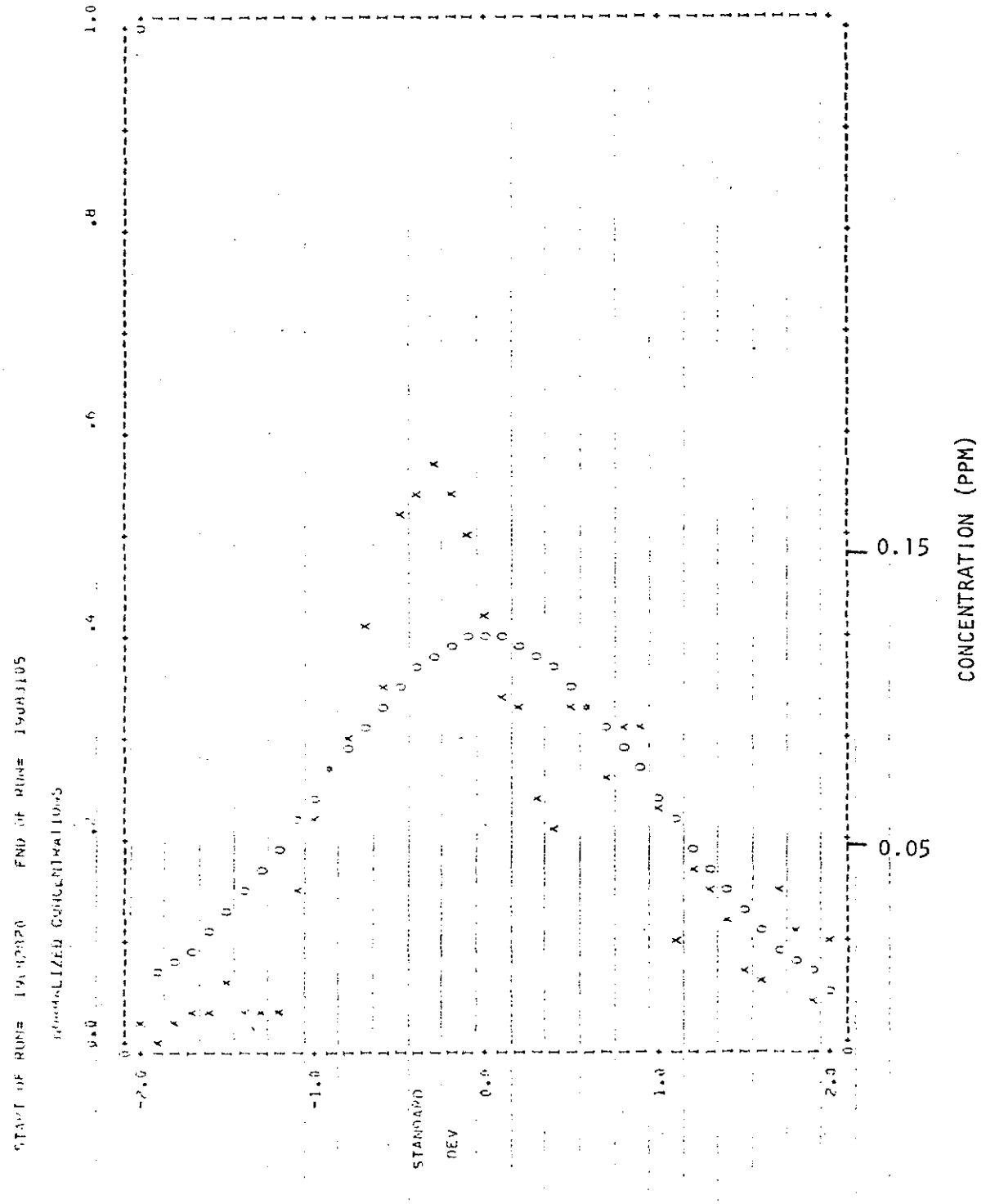

Figure 58. Run 1, 19 June 1977.

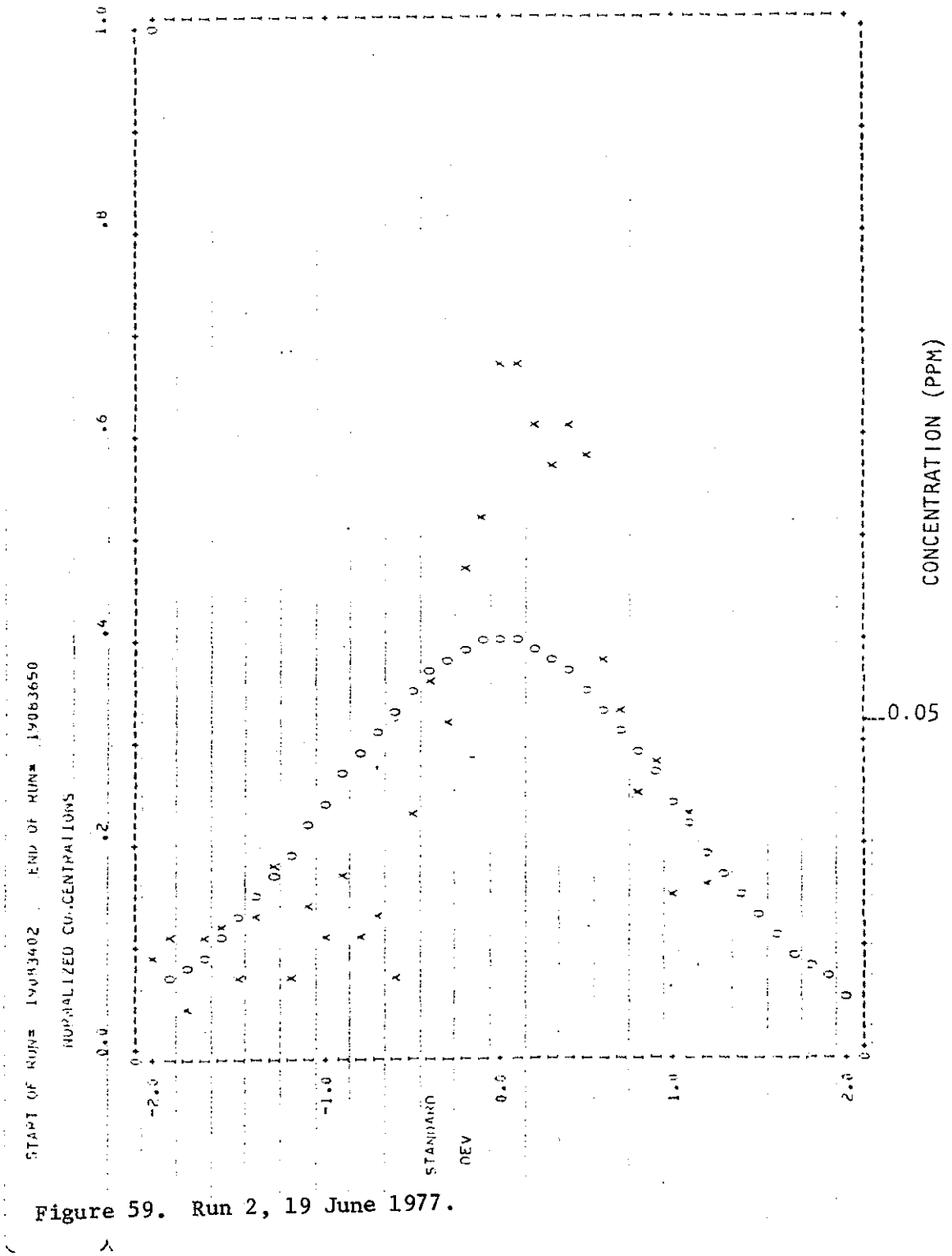

Figure 59. Run 2, 19 June 1977.

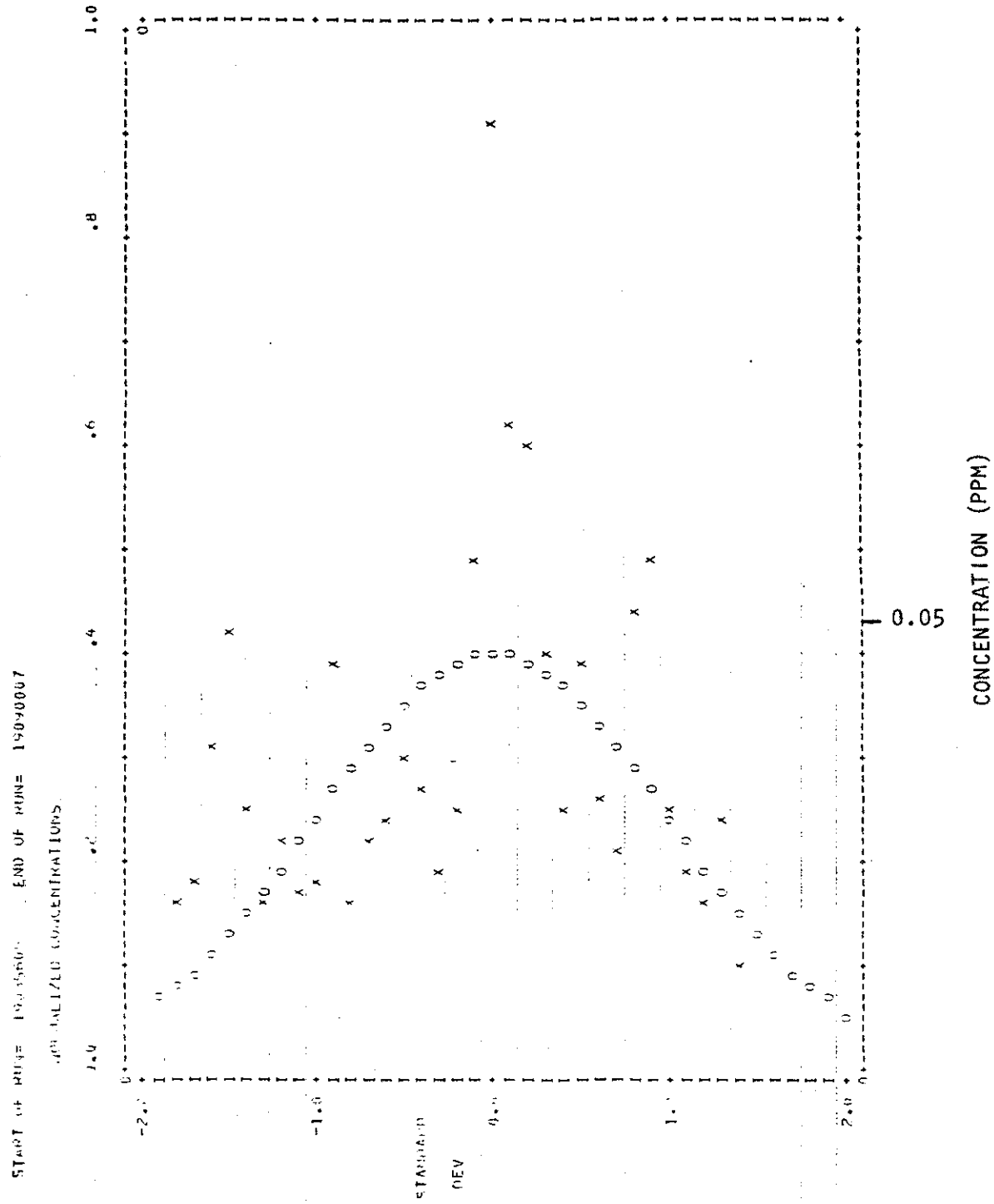

Figure 60. Run 5, 19 June 1977.

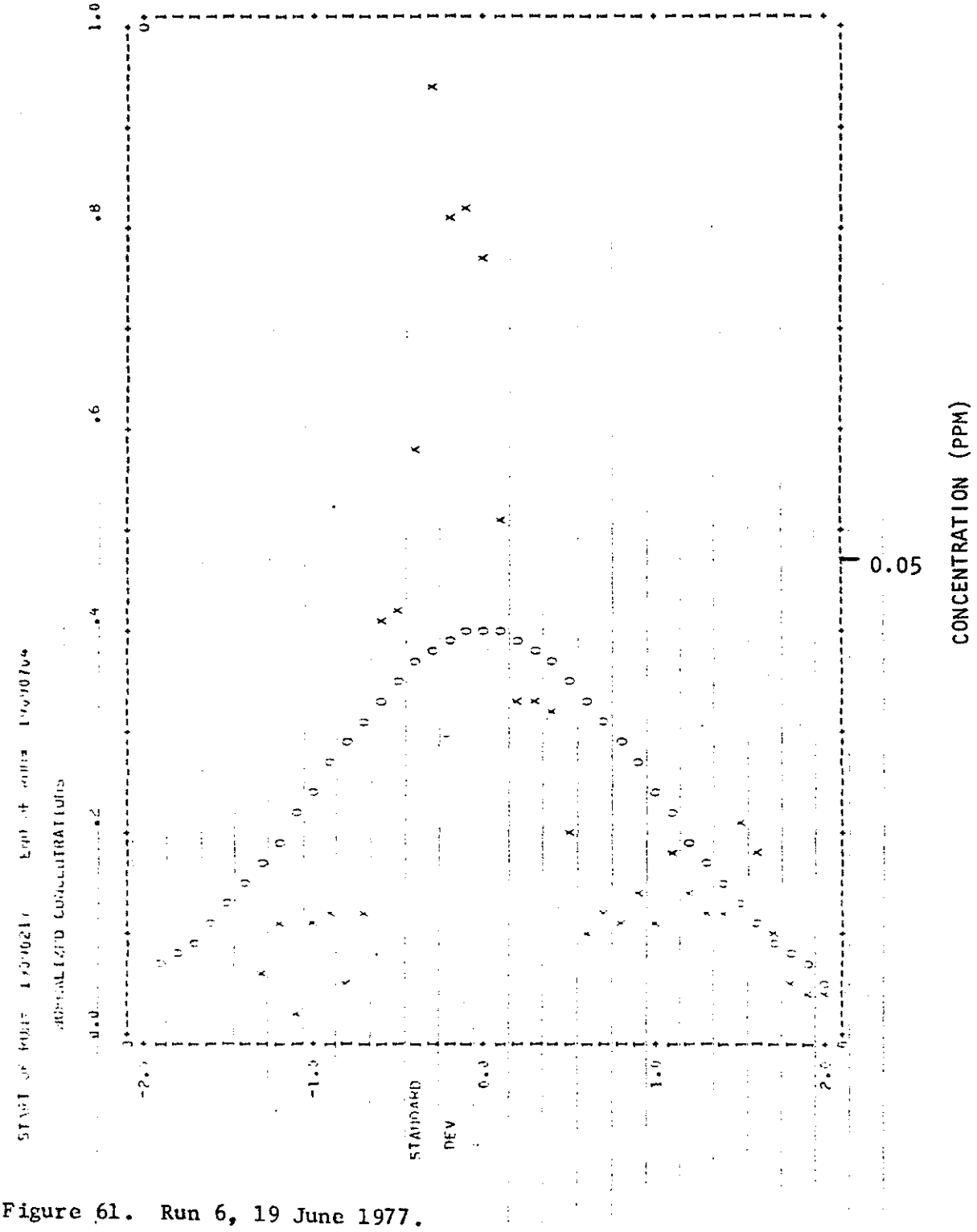

Figure 61. Run 6, 19 June 1977.

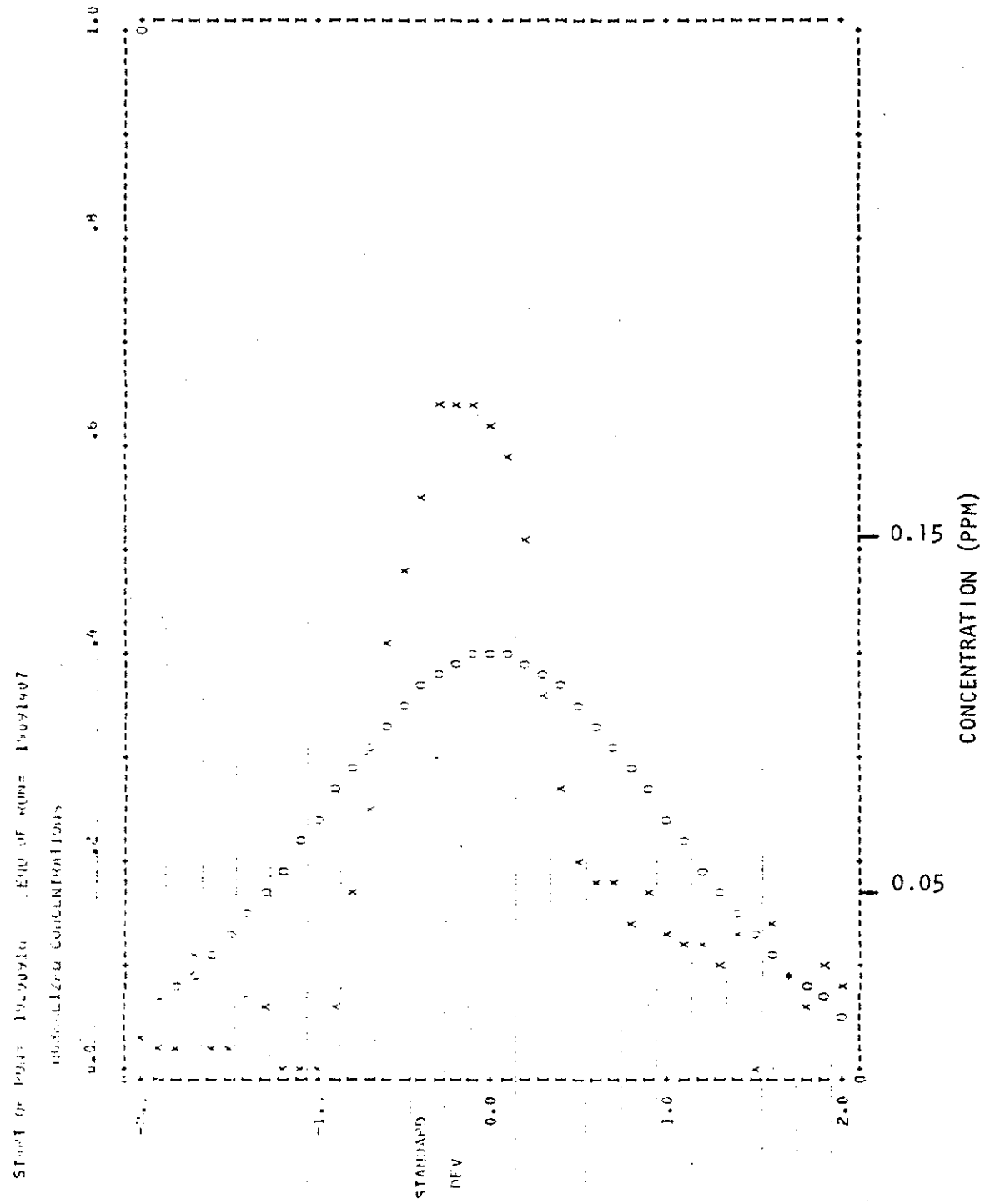

Figure 62. Run 7, 19 June 1977.

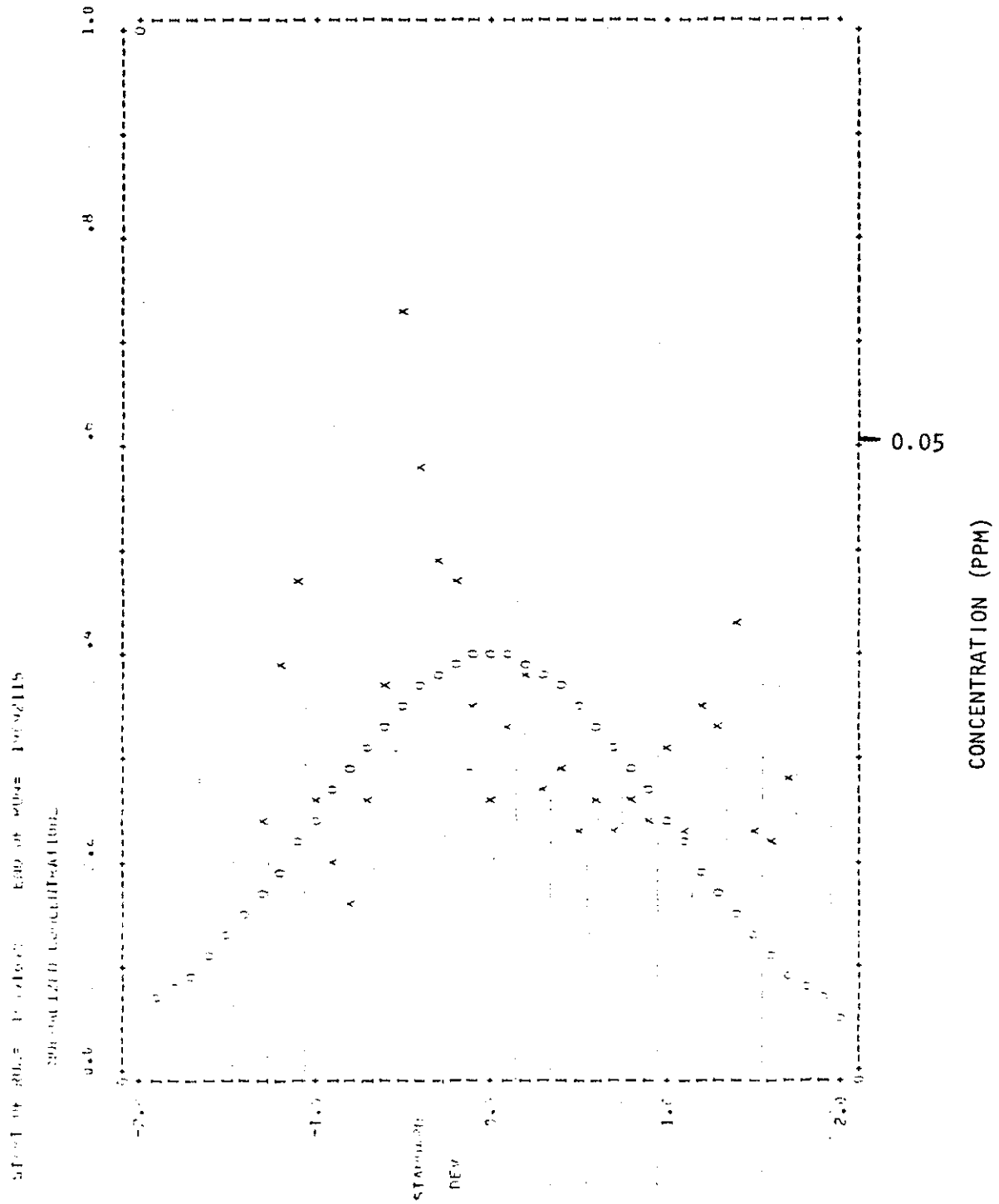

Figure 63. Run 8, 19 June 1977.

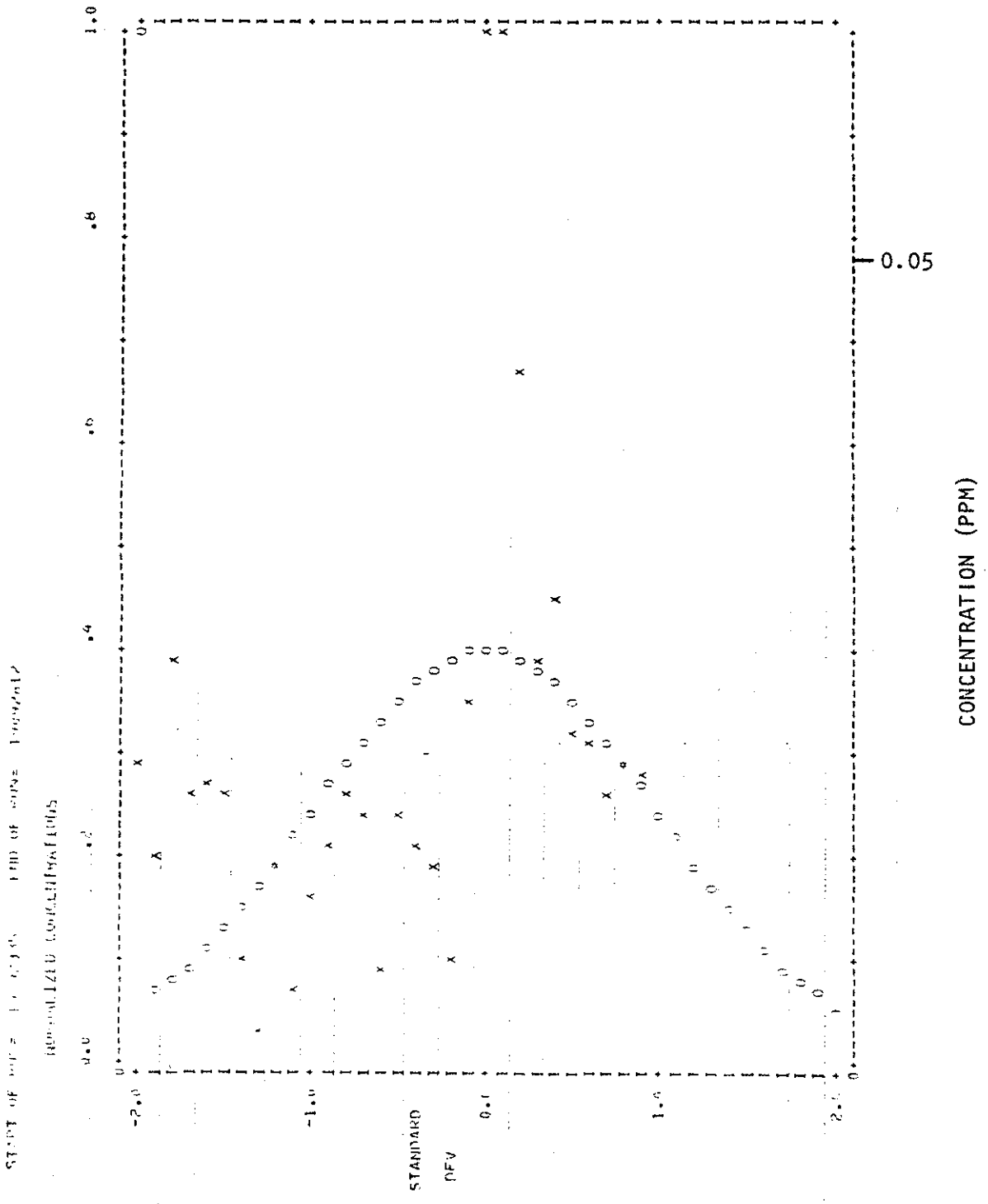

Figure 64. Run 9, 19 June 1977.

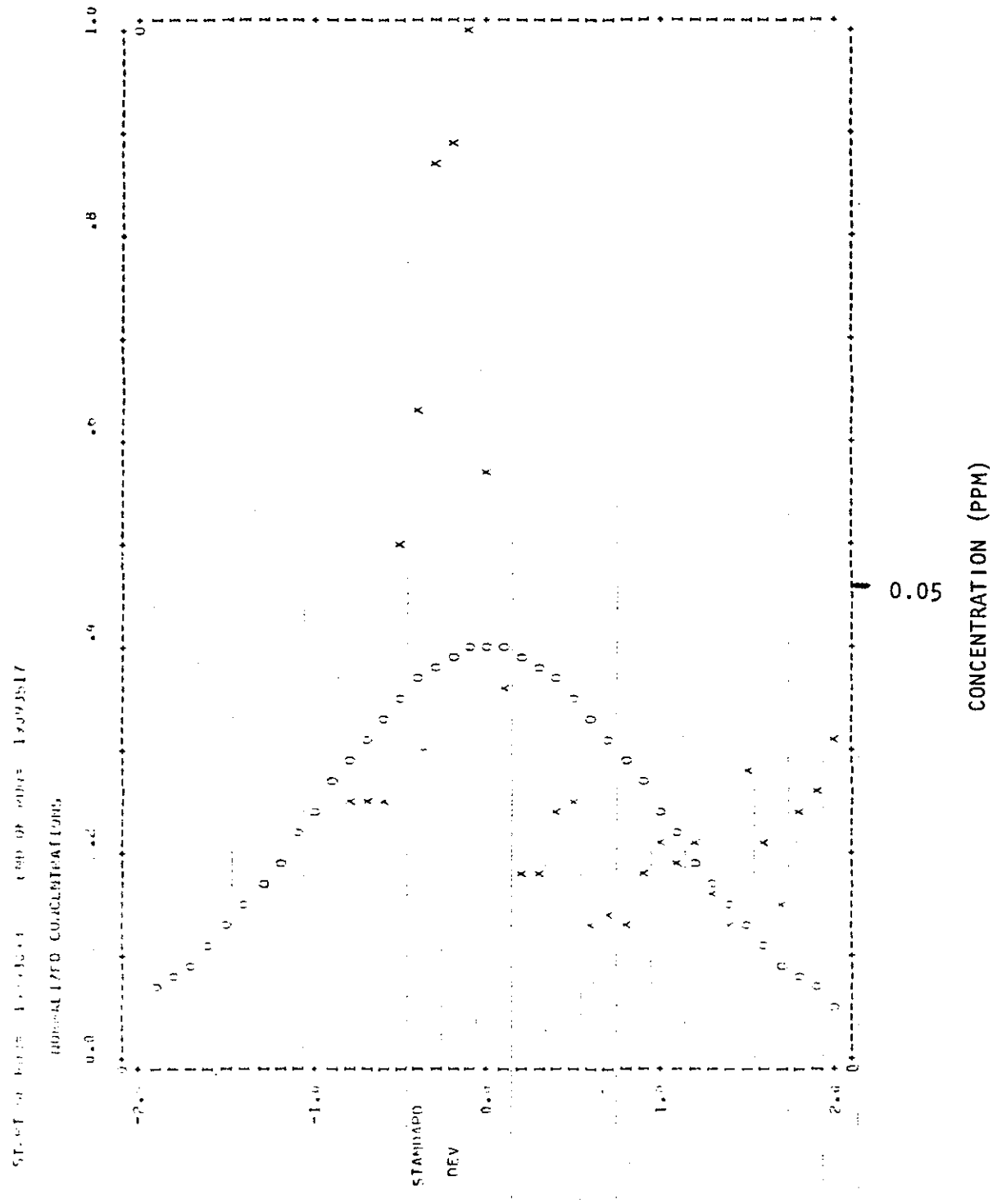

Figure 65. Run 10, 19 June 1977.

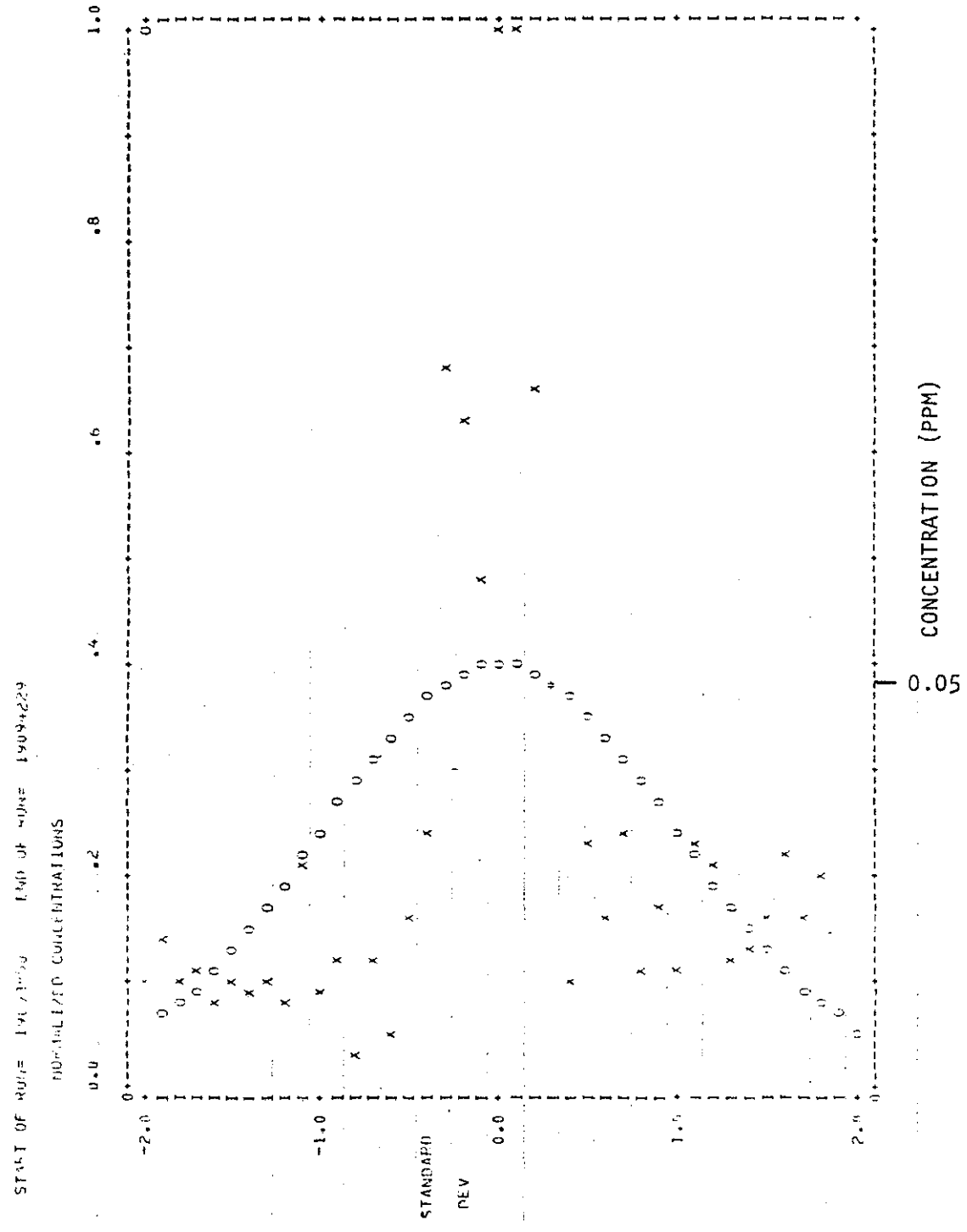

Figure 66. Run 11, 19 June 1977.

8.4 ADDITIONAL DETAILS OF SO_2 CONCENTRATIONS AND TURBULENCE STATISTICS FOR THE FLIGHT OF 19 JUNE 1977 (1335-1735 MDT).

Table 23. Run information for flight of 19 June 1977 (1335-1735 MDT).

Run Number	Start Time (MDT)	Altitude (m AMSL) ± 20	Downwind Distance (km) ± 0.3	σ_y (m) ± 100	Max. Conc. (ppm) ± 0.02	Integrated Conc. (ppm-m) ± 50	Flight Dir. (from-to)
1	1416	915	3.2	5137	0.088	221	E-W
2	1423	915	8.0	2628	0.092	303	W-E
3	1431	610	3.2	6251	0.098	423	E-W
4	1437	610	8.0	3747	0.070	225	W-E
5[a]	1445	1219	3.2	-	-	-	E-W
6[a]	1451	1219	8.0	-	-	-	W-E
7	1459	763	3.2	6641	0.19	479	E-W
8	1506	763	8.0	8003	0.079	368	W-E
9	1518	1373	3.2	517	0.067	68	E-W
10[a]	1524	1373	8.0	-	-	-	W-E
11	1532	1068	3.2	4798	0.073	160	E-W
12	1539	1068	8.0	1771	0.082	107	W-E
13	1549	519	3.2	6723	0.10	531	E-W
14[a]	1556	549	8.0	-	-	-	W-E
15	1602	793	3.2	5072	0.14	433	E-W
16	1609	793	3.2	5121	0.12	332	W-E
17T	1618	610	-	-	-	-	S-N
18T	1630	610	-	-	-	-	N-S
19T	1648	1220	-	-	-	-	S-N
20T	1701	1220	-	-	-	-	N-S

[a]No detectable SO_2.

T - turbulence run.

Table 24. Turbulence statistics from each run for the flight of 19 June 1977 (1335-1735 MDT).

Run No.	HT. m AMSL	X km	σ_w	σ_v	$\overline{W'V'}$	$\overline{W'T'}$	ℓ_w	ℓ_v	ε	N
1	915	3.2	1.69	1.28	-0.02	0.09	140	100	90	4
2	915	8.0	1.38	1.41	-0.40	-0.01	140	150	80	3
3	610	3.2	1.76	1.45	+0.03	-0.17	220	140	95	3
4	610	8.0	1.74	1.65	-0.44	0.03	170	150	105	4
5[a]	1219	3.2	1.74	1.65	+0.02	-0.03	180	230	50	2
6[a]	1219	8.0	1.22	1.25	-0.00	0.03	90	150	50	4
7	763	3.2	1.42	1.49	-0.69	0.14	140	160	70	4
8	763	8.0	1.46	1.53	-0.74	0.18	160	250	50	3
9	1373	3.2	1.30	1.20	-0.17	-0.01	160	140	35	4
10[a]	1373	8.0	1.43	1.34	0.10	0.02	250	240	50	2
11	1068	3.2	1.95	1.14	+0.39	0.00	260	90	55	4
12	1068	8.0	1.38	1.77	0.20	0.05	200	190	50	4
13	519	3.2	1.38	1.80	+0.42	0.04	190	210	60	3
14[a]	549	8.0	1.84	1.98	0.69	0.00	220	250	80	3
15	793	3.2	1.66	1.58	-0.11	-0.02	290	170	60	4
16	793	3.2	1.29	1.83	-0.42	0.05	130	230	65	3
17T	610	-	1.49	1.53	-0.34	0.13	170	140	75	5
18T	610	-	1.47	1.28	+0.13	0.06	190	130	45	8
19T	1220	-	1.57	1.39	0.08	0.05	150	160	55	7
20T	1220	-	1.30	1.21	-0.07	0.04	150	180	35	8

Notes: All units are MKS except dissipation, ε, which is expressed in $cm^2\ sec^{-3}$.

X downwind distance from GCOS stack for crosswind flights

σ_w standard deviation of the vertical velocity

σ_v standard deviation of the lateral velocity with respect to the aircraft

$\overline{W'V'}$ product of fluctuating vertical and lateral velocities with sign changes so that crosswind flights express $\overline{W'U'}$ with respect to ground and along wind flights express $\overline{W'V'}$ with respect to ground using a right hand co-ordinate system with positive u in direction of wind.

$\overline{W'T'}$ product of fluctuating temperature and vertical velocity

ℓ_w integral length scale for vertical velocity

ℓ_v integral length scale for lateral velocity with respect to the aircraft

ε dissipation

Continued ...

Table 24. Concluded.

N number of 65 sec analysis blocks in the run

T turbulence run flown parallel to wind.

[a]No detectable SO_2.

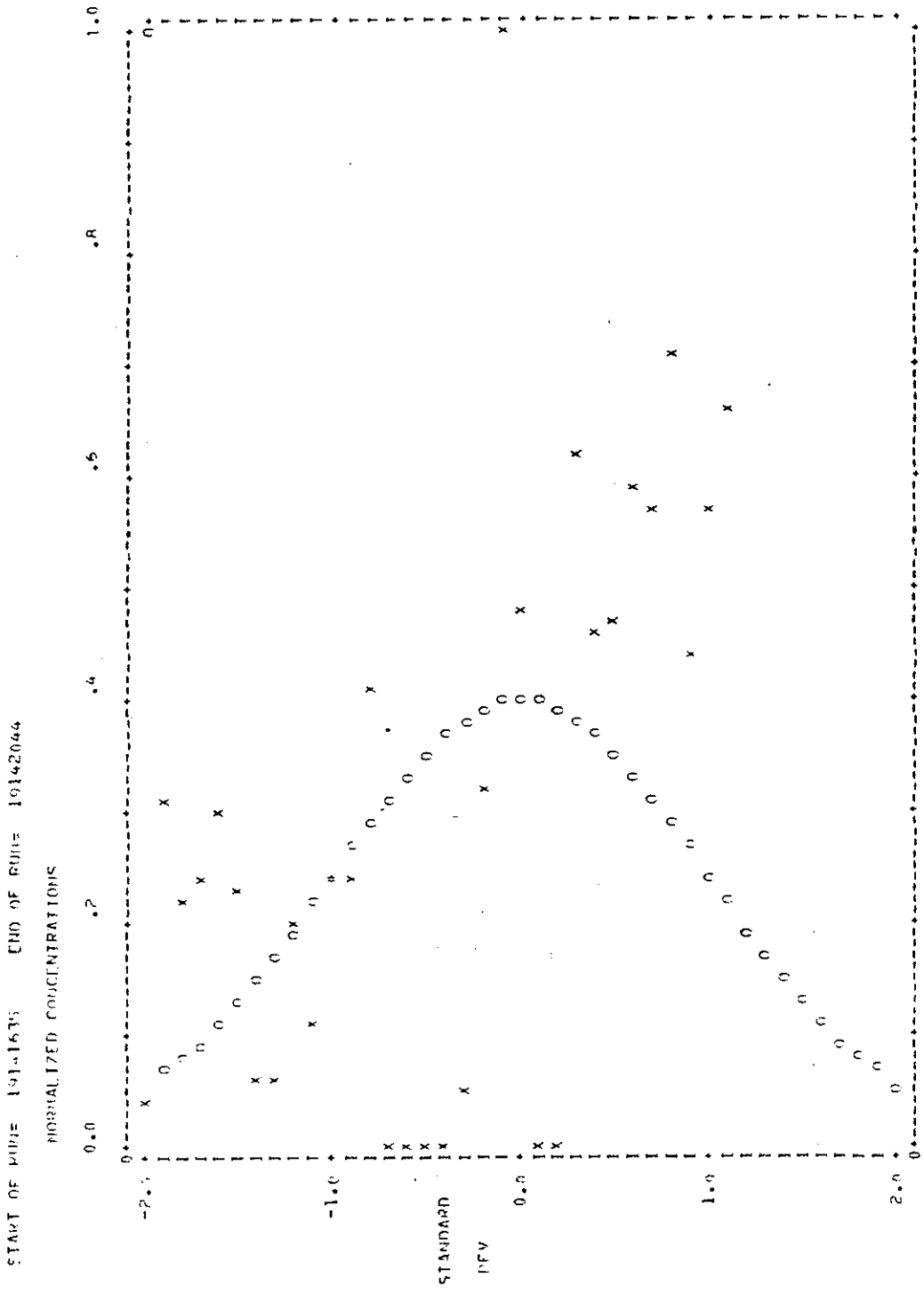

Figure 67. Run 1, 19 June 1977.

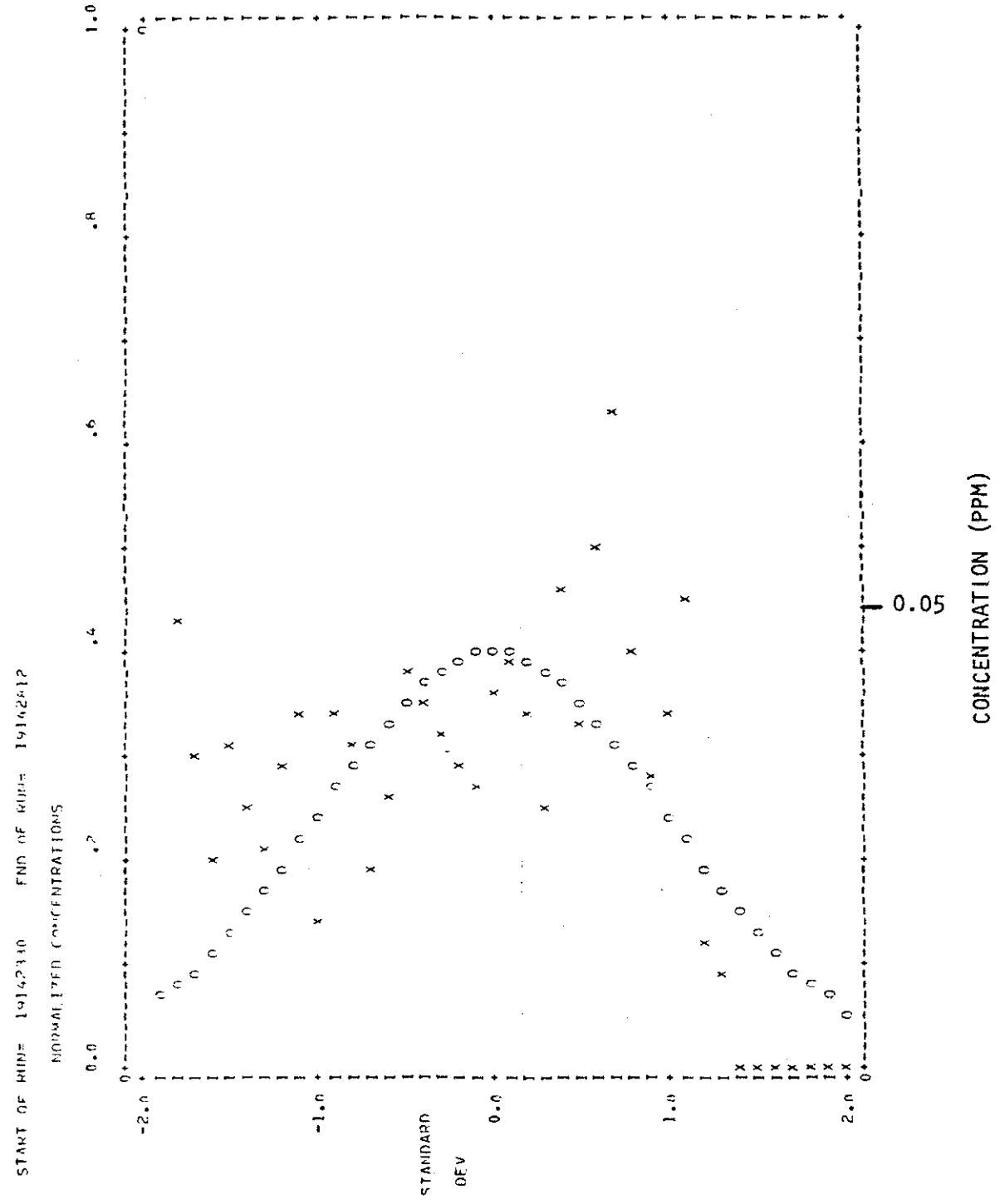

Figure 68. Run 2, 19 June 1977.

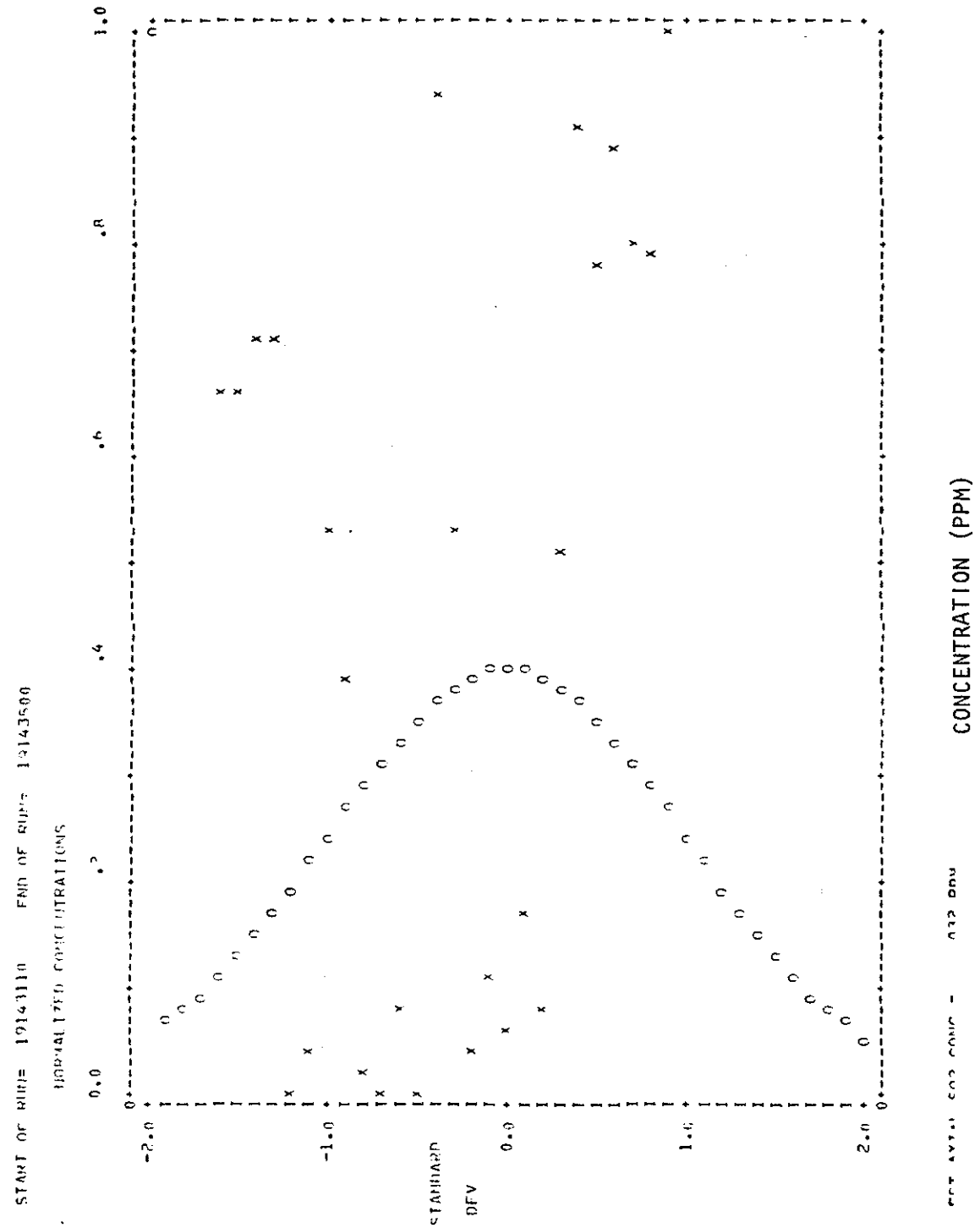

Figure 69. Run 3, 19 June 1977.

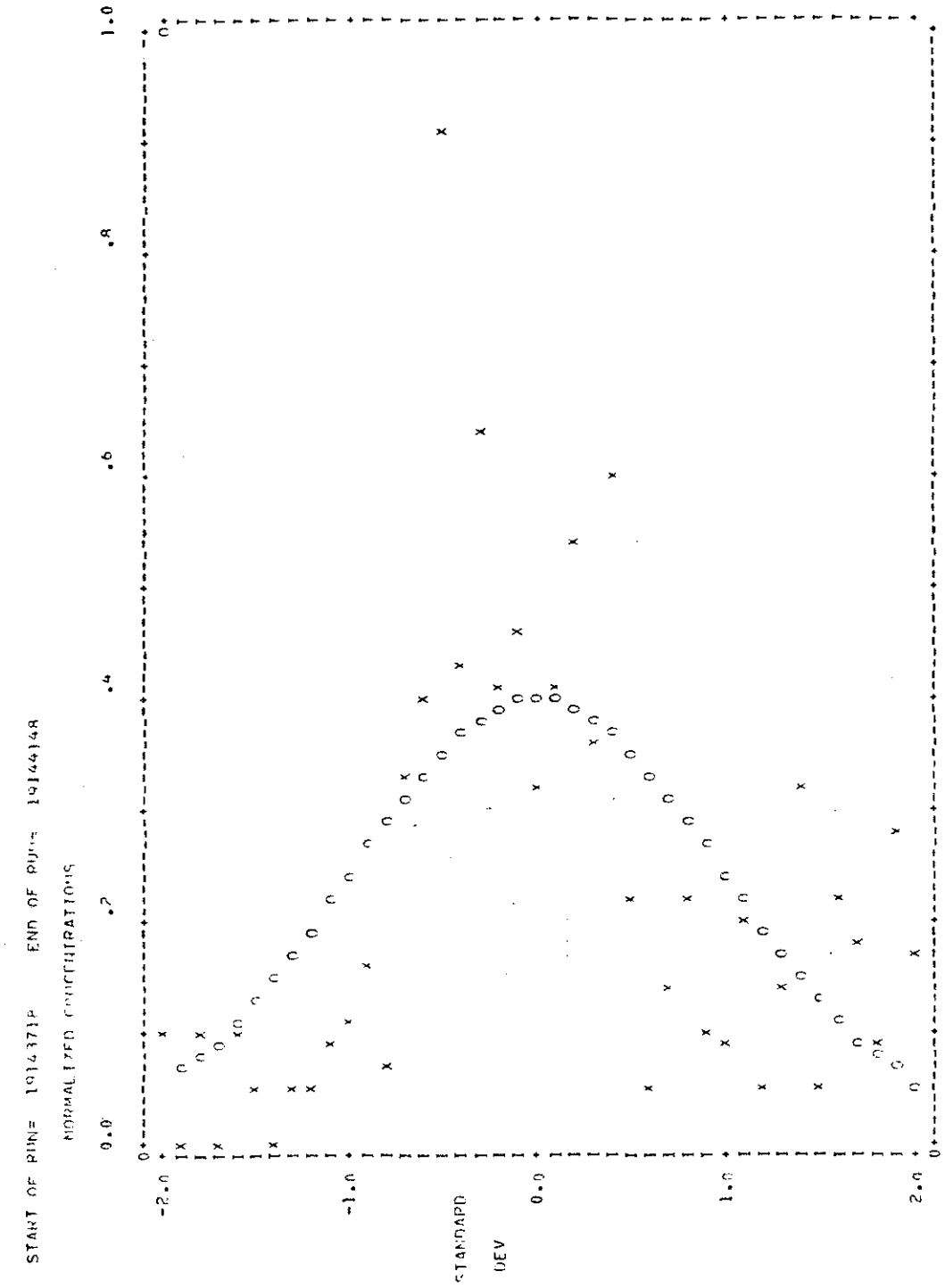

Figure 70. Run 4, 19 June 1977.

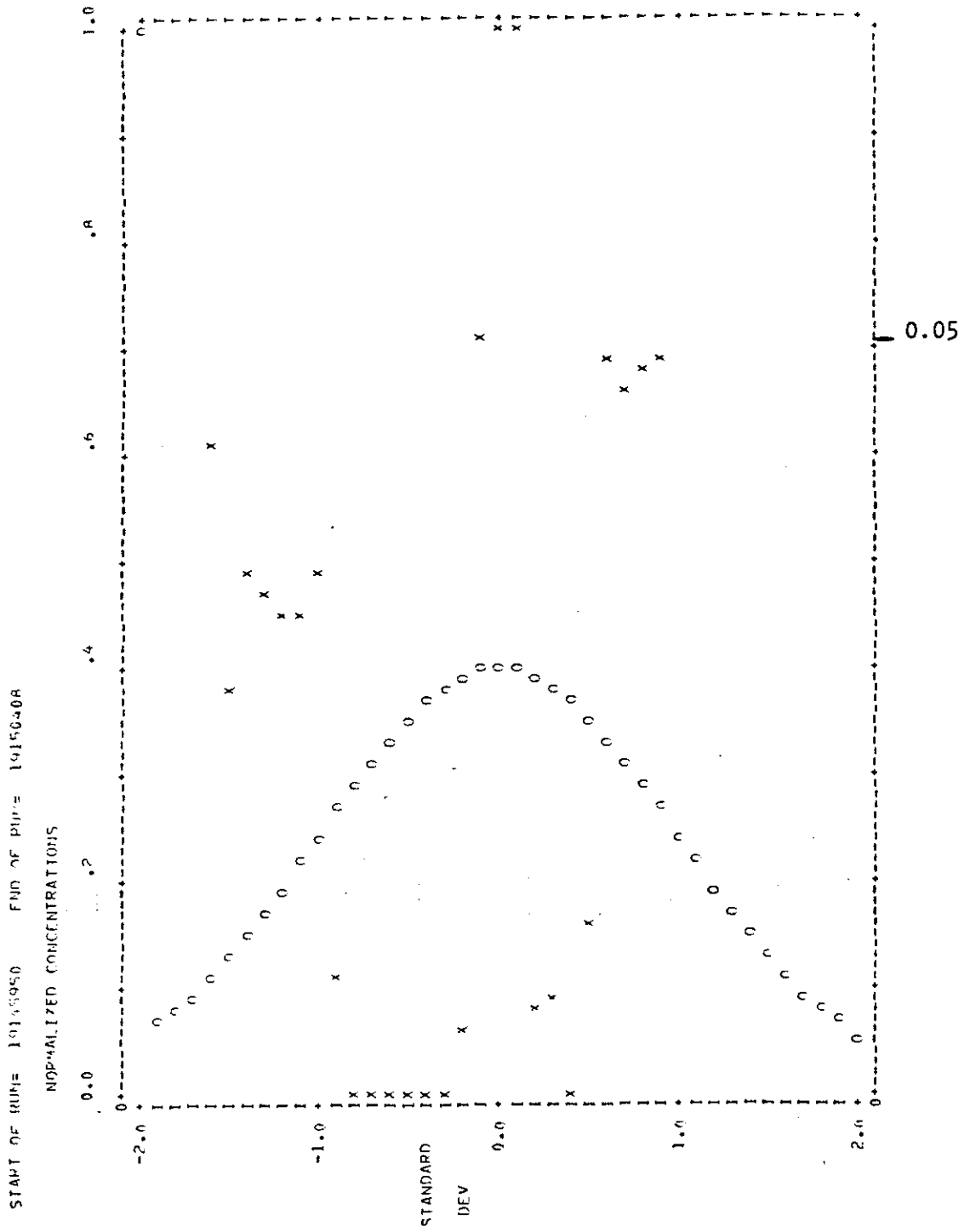

Figure 71. Run 7, 19 June 1977.

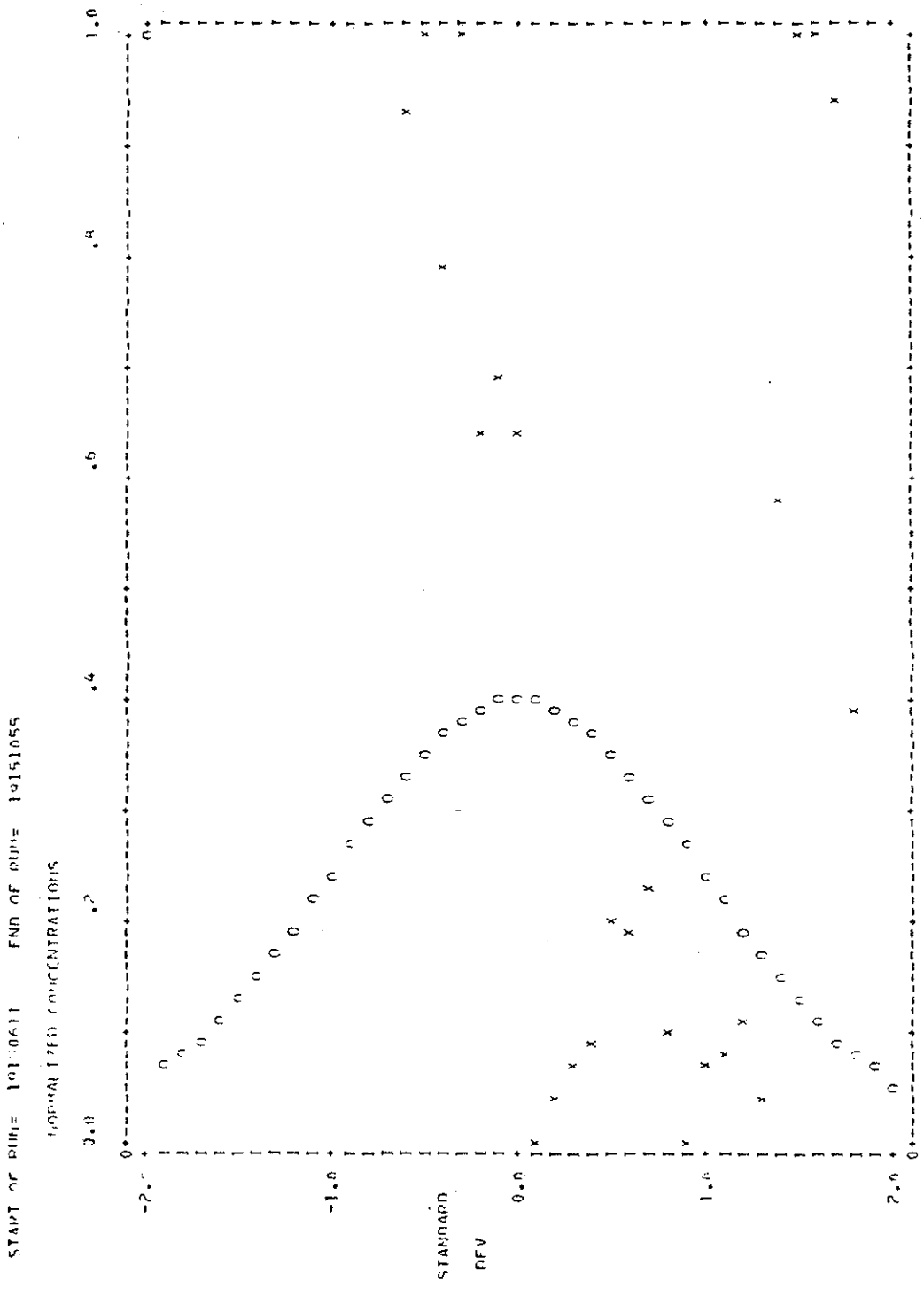

Figure 72. Run 8, 19 June 1977.

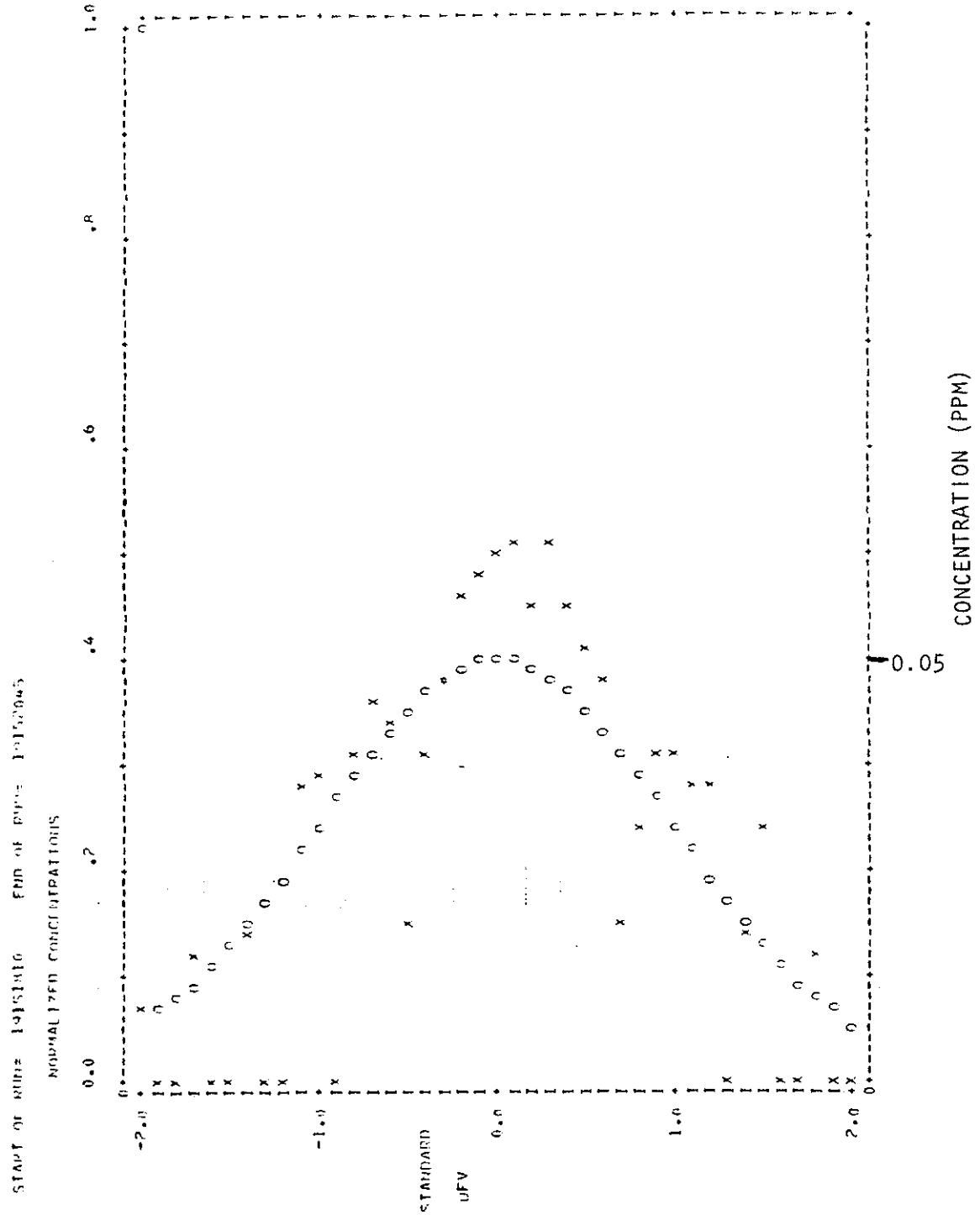

Figure 73. Run 9, 19 June 1977.

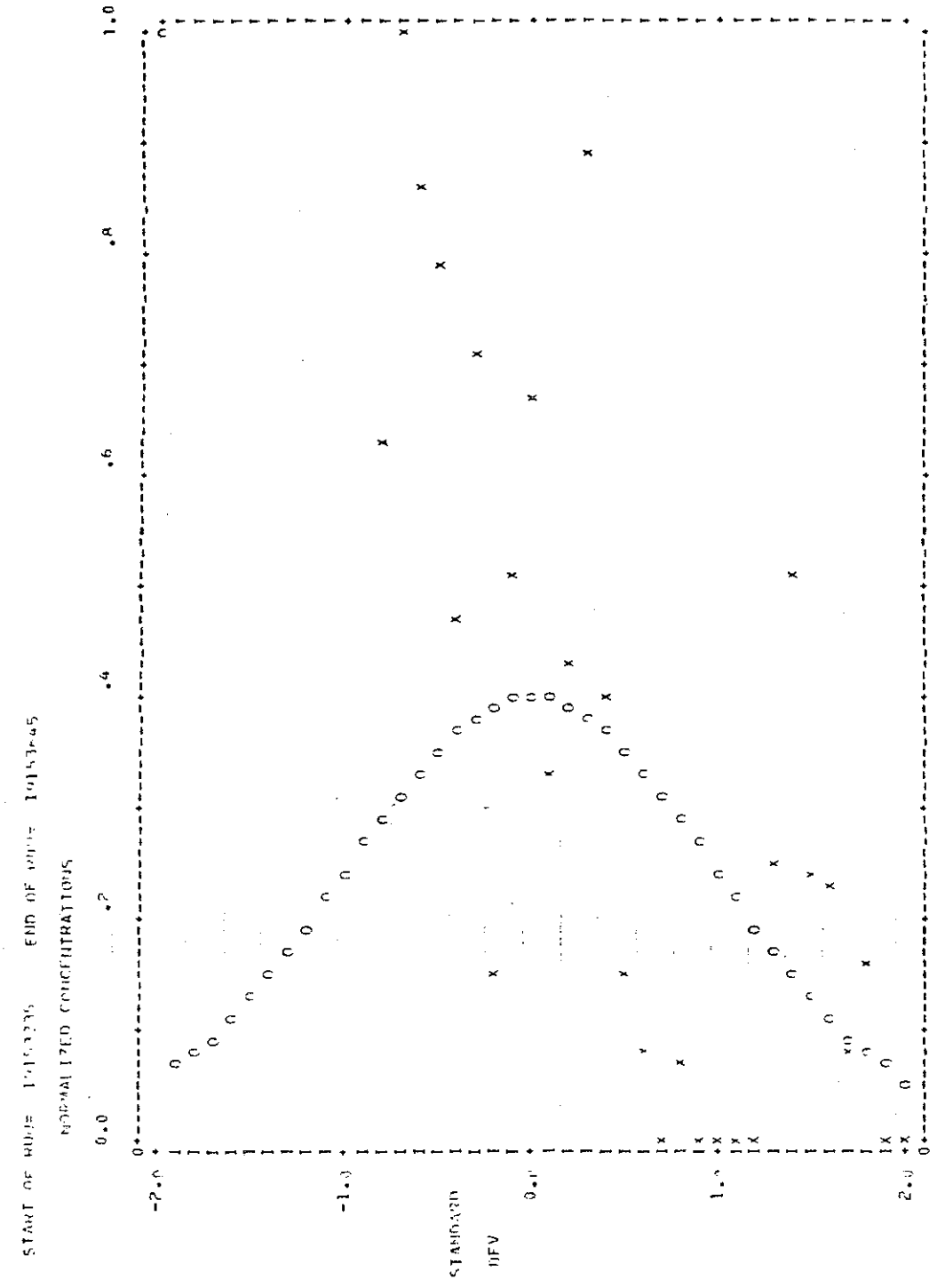

Figure 74. Run 11, 19 June 1977.

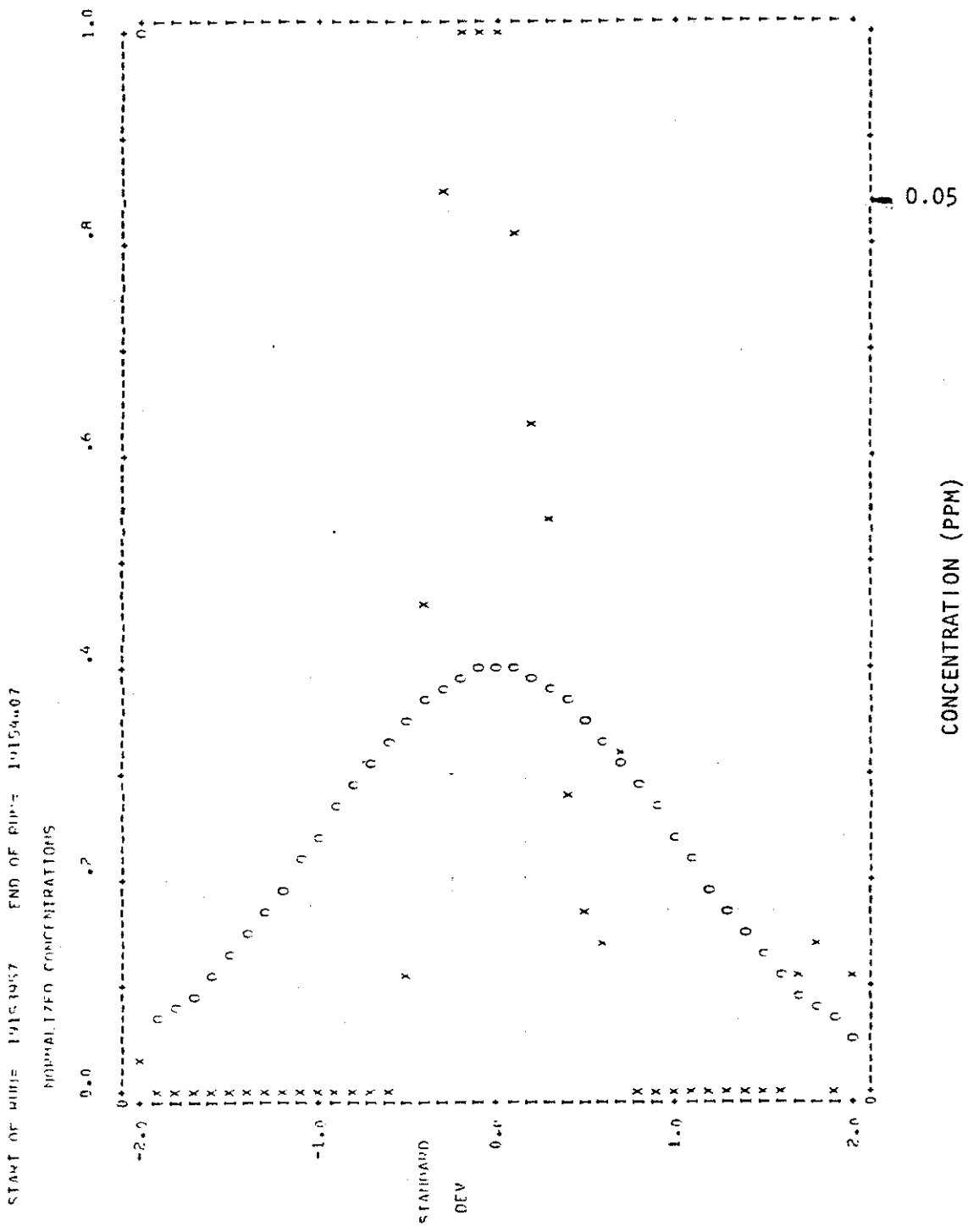

Figure 75. Run 12, 19 June 1977.

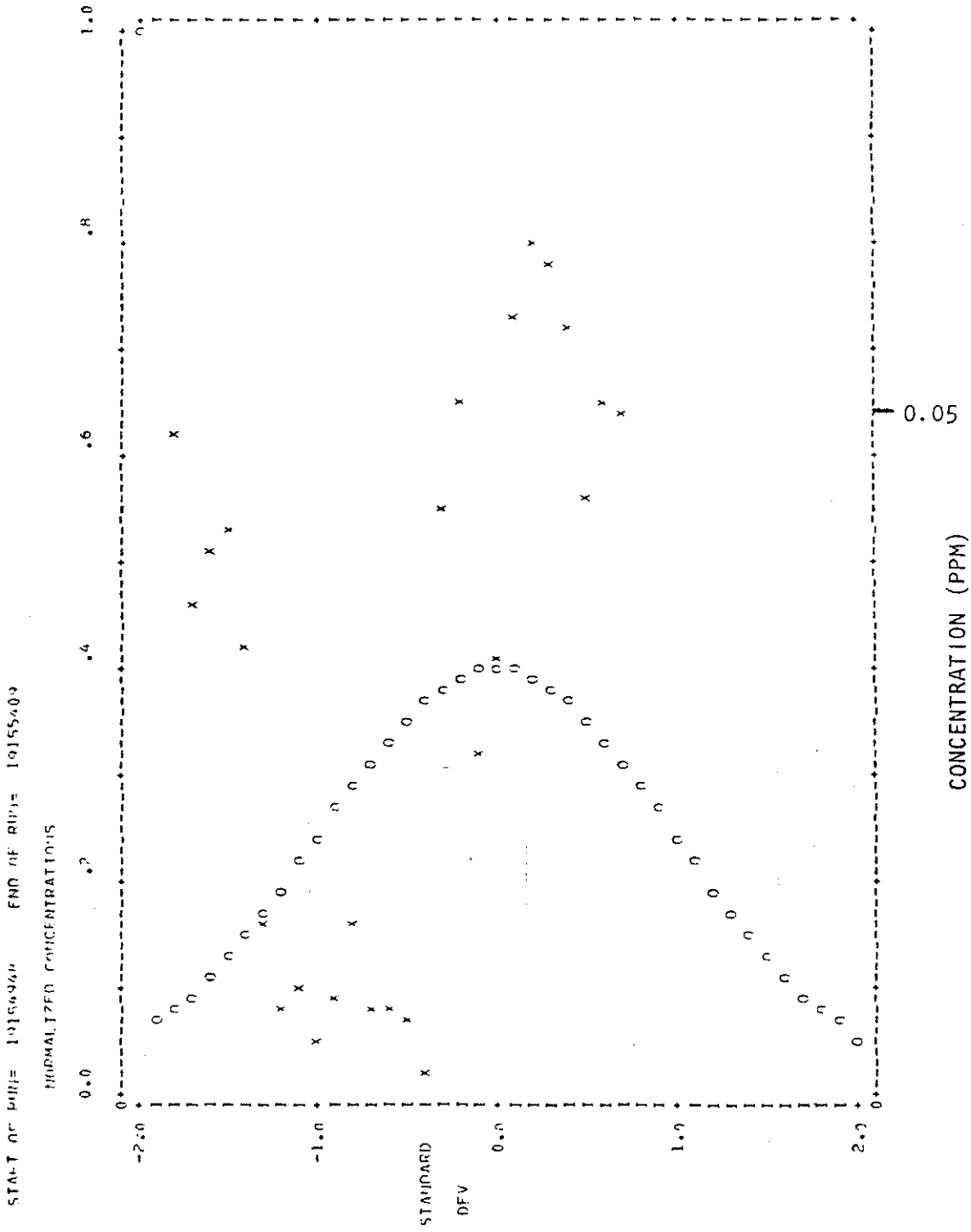

Figure 76. Run 13, 19 June 1977.

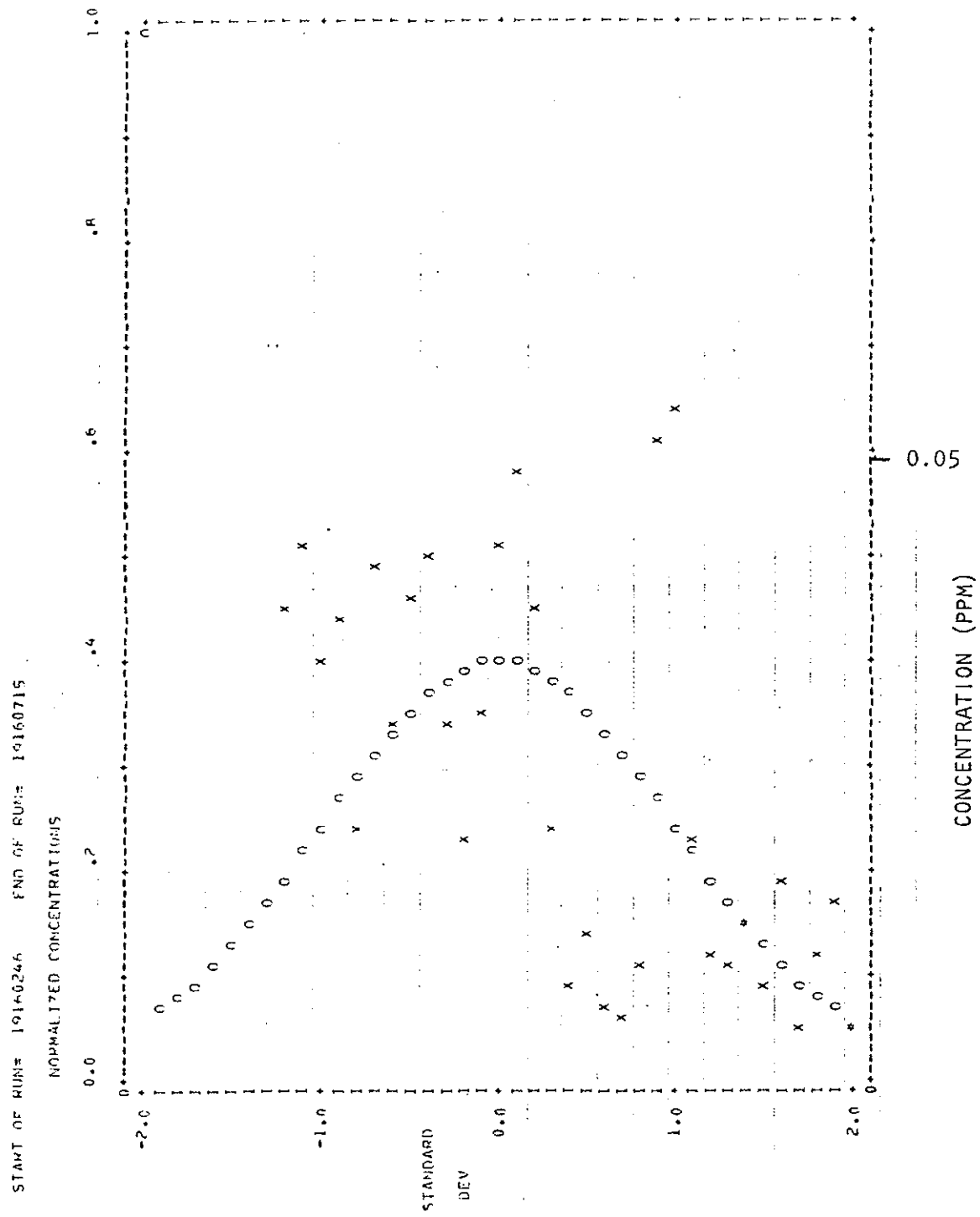

Figure 77. Run 15, 19 June 1977.

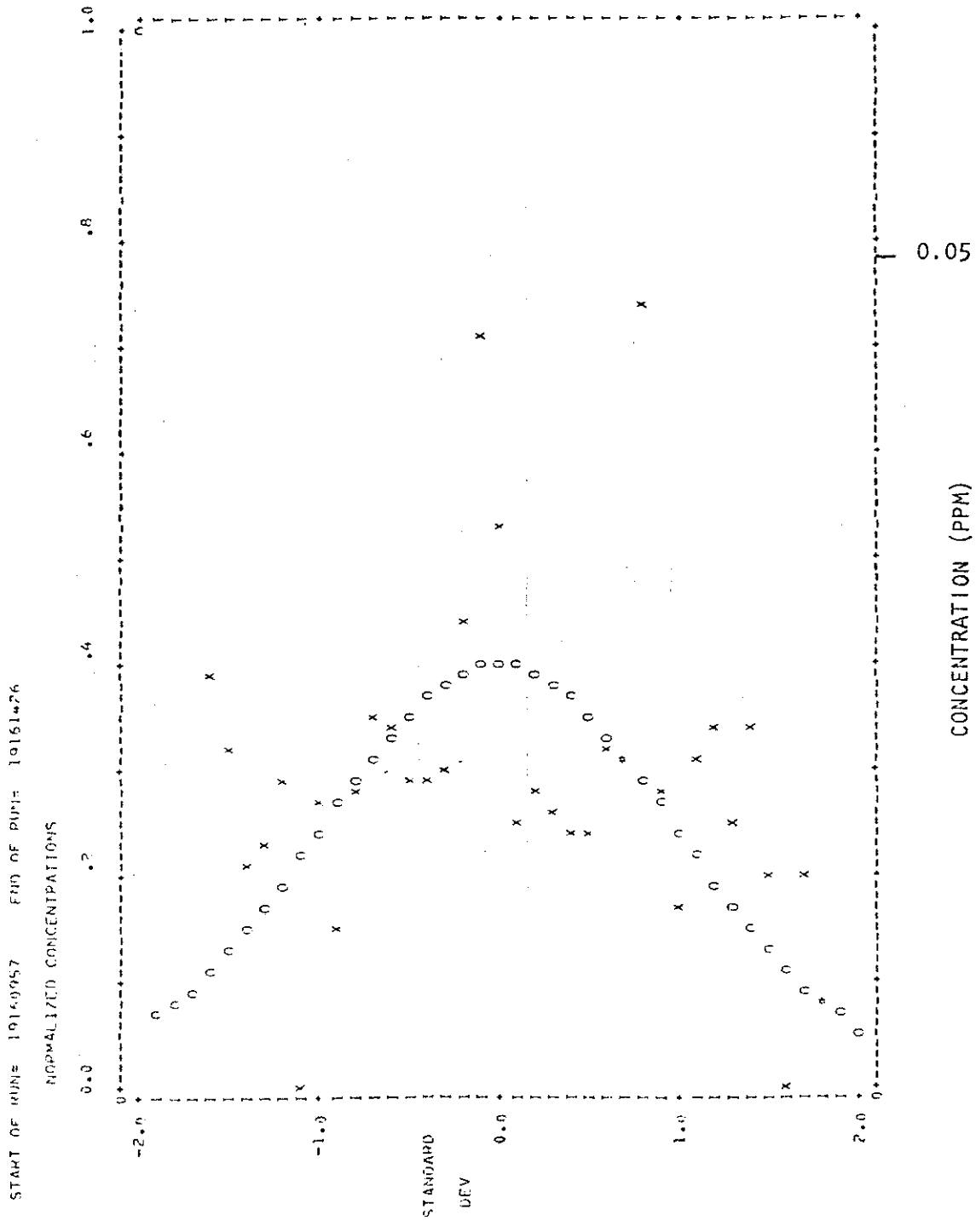

Figure 78. Run 16, 19 June 1977.

8.5 ADDITIONAL DETAILS OF SO_2 CONCENTRATIONS AND TURBULENCE STATISTICS FOR THE FLIGHT OF 20 JUNE 1977 (1000-1500 MDT).

Table 25. Run information for flight of 20 June 1977 (1000-1500 MDT).

Run Number	Start Time (MDT)	Altitude (m AMSL) ± 20	Downwind Distance (km) ± 0.3	σ_y (m) ± 100	Max. Conc. (ppm) ± 0.02	Integrated Conc. (ppm-m) ± 50	Flight Dir. (from-to)
1	1131	763	3.2	501	0.47	471	E-W
2	1137	763	8.0	726	0.24	384	W-E
3[a]	1146	1070	3.2	-	-	-	E-W
4[a]	1153	1070	8.0	-	-	-	W-E
5	1202	610	3.2	443	0.23	231	E-W
6	1208	610	8.0	1137	0.21	377	W-E
7[a]	1217	915	3.2	-	-	-	E-W
8	1224	915	8.0	6745	0.04	29	W-E
9	1231	519	3.2	585	0.35	406	E-W
10	1237	519	8.0	699	0.23	318	W-E
11	1246	839	3.2	516	0.64	552	E-W
12	1253	839	8.0	401	0.08	78	W-E
13	1259	686	3.2	508	0.38	387	E-W
14	1306	686	8.0	972	0.20	426	W-E
15	1313	763	3.2	502	0.20	195	E-W
16	1321	763	3.2	559	0.62	608	W-E
17	1335	839	3.2	534	0.25	276	E-W
18	1341	839	3.2	361	0.35	250	W-E
19T	1350	763	-	-	-	-	S-N
20T	1402	763	-	-	-	-	N-S
21T	1421	1070	-	-	-	-	S-N
22T	1435	1070	-	-	-	-	N-S

[a]No detectable SO_2.

T - turbulence run.

Table 26. Turbulence statistics from each run for the flight of 20 June 1977 (1000-1500 MDT).

Run No.	HT. m AMSL	X km	σ_w	σ_v	$\overline{W'V'}$	$\overline{W'T'}$	ℓ_w	ℓ_v	ϵ	N
1	763	3.2	0.62	1.19	+0.06	-0.02	50	150	20	1
2[a]	763	8.0	1.00	1.18	0.26	0.15	200	200	15	3
3[a]	1070	3.2	0.66	0.53	-0.08	0.00	240	380	1	4
4[a]	1070	8.0	0.47	1.30	0.01	-0.01	240	360	2	2
5	610	3.2	1.01	1.42	-0.06	0.01	110	210	40	3
6[a]	610	8.0	1.67	1.35	-0.83	-0.01	170	170	65	2
7[a]	915	3.2	1.25	0.97	-0.18	-0.04	320	320	8	4
8	915	8.0	1.31	0.85	0.17	0.06	310	360	7	3
9	519	3.2	1.18	1.85	-0.05	-0.02	150	220	50	3
10	519	8.0	1.42	1.60	0.31	0.04	150	190	60	3
11	839	3.2	1.17	1.21	-0.04	-0.23	200	180	25	2
12	839	8.0	1.41	1.64	0.55	0.12	150	220	60	4
13	686	3.2	1.56	1.52	+0.47	0.10	170	230	50	4
14	686	8.0	unreliable data							
15	763	3.2	1.17	1.87	+0.13	0.02	130	230	60	4
16	763	3.2	1.66	1.78	-0.34	0.06	150	180	95	4
17	839	3.2	2.16	1.77	+0.27	0.08	160	160	105	2
18	839	3.2	1.94	2.01	-0.61	0.22	240	180	85	3
19T	763	-	2.05	1.91	-0.20	0.06	180	200	135	7
20T	763	-	1.53	1.45	+0.30	0.03	130	180	85	7
21T	1070	-	2.10	2.13	-0.08	0.07	210	240	80	5
22T	1070	-	1.59	1.42	+0.03	0.03	200	130	65	5

Notes: all units are MKS except dissipation, ϵ, which is expressed in $cm^2\ sec^{-3}$.

X downwind distance from GCOS stack for crosswind flights

σ_w standard deviation of the vertical velocity

σ_v standard deviation of the lateral velocity with respect to the aircraft

$\overline{W'V'}$ product of fluctuating vertical and lateral velocities with sign changes so that crosswind flights express $\overline{W'U'}$ with respect to ground and along wind flights express $\overline{W'V'}$ with respect to ground using a right hand co-ordinate system with positive u in direction of wind.

$\overline{W'T'}$ product of fluctuating temperature and vertical velocity

ℓ_w integral length scale for vertical velocity

ℓ_v integral length scale for lateral velocity with respect to the aircraft.

continued ...

Table 26. Concluded.

ε dissipation

N number of 65 sec analysis blocks in the run

T turbulence run flown parallel to wind.

[a]No detectable SO_2.

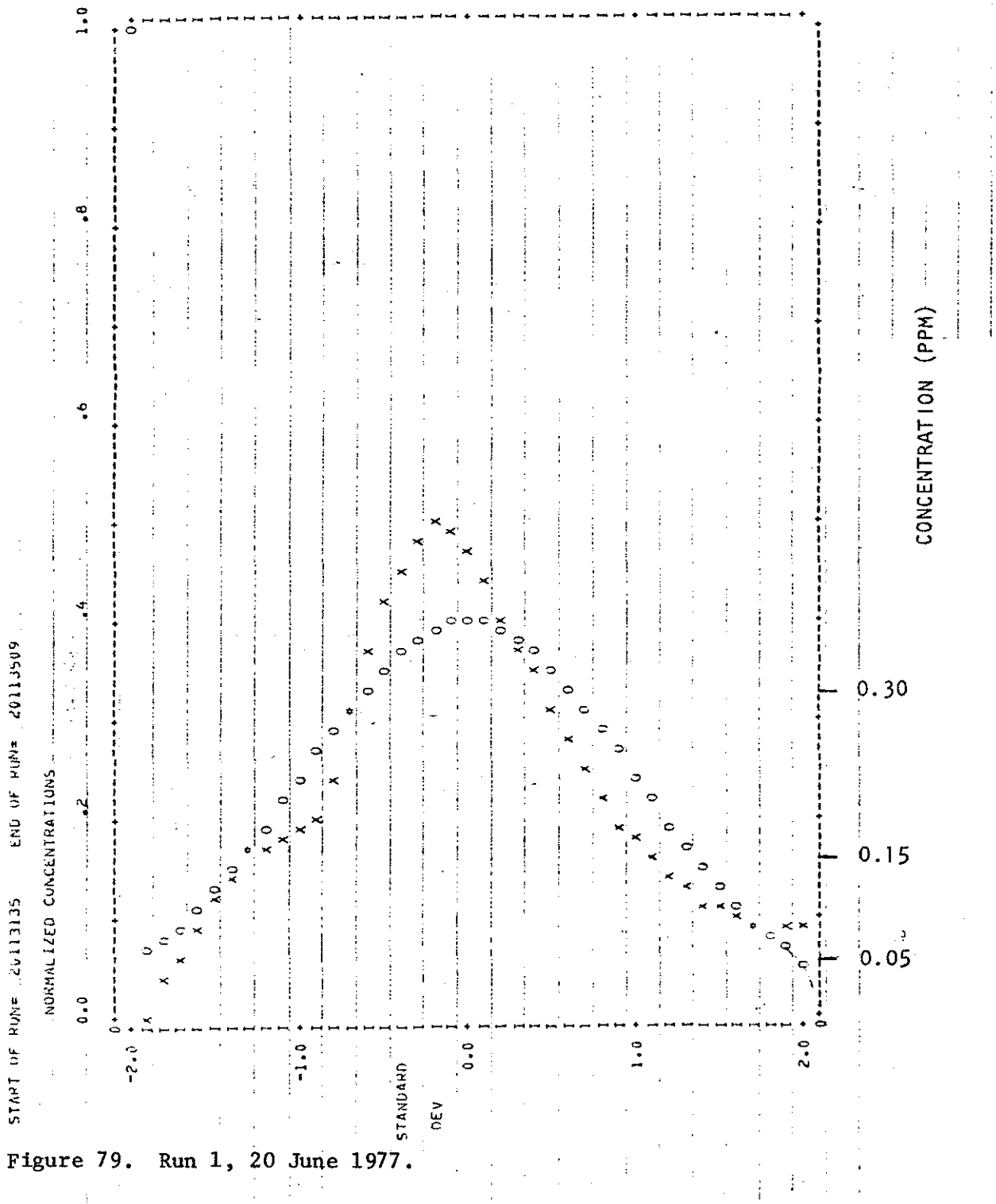

Figure 79. Run 1, 20 June 1977.

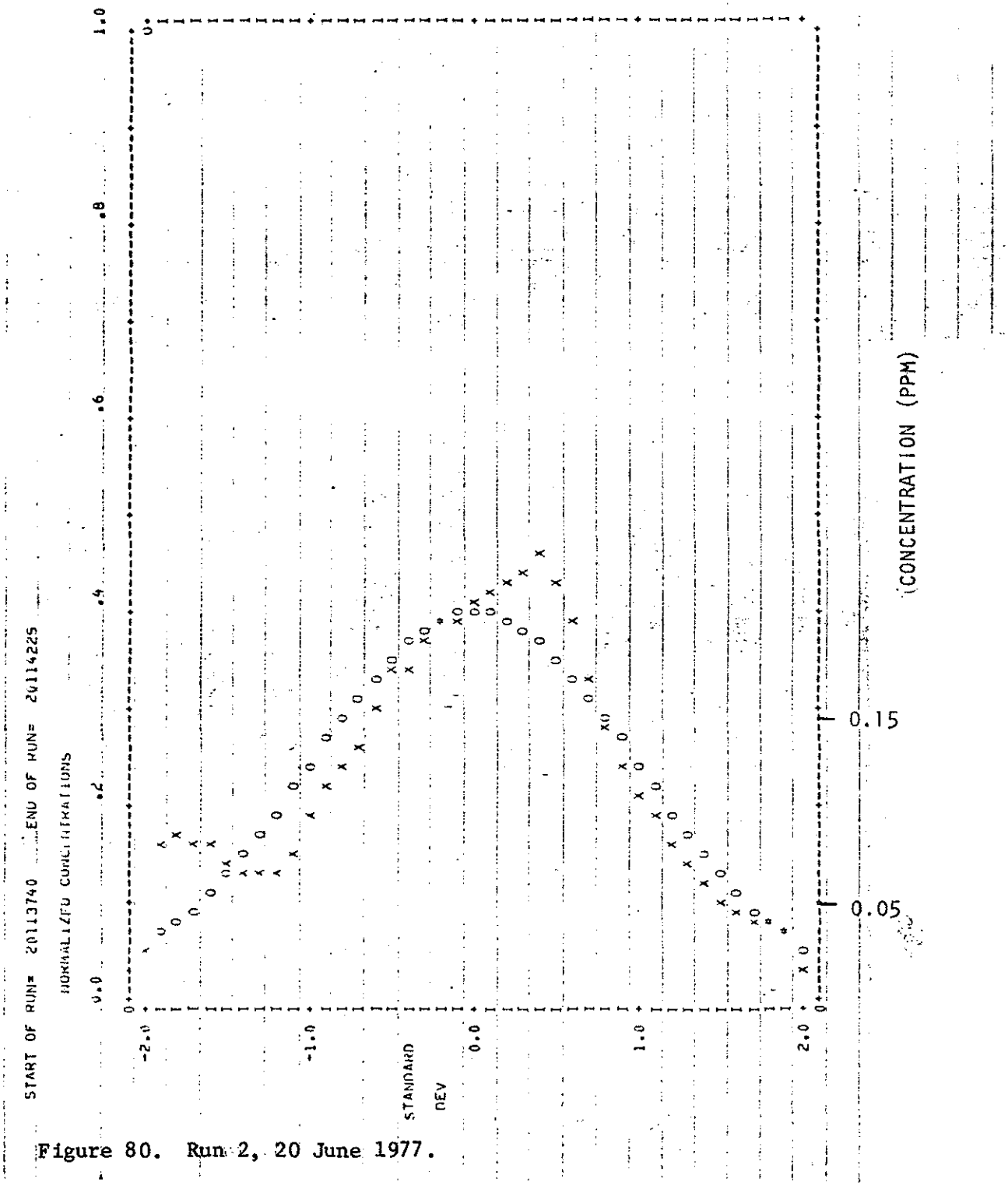

Figure 80. Run 2, 20 June 1977.

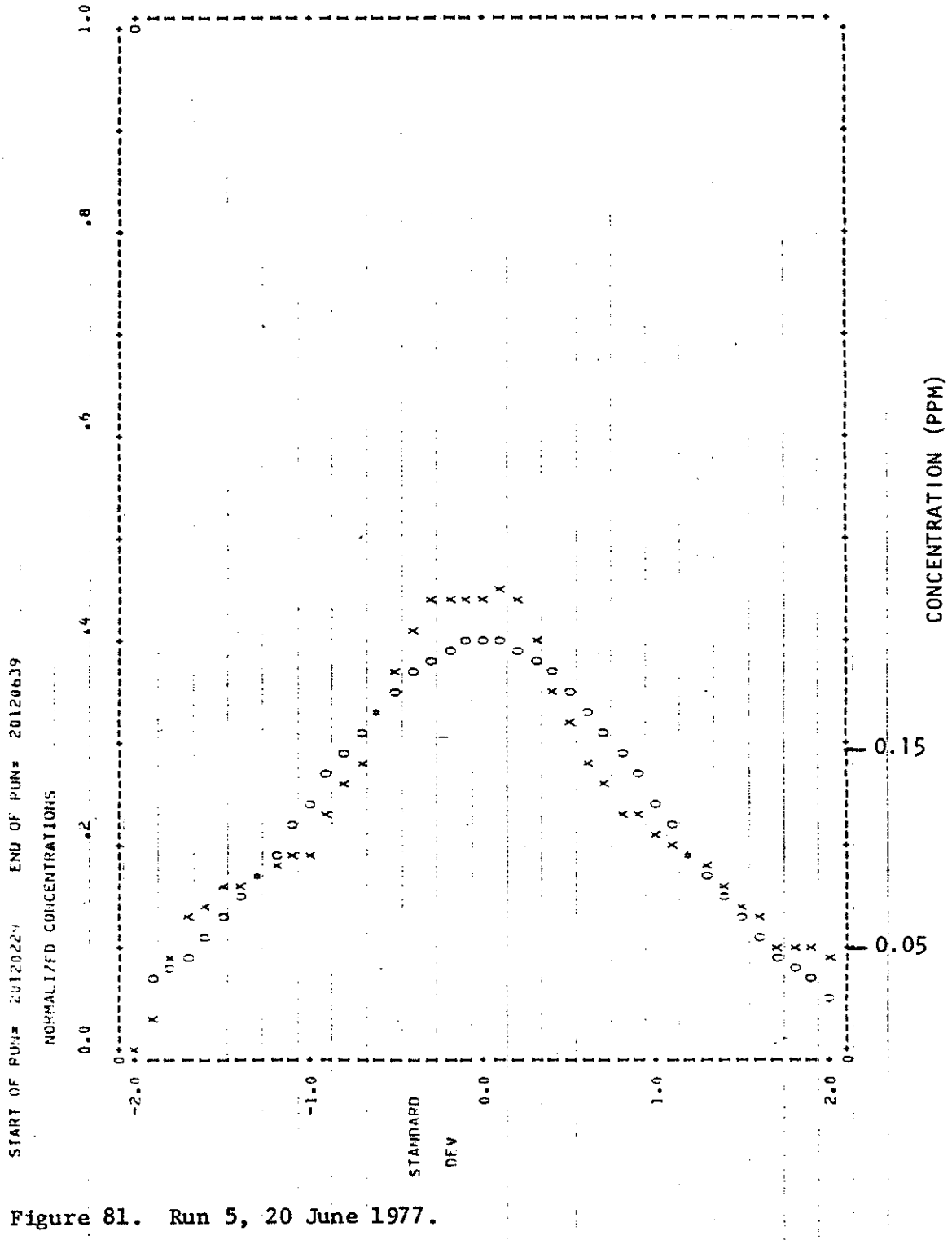

Figure 81. Run 5, 20 June 1977.

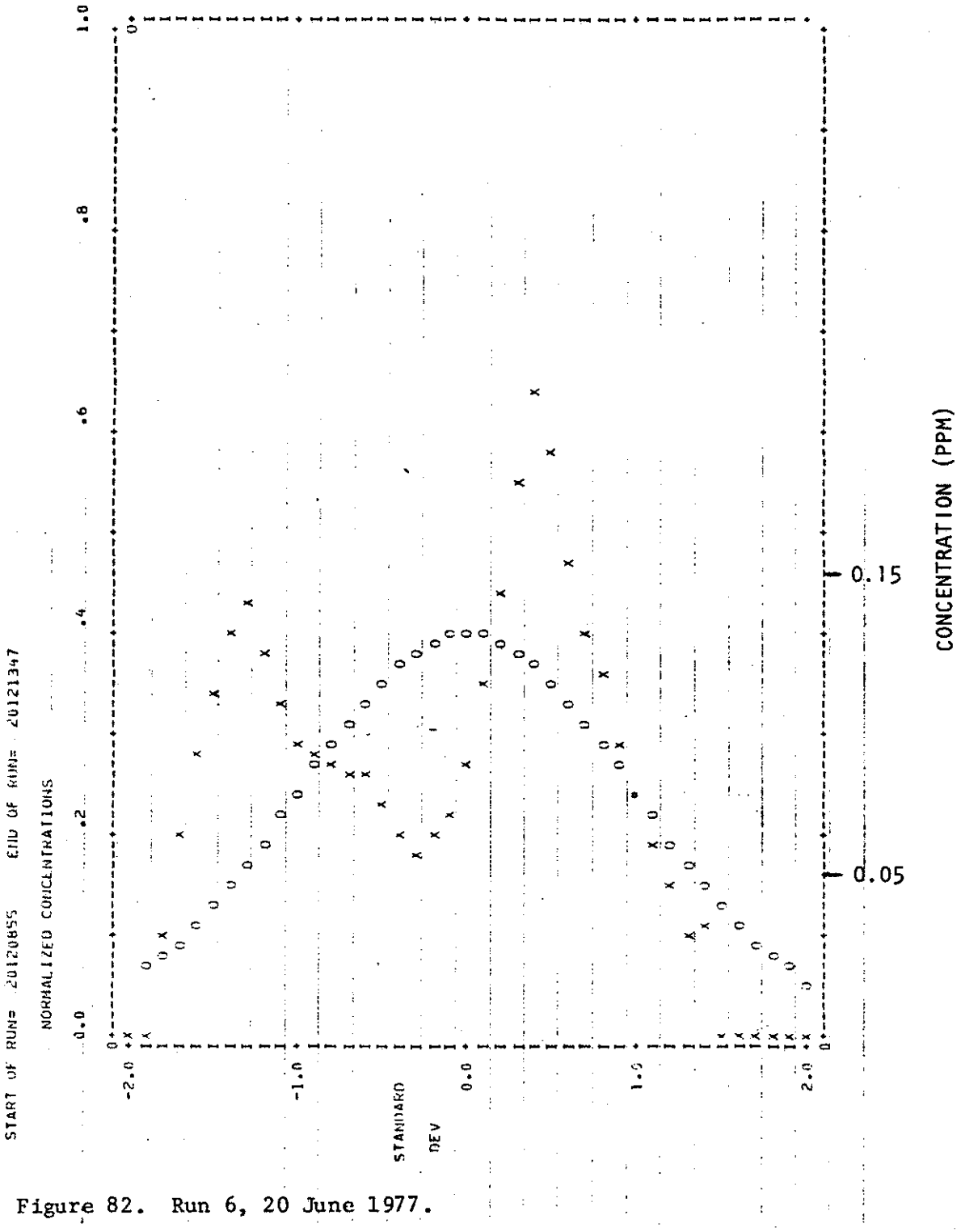

Figure 82. Run 6, 20 June 1977.

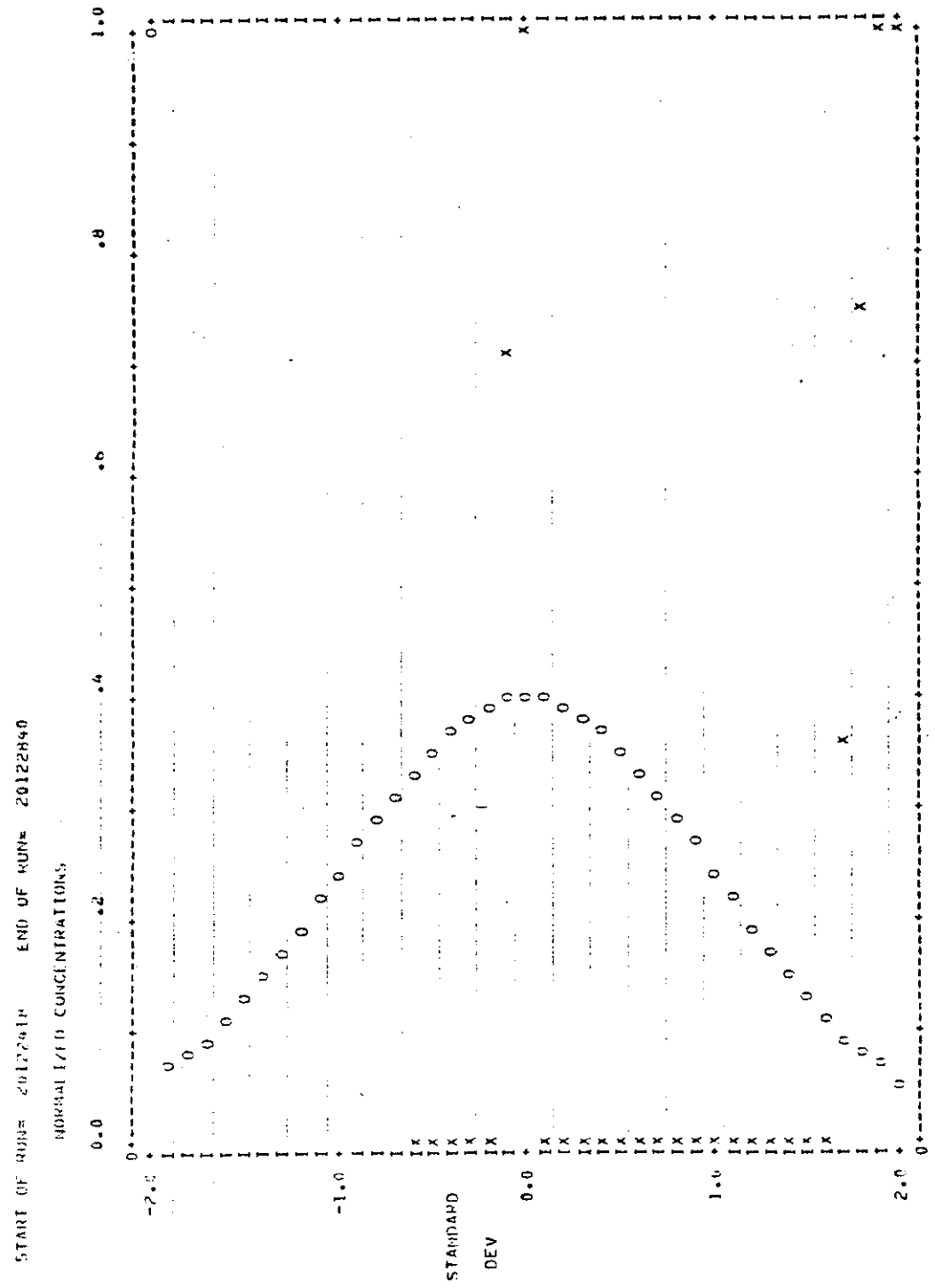

Figure 83. Run 8, 20 June 1977.

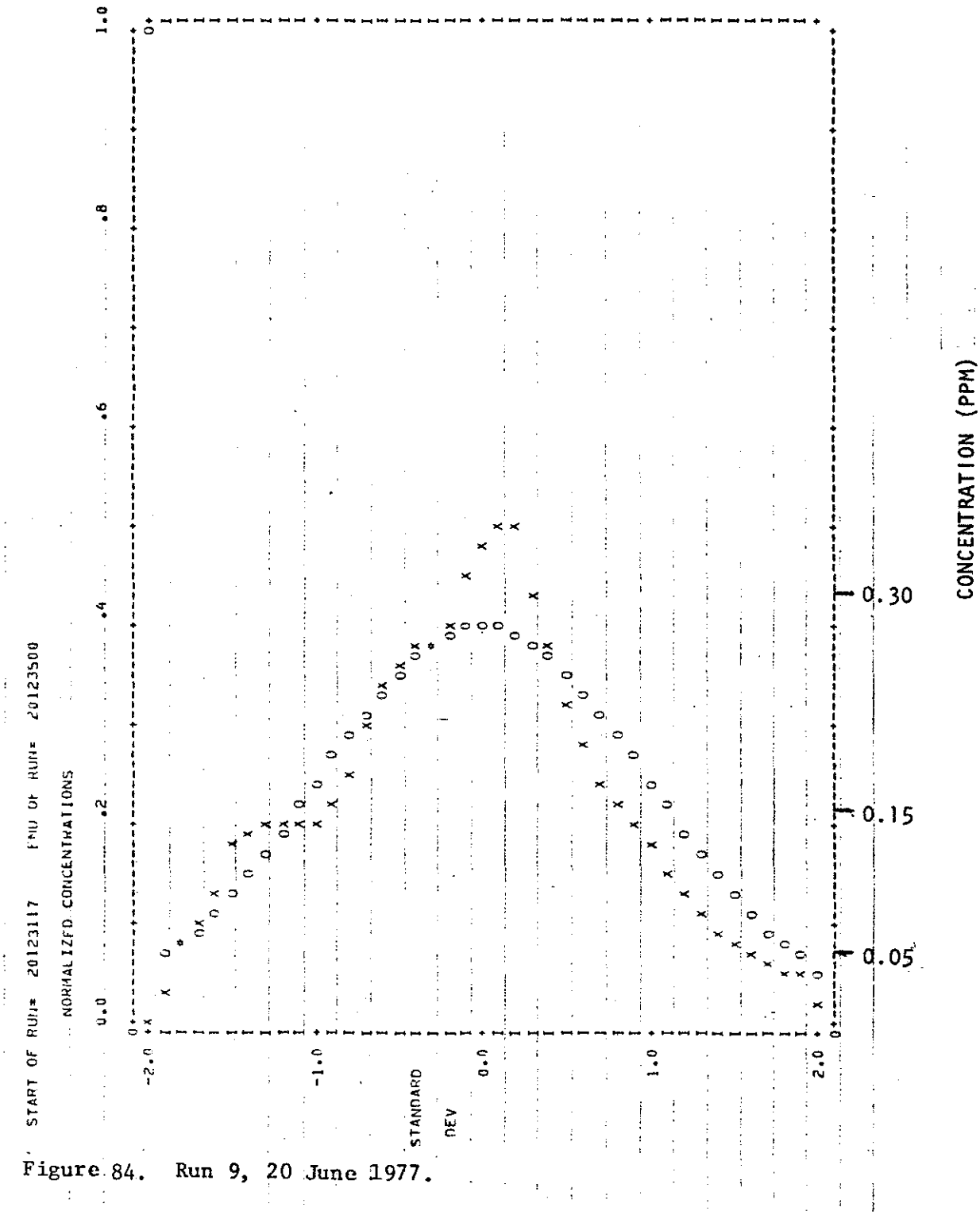

Figure 84. Run 9, 20 June 1977.

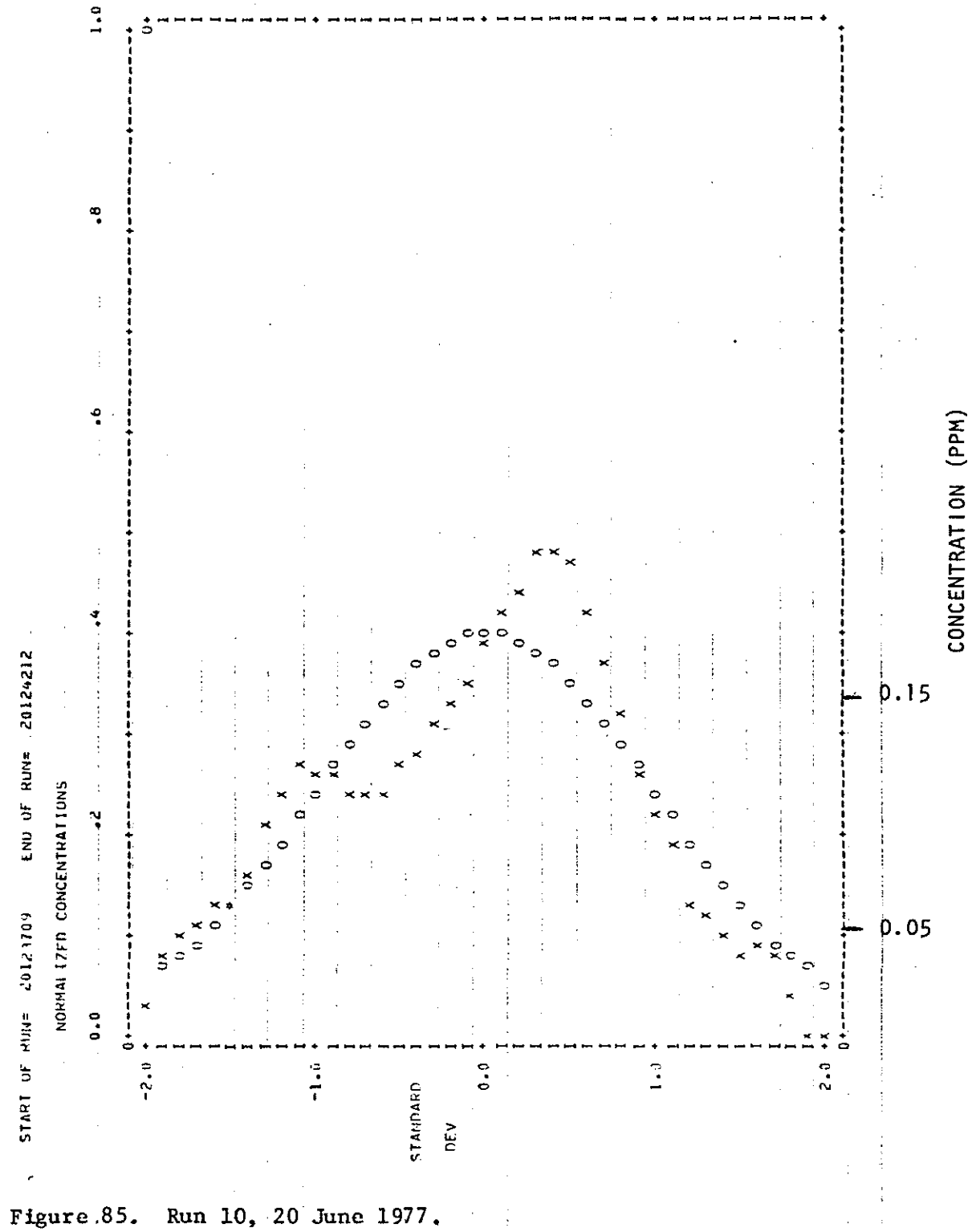

Figure 85. Run 10, 20 June 1977.

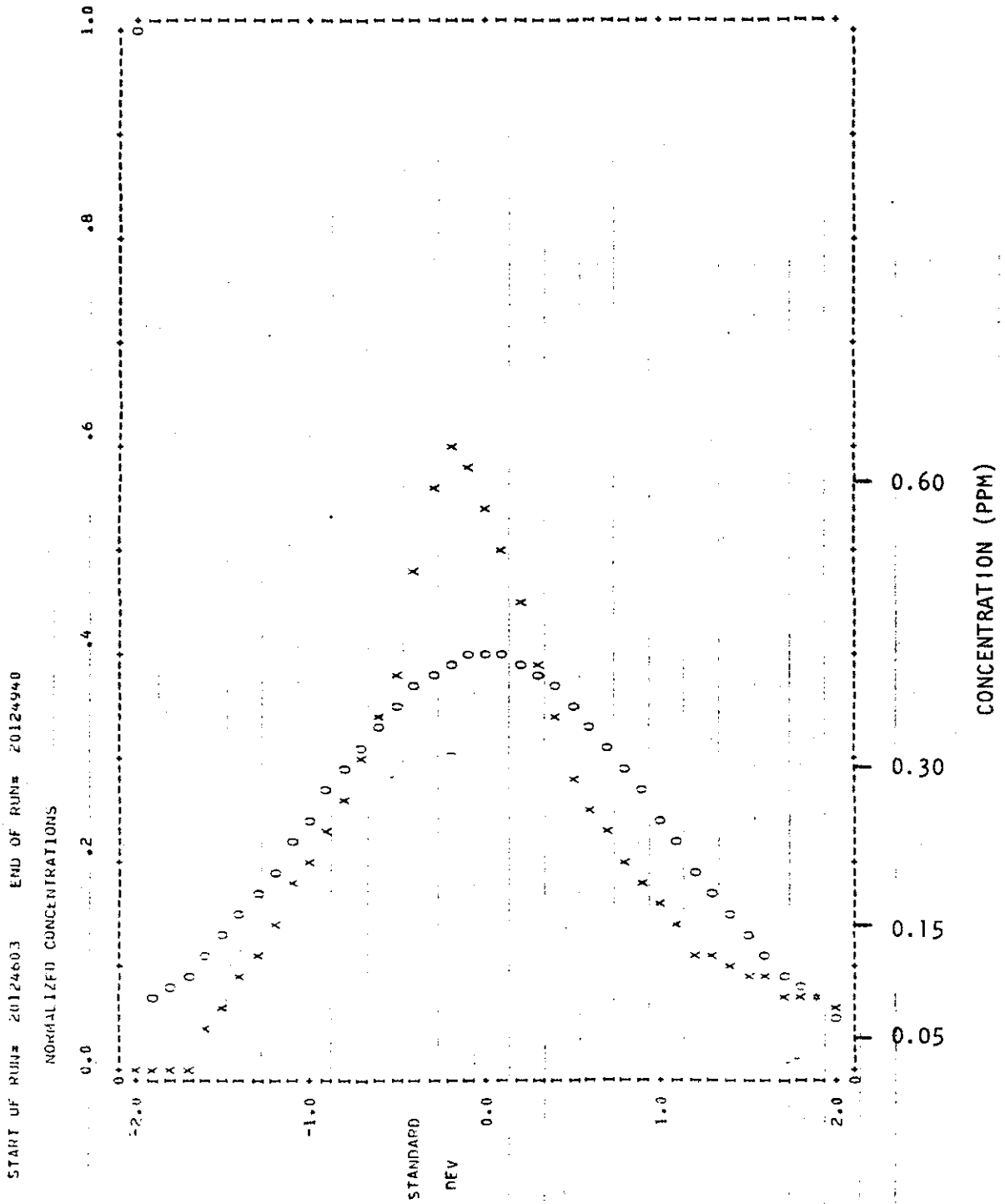

Figure 86. Run 11, 20 June 1977.

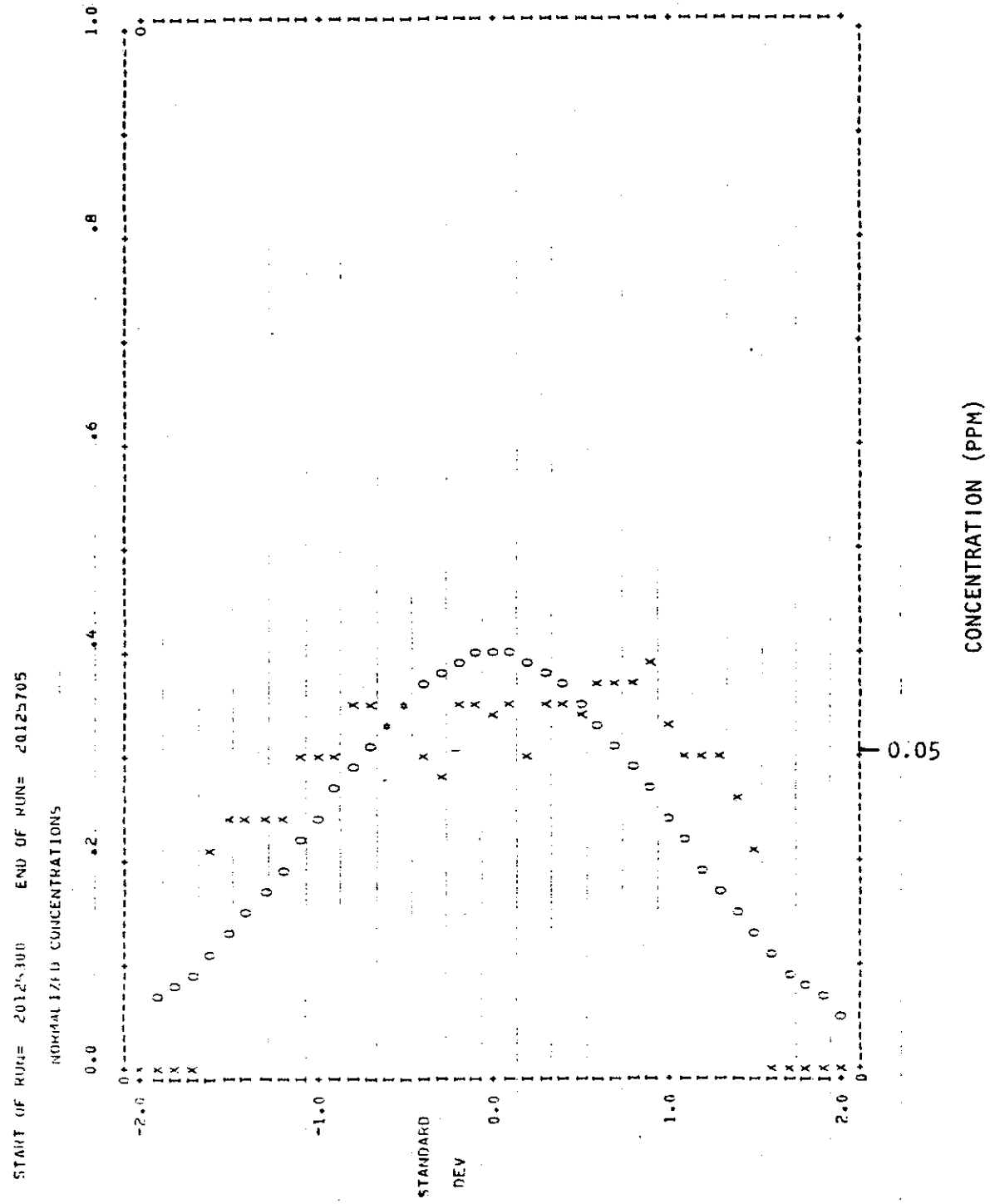

Figure 87. Run 12, 20 June 1977.

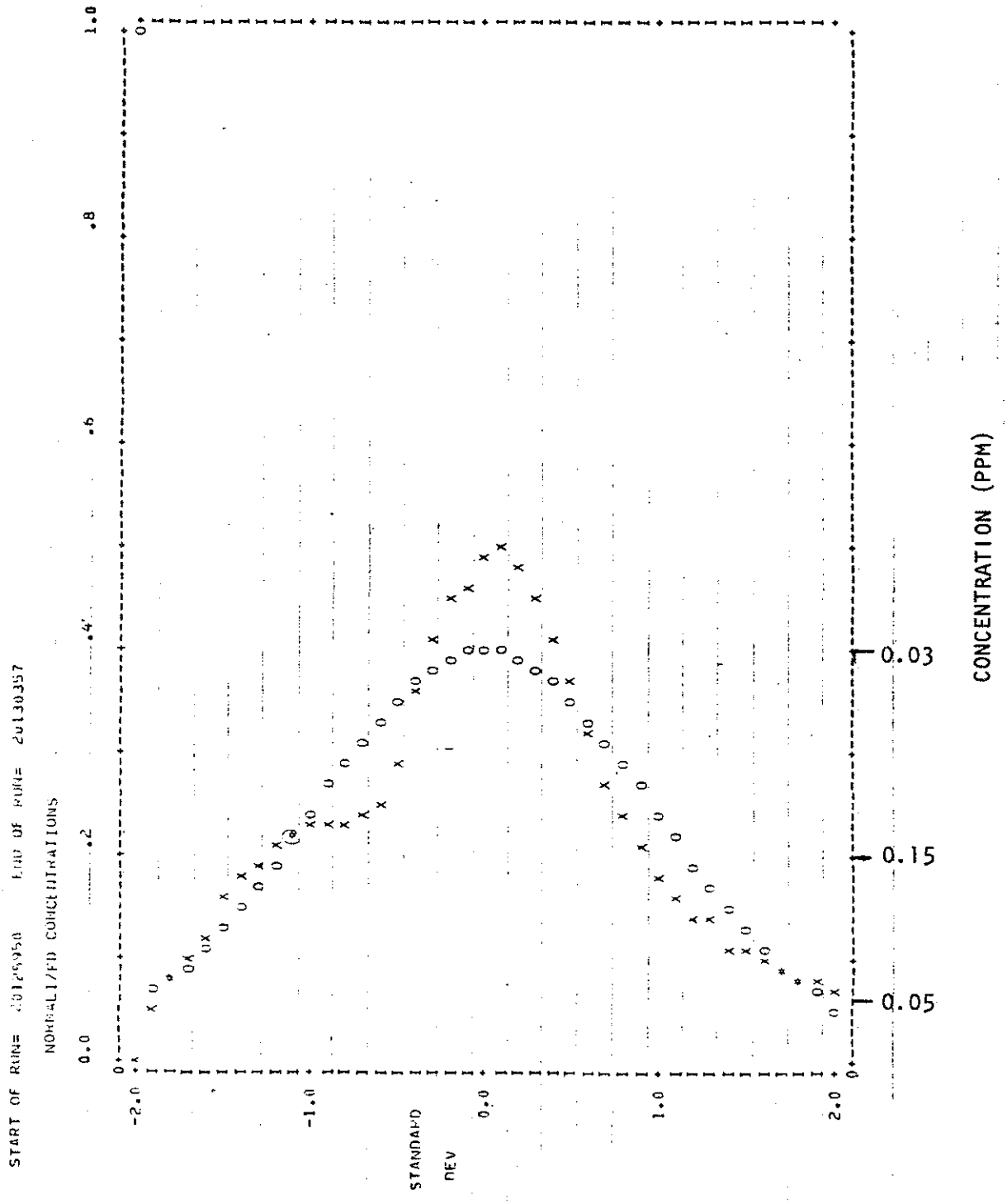

Figure 88. Run 13, 20 June 1977.

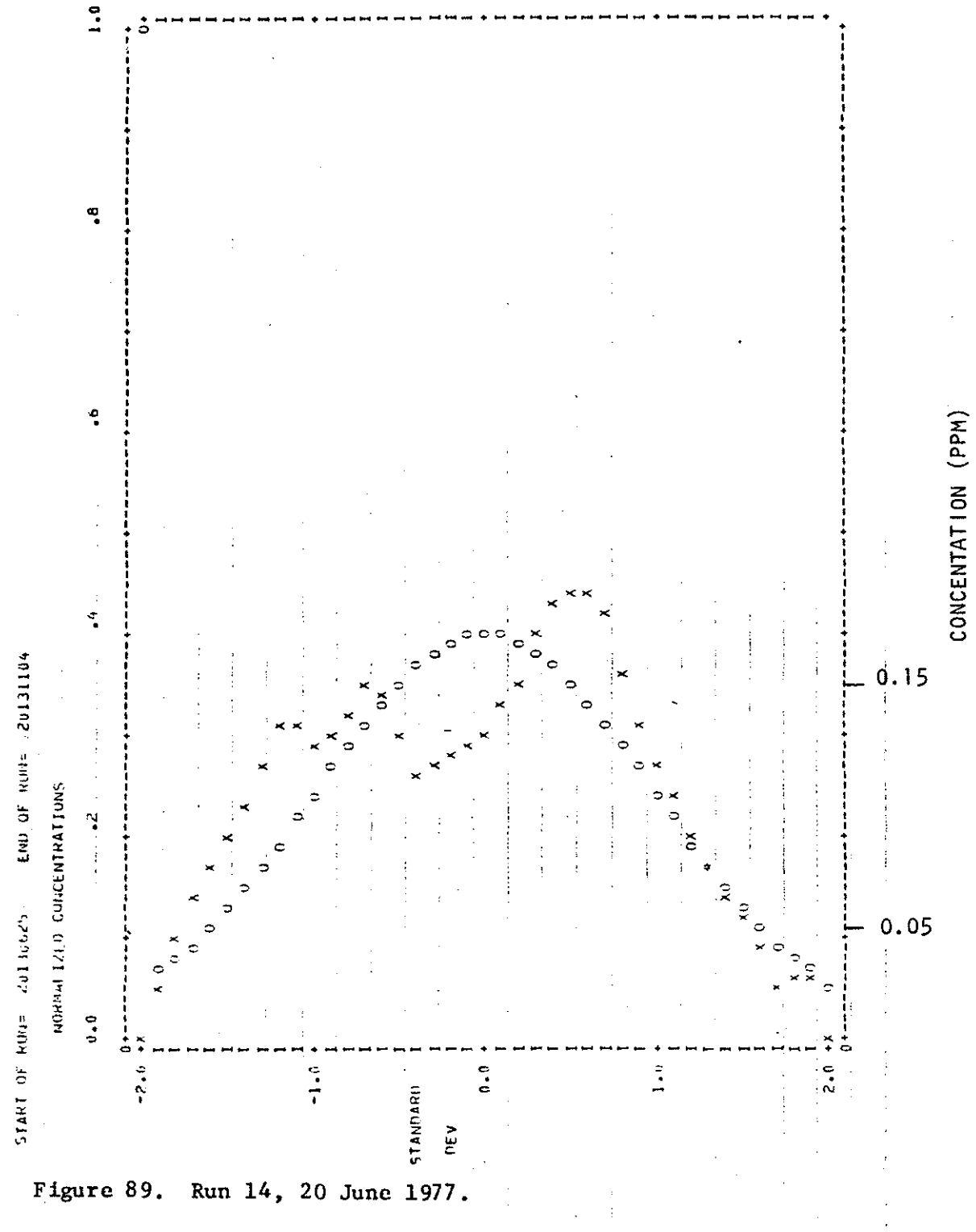

Figure 89. Run 14, 20 June 1977.

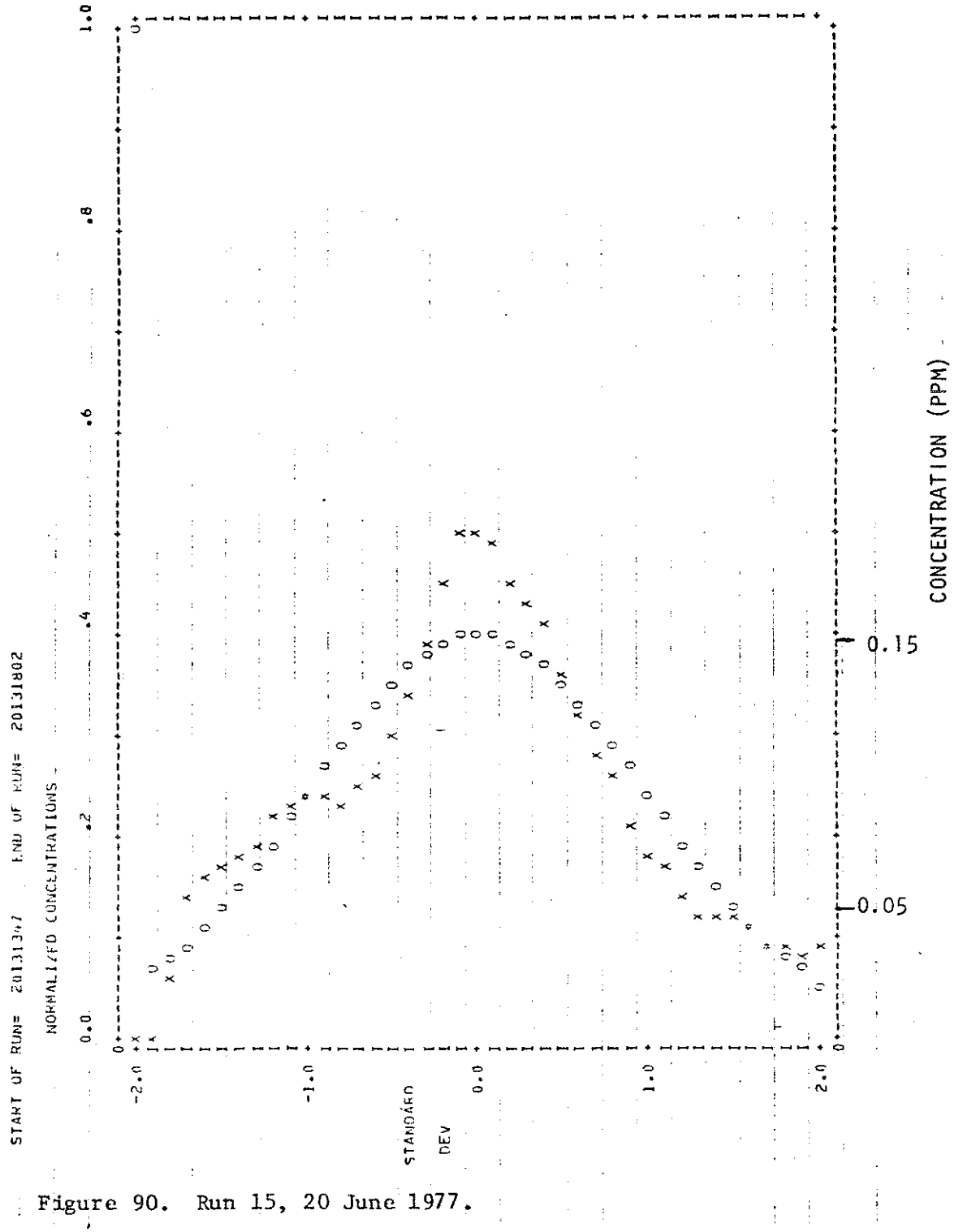

Figure 90. Run 15, 20 June 1977.

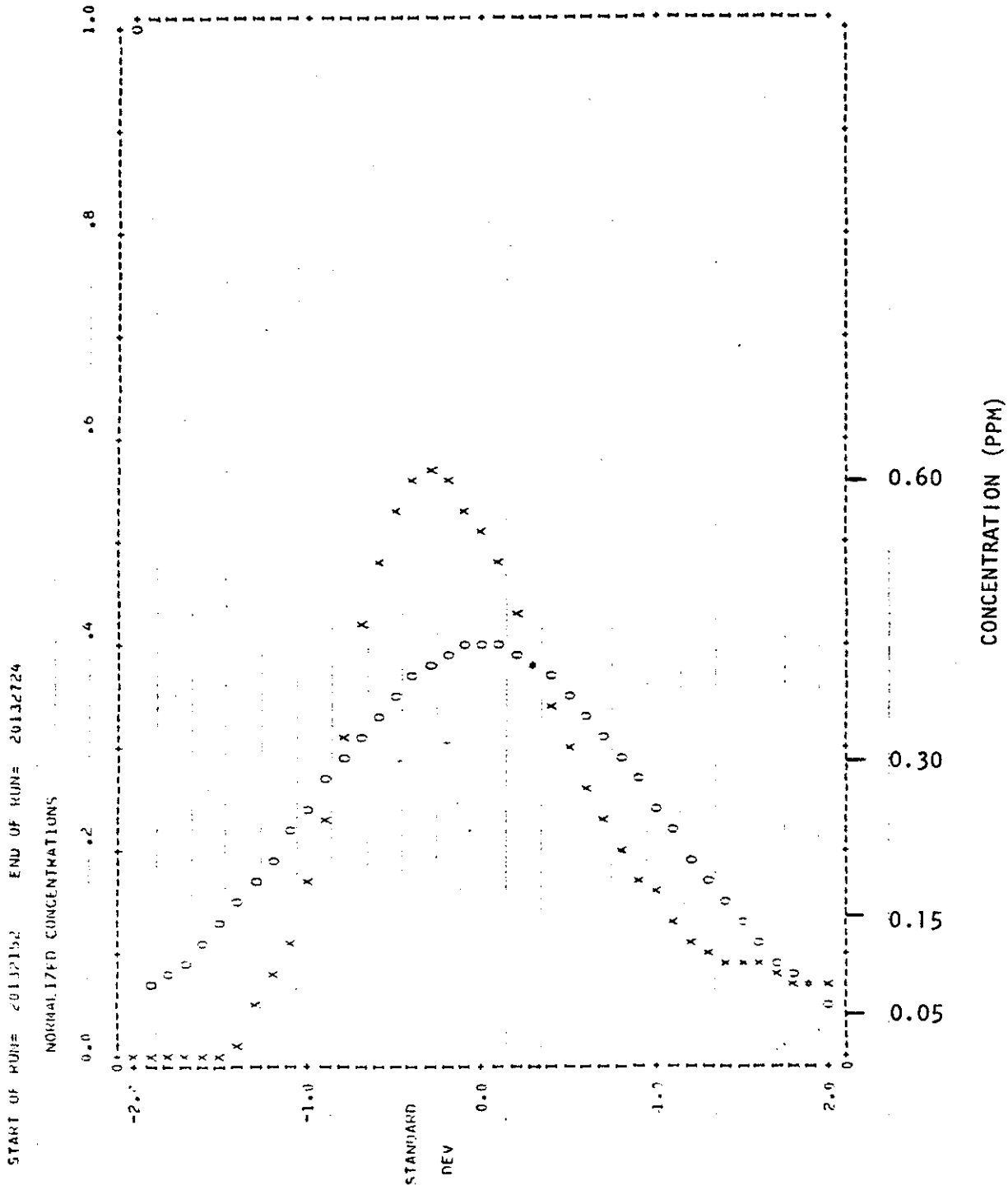

Figure 91. Run 16, 20 June 1977.

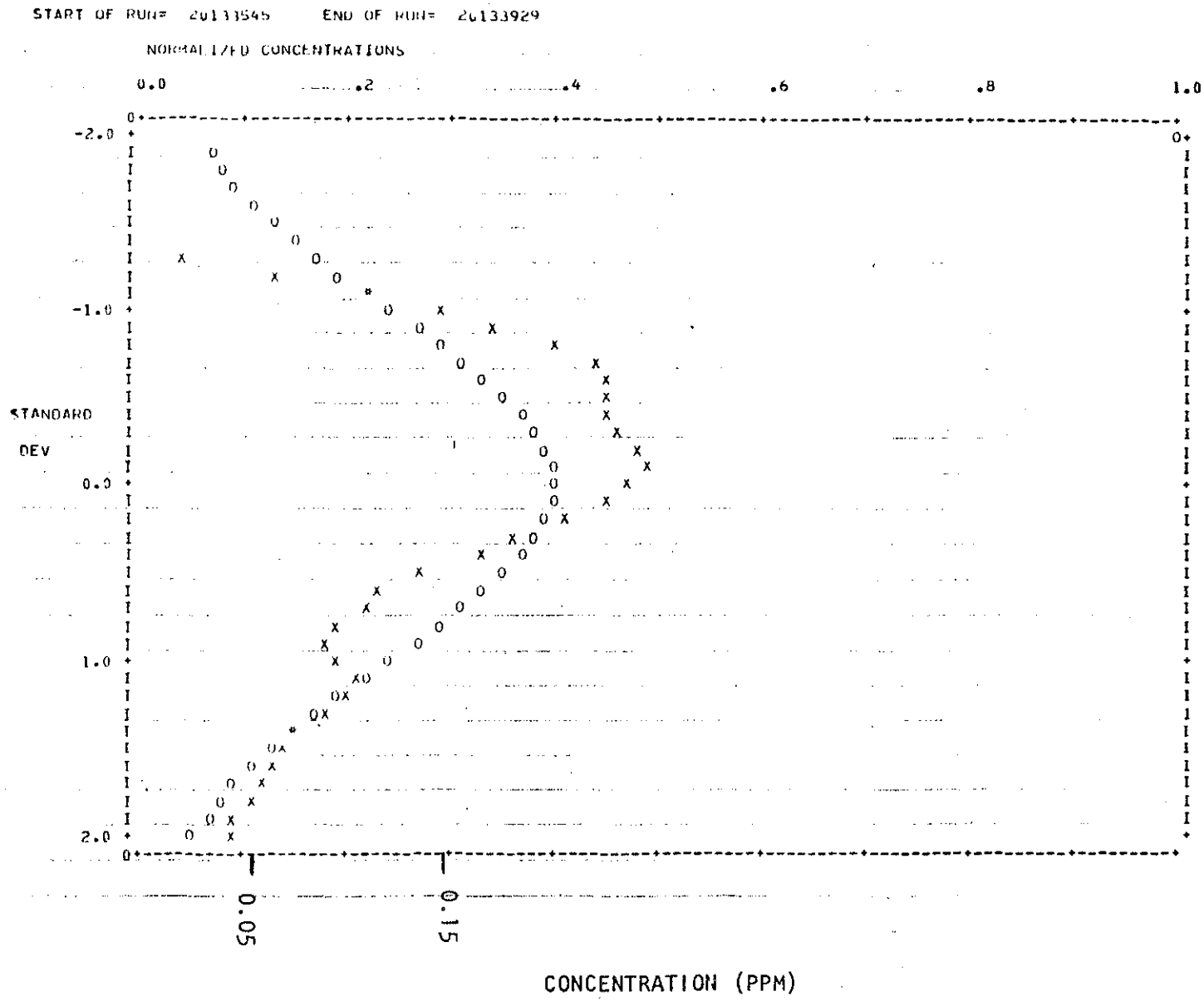

Figure 92. Run 17, 20 June 1977.

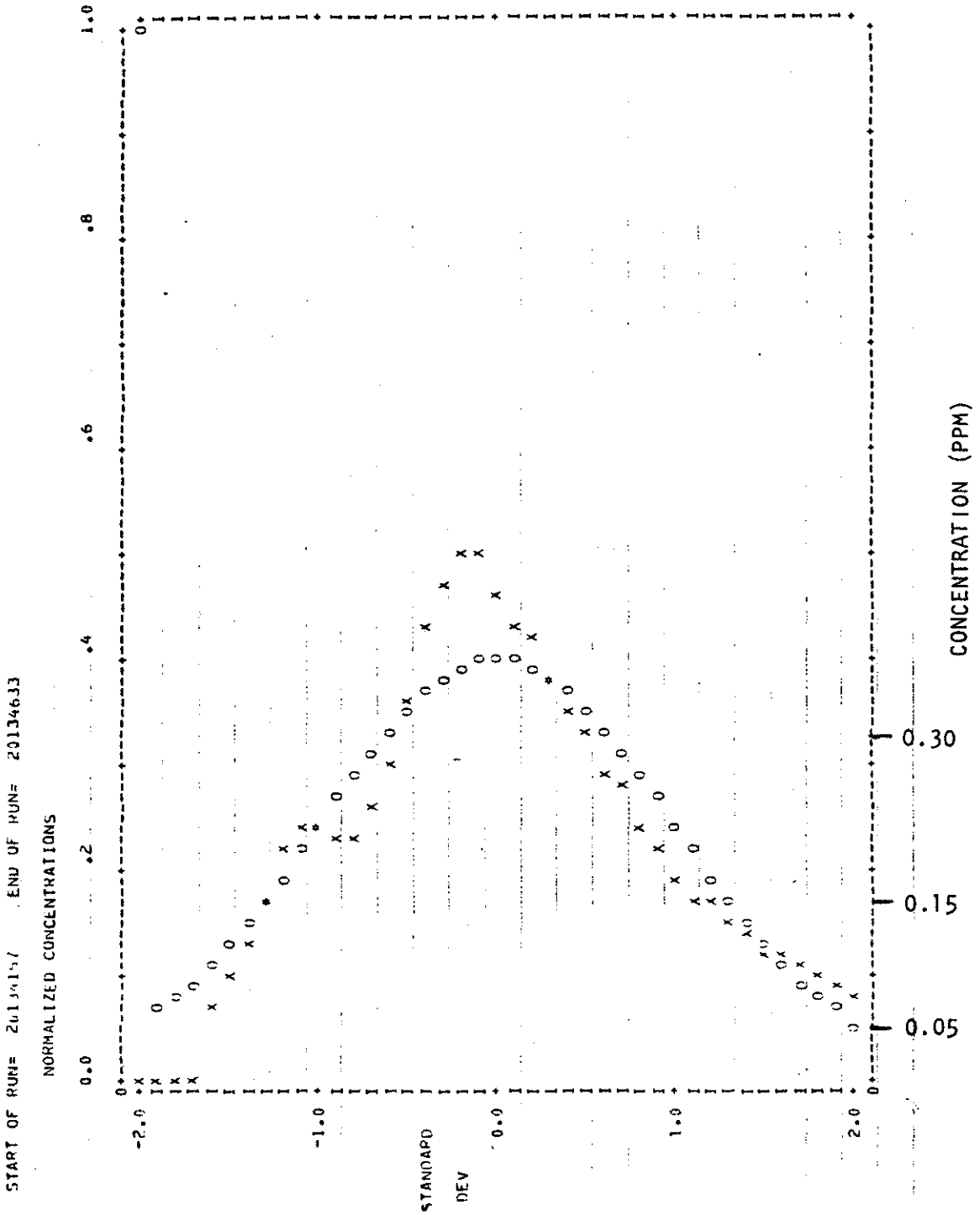

Figure 93. Run 18, 20 June 1977.

8.6 ADDITIONAL DETAILS OF SO_2 CONCENTRATIONS AND TURBULENCE STATISTICS FOR THE FLIGHT OF 22 JUNE 1977 (1915-2305 MDT).

Table 27. Run information for flight of 22 June 1977 (1915-2305 MDT).

Run Number	Start Time (MDT)	Altitude (m AMSL) ± 20	Downward Distance (km) ± 0.3	σ_y (m) ± 100	Max. Conc. (ppm) ± 0.02	Integrated Conc. (ppm-m) ± 50	Flight Dir. (from-to)
1[a]	1953	1526	3.2	-	-	-	N-S
2[a]	1959	1526	8.0	-	-	-	S-N
3[a]	2012	915	3.2	-	-	-	N-S
4	2018	915	8.0	341	0.13	98	S-N
5	2025	610	3.2	435	0.43	313	N-S
6	2033	610	8.0	1448	0.08	75	S-N
7[a]	2045	1220	3.2	-	-	-	N-S
8	2053	1220	8.0	210	0.08	42	S-N
9[a]	2101	763	3.2	-	-	-	N-S
10	2108	763	8.0	438	0.17	182	S-N
11[a]	2121	1068	3.2	-	-	-	N-S
12	2130	1068	8.0	318	0.20	146	S-N
13[a]	2137	915	3.2	-	-	-	N-S
14	2144	915	8.0	728	0.09	78	S-N
15	2152	610	3.2	375	0.93	667	N-S
16	2159	610	8.0	452	0.31	303	S-N
17	2205	534	3.2	403	0.49	427	N-S
18	2212	549	8.0	796	0.19	362	S-N
19[a]	2221	763	3.2	-	-	-	N-S
20	2228	763	8.0	307	0.14	101	S-N
21[a]	2236	671	3.2	-	-	-	N-S
22	2243	671	8.0	482	0.77	642	S-N

[a]No detectable SO_2.

T - turbulence run.

Table 28. Turbulence statistics from each run for the flight of 22 June 1977 (1915-2305 MDT).

Run No.	HT. m AMSL	X km	σ_w	σ_v	$\overline{W'V'}$	$\overline{W'T'}$	ℓ_w	ℓ_v	ε	N
1[a]	1526	3.2	1.09	+0.82	-0.10	0.00	380	220	6	3
2[a]	1526	8.0	0.82	0.82	-0.12	0.01	200	320	4	2
3	915	3.2	1.07	0.99	-0.67	-0.03	270	190	7	2
4	915	8.0	1.24	1.64	-0.79	0.02	250	310	15	3
5	610	3.2	1.42	1.48	-0.32	0.02	160	190	55	4
6	610	8.0	1.33	2.03	-0.19	0.03	250	220	50	3
7[a]	1220	3.2	0.95	0.58	0.02	0.01	250	220	4	3
8	1220	8.0	0.96	0.89	-0.16	0.00	300	240	7	3
9[a]	763	3.2	1.24	2.03	-0.87	0.02	230	330	22	1
10	763	8.0	0.61	0.99	-0.06	0.02	100	210	12	2
11[a]	1068	3.2	0.68	0.79	0.42	0.02	250	320	2	3
12	1068	8.0	0.57	0.63	-0.05	0.00	260	320	1	2
13[a]	915	3.2	0.68	0.64	0.13	0.01	230	250	3	2
14	915	8.0	0.71	0.80	+0.35	0.02	300	370	1	2
15A	610	3.2	1.27	1.63	-0.65	0.01	135	135	65	1
15B	610	3.2	0.78	1.43	0.29	0.00	180	350	12	3
16	610	8.0	0.81	1.20	+0.20	0.02	170	170	12	4
17A	534	3.2	1.36	1.45	-1.07	0.02	170	170	50	2
17B	534	3.2	0.62	0.82	-0.08	0.01	180	180	9	2
18	549	8.0	0.69	1.22	+0.08	0.00	120	200	17	3
19[a]	763	3.2	0.52	0.80	-0.03	-0.01	200	310	2	3
20	763	8.0	0.74	0.84	-0.25	0.03	230	280	3	2
21[a]	671	3.2	Data Logger Malfunction							
22	671	8.0	0.46	0.76	-0.23	0.01	400	370	2	1

Notes: all units are MKS except dissipation, ε, which is expressed in $cm^2 \cdot sec^{-3}$.

X downwind distance from GCOS stack for crosswind flights

σ_w standard deviation of the vertical velocity

σ_v standard deviation of the lateral velocity with respect to the aircraft

$\overline{W'V'}$ product of fluctuating vertical and lateral velocities with sign changes so that crosswind flights express $\overline{W'U'}$ with respect to ground and along wind flights express $\overline{W'V'}$ with respect to ground using a right hand co-ordinate system with positive u in direction of wind.

$\overline{W'T'}$ product of fluctuating temperature and vertical velocity

ℓ_w integral length scale for vertical velocity

ℓ_v integral length scale for lateral velocity with respect to the aircraft

continued ...

Table 28. Concluded.

ϵ dissipation

N number of 65 sec analysis blocks in the run

T turbulence run flown parallel to wind.

[a]No detectable SO_2.

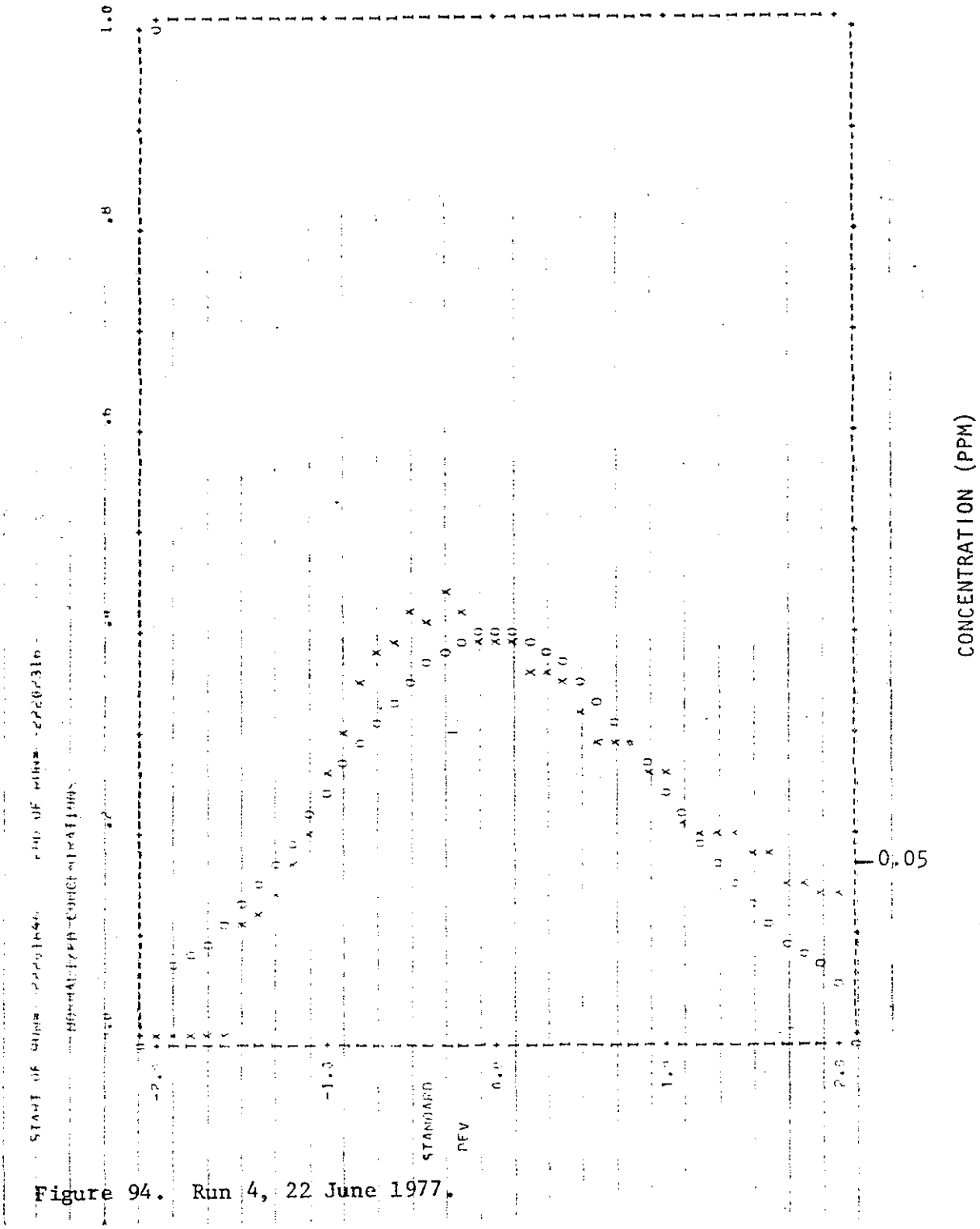

Figure 94. Run 4, 22 June 1977.

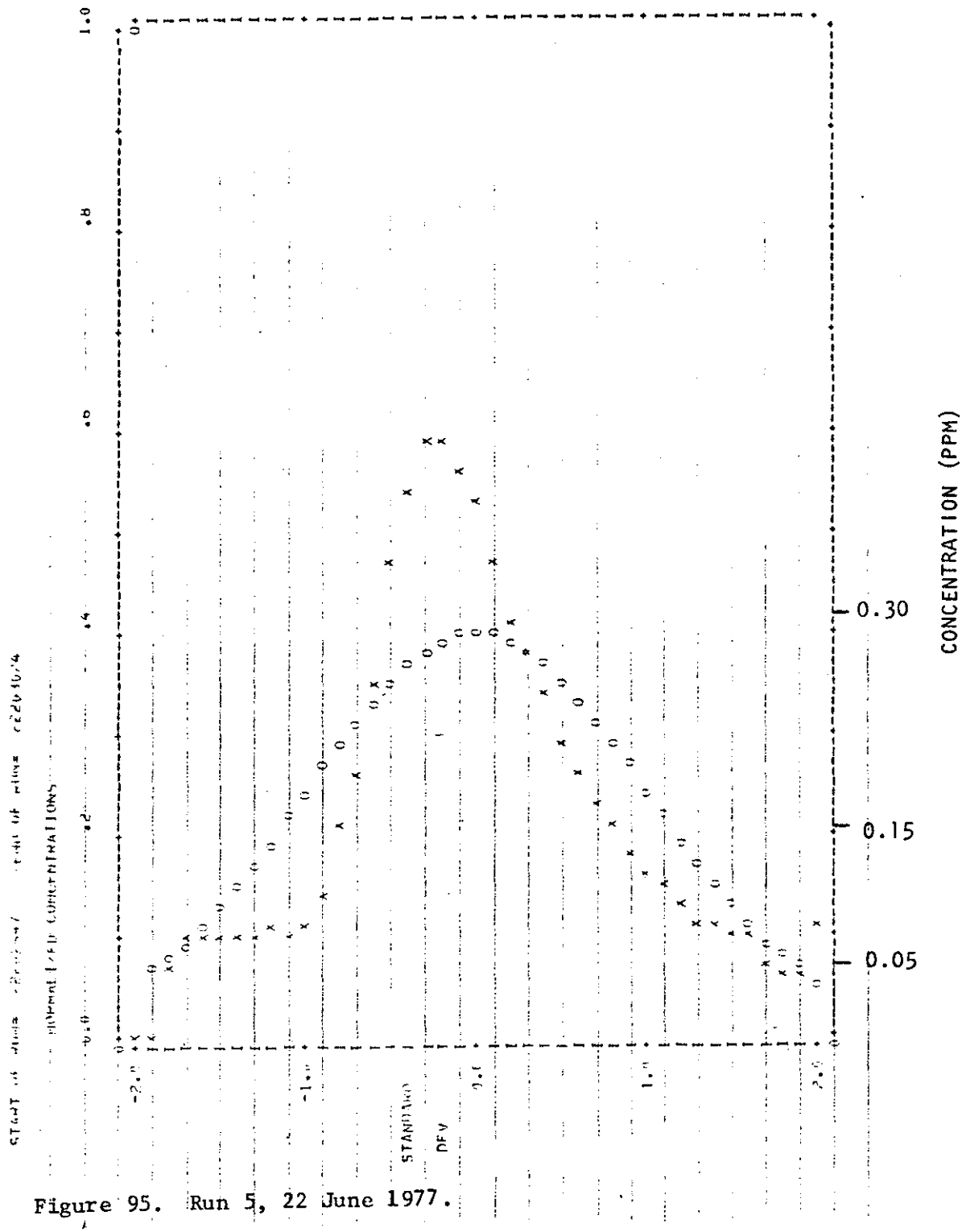

Figure 95. Run 5, 22 June 1977.

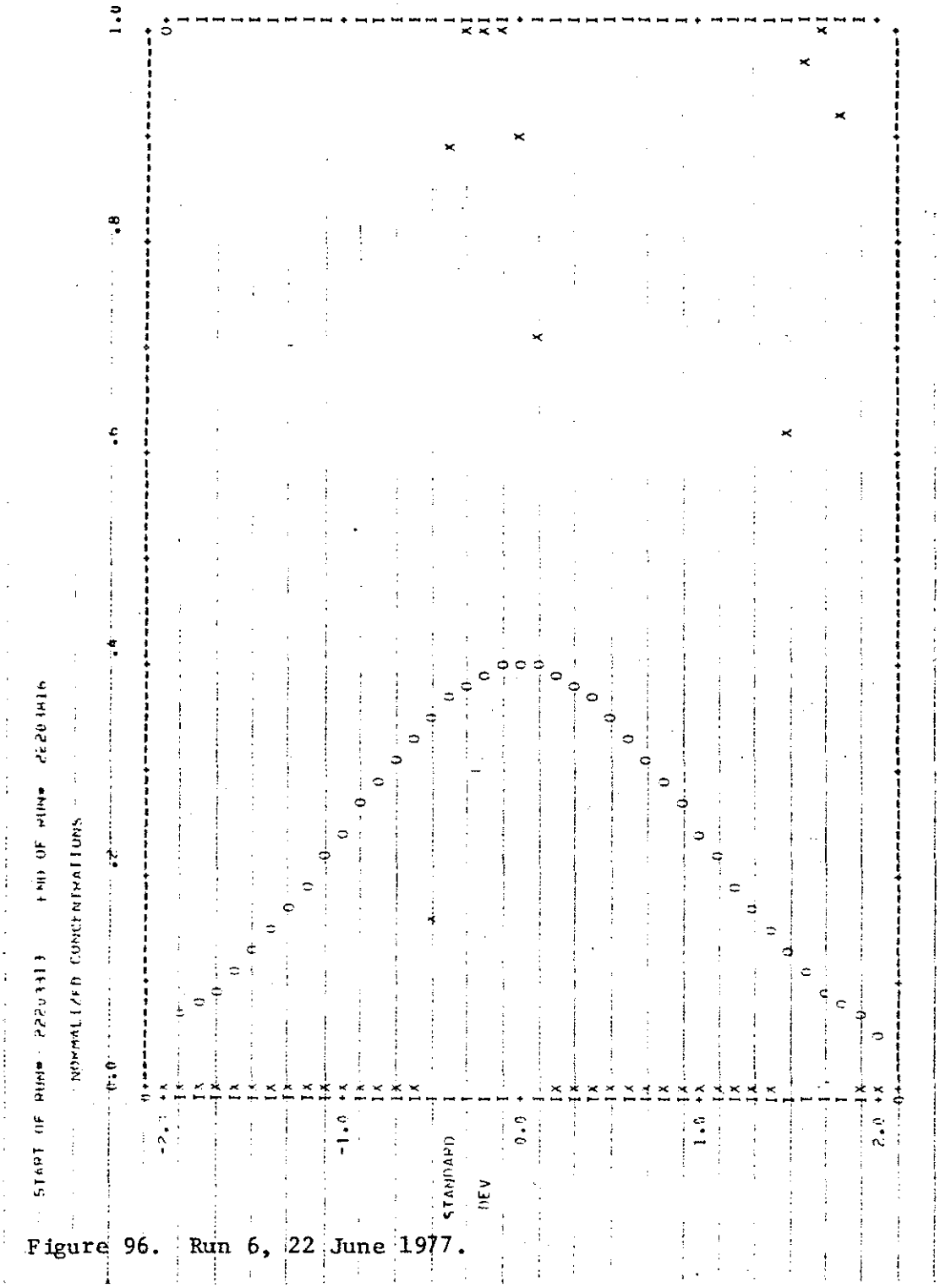

Figure 96. Run 6, 22 June 1977.

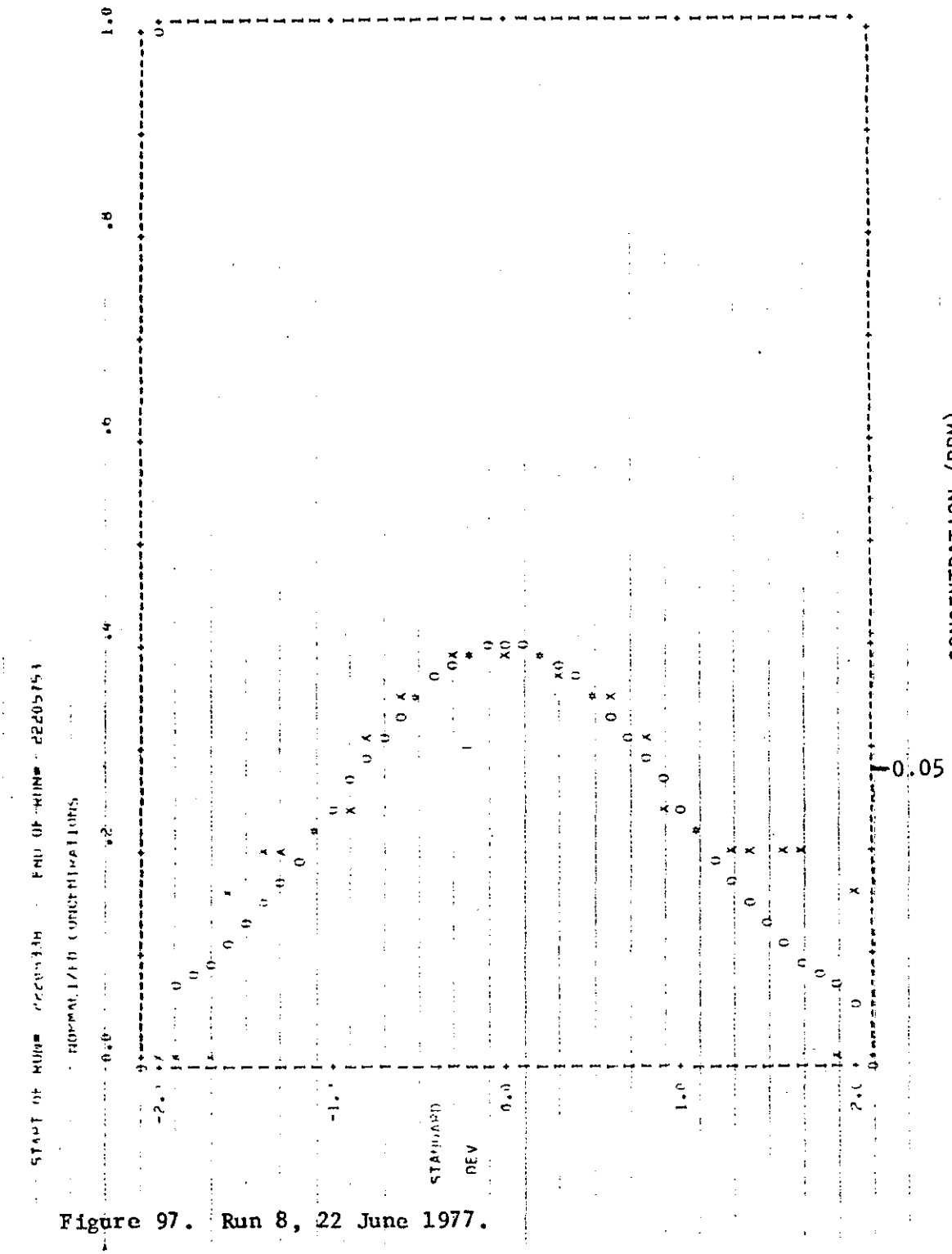

Figure 97. Run 8, 22 June 1977.

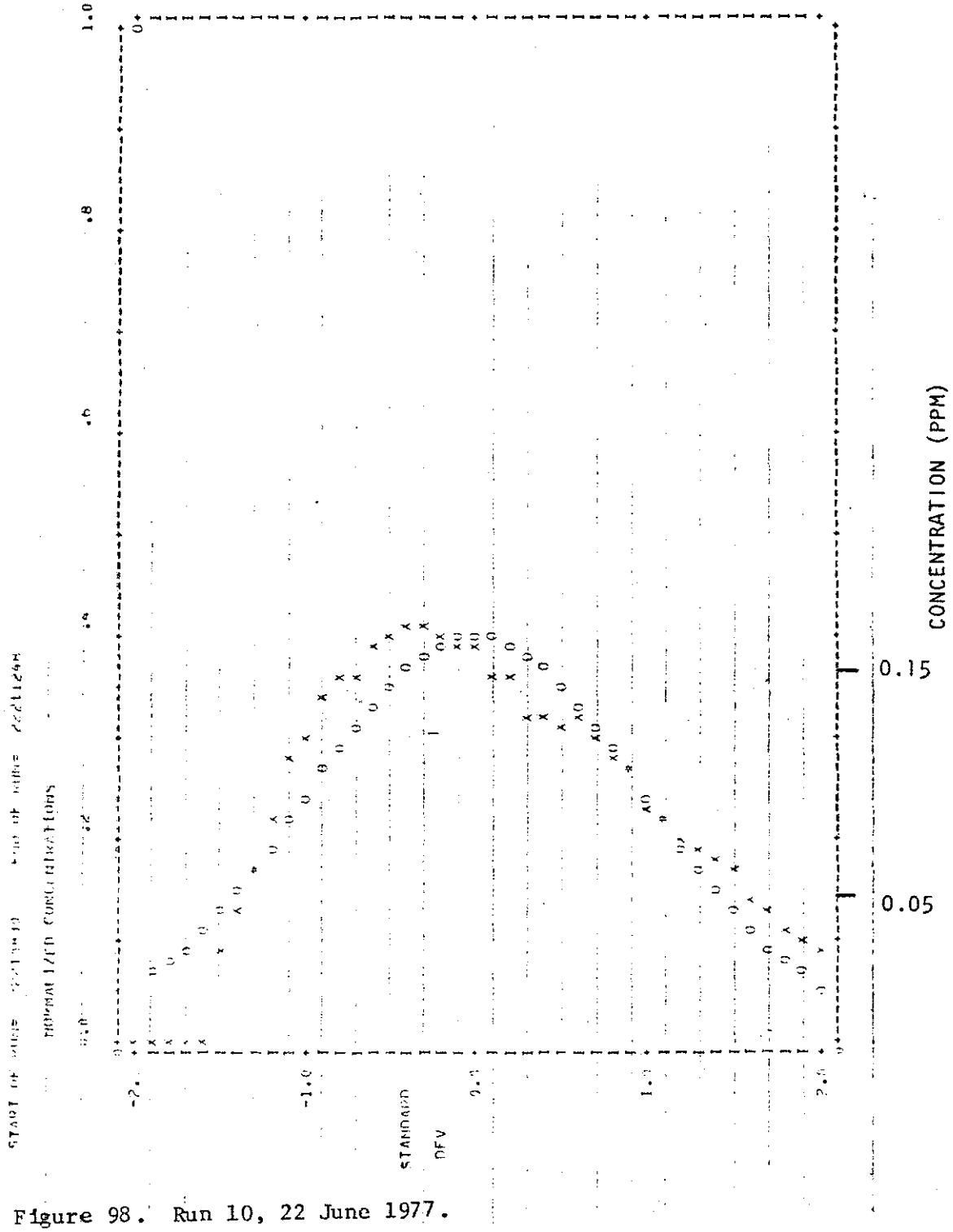

Figure 98. Run 10, 22 June 1977.

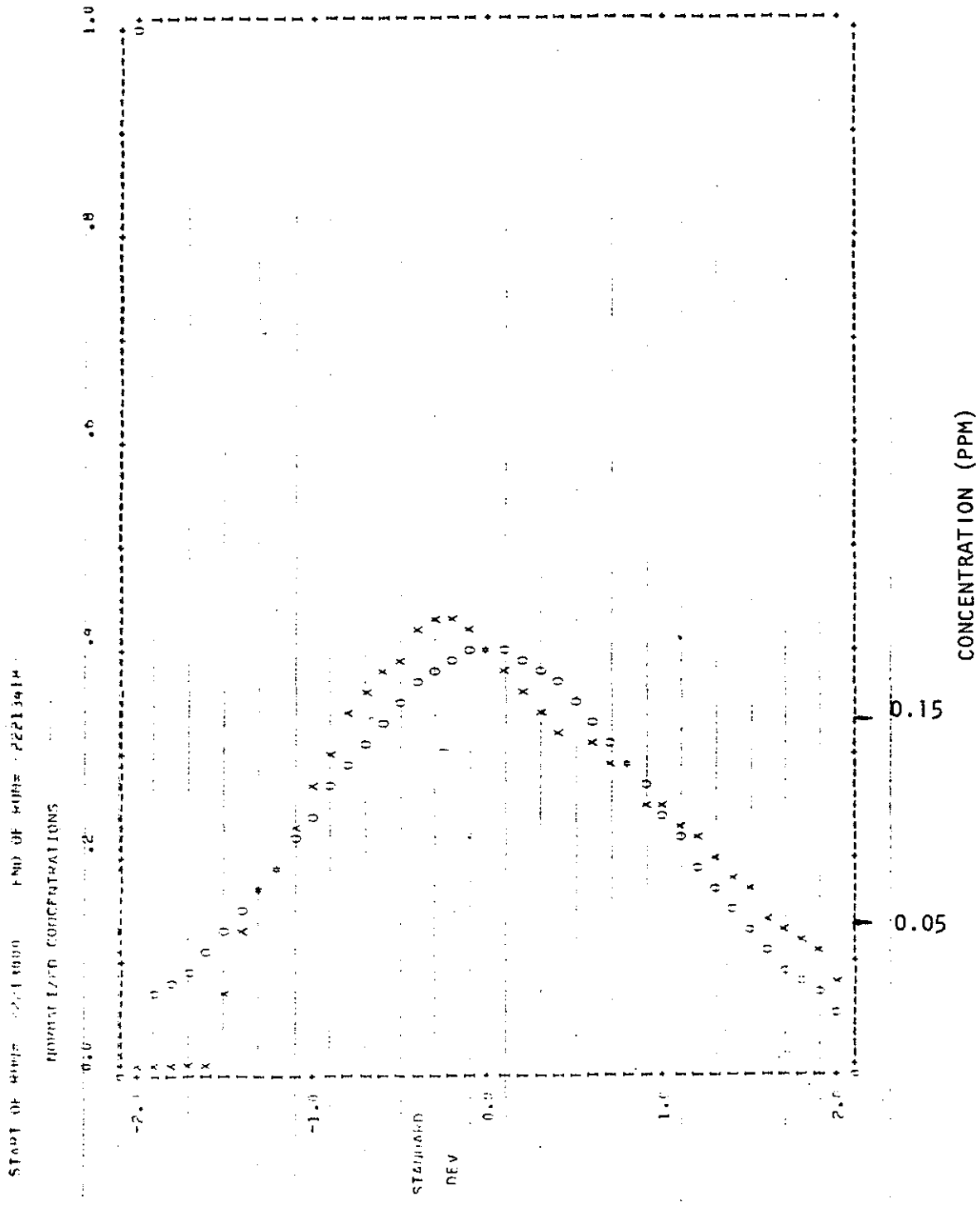

Figure 99. Run 12, 22 June 1977.

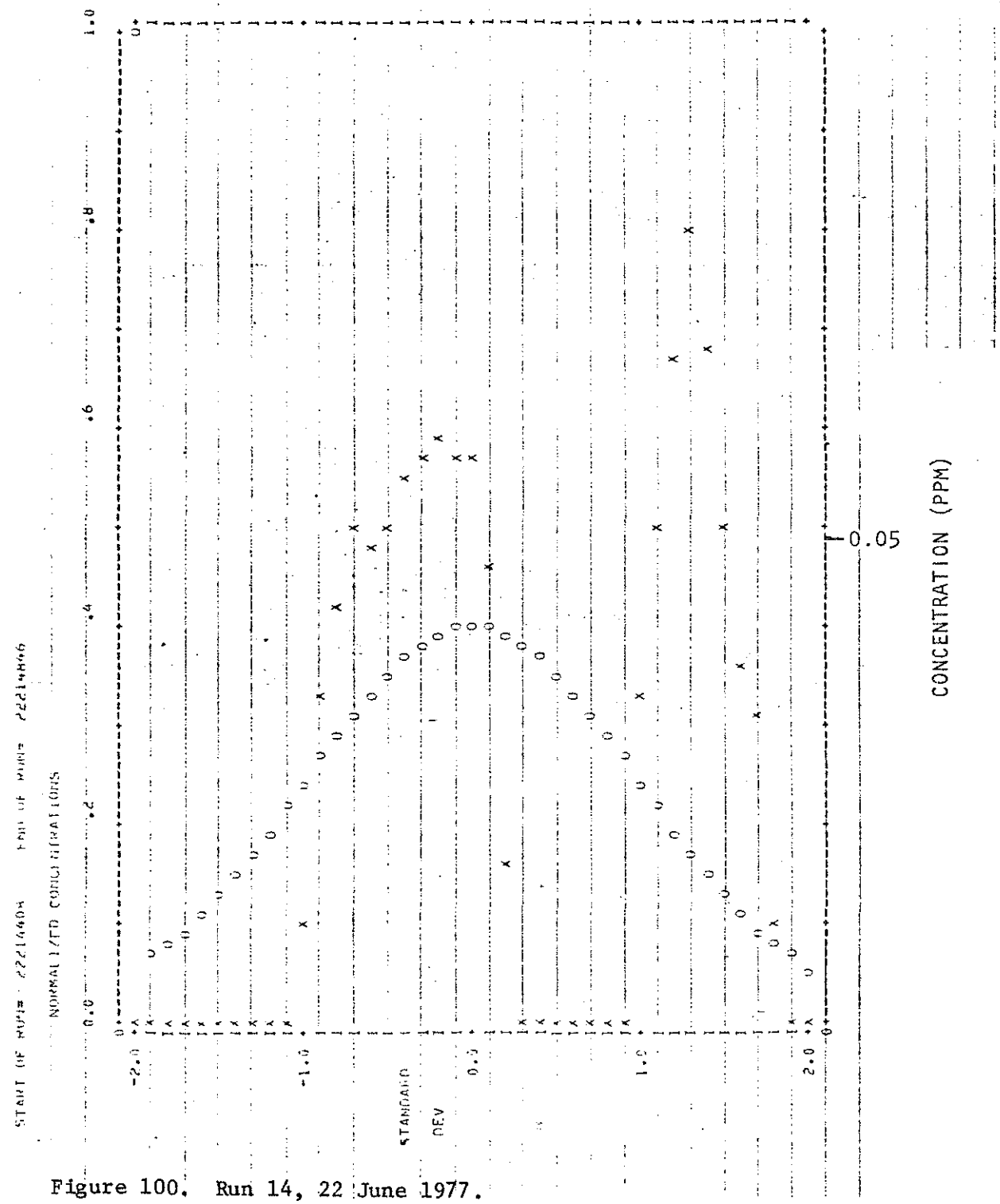

Figure 100. Run 14, 22 June 1977.

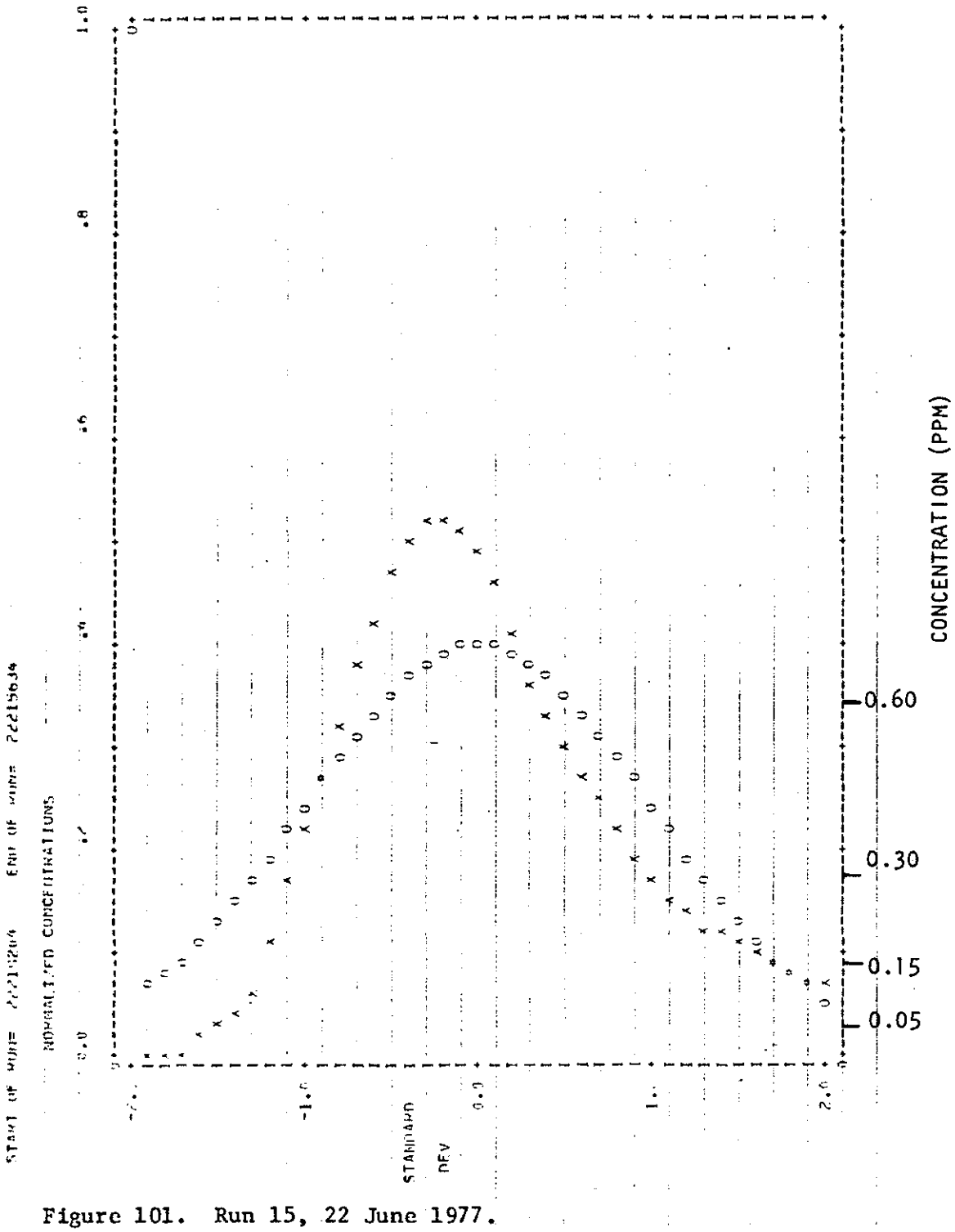

Figure 101. Run 15, 22 June 1977.

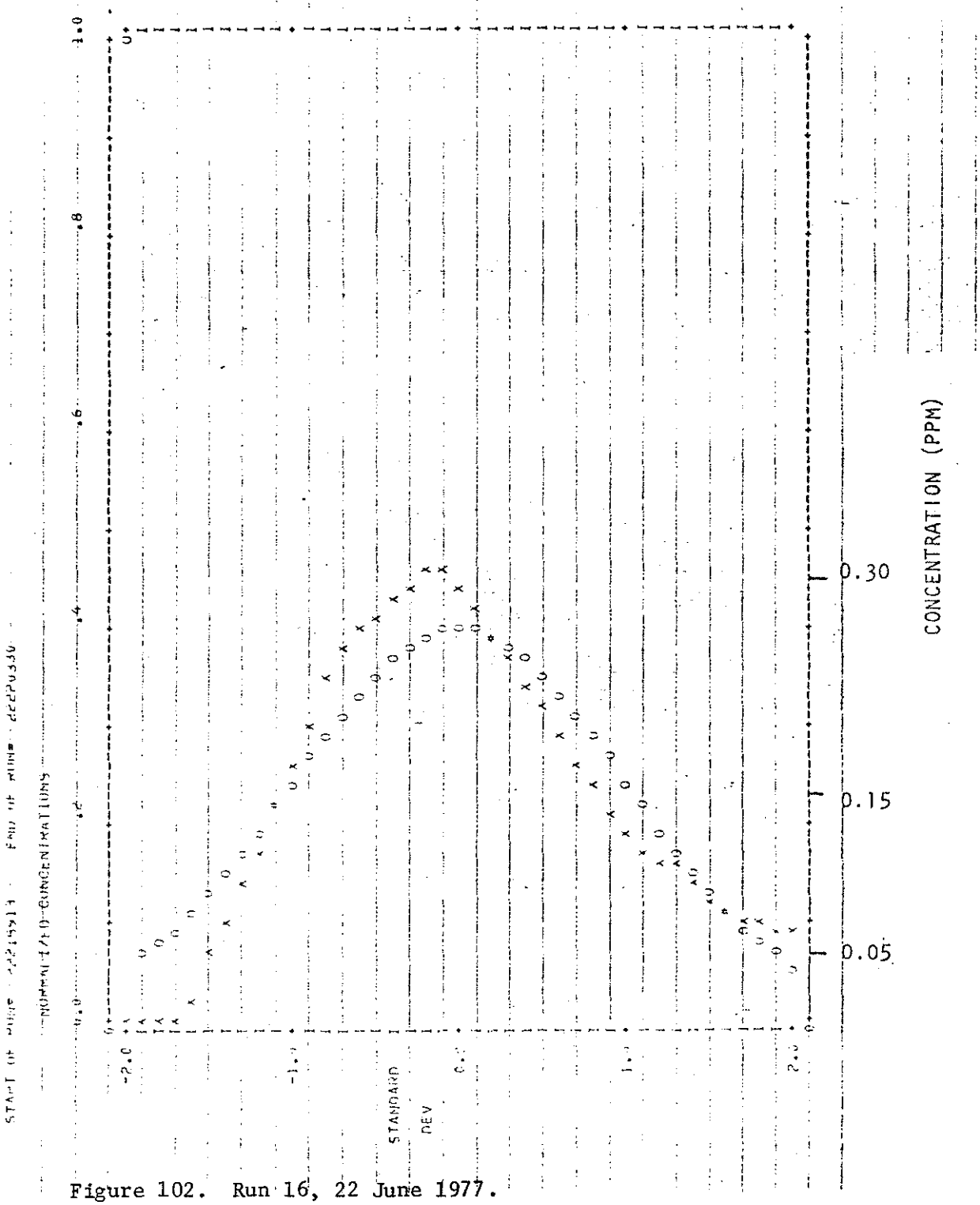

Figure 102. Run 16, 22 June 1977.

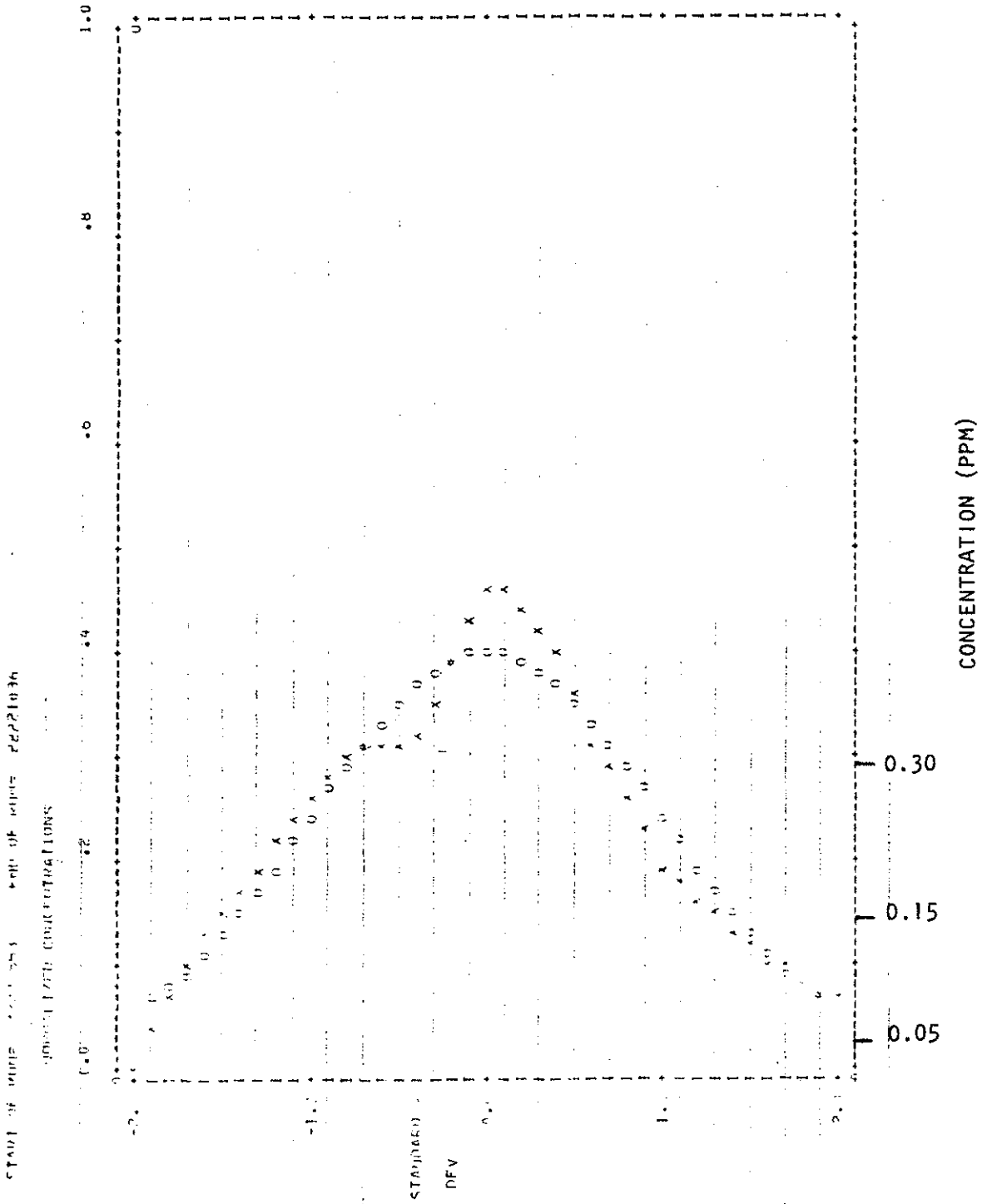

Figure 103. Run 17, 22 June 1977.

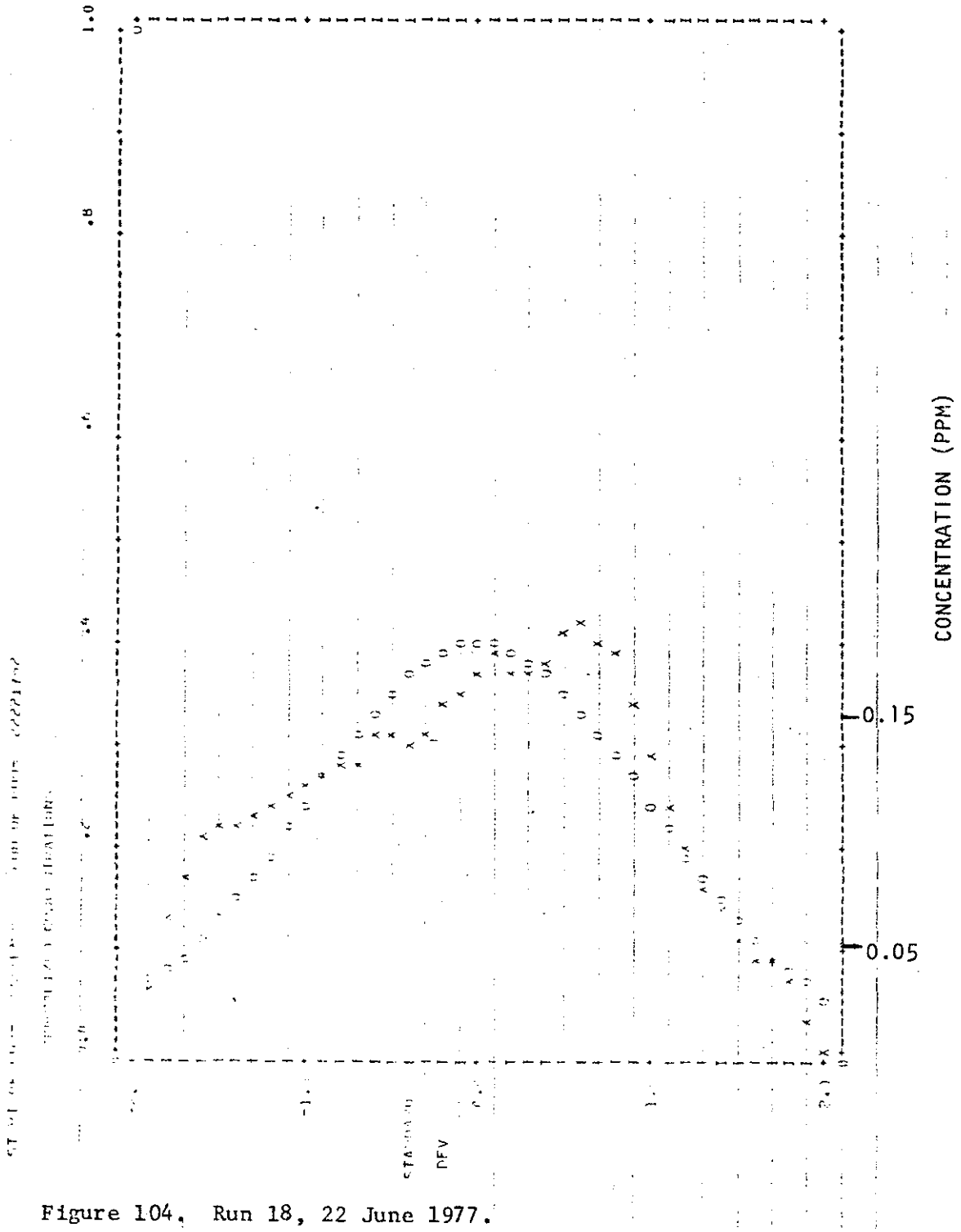

Figure 104. Run 18, 22 June 1977.

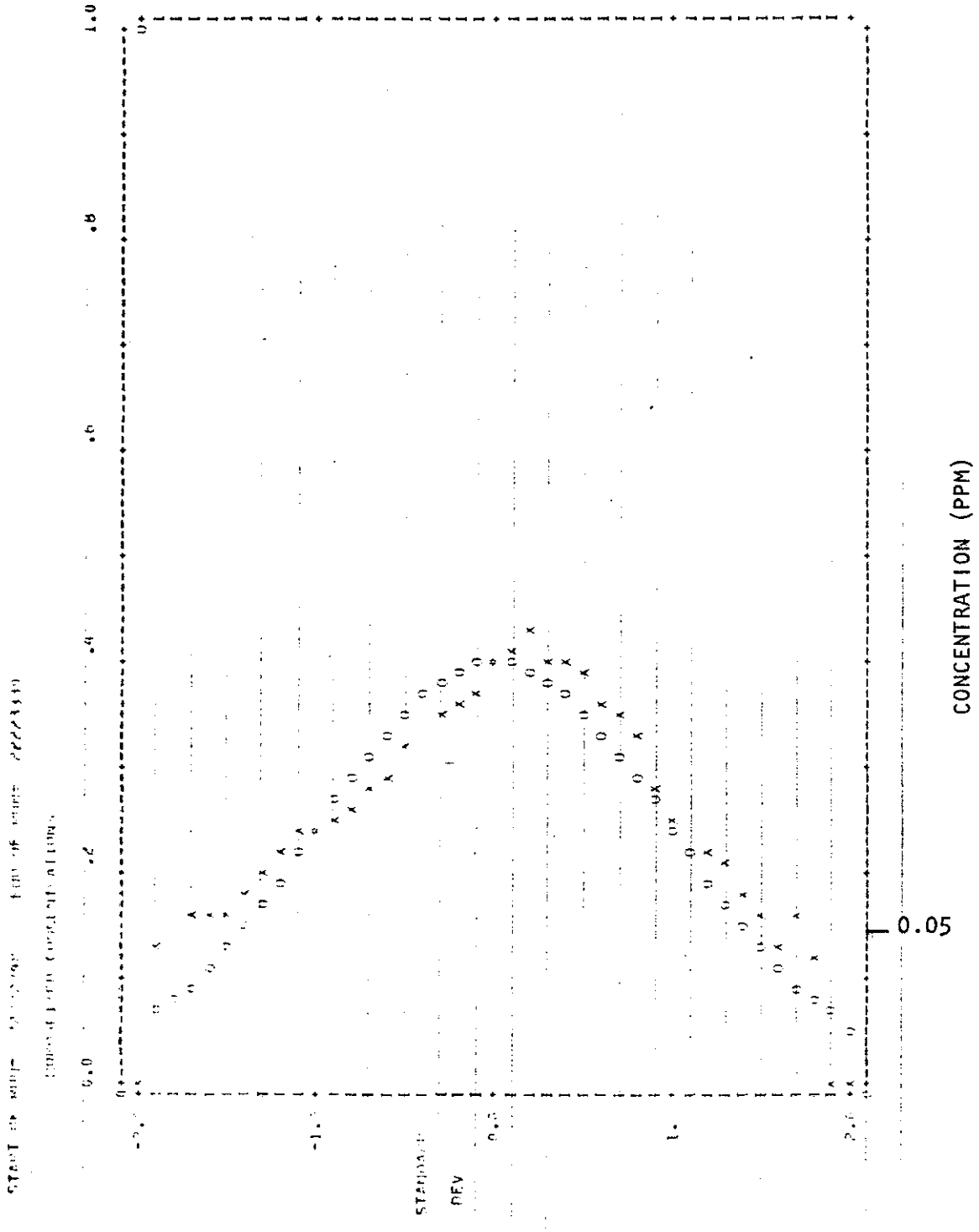

Figure 105. Run 20, 22 June 1977.

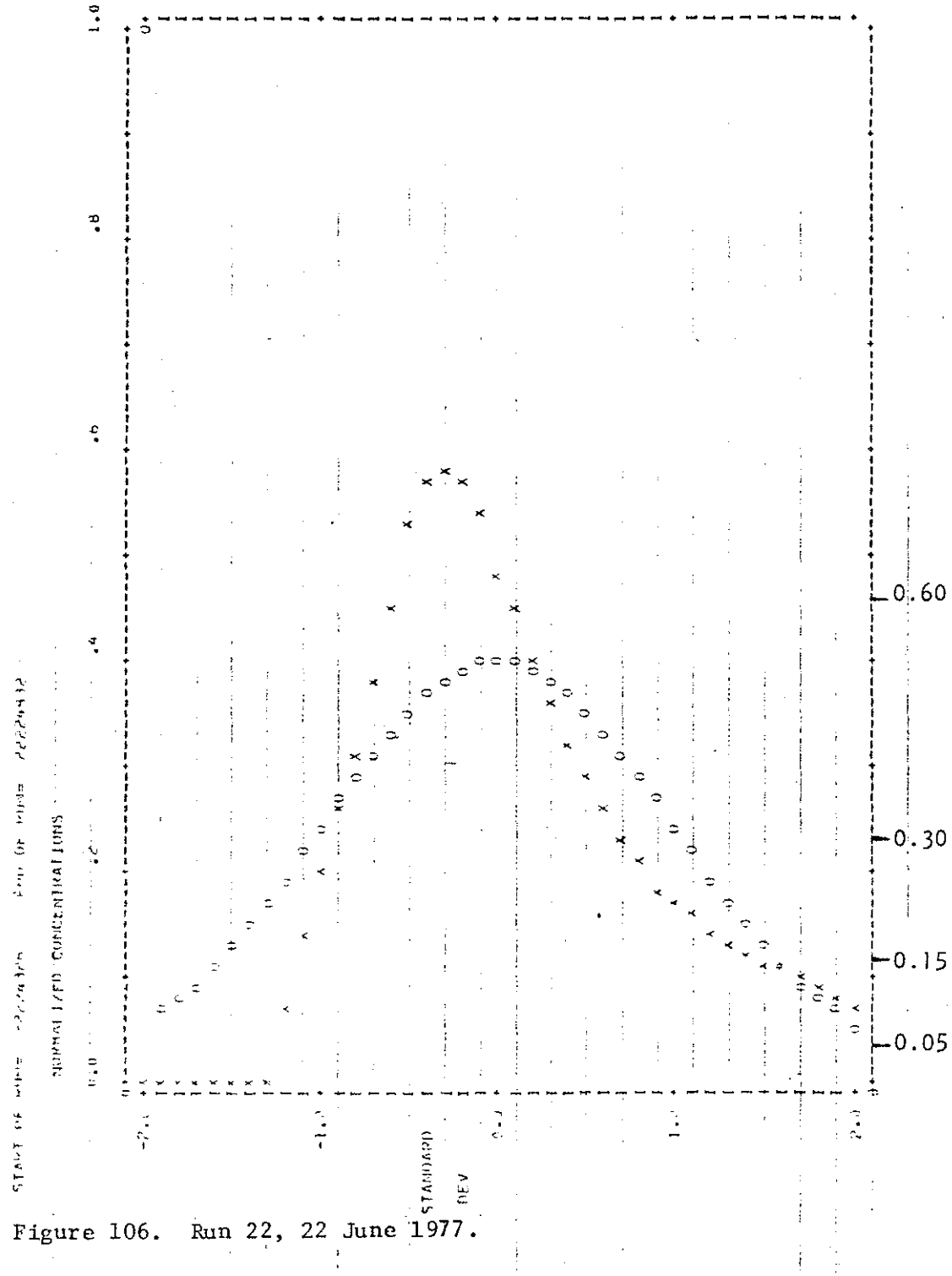

Figure 106. Run 22, 22 June 1977.

8.7 LIST OF SYMBOLS

e (subscript)	environmental, ground-based co-ordinate system
f(x)	Pasquill's downwind decay function
f	frequency
H	effective stack height
k	wave number ($k = 2^{o}f/TAS$)
L	Monin Obukhov length
ℓ_E	Eulerian integral length scale
ℓ_L	Lagrangian integral length scale
R	Lagrangian autocorrelation function for velocities
T^i	temperature fluctuation
T	dispersion time or temperature
t_E	Eulerian integral time scale
t_L	Lagrangian integral time scale
TAS	aircraft true air speed
$\overline{U}$	mean wind speed
U'	fluctuations in longitudinal wind component
u_*	friction velocity $u_*^2 = -\overline{U'W'}$
V'	fluctuations in lateral wind component
W'	fluctuations in vertical wind component
X	downwind distance from source
β	ratio of Lagrangian to Eulerian length scales
ε	dissipation
σ	standard deviation of a distribution or time series
Θ	wind direction

8.8 RECOMMENDATIONS FOR FUTURE AERIAL PROGRAMS

As required by contract, the recommendations arising from the Plume Dispersion Study, June 1977 (AOSERP Project ME 2.3.2) are presented under separate cover.

Based upon the experience gained during the field programs and subsequent analyses of both the March 1976 and 1977 field studies, specific recommendations are presented below.

8.8.1 Position Recovery

Accurate navigation using visual flight positioning is very difficult, particularly on the east side of the Athabasca River. It is recommended that position recovery instrumentation be used on subsequent field trips. The Ontrac III VLF Omega Navigation System used in the June 1977 field study was found to be adequate for position recovery.

8.8.2 Stationarity Problems

The main plume from GCOS generally has a high effective stack height, and so the vertical depth over which stacked traverses are required is large. It is recommended that in order to avoid significant changes in the plume structure, the number of downwind distances for the stacked traverses to be kept to two. It is better to have increased vertical resolution than another downwind distance. Detailed turbulence analysis showed that conditions often were changing continuously. Thus, a staggering of flight levels is needed to distinguish time from height variations. Particular care must be paid to changes in centerline height; mass flux computations are valuable for this problem.

8.8.3 Aircraft Operational Base

In the report for the March 1976 field study, it was recommended that the Fort McMurray airport be used as the operational base for subsequent field programs. The advantages of heated hangar and availability of an aircraft mechanic were considered to be very significant.

It is recommended that even in warm-weather field trips, the conveniences of aircraft servicing outweighs the isolation of the aircraft crew and the slightly increased costs of staying at Fort McMurray. In the June 1977 study, the field camp was visited several times, and it was felt that the visits together with telephone discussions provided sufficient communication between the aircraft operations and the rest of the field program.

8.8.4 Types of Aircraft Measurements Desired

The analysis of the June 1977 data demonstrated that-bulence data are very helpful in interpreting the SO_2 data. The turbulence data applied to the statistical theory gave very promising indications that plume dispersion may be predictable directly from turbulence measurements. Because of these encouraging results, it is recommended that airborne measurements include the measurement of the turbulence characteristics required for Taylor's statistical theory.

8.8.5 Subsequent Data Analysis and Field Trips

The recommendations for subsequent data analysis have already been enacted through the awarding of the contract for plume sigma analysis--AOSERP Project ME 3.8.3. The meteorological data from all available AOSERP sources needs to be brought together, standardized, and analysed. In this way, the completeness of the data set and its usefulness in formulating a prediction scheme for the plume sigma values can be determined. Recommendations for the timing of subsequent field trips should await the results of the plume sigma analysis.

9. AOSERP RESEARCH REPORTS

1.		AOSERP First Annual Report, 1975
2.	AF 4.1.1	Walleye and Goldeye Fisheries Investigations in the Peace-Athabasca Delta--1975
3.	HE 1.1.1	Structure of a Traditional Baseline Data System
4.	VE 2.2	A Preliminary Vegetation Survey of the Alberta Oil Sands Environmental Research Program Study Area
5.	HY 3.1	The Evaluation of Wastewaters from an Oil Sand Extraction Plant
6.		Housing for the North--The Stackwall System
7.	AF 3.1.1	A Synopsis of the Physical and Biological Limnology and Fisheries Programs whithin the Alberta Oil Sands Area
8.	AF 1.2.1	The Impact of Saline Waters upon Freshwater Biota (A Literature Review and Bibliography)
9.	ME 3.3	Preliminary Investigations into the Magnitude of Fog Occurrence and Associated Problems in the Oil Sands Area
10.	HE 2.1	Development of a Research Design Related to Archaeological Studies in the Athabasca Oil Sands Area
11.	AF 2.2.1	Life Cycles of Some Common Aquatic Insects of the Athabasca River, Alberta
12.	ME 1.7	Very High Resolution Meteorological Satellite Study of Oil Sands Weather: "A Feasibility Study"
13.	ME 2.3.1	Plume Dispersion Measurements from an Oil Sands Extraction Plant, March 1976
14.		
15.	ME 3.4	A Climatology of Low Level Air Trajectories in the Alberta Oil Sands Area
16.	ME 1.6	The Feasibility of a Weather Radar near Fort McMurray, Alberta
17.	AF 2.1.1	A Survey of Baseline Levels of Contaminants in Aquatic Biota of the AOSERP Study Area
18.	HY 1.1	Interim Compilation of Stream Gauging Data to December 1976 for the Alberta Oil Sands Environmental Research Program
19.	ME 4.1	Calculations of Annual Averaged Sulphur Dioxide Concentrations at Ground Level in the AOSERP Study Area
20.	HY 3.1.1	Characterization of Organic Constituents in Waters and Wastewaters of the Athabasca Oil Sands Mining Area
21.		AOSERP Second Annual Report, 1976-77
22.		Alberta Oil Sands Environmental Research Program Interim Report to 1978 covering the period April 1975 to November 1978
23.	AF 1.1.2	Acute Lethality of Mine Depressurization Water on Trout Perch and Rainbow Trout
24.	ME 1.5.2	Air System Winter Field Study in the AOSERP Study Area, February 1977.
25.	ME 3.5.1	Review of Pollutant Transformation Processes Relevant to the Alberta Oil Sands Area

26.	AF 4.5.1	Interim Report on an Intensive Study of the Fish Fauna of the Muskeg River Watershed of Northeastern Alberta
27.	ME 1.5.1	Meteorology and Air Quality Winter Field Study in the AOSERP Study Area, March 1976
28.	VE 2.1	Interim Report on a Soils Inventory in the Athabasca Oil Sands Area
29.	ME 2.2	An Inventory System for Atmospheric Emissions in the AOSERP Study Area
30.	ME 2.1	Ambient Air Quality in the AOSERP Study Area, 1977
31.	VE 2.3	Ecological Habitat Mapping of the AOSERP Study Area: Phase I
32.		AOSERP Third Annual Report, 1977-78
33.	TF 1.2	Relationships Between Habitats, Forages, and Carrying Capacity of Moose Range in northern Alberta. Part I: Moose Preferences for Habitat Strata and Forages.
34.	HY 2.4	Heavy Metals in Bottom Sediments of the Mainstem Athabasca River System in the AOSERP Study Area
35.	AF 4.9.1	The Effects of Sedimentation on the Aquatic Biota
36.	AF 4.8.1	Fall Fisheries Investigations in the Athabasca and Clearwater Rivers Upstream of Fort McMurray: Volume I
37.	HE 2.2.2	Community Studies: Fort McMurray, Anzac, Fort MacKay
38.	VE 7.1.1	Techniques for the Control of Small Mammals: A Review
39.	ME 1.0	The Climatology of the Alberta Oil Sands Environmental Research Program Study Area
40.	WS 3.3	Mixing Characteristics of the Athabasca River below Fort McMurray - Winter Conditions
41.	AF 3.5.1	Acute and Chronic Toxicity of Vanadium to Fish
42.	TF 1.1.4	Analysis of Fur Production Records for Registered Traplines in the AOSERP Study Area, 1970-75
43.	TF 6.1	A Socioeconomic Evaluation of the Recreational Fish and Wildlife Resources in Alberta, with Particular Reference to the AOSERP Study Area. Volume I: Summary and Conclusions
44.	VE 3.1	Interim Report on Symptomology and Threshold Levels of Air Pollutant Injury to Vegetation, 1975 to 1978
45.	VE 3.3	Interim Report on Physiology and Mechanisms of Air-Borne Pollutant Injury to Vegetation, 1975 to 1978
46.	VE 3.4	Interim Report on Ecological Benchmarking and Biomonitoring for Detection of Air-Borne Pollutant Effects on Vegetation and Soils, 1975 to 1978.
47.	TF 1.1.1	A Visibility Bias Model for Aerial Surveys for Moose on the AOSERP Study Area
48.	HG 1.1	Interim Report on a Hydrogeological Investigation of the Muskeg River Basin, Alberta
49.	WS 1.3.3	The Ecology of Macrobenthic Invertebrate Communities in Hartley Creek, Northeastern Alberta
50.	ME 3.6	Literature Review on Pollution Deposition Processes
51.	HY 1.3	Interim Compilation of 1976 Suspended Sediment Date in the AOSERP Study Area
52.	ME 2.3.2	Plume Dispersion Measurements from an Oil Sands Extraction Plan, June 1977

53.	HY 3.1.2	Baseline States of Organic Constituents in the Athabasca River System Upstream of Fort McMurray
54.	WS 2.3	A Preliminary Study of Chemical and Microbial Characteristics of the Athabasca River in the Athabasca Oil Sands Area of Northeastern Alberta
55.	HY 2.6	Microbial Populations in the Athabasca River
56.	AF 3.2.1	The Acute Toxicity of Saline Groundwater and of Vanadium to Fish and Aquatic Invertebrates
57.	LS 2.3.1	Ecological Habitat Mapping of the AOSERP Study Area (Supplement): Phase I
58.	AF 2.0.2	Interim Report on Ecological Studies on the Lower Trophic Levels of Muskeg Rivers Within the Alberta Oil Sands Environmental Research Program Study Area
59.	TF 3.1	Semi-Aquatic Mammals: Annotated Bibliography
60.	WS 1.1.1	Synthesis of Surface Water Hydrology
61.	AF 4.5.2	An Intensive Study of the Fish Fauna of the Steepbank River Watershed of Northeastern Alberta
62.	TF 5.1	Amphibians and Reptiles in the AOSERP Study Area
63.		Calculate Sigma Data for the Alberta Oil Sands Environmental Research Program Study Area.
64.	LS 21.6.1	A Review of the Baseline Data Relevant to the Impacts of Oil Sands Development on Large Mammals in the AOSERP Study Area
65.	LS 21.6.2	A Review of the Baseline Data Relevant to the Impacts of Oil Sands Development on Black Bears in the AOSERP Study Area
66.	AS 4.3.2	An Assessment of the Models LIRAQ and ADPIC for Application to the Athabasca Oil Sands Area
67.	WS 1.3.2	Aquatic Biological Investigations of the Muskeg River Watershed
68.	AS 1.5.3 AS 3.5.2	Air System Summer Field Study in the AOSERP Study Area, June 1977
69.	HS 40.1	Native Employment Patterns in Alberta's Athabasca Oil Sands Region
70.	LS 28.1.2	An Interim Report on the Insectivorous Animals in the AOSERP Study Area
71.	HY 2.2	Lake Acidification Potential in the Alberta Oil Sands Environmental Research Program Study Area
72.	LS 7.1.2	The Ecology of Five Major Species of Small Mammals in the AOSERP Study Area: A Review
73.	LS 23.2	Distribution, Abundance and Habitat Associations of Beavers, Muskrats, Mink and River Otters in the AOSERP Study Area, Northeastern Alberta
-	--	Interim Report to 1978
74.	AS 4.5	Air Quality Modelling and User Needs
75.	LS 2.1	Interim Report on the Soils Inventory of the AOSERP Study Area

76. AF 4.5.1 An Intensive Study of the Fish Fauna of the Muskeg River Watershed of Northeastern Alberta

77. HS 20.1 Overview of Local Economic Development in the Athabasca Oil Sands Region Since 1961.

78. LS 22.1.1 Habitat Relationships and Management of Terrestrial Birds in Northeastern Alberta.

79. AF 3.6.1 The Multiple Toxicity of Vanadium, Nickel, and Phenol to Fish.

These reports are not available upon request. For further information about availability and location of depositories, please contact:

Alberta Oil Sands Environmental Research Program
15th Floor, Oxbridge Place
9820 - 106 Street
Edmonton, Alberta
T5K 2J6

DATE DUE SLIP

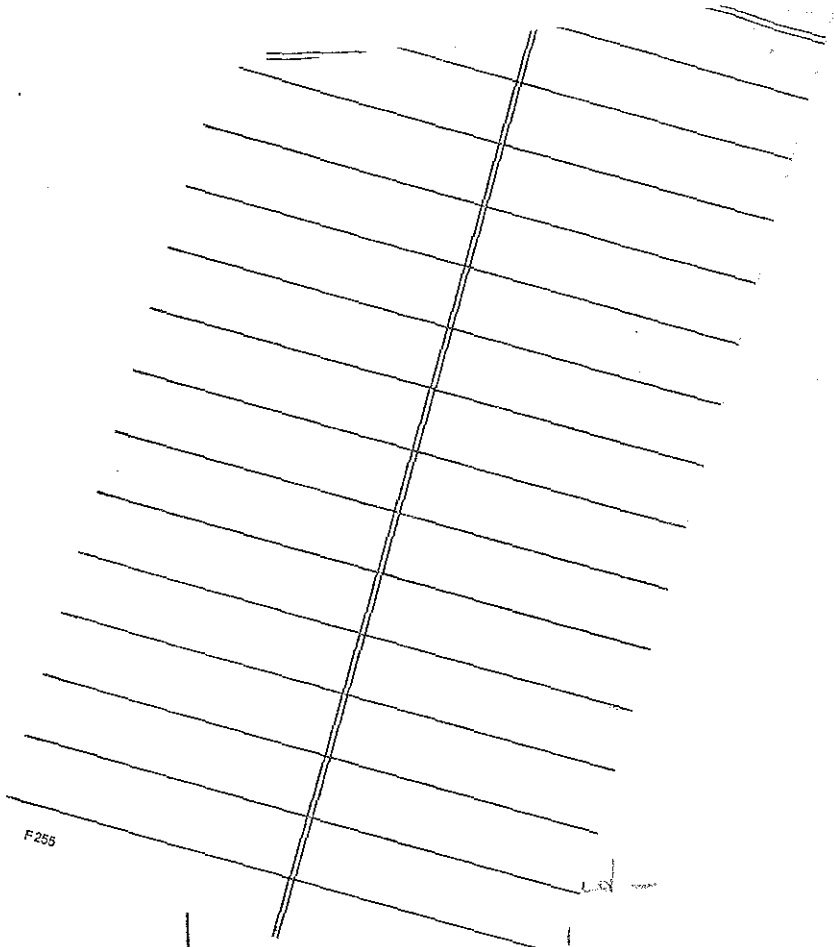

F255

X-Ref. Acid mu

Locational